

INVESTIGATION TO DIRECT ETHANOL INJECTION IN SPARK IGNITION GASOLINE ENGINES

By
Yuan ZHUANG

Thesis submitted as a requirement for the degree of
Doctor of Philosophy

School of Electrical, Mechanical and Mechatronic Systems
Faculty of Engineering and Information Technology

University of Technology, Sydney (UTS)
July, 2014

Declaration of Authorship

I, Yuan ZHUANG, certify that the work in this thesis has not previously been submitted for a degree nor has it been submitted as part of requirements for a degree except as fully acknowledged within the text.

I also certify that the thesis has been written by me. Any help that I have received in my research work and the preparation of the thesis itself has been acknowledged. In addition, I certify that all information sources and literature used are indicated in the thesis.

Signed:

Date:

Acknowledgements

I would like to take this opportunity to express my gratitude to all of the people who have offered me help and support during the past four years of my candidature. First and foremost, I would like to give my sincere thanks to my supervisor A/Prof. Guang Hong for providing the project and for her guidance, inspiration, numerous hours of discussion, and revision of the papers. From her I acquired not only knowledge but also high order research methodology skills which will benefit me throughout my career.

I wish to acknowledge my co-supervisor Dr. Jianguo Wang and visiting scholar Dr. Zhipeng Li who respectively helped me to solve the software problems of our engine control unit. I benefited greatly from their support, and I sincerely appreciated their contribution to the project.

I wish to acknowledge the strong support that I received from staff in Mechanical engineering Laboratories and FEIT workshop at UTS, including Len D'Arcy, Chris Chapman, Holger Roser, Jack Liang, Laurence Stonard, John Funnell, and Ron Smith. Without their excellent technical assistance, the building up, calibration and maintenance of the testing rig system would not have been possible.

Many thanks to the capstone students, Gim Lim Ong, Tin Shea, Kelvin Tran, Fabio Perri, Michael Milledge and Kiel D'Arcy who assisted with the experimental work. I also want to thank Dr. Ding Fei, A/Prof. Bin Zhou, Dr. Cliff Wang and Mr. Yuhan Huang who gave me great assistance in both my studies and daily life.

My deep thanks go to my parents and friends, who have always been proud of my achievements and who have consistently supported and cared for me throughout the years.

I extend my gratitude to the China Scholarship Council who provided the scholarship for my four years of study. I also would like to express my great appreciation for the financial support from the Faculty of Engineering & IT, including my top-up scholarship for four years and the funding for setting up the engine rig. Manildra Group, the supplier of the ethanol fuel is also gratefully acknowledged.

Finally, I would like to thank Shale Preston for proofreading my thesis.

Publications

Journal Papers:

Yuan Zhuang and Guang Hong. "Primary investigation to leveraging effect of using ethanol fuel on reducing gasoline fuel consumption." *Fuel* 105 (2013): 425-431.

Yuan Zhuang and Guang Hong. " Effects of direct injection timing of ethanol fuel on engine knock and lean burn in a port injection gasoline engine." *Fuel* 135 (2014) 27–37.

Conference Papers:

Yuan Zhuang and Guang Hong. "Investigation to Leveraging Effect of Ethanol Direct Injection (EDI) in a Gasoline Port Injection (GPI) Engine." SAE Technical Paper 2013-04-08, 2013, doi: 10.4271/2013-01-1322.

Yuan Zhuang and Guang Hong. The Effect of Direct Injection Timing and Pressure on Engine Performance in an Ethanol Direct Injection Plus Gasoline Port Injection (EDI+ GPI) SI Engine. SAE Technical Paper 2013-01-0892, 2013, doi:10.4271/2013-01-0892.

Yuan Zhuang, Guang Hong, and Jianguo Wang. "Preliminary investigation to combustion in a SI engine with direct ethanol injection and port gasoline injection (EDI+ GPI)." (2012), 18th Australasian Fluid Mechanics Conference, Launceston, Australia.

Yuan Zhuang, Jianguo Wang, and Guang Hong. "A single cylinder research engine for investigating combustion of direct ethanol injection and port gasoline injection." (2012), 18th Australasian Fluid Mechanics Conference, Launceston, Australia.

Papers Submitted for Publications:

Yuan Zhuang and Guang Hong. "Effects of spark timing on the performance of an ethanol direct injection plus gasoline port injection (EDI+GPI) engine" Submitted to *Applied Energy*, in review.

Abstract

Ethanol is a promising alternative fuel in terms of addressing future energy and environmental problems. The existing method of using ethanol fuel by blending gasoline and ethanol fuel does not fully exploit ethanol's advantages. The dual-fuel injection strategy, ethanol direct injection plus gasoline port injection (EDI+GPI), offers a potentially new way to make use of ethanol fuel more effectively and efficiently. The effect of EDI+GPI on engine performance has been experimentally investigated on a 249cc, 4 stroke, air cooled single cylinder engine which was modified by adding an ethanol fuel direct injection system. The research purpose was focused on efficiency improvement (leveraging effect) and emissions reduction. Engine performance at original engine spark timing setting (15 CAD BTDC), knock margin and lean conditions was carried out to assess EDI+GPI's effectiveness. The impacts of EDI+GPI on engine control parameters, such as start of injection (SOI) timing and spark timing, were also evaluated in order to best match this new fuelling system to conventional SI engines.

When the engine was operating at the original engine spark timing setting (15 CAD BTDC), less energy input was required in a SI engine equipped with EDI+GPI to achieve comparable engine power output. Thus, the total fuel consumption could be reduced by leveraging the use of ethanol fuel. At engine speed of 3500rpm, when the ethanol energy ratio (EER) was less than 42.4% at light load and 36.3% at medium load, the EDI+GPI showed a positive impact in relation to combustion with reduced combustion duration and advanced central combustion phasing. However, with further increase of EER, the combustion duration prolonged and central combustion phasing retarded. This may be caused by over cooling due to increased ethanol fuel directly injected.

EDI+GPI effectively mitigated engine knock and permitted more advanced spark timing and higher inlet air pressure. At three tested engine loads of indicated mean effective pressure (IMEP), 7.2 Bar, 7.8 Bar and 8.5 Bar, every 2% or 3% increment of EER permitted about 2 CAD advance of knock limited spark advance (KLSA) when the EER was in the range from 15% to 35%. The highest load achieved in this investigation was 10.5 Bar IMEP at inlet (compressed) air pressure of 1.4 Bar. The EER level at this condition was 36.9%.

Early ethanol direct injection (EEDI) was more suitable to the EDI+GPI engine since the IMEP in EEDI conditions was greater than that in later ethanol direct injection (LEDI) conditions due to improved volumetric efficiency and combustion. LEDI was less effective on increasing IMEP

because its major combustion duration was longer than that in the EEDI condition. In lean burn, EEDI was more effective on extending the lean burn limit than LEDI. The maximum lean burn limit (λ) achieved by EEDI was 1.29. LEDI only slightly increased the lean burn limit which was just over the stoichiometric air-fuel ratio (AFR).

When the EER varied, spark timing required corresponding changes to achieve the best efficiency. At IMEP of around 4.0 Bar, spark timing of 25 CAD BTDC resulted in the highest indicated thermal efficiency when the EER was less than 29%, whilst when the EER was greater than 39%, the maximum indicated thermal efficiency was at spark timing of 30 CAD BTDC.

Contents

1. Chapter One	
1. Introduction	1
1.1 Properties of Ethanol Fuel.....	2
1.2 Application of ethanol fuel to CI engines	3
1.2.1 Assisted-ignition CI engine.....	4
1.2.2 Diesel/ethanol (Diesohol) fuel blends.....	5
1.2.3 Ethanol-diesel dual-fuel injection	7
1.3 Application of ethanol fuel to SI engines.....	10
1.3.1 Pure ethanol engine and gasoline/ethanol dual port injection.....	10
1.3.2 Ethanol/gasoline blends	11
1.3.3 Existing problem of using ethanol fuel in SI engine.....	13
2. Chapter Two	
2. Review of direct injection plus port injection SI engines	17
2.1 Introduction	17
2.2 Potential impact of EDI+GPI on engine performance	18
2.2.1 Inlet air flow and mixture quality.....	18
2.2.2 In-cylinder temperature and knock tendency	20
2.2.3 Mixture preparation.....	22
2.2.4 Combustion process	24
2.2.5 Lean burn	24
2.2.6 Pollutant emissions	27
2.3 Research up to date	28
2.4 Existing problems and research objectives	31
2.5 Outlines	33
3. Chapter Three	
3. Experimental setup and test facilities.....	35
3.1 General description	35
3.2 Research engine system	37
3.2.1 Research engine	37
3.2.2 High pressure ethanol fuel supply system.....	39
3.2.3 Control unit	40
3.2.4 Engine control strategy	41
3.2.5 Dynamometer.....	42
3.3 Instruments and measurements	42
3.3.1 In-cylinder pressure measurement	42
3.3.2 Data acquisition system.....	43

3.3.3 Exhaust gas emission measurement	44
3.3.4 Fuel mass flow, air mass flow and other measurements	45
3.4 Data processing and analysis	46
3.4.1 Indicated mean effect pressure	46
3.4.2 Heat release rate	47
3.4.3 Coefficient of variation	48
3.4.4 Fuel efficiency	48
3.4.5 Knock detection	49
3.4.6 Mass burnt fraction	51
3.4.7 Calculation of lambda	53
3.4.8 Combustion efficiency	54
3.5 Tested fuels	54
4. Chapter Four	
4. Leveraging effect of EDI	56
4.1 Influence of EER	56
4.1.1 Engine performance	57
4.1.2 Possible reasons for the increased IMEP	59
4.1.3 Combustion characteristics	68
4.1.4 Exhaust gas emissions	75
4.2 Comparison of EDI+GPI and GDI+GPI	77
4.2.1 Engine performance	77
4.2.2 Combustion characteristics	80
4.2.3 Emissions	83
4.3 Summary	86
5. Chapter Five	
5. Leveraging effect of EDI enhanced by spark advance and inlet air pressure increment	88
5.1 Effect of spark timing on EDI+GPI engine	88
5.1.1 Effect of spark timing on combustion at different EERs	89
5.1.2 Effect of spark timing on emissions and efficiency at different EERs	99
5.2 Leveraging effect enhanced by spark advance and inlet air pressure increment	103
5.2.1 Leveraging effect enhanced by spark advance	105
5.2.2 Leveraging effect enhanced by inlet air pressure increment	116
5.3 Summary	124
6. Chapter Six	
6. Influence of SOI timing and injection pressure on EDI+GPI engine performance	127

6.1	Effect of SOI timing and injection pressure.....	127
6.1.1	Engine performance	128
6.1.2	Combustion characteristics	134
6.1.3	Engine exhaust gas emissions	139
6.2	Effect of SOI timing on knock mitigation	143
6.2.1	Engine performance.....	144
6.2.2	Combustion characteristics.....	147
6.2.3	Emissions.....	149
6.3	Effect of SOI timing on lean burn.....	151
6.3.1	Engine performance.....	151
6.3.2	Combustion.....	157
6.3.3	Emissions.....	159
6.4	Summary	161
7.	Chapter Seven	
7.	Conclusions and future work	164
7.1	Conclusions	164
7.2	Future work	168

List of Tables

Table 1. 1 Properties of Diesel/Ethanol/Gasoline	2
Table 3. 1 Specifications of Yamaha YBR250 engine.....	37
Table 3. 2 Resolution of the gas analyser.....	45
Table 3. 3 Test fuel properties.....	55
Table 4. 1 Experimental conditions for Section 4.1	56
Table 4. 2 Experimental conditions for Section 4.2	78
Table 5. 1 Experimental conditions for Section 5.1	89
Table 5. 2 Experimental conditions for Section 5.2.1	104
Table 5. 3 Experimental conditions for Section 5.2.2	105
Table 6. 1 Experimental conditions for Section 6.1	128
Table 6. 2 Experimental conditions for Section 6.2	144
Table 6. 3 Experimental conditions for Section 6.3	153

List of Figures

Figure 1.1–(a) Injecting the ethanol fuel into the inlet manifold; (b) Direct injecting ethanol fuel into combustion chamber.....	7
Figure 2.1–Tumble intensity vs.flow coefficient.....	20
Figure 2.2–Distillation characteristics of ethanol blends	22
Figure 2.3–Vaporization curve for ethanol, gasoline and Isooctane	23
Figure 3.1–Schematic description of the entire experimental setup.....	36
Figure 3.2–Components and links of the control system	36
Figure 3.3–Relative position of direction injector on cylinder head (External View) ...	38
Figure 3.4–Relative position of direction injector on cylinder head (Internal View)	38
Figure 3.5–Images of injector in combustion chamber and external cylinder	39
Figure 3.6–Schematic diagram of high pressure ethanol fuel system	39
Figure 3.7–Nominal spray pattern of the injector	40
Figure 3.8–Function of ECU	41
Figure 3.9–Roadmap of control strategy	41
Figure 3.10–Schematic of Kistler 6115B pressure transducer	43
Figure 3.11–Photo of MEXA-584L Gas analyser.....	44
Figure 3.12–HC concentrations from NDIR and FID analysis	45
Figure 3.13–Gravimetric calibration of DI and PFI injectors	46
Figure 3.14– Original cylinder pressure trace and 3-20 kHz band pass filtered pressure for different engine body temperature conditions	51
Figure 3.15–Pressure-Volume diagram to show the pressure values in calculating MBF.....	52
Figure 4.1–Variation of IMEP with EER.....	57
Figure 4.2–Variation of volumetric efficiency with EER	58
Figure 4.3–Variation of ISFC with EER	59
Figure 4.4–Variation of BSEC with EER.....	59
Figure 4.5–Variation of heat of vaporization of stoichiometric mixture.....	61
Figure 4.6–Maximum thermodynamic charge cooling and volumetric efficiency increment for a Gasoline-Ethanol Blend vs. Volumetric Ethanol Content.	62
Figure 4.7–In-cylinder temperature before combustion.....	62
Figure 4.8–Variation of LHV per unit mass of air and LHV of ethanol/gasoline air mixture.....	63
Figure 4.9–Variation of γ with temperature at stoichiometric air/fuel reactants and complete stoichiometric products.....	65
Figure 4.10–Variation of γ with ethanol/gasoline ratio.....	66
Figure 4.11–Variation of mole multiplier with ethanol/gasoline ratio.....	67
Figure 4.12– In-cylinder pressure trace and maximum in-cylinder pressure at different EERs at 3500rpm.....	70
Figure 4.13– Heat release rate and CA50 at different EERs at 3500rpm.....	71

Figure 4.14–Variation of CA0-5% with EER	72
Figure 4.15–Variation of CA5-50% with EER	73
Figure 4.16–Variation of indicated CA5-90% with EER.....	73
Figure 4.17–Variation of COV_{IMEP} with EER.....	74
Figure 4.18–Variation of indicated thermal efficiency with EER.....	75
Figure 4.19–Variation of ISHC with EER	76
Figure 4.20–Variation of ISCO with EER	76
Figure 4.21–Variation of ISNO with EER	77
Figure 4.22–Variation of volumetric efficiency with DI/PFI energy ratio at 3500rpm .	78
Figure 4.23–Variation of IMEP with DI/PFI energy ratio at 3500rpm.....	79
Figure 4.24–Variation of CA5-50% with DI/PFI energy ratio at 3500rpm	80
Figure 4.25–Variation of CA5-90% with DI/PFI energy ratio at 3500rpm	82
Figure 4.26–Variation of indicated thermal efficiency with DI/PFI energy ratio at 3500rpm.....	83
Figure 4.27–Variation of ISCO with DI/PFI energy ratio at 3500rpm	84
Figure 4.28–Variation of ISHC with DI/PFI energy ratio at 3500rpm	85
Figure 4.29–Variation of ISNO with DI/PFI energy ratio at 3500rpm	86
Figure 5.1–Variation of IMEP with spark timing (a) and EERs (b)	90
Figure 5.2–Variation of CA0-5% with spark timing (a) and EERs (b).....	92
Figure 5.3–Variation of CA5-50% with spark timing (a) and EERs (b).....	93
Figure 5.4–Variation of CA5-90% with spark timing (a) and EERs (b).....	95
Figure 5.5–Variation of P_{max} with spark timing (a) and EERs (b)	96
Figure 5.6–Variation of COV_{IMEP} with spark timing (a) and EERs (b)	97
Figure 5.7–Variation of exhaust temperature with spark timing (a) and EERs (b).....	98
Figure 5.8–Variation of ISNO with spark timing (a) and EERs (b).....	99
Figure 5.9–Variation of ISCO with spark timing (a) and EERs (b).....	100
Figure 5.10–Variation of ISHC with spark timing (a) and EERs (b).....	101
Figure 5.11–Variation of indicated thermal efficiency with spark timing (a) and EERs (b).....	102
Figure 5.12–Variation of KLSA with EER	106
Figure 5.13–Variation of ethanol volumetric flow rate with KLSA	107
Figure 5.14–Variation of P_{max} with KLSA	108
Figure 5.15–Variation of combustion efficiency with KLSA	109
Figure 5.16–Variation of CA50 with KLSA	111
Figure 5.17–Variation of CA5-90% with KLSA	112
Figure 5.18–Variation of indicated thermal efficiency at KLSA	113
Figure 5.19–Variation of ISHC with KLSA.....	114
Figure 5.20–Variation of ISCO with KLSA.....	115
Figure 5.21–Variation of ISNO with KLSA	116
Figure 5.22– Variation of IMEP and MBT spark timing with inlet air pressure	117

Figure 5.23–Variation of EER and ethanol volumetric flow rate with inlet air pressure	118
Figure 5.24– Variation of P_{max} with Inlet air pressure	119
Figure 5.25– Variation of CA5-90% with inlet air pressure	120
Figure 5.26– Variation of indicated thermal efficiency with inlet air pressure.....	121
Figure 5.27– Variation of ISCO with inlet air pressure	122
Figure 5.28– Variation of ISNO with inlet air pressure	123
Figure 5.29– Variation of ISHC with inlet air pressure	124
Figure 6.1–Experimental engine SOI timing windows	128
Figure 6.2–Variation of IMEP with SOI timing and pressure in EDI+GPI (a) and EDI+GPI (b) conditions	129
Figure 6.3–Variation of Volumetric efficiency with SOI timing and pressure in EDI+GPI (a) and EDI+GPI (b) conditions.....	131
Figure 6.4–Variation of ISEC with SOI timing and pressure in EDI+GPI (a) and EDI+GPI (b) conditions	133
Figure 6.5–Variation of CA5-90% with SOI timing and pressure in EDI+GPI (a) and EDI+GPI (b) conditions	134
Figure 6.6–Variation of CA50 with SOI timing and pressure in EDI+GPI (a) and EDI+GPI (b) conditions	136
Figure 6.7–Variation of indicated thermal efficiency with SOI timing and pressure in EDI+GPI (a) and EDI+GPI (b) conditions.....	138
Figure 6.8–Variation of ISCO with SOI timing and pressure in EDI+GPI (a) and EDI+GPI (b) conditions	139
Figure 6.9–Variation of ISHC with SOI timing and pressure in EDI+GPI (a) and EDI+GPI (b) conditions	141
Figure 6.10–Variation of ISNO with SOI timing and pressure in EDI+GPI (a) and EDI+GPI (b) conditions	142
Figure 6.11–Variation of KLSA with SOI timing.....	144
Figure 6.12–Variation of IMEP with SOI timing at KLSA	145
Figure 6.13–Variation of volumetric efficiency with SOI timing at KLSA.....	146
Figure 6.14–Variation of CA0-5% with SOI timing at KLSA.....	147
Figure 6.15–Variation of CA5-90% with SOI timing at KLSA.....	148
Figure 6.16–Variation of indicated thermal efficiency with SOI timing at KLSA	149
Figure 6.17–Variation of ISNO with SOI timing at KLSA.....	150
Figure 6.18–Variation of ISHC with SOI timing at KLSA.....	151
Figure 6.19 –Variation of lean burn limit with SOI timing.....	154
Figure 6.20– Variation of IMEP at lean burn limit	155
Figure 6.21– Variation of indicated thermal efficiency at lean burn limit.....	156
Figure 6.22–Variation of COV_{IMEP} with SOI timing at lean burn limit.....	157
Figure 6.23– Variation of CA0-10% at lean burn limit.....	158
Figure 6.24– Variation of CA10-90% at lean burn limit.....	159
Figure 6.25– Variation of ISNO at lean burn limit.....	160

Figure 6.26– Variation of ISHC at lean burn limit..... 161

Acronyms and Abbreviations

HE: Heating energy

HC: Hydrocarbon

ATDC: After top dead center

BTDC: Before top dead center

CI: Compression ignition

CO: Carbon monoxide

DI: Direct fuel injection

ECU: Electronic control unit

EDI: Ethanol fuel direct injection

EEDI: Early ethanol direct injection

EGDI: Early gasoline direct injection

ERR: Ethanol/gasoline energy ratio

FFV: Fuel flexible vehicle

GDI: Gasoline direct injection

GPI: Gasoline port injection

HC: Hydrocarbon

IMEP: Indicated mean effective pressure

ISCO: Indicated specific carbon monoxide

ISHC: Indicated specific hydrocarbon

ISNO: Indicated specific nitric oxide

KLSA: Knock limited spark advance

LEDI: Late ethanol direct injection

LGDI: Late gasoline direct injection

MBT: Maximum advanced for best torque

NO_x: Nitric oxygen

PFI: Port fuel injection

SIDI: Spark ignition direct injection

SOI: Start of injection

ST: Spark timing

SI: Spark ignition

TDC: Top dead center

RPM: Revolutions per minute

Variables

CA0-5%: Combustion initiation duration (degree)

CA50: Crank angle position where the accumulated heat release reaches 50% of the total released heat (degree)

CA5-50%: Early combustion duration (degree)

CA5-90%: Major combustion duration (degree)

CAD: Crank angle degree (degree)

HE: Heating energy (kW)

Lambda (λ): Air/fuel equivalence ratio (dimensional)

MBF: Mass burnt fraction (dimensional)

Chapter One

1. Introduction

Nowadays, the demand for crude oil has rapidly increased with the development of the world economy. The consequent problems initiated by the wide use of fossil fuels, such as depletion of fossil fuel resources, global warming and environmental degradation have become serious problems obstructing the continuous development and sustainable progress of human society.

In order to address the resultant environmental and energy problems, several technical approaches have been proposed by the automotive industry, for example fuel cell vehicles, electrical automobiles, hydrogen cars and hybrid vehicles. These technical solutions have been in development for decades. However, due to the colossal requirements for infrastructure construction, great technical obstacles and added cost to the vehicle price, these technical approaches are still in their infancy [1] [2]. The most logical near term solutions still rely on the continual improvement of internal combustion (IC) engines.

Using liquid biofuels is one of the most promising ways to improve the current IC engine due to the ease of implementation in the existing combustion systems and infrastructure. Another merit of using liquid biofuels is that they may simultaneously increase engine efficiency and reduce pollutant emissions, owing to the favorable features of these fuels. Ethanol is the most promising biofuel among all of the possible candidates.

The application of ethanol as a fuel in the SI engine can be traced back to 1908, the year in which the Ford Motor Company's first car, the Model T, used ethanol corn alcohol gasoline for fuel energy [3]. Ethanol is a renewable energy source that can be produced from multiple bio-sources such as sugar cane, maize, grain straw and brown seaweed [4]. The use of ethanol fuel has the potential to reduce the greenhouse gas emissions, as it absorbs carbon dioxide (CO₂) while undergoing the growth process. In 2013, about 22.4 billion gallons of ethanol was

consumed for the transportation sector as a fuel [4].

1.1 Properties of Ethanol Fuel

Ethanol, like most short-chain alcohols, is a volatile, flammable, colourless liquid. It is miscible with water and with most organic liquids, including non-polar liquids such as aliphatic hydrocarbons. It can be produced both as a petrochemical, through the hydration of ethylene, and biologically, by fermenting sugars with yeast. The chemical formula of ethanol is C_2H_5OH .

Currently, the ethanol is used in internal combustion engines in the following major ways: Ethanol/Gasoline blended fuel, Ethanol/Diesel blended fuel, Gasoline and Ethanol separated injection on SI engine, Diesel and Ethanol separated injection on CI engine and pure ethanol fuel. Table 1.1 lists the properties of diesel, ethanol and gasoline.

Table 1. 1 Properties of Diesel/Ethanol/Gasoline [5]

	Diesel	Ethanol	Gasoline
Formula	C_{15-16}	CH_3-CH_2-OH	C_{4-12}
Low heating value (MJ/kg)	42.5	27.0	43.5
Density(g/ml)	0.84	0.81	0.70~0.78
Cetane Number	40~55	8	0-10
Auto Ignition Temperature (K)	473-493	693	493-533
Octane Number	20-30	111	90-95
Air/Fuel ratio	14.6	9.0	14.7-15
Heat of Vaporization (kJ/Kg)	251 ~ 270	854 ~ 904	310 ~320
Boiling Point (K)	453-633	351.5	303-473
Kinematic viscosity ($10^{-6}m^3 /s$)	2.5-8.5	1.51	0.65-0.85

From table 1.1, the following information can be drawn for the use of ethanol fuel in internal combustion engines.

1. The usage of ethanol fuel can reduce the requirements on the engine intake system, because the stoichiometric AFR of ethanol is 9.0 which is, lower than gasoline and diesel, and the ethanol is oxygen contained (34.8%, mass based) [6].

2. Ethanol has a high octane number and a low cetane number. Thus it has a poor spontaneous combustion performance and a high knock resistance property.
3. Ethanol boasts a high volatility compared with diesel. Adding ethanol to the major fuel can improve the formation of the homogeneous mixture and improve the combustion process of the engine.
4. The flame propagation speed of ethanol is faster than gasoline and diesel in a relatively wide AFR range. It can accelerate the combustion process of the mixture and consequently improve the combustion [7] [8].
5. The latent heat vaporisation of ethanol is much higher than gasoline and diesel. This property can be used to lower the in-cylinder temperature, which improves volumetric efficiency, reduces combustion emission and increases the compression rate or boost pressure of a SI engine [9].
6. The low heat value of ethanol is about 62.8% of diesel and 63.5% of gasoline. This requires the improvements on the fuel delivery system to regain the same engine power, as more mass of ethanol fuel is needed.

1.2 Application of ethanol fuel to CI engines

The implementation of ethanol fuel on the compression ignition (CI) engine has been studied for a long time. Detailed studies have been conducted by many scholars. However, due to various reasons, the commercialisation of using ethanol fuel in the CI engine is still in its infancy. Only small scale commercialised real-world applications were carried out in some parts of west China, Belgium and Brazil. Generally, the technical approaches for implementing ethanol on the CI engine can be concluded as three major methods: assisted-ignition,

diesel/ethanol (Diesohol) fuel blends and dual-fuel injection.

1.2.1 Assisted-ignition CI engine

In a conventional diesel engine, the hot air that prevails at the end of the compression stroke is sufficient for igniting the diesel fuel. However, in the CI engine fueled with pure ethanol or ethanol/diesel blends, ignition-assistance is needed to ensure continuous combustion, due to the high self-ignition temperature of ethanol (693 K). This high self-ignition temperature can be useful for SI engines as it enhances the engine knock resistance, however, in the CI engine it results in negative effects on continuous self-ignition. The ignition assistance can be by means of a sparkplug, a glow plug or other heated surface [10]. Normally, in these systems the ethanol is injected through the original injector and the fuel supply system is modified by increasing the fuel flow rate due to the low lower heating value of the ethanol fuel. Modifications on the combustion chamber and compression ratio are also needed, owing to ethanol fuel's high latent heat of vaporisation, high auto-ignition temperature and high flame propagation speed [10] [11].

When using ignition-assistance, its position in the combustion chamber, operating temperature and the length of the intruding part are the key factors that affect performance. For example, when using a glow-plug, the tip of the glow-plug is normally positioned in the vicinity of the injector nozzle, and the protrusion into the combustion chamber should be long enough. Thus, a better impingement of the fuel spray with the glow-plug can be achieved and the mixture temperature can be easily increased [10]. When using a spark plug, the improperly installed position and length of the intruding part can lead to the short life of the plug. If the fuel spray can easily contaminate the spark plug and the protrusion of the spark plug cannot be sufficiently cooled down, the plug may be damaged in a short period of time. The hot surface assisted-ignition method is also sensitive to the installed position. However, its working temperature is lower than that of glow-plug. Over 573 K is high enough to ensure continuous self-ignition of ethanol fuel [11]. Thus thermal damage is not usual in this method. Generally, due to the reliability of the ignition-assistance, the assisted-ignition CI engine is not an optimal

solution for using ethanol fuel. However, the research results of the threshold temperature for ethanol self-ignition may be used as references for future anti-knock studies of ethanol fueled SI engines.

Although the assisted-ignition CI engines possess some shortcomings in ensuring continuous combustion, the engine test results in [12] showed positive effects in terms of using ethanol fuel. Investigations into using ethanol fuel in the assisted-ignition CI engine have demonstrated substantial improvements in engine thermal efficiency and emissions. Lorusso et al. conducted their research on a single cylinder engine which was modified from a 6.6L, 6-cylinder diesel engine. The engine was equipped with a glow-plug. Experimental results showed that the DI ethanol resulted in a 9% to 15% increase in full load BMEP, and a 1% to 1.5% reduction in energy consumption based on the EPA 13-mode transient cycle relative to the baseline DI diesel mode [12]. Can et al. conducted research on using ethanol fuel on a single cylinder CI engine equipped with a spark assistance ignition system. The results indicated that the combination of using ethanol fuel and the “ ω ” sharp combustion chamber largely increased diesel engine thermal efficiency. The maximum brake thermal efficiency was 42% in their study, which was much higher than other CI engines fueling with diesel that was normally between 35% and 37% [13]. Other investigations into the assisted-ignition CI engine also reported an increase in thermal efficiency when using ethanol fuel. Nitrogen oxides (NO_x) emissions were reduced as well [14] [15]. Despite the merits of increasing thermal efficiency, the life-time of the spark plug or glow-plug is problematic in relation to the assisted-ignition ethanol engine. This factor seriously constrains the commercialisation of this technique [16].

1.2.2 Diesel/ethanol (Diesohol) fuel blends

Currently, the research on diesohol fuel or diesel/ethanol fuel blends is mainly focused on the following directions: dissolvability of ethanol and diesel, the development of solvent, and combustion and emission characteristics of the fuel. The ethanol solubility in diesel is affected mainly by two factors, these being the temperature and water content of the blend [17]. At warm

ambient temperatures, dry ethanol blends readily with diesel fuel. However, when the temperature is below about 280 K (a temperature limit that is easily exceeded in many parts of the world for a large portion of the year) the two fuels separate. Prevention of this separation can be accomplished in two ways: by adding an emulsifier which acts to suspend small droplets of ethanol within the diesel fuel, or by adding a co-solvent that acts as a bridging agent through molecular compatibility and bonding to produce a homogeneous blend [18]. Gasoline and biodiesel can be used as co-solvent for the ethanol and diesel blend. They can help to produce a complete soluble compound fuel whereby a higher substitution rate is possible. The combustion performance of the compound can be optimised by them because gasoline and biodiesel are both fuels and co-solvents [19].

Experimental investigations on the combustion and emission characteristics of diesohol fuel showed that when using an appropriate ratio of the ethanol-diesel-gasoline blend (ethanol 10%~20%, diesel 70%~80%, gasoline 10%~20%) the engine power output and equivalent specific fuel consumption (ESFC) remained unchanged. Soot and NO_x emissions reduced remarkably, primarily due to the oxygen content and low adiabatic flame temperature of ethanol [20]. The ignition delay period was found to be elongated when using diesohol fuel. Ethanol's high self-ignition temperature and great latent heat of vaporisation were regarded as the causes for the elongated ignition delay. The cylinder pressure, maximum rate of pressure rise and heat release rate increased with higher ethanol concentration due to the longer ignition delay. The average temperature in the cylinder and the combustion duration was reduced [21] [22]. Pan et al. reported that better combustion performance and lower emissions could be achieved by introducing an umbrella nozzle. It was found that when using the umbrella nozzle, the mixture released the heat at a more intensive rate, and the combustion duration reduced by an average of 5 CAD in all tested conditions. Soot formation declined 50% in certain SOI timings and carbon monoxide (CO) emissions decreased as well. It was also found that the injection advance angle should be adjusted correspondingly in order to achieve better engine performance [23]. Other research reported that the addition of ethanol in the fuel led to an increase in terms of ignition delay and a lag in relation to combustion phasing. The engine thermal efficiency and fuel

consumption could be kept at a similar level to that of the diesel fueled counterpart through adjusting the SOI timing. The maximum cylinder pressure was almost unaffected by adding ethanol [24] [25]. The exhaust temperature decreased with the increase of ethanol/diesel blending ratio, which was attributed to the low adiabatic flame temperature of the ethanol. Emissions of NO_x and CO were largely reduced, but hydrocarbon (HC) emissions increased by 50% or more [26] [27].

1.2.3 Ethanol-diesel dual-fuel injection

Dual-fuel injection is another way of ensuring continuous and stable ignition when using ethanol fuel in the CI engine. It is realised by using pilot diesel to ignite the ethanol fuel. The ethanol fuel can be introduced by aspiration or injection into the inlet manifold, or direct injection in the combustion chamber. Figure 1.1 shows the layout of these two methods.

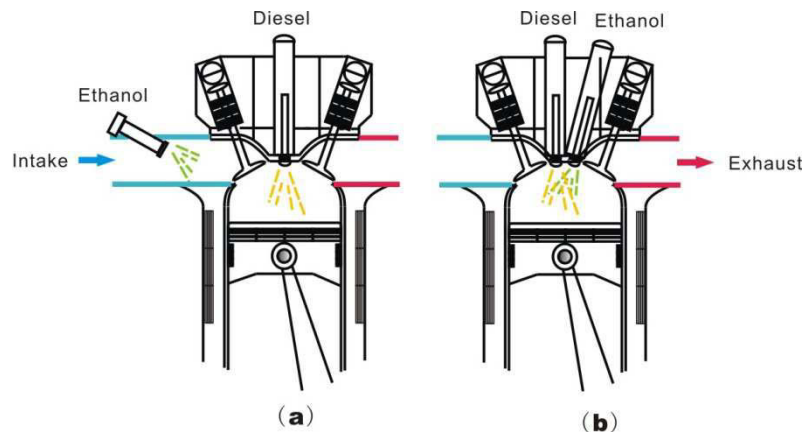


Figure 1.1–(a) Injecting the ethanol fuel into the inlet manifold; (b) Direct injecting ethanol fuel into combustion chamber [28]

A dual-fuel direct injection CI engine requires the engine to incorporate two types of fuel injection systems. One is for ethanol fuel, the other one is for diesel. In this way, the ethanol fuel usage (volumetric percentage) can be largely increased, because the diesel/ethanol ratio can be adjusted according to the engine operating conditions and high ratios can be used in the conditions at which continuous combustion can be ensured. According to Anisits et al., 10% of diesel (volumetric based) was enough to ensure stable ignition. Higher ethanol/diesel percentage was achievable, but the ignition timing was delayed and the HC and CO emissions were

increased largely. This increase in ignition delay and emission was possibly due to the great latent heat of the vaporisation of ethanol which may significantly decrease the in-cylinder temperature and deteriorate the combustion process [28]. In dual-fuel direct injection CI engines, pilot diesel fuel spray angle and ethanol fuel injection timing are the two factors which significantly affect the engine performance [29]. Improper pilot spray angle may cause difficulties in igniting ethanol fuel which may in turn lead to an increase in fuel consumption and HC emissions. The ethanol fuel injection timing affects the engine performance in both light and heavy engine loads, because earlier ethanol fuel injection greatly reduces the in-cylinder temperature and deteriorates the combustion process. Thus engine power output decreases and fuel consumption increases [30]. Pischinger et al. conducted experimental investigations on a CI engine equipped with ethanol and diesel dual-fuel direct injection systems. It was found that the maximum pressure increase rate was related to ethanol fuel injection timing and engine speed. The proper ethanol injection timing and quantity (40%-65% and 8-12 CAD BTDC in the study) improved the engine performance, decreased the fuel consumption, and reduced the CO emission. It was also found that the use of ethanol remarkably decreased soot formation and NO_x exhaust. The diesel engine could operate in a relatively higher compression ratio (18-20) and mechanics load to gain the same engine performance if ethanol fuel was used [31] [32]. As the dual-fuel direct injection CI engine requires an extra high-pressure fuel injection system and major changes of the cylinder head, this method was considered uneconomic and consequently these kinds of engines have seldom been commercially used.

Injecting ethanol fuel into the manifold is another way of using ethanol fuel in the CI engine. This method does not require major changes to the engine structure, and the additional cost of the port ethanol fuel injection system is low. Therefore, it has been more widely studied. Small-scale commercialisation has been carried out in some countries, for example, China and Belgium [31]. In the ethanol fuel port injection diesel engine, the heat of the fresh charge, manifold, cylinder head and inlet valve can be utilised for ethanol evaporating, thus the ethanol fuel can be well vaporised before it enters the combustion chamber. Volumetric efficiency is therefore increased and negative impact of ethanol's great latent heat of vaporisation (which can

significantly decrease the in-cylinder mixture temperature and lead to problems of self-ignition) no longer exists. Thermal efficiency is also increased [32].

The study of the ethanol fuel port injection diesel engine can be traced back to the 1980s. Shi et al. [33] and Cui et al. [34] conducted an investigation into the CI engines equipped with the ethanol fuel port injection system. It was found that by using ethanol fuel port injection, engine thermal efficiency substantially increased by up to 4.7%. CO and HC emissions increased with increases in the ethanol/diesel percentage, smoke and soot emissions decreased with increases in the ethanol/diesel percentage. Lu et al. [35] and Abu et al. [36] found that the ethanol fuel port injection could largely reduce NO_x and soot emissions due to the ethanol oxygen containing properties. Fuel consumption and engine thermal efficiency were partially improved in certain engine conditions. Pidol et al. [37] and Yao et al. [38] investigated the engine performance in an ethanol fuel port injection diesel engine. The experiments indicated that the use of port ethanol fuel injection could leverage diesel fuel usage and conserve its consumption. In some ideal conditions, up to 30% diesel fuel can be saved by using ethanol fuel port injection .

Previous research on the ethanol fuel port injection diesel engine was mainly focused on using ethanol fuel to reduce fossil oil consumption and improve CI engine efficiency. Recently, with the development of combustion technology, more attention is focused on using port injected ethanol fuel as a mixture property regulator to real-time adjust the mixture's chemical and physical properties in order to realize high efficiency combustion, for example, homogeneous charge compression ignition (HCCI). The ethanol fuel port injection system can provide homogeneous ethanol/air mixture, as well as real-time control in terms of the ethanol/diesel blending ratio. These can offer more feasibility in relation to adjusting the mixture's physicochemical properties and thereby improving the HCCI combustion. It was found that ethanol fuel port injection in the diesel engine showed strong potential towards achieving low temperature homogeneous combustion (HCCI), extending the operating range and reducing NO_x and smoke emissions. The engine maximum power output was also found to increase when implementing this dual-injection method [39] [40]. The ethanol's high latent heat of

vaporisation and great octane rating were deemed to contribute to the extension of the HCCI window in the port ethanol fuel injection diesel engine. The presence of oxygen compounds and the low ratio of soot precursors (aromatics) in ethanol fuel were considered to be the reasons for low levels of smoke [41] [42].

Generally, ethanol's high self-ignition temperature and low lower heating value pose negative effects on conventional CI engines and necessitate sufficient engine modifications in order to ensure mixture preparation and continuous combustion. Moreover, ethanol's properties are not well utilised in CI engines. Thus, it is not an ideal alternative fuel for replacing diesel.

1.3 Application of ethanol fuel to SI engines

From the beginning of the 21st century, large scale commercial use of ethanol as a fuel has commenced [43]. Currently, there are three ways of using ethanol fuel in SI engines: ethanol/gasoline blends, pure ethanol engine and gasoline/ethanol dual-fuel port injection.

1.3.1 Pure ethanol engine and gasoline/ethanol dual port injection

Pure ethanol fuel is only used in areas rich in ethanol production resources, such as Brazil, or countries like, Belgium and Sweden [44]. Up to 2011, there were about one million pure ethanol vehicles in the world, which only accounted for a tiny fraction of the world's total automobiles [45].

The merit of the pure ethanol engine is that it can fully take the advantages of ethanol fuel via the modification of engine structure and parameters such as, combustion chamber geometry, manifold, fuel delivery system, compression ratio, boost pressure, and spark advance. Ethanol can substantially enhance engine anti-knock ability, allowing the use of higher compression ratio, boost pressure and more optimum spark advance. It was found that when a direct injection

spark ignition (DISI) engine was fuelled with pure ethanol, the engine compression ratio (when spark timing was kept at the maximum brake torque (MBT) timing of most heavy load conditions or even full load conditions) had the potential to be increased by up to 5 units [46] [47]. The subsequent engine power output was increased by 35% or more [48] [49]. Furthermore, the pure ethanol engine could largely reduce engine emissions. It was found that when using pure ethanol, the reduction in NO_x emissions were up to 20%. HC and CO emissions were reduced by 30% [50] [51]. Although the engine efficiency could be increased in the pure ethanol engine, the ethanol's low heating value is only about 60% of gasoline (Table 1.1), which inevitably leads to an increase in vehicle fuel consumption. Thus, the pure ethanol vehicle is currently used only in areas with rich ethanol production resources and it is uneconomic to implement in other areas of the world [52] [53].

The gasoline/ethanol dual port injection method has seldom been reported. The advantage of this method is that it can flexibly adjust the ethanol/gasoline fuel ratio at any time depending on the engine operating conditions and fuel availability. As reported in [54] and [55], the dual port injection method can increase the engine power output and efficiency by up to 6.8% and 3.2%, respectively and decrease the NO_x emissions by about 20%. In addition, with a separate ethanol fuel delivery system, the engine can use fusel oil which is not solute with gasoline. The use of fusel oil can reduce the expenses on the fuel, because the fusel oil is about 30% cheaper than pure ethanol [54]. However, due to the additional cost and low merits of the injection fuel supply system, the gasoline/ethanol dual port injection vehicles quickly disappear in the market [56].

1.3.2 Ethanol/gasoline blends

Ethanol/gasoline blends are the most widely used method to apply ethanol to SI engines. Due to ethanol and gasoline's physical and chemical properties, these two kinds of fuel can be blended at any ratio without worrying about the solubility problem [57]. Currently, the ethanol/gasoline blended fuel sold on the market is normally mixed with 10%~20% of ethanol. These kinds of

ethanol/gasoline blends can be used directly in the current SI engine without modification. In some countries, like the United States, Australia and parts of UE countries, high ethanol/gasoline ratio blends such as E50 (contains 50% ethanol) and E85 (contains 85% ethanol) are also commercially available. However, they can only be used in the fuel flexible vehicle (FFV) which is specially designed to suite different ethanol/gasoline blends.

The use of ethanol/gasoline blends has a positive impact on fuel physicochemical properties, engine combustion and emissions. When ethanol is added to gasoline, the vapor pressure of the mixture is greater than the vapor pressure of gasoline or even ethanol alone. This is because the molecules of ethanol are strongly hydrogen-bonded, but with small amounts of ethanol in a non-polar material for example gasoline, the hydrogen bonding is much less extensive and the ethanol molecules behave in a manner more in keeping with their low molecular weight [17] [57]. Thus the ethanol/gasoline blends become more volatile and the mixture formation process is improved, resulting in more complete combustion and improved engine performance.

The engine combustion process can also be optimised by adding ethanol fuel. The mixture chemical reaction rate and flame propagation speed of ethanol are higher than gasoline. Its combustion duration is shorter than gasoline. These can contribute to short ignition delay, increased maximum cylinder pressure and more intensified heat release. Therefore, at the same energy input level (lower heating value), the power output of the ethanol/gasoline blend fueled engine is normally higher than the gasoline fueled only engine [58] [59].

Adding ethanol into gasoline can increase the fuel's octane number. Normally, the initial octane number increase for the first 10% of ethanol (volumetric based) added is greater than each subsequent 10% increase [60]. Thus, adding small amount of ethanol, such as 10% or 20%, into gasoline can lead to obvious increments in the octane number. Adding ethanol into gasoline also increases the heat required by blended fuel's evaporation due to ethanol's greater latent heat of vaporisation. Charge temperature can then be further reduced. The engine anti-knock ability is therefore enhanced. Thus, engine full/heavy load performance is improved and thermal

efficiency is increased [59].

Generally, fueling the SI engine with the ethanol/gasoline blend can increase the SI engine thermal efficiency, because of the improvements in the fuel volatility, octane number and combustion [61] [62].

Using ethanol/gasoline blends can reduce engine-out emissions. It is generally reported that HC and CO emissions decreased with the increase of the ethanol/gasoline percentage in medium and high load engine conditions. About 33% of CO and HC emissions were reduced when 65% ethanol/gasoline was used [63] [64]. However, it is reported that in full load and light load conditions, HC and CO emissions increased with the increase of ethanol usage when the ethanol/gasoline ratio was above 80%. The increase of HC and CO emissions in full load conditions was caused by deterioration of combustion, possibly due to the poor mixture homogeneous quality. The increase of HC and CO emissions in light load conditions was attributed to the great charge cooling effect of ethanol evaporation, which may significantly decrease the in-cylinder temperature [65] [66]. NO_x emissions were generally decreased with the increase of the ethanol/gasoline ratio [65] [63]. However, in some of the tests, NO_x emissions were found to increase when ethanol was used in medium and heavy engine load conditions [64].

Although ethanol/gasoline blends have been widely used in many countries, and have shown the potential in decreasing engine emissions whilst moderately increasing engine performance, they still have many disadvantages which are mainly caused by the fixed ethanol/gasoline ratio.

1.3.3 Existing problem of using ethanol fuel in SI engine

When an original gasoline SI engine is fuelled with ethanol/gasoline blends, the engine may suffer a decrease in the engine power output if the fuel delivery system is not modified correspondingly. This is mainly because of the low energy content of ethanol fuel (about 60% of

gasoline). Other factors that may contribute to a power decrease include the high viscosity of ethanol fuel and high latent heat of vaporisation. The viscosity of the ethanol is about three times larger than gasoline. When the engine is operated in high load conditions at which a large amount of fuel delivery is required, the fuel flow rate is high. High fuel flow rate and high fuel viscosity will lead to high flow resistance and consequently the fuel delivery in every cycle will decrease [67]. The latent heat of vaporisation of ethanol is greater than gasoline. When the engine is operated at high load and high speed, the time for ethanol fuel vaporisation may not be sufficient to ensure that such an amount of fuel completely vaporises, and this can lead to deterioration of the mixture combustion [68].

Cold startability is another problem when the SI engine is fuelled with pure ethanol fuel or ethanol/gasoline blends. Cold startability is highly dependent on the fuel's ability to vaporise effectively at low temperatures and provide an ignitable mixture at the time of ignition. Although, the ethanol fuel's volatility is greater than gasoline, its high heat of vaporisation requires more heat than pure gasoline to vaporise [69]. This characteristic is favourable in relation to enhancing the engine anti-knock properties in warm engine conditions. But in cold start, it may cause problems. When an engine is cold and the ambient temperature is low, a large portion of the fuel may form a liquid film in the inner of the inlet manifold or combustion chamber. It is the lack of enough heat for vaporisation that gives rise to the film and difficulties in ignition which in turn leads to engine start problems and an unstable cold operation. The modern DI engine with the later start of injection timing can create a higher in-cylinder temperature for ethanol or ethanol blends vaporisation when the ambient temperature is low, because the compression of the fresh charge rises the mixture temperature. However, the testing results on DI engines indicated that the improvement was not significant [70]. In the port injection or carbureted engine, the difficulties in cold start become more obvious because the temperature for fuel vaporisation in cold start is close to the ambient temperature. Therefore, the cold start is an important issue in terms of the use of ethanol as a fuel.

The use of ethanol also poses durability problems to the engine components. The investigation

on the metal to metal wear difference due to the impact of using alcohol and alcohol blends showed that the ethanol or ethanol blends offer less lubrication to metal parts. Potential wear engine may happen because of the ethanol washing away of lubrication film [71].

In the port injection engine, it was reported that the intake system deposits were more prevalent with fuels containing alcohol and the deposits on intake valve were referenced as the area of most concern due to the intake valve and seat area presenting the flow restriction point in the intake tract of modern engines [72].

Corrosion in metallic fuel system components is another problem in terms of the use of ethanol fuel. For most modern engines, the materials in fuel systems are normally upgraded in order to be suitable for up to 10% ethanol gasoline fuel blends [73]. However, corrosion problems may also happen when the phase separation occurs because the ethanol-water phase tends to be more corrosive than the ethanol/gasoline blend. Indeed, it can even cause damage to the steel, zinc, diecastings and aluminum components of the fuel system [74].

The use of ethanol also increases gum and deposit formation in the fuel system. The ethanol in gasoline fuel can increase the solubility of gasoline fuel deposits leading to the release of gum bound debris followed by blockage of filters and fuel metering components. Gum formation during equipment storage is also a particular concern particularly for equipment that does not get used on a regular basis [75] [76].

Another issue that may seriously impede the wide usage of ethanol fuel is production. The current way of producing ethanol is mainly from a range of agricultural crops, such as wheat, corn, sugar and the byproducts of corn production. Large scale ethanol production may pose challenges to availability and the price of food supply [77]. This has already been realised by the Chinese when at the beginning of the 21st century, the Chinese government launched large scale ethanol fuel application projects in its three major grain production provinces. After three years, the government found that the ethanol fuel projects seriously impacted the food supply.

Ethanol fuel's price also soared due to the lack of material for production. As stable food prices and supply are vital for a country like China with its huge population, the ethanol fuel application projects were suspended. Similar problems also happened in Mexico where the large use of ethanol fuel increased the grain food price and led to protests [78]. In addition to the influence on food availability, the ethanol fuel price is another problem. The current way of producing ethanol fuel requires about 3~4 tons of grain to produce 1 ton of ethanol, and lots of energy is also required [77]. These hinder the potential reductions in the ethanol fuel price and also influence its acceptance by the public. Although the production of cellulosic ethanol and algal ethanol hold the promise of dramatically increasing ethanol production and reducing the impact on food supply and land use, they have not yet reached a large commercial scale [79].

From the above, it can be seen that the current ways of using ethanol, either pure ethanol fuel or ethanol pre-blended with other fuels, have not fully exploited the advantages of ethanol fuel. Problems have also arisen because the engine components, such as fuel delivery system, combustion system and ignition system are not well optimised to adapt to the characteristics of ethanol fuel. Therefore, in order to optimise ethanol fuel performance in conventional SI engines, modifications to the engine components are required.

Chapter Two

2. Review of direct injection plus port injection SI engines

2.1 Introduction

The current ways of using ethanol as a pure gasoline substitute in SI engines pose many challenges, as some good properties of ethanol are not well utilised and they can cause many problems. Facing increasingly severe environmental and energy issues, ethanol's renewable and environmental friendly features have regained attention, as many countries, for example the USA, China, Australia and the EU have implemented ethanol fuel promotion plans. In this context, optimising the ethanol fuel usage in the conventional SI engine becomes imperative. The low productive efficiency of current methods of producing ethanol also adds incentives to this motivation. Therefore, finding an efficient and effective way of using ethanol fuel, which can overcome the current shortcomings, fully exploit ethanol's advantages, and possibly use a relatively small amount of ethanol to leverage engine performance and reduce emissions, is becoming an urgent task for the automobile sector.

In order to meet the requirements of effectively using ethanol and trying to develop a high efficiency, clean and downsized SI engine which performs like a full-size one but offers the fuel efficiency approaching that of a hybrid electric car, the dual-injection, ethanol boosted gasoline engine was proposed in 2005 [80]. In this engine, the ethanol fuel was directly injected into the combustion chamber through a fuel delivery system which was separate from the port injected gasoline fuel system. The ethanol was used for knock constraint. The fraction of ethanol fuel was varied according to the need for knock suppression. It was zero at low torque where knock suppression was not needed and it could reach a high ratio when maximum knock suppression was required at high torque [81]. According to numerical simulations, this method could result in up to 38% of ethanol consumption reduction and save up to 30% gasoline usage for the same engine power output relative to the conventional SI engine fueled with E10. The time interval

for topping up the small ethanol fuel tank could be extended up to three months [82].

In this dual-fuel injection method, the ethanol fuel is not simply used as a substitution of gasoline but as a knock suppressor to be effectively applied in the conditions where knock occurs. The ethanol consumption can therefore be largely reduced and the energy efficiency is greatly increased. Ethanol has been efficiently used. Moreover, the ethanol's properties of great latent heat of vaporisation and high temperature self-ignition are fully exploited in this technical approach and their negative impact on engine cold start is completely removed because the gasoline port injection system can provide a more readily ignitable mixture during the cold start. The ethanol fuel delivery system is specially designed to meet the requirements for high ethanol flow rate at high engine speeds and loads. Corrosion on the ethanol fuel system can be solved by using specially designed fluoroelastomers material and coated material components with anti-corrosion film. (These materials have already been developed and commercialised by several major automobile parts providers.) Engine wear could also be alleviated due to less ethanol being used in the real engine operation.

Apart from the aforementioned merits, through review of previous studies on using ethanol fuel and dual-injection, the ethanol direct injection plus gasoline port injection (EDI+GPI) method may also have the potential to benefit engine performance in the following aspects detailed below.

2.2 Potential impact of EDI+GPI on engine performance

2.2.1 Inlet air flow and mixture quality

As shown in Table 1.1, ethanol's high latent heat of vaporisation is about three times that of gasoline. Higher heat of vaporisation means that more heat is needed for fuel vaporising. In the EDI+GPI engine, the early injection (before the close of the inlet valve) of ethanol cools the charge at an early time, which decreases the charge temperature, increases the mixture density and subsequently improves the volumetric efficiency. Additionally, with EDI, the mass of port injected gasoline decreases. This decreased mass of gasoline fuel reduces the gasoline fuel

partial pressure and increases the partial pressure of fresh air. This also contributes to the increase of volumetric efficiency. When the volumetric efficiency increases, the mass of air per engine cycle increases, which allows more fuel to be burned and results in more work being done per cycle and a greater amount of power being produced by the engine [46].

The intake-port efficiency in DISI engines can also be improved by the dual-injection method. DISI engines have the disadvantage of forming a homogeneous air/fuel mixture, which consequently leads to the need to refine engine performance. The less homogeneous air/fuel mixture formed in DISI engines is mainly because of the lack of time from the point where fuel is injected to ignition. This causes in-cylinder mixture stratification. Owing to this, the combustion efficiency and stability are negatively affected at high load and low engine speed due to weak in-cylinder air-motion. In order to overcome these combustion deteriorations, some devices such as the tumble intake-port, helical intake-port, swirl control valve (SCV) and so on, have been implemented in conventional DISI engines to enhance in-cylinder air-motion for the purposes of forming a homogeneous mixture. However, the introduction of these devices decreases the intake-port flow efficiency compared to that of a port injection engine. There is a trade-off between the flow coefficient and tumble intensity (See Figure 2.1). Therefore, the DISI engines suffer low intake-port efficiency and consequent power losses at high load and low speed conditions. The use of the port fuel injection system in the DISI engine provides a novel solution to overcome this drawback. The port injector together with the direct injection injector can reduce the requirement for high tumble intensity whilst producing a more homogeneous air/fuel mixture which when compared to a conventional DISI engine [83] improves combustion, reduces fuel consumption and decreases unburned emissions.

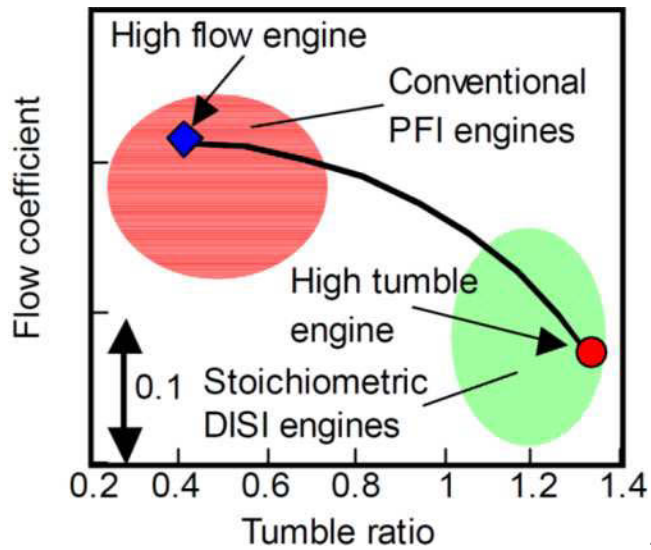


Figure 2.1–Tumble intensity vs.flow coefficient [83]

2.2.2 In-cylinder temperature and knock tendency

In a SI engine, the phenomenon of knock is a major obstacle that prevents further increase in engine efficiency. Knock is an abnormal combustion phenomenon. In a SI engine, when the mixture is ignited by spark, combustion occurs and the flame front subsequently propagates outwards and consumes the unburned mixture on the outside of the flame (called “end gas”), and this in turn releases heat and increases the mixture (burned and unburned) pressure. As the end gas pressure and temperature rises due to the compression caused by this process, auto-ignition of the fuel may occur in certain spots, creating pressure oscillation which can potentially result in significant hardware damage to the engine [84] [85]. The knock can be caused by advancing spark timing, increasing the compression ratio and raising the inlet air pressure through turbocharge or supercharge. These three factors are also the major technical approaches to increase SI engines power output and efficiency. Therefore, knock is the most severe obstacle to further improvements in engine efficiency.

The occurrence of engine knock is usually related to the unburned mixture temperature and pressure and available time (dependent on fuel chemistry and the octane number). Therefore, decreasing the charge temperature and increasing the fuel chemistry (octane number) are effective ways to suppress knock. Ethanol has excellent anti-knock qualities as indicated by its

111 octane number. In addition to the chemical benefit in preventing knock, which can be realised in both DI and port fuel injection (PFI) engines, ethanol has a significant synergy with DI that has a strong cooling effect due to fuel evaporation (854 ~ 904 kJ/Kg). This effect in addition to the chemical anti-knock effect may effectively suppress knock and permit the engine to work at more advanced spark timing, higher compression and greater inlet air pressure.

Investigation to charge the cooling effect has shown that the charge cooling effect of DI gasoline can merely increase the effective octane for about 5 units (equivalent to an increase in the fuel octane number by 5 units). In contrast, the charge cooling effect of DI pure ethanol can increase the effective octane number by about 18 units. This increase in the effective octane number is mainly due to ethanol vaporisation which reduces the in-cylinder temperature to about 40 K, and ethanol's low adiabatic flame temperature [86] [87]. Other investigations have shown that when using high ethanol/gasoline content blends, such as E85 or pure ethanol in the DISI engine, the engine knock can be sufficiently suppressed due to the charge cooling and ethanol's high octane number. The engine compression ratio can also be increased by 2-4 units and the indicated thermal efficiency improvement is up to 5% [88].

In PFI engines, the merits of ethanol in knock mitigation are not well utilised because the ethanol is completely vaporised before it enters the combustion chamber and the fuel vaporisation is mainly by absorbing heat from the fresh air, manifold and the back of intake valve. The merits of ethanol in in-cylinder temperature reduction and knock mitigation are also not well utilised by low ethanol/gasoline blends. Investigation has shown that when the ethanol/gasoline ratio is increased from 0 to 20%, the effective octane number of the ethanol/gasoline blends increases more quickly in this range than that in the range from 20% to 100%. However, the final charge cooling effect of low ethanol/gasoline blends cannot be compared to that of high ethanol/gasoline blends or pure ethanol [60] [86]. Therefore, using ethanol DI is the most effective way to exploit ethanol's advantages in in-cylinder temperature reduction and knock mitigation.

2.2.3 Mixture preparation

For EDI+GPI engines, SOI timing directly affects the heat transfer and mixture temperature. Earlier fuel injection cools the gas at an earlier time and results in increased volumetric efficiency but it can also increase the heat transfer from the wall to the gases. Thus, the cooling effect on the final charge temperature is compromised. For late injection, the cooling effect due to fuel evaporation can be well preserved, which leads to a lower knocking tendency, but the mixture's homogeneous quality may be negatively affected and the combustion may deteriorate [89] [90].

In DI engines, the vaporisation of fuel plays a critical role due to the short time interval between SOI and ignition. The SOI timing should be carefully adjusted in order to ensure the fuel is completely vaporised. The distillation characteristics feature the vaporisation capability of a fuel. Figure 2.2 shows the distillation characteristics of ethanol/gasoline blends. It can be seen that the ethanol fuel boils at relatively lower temperature than gasoline. This is mainly due to the single alcohol component of ethanol which has a defined boiling point of 77°C (350 K). On the other hand, due to the content of heavy fuel fraction, the boiling points for complete evaporation of gasoline are normally up to 204°C (477 K) [91].

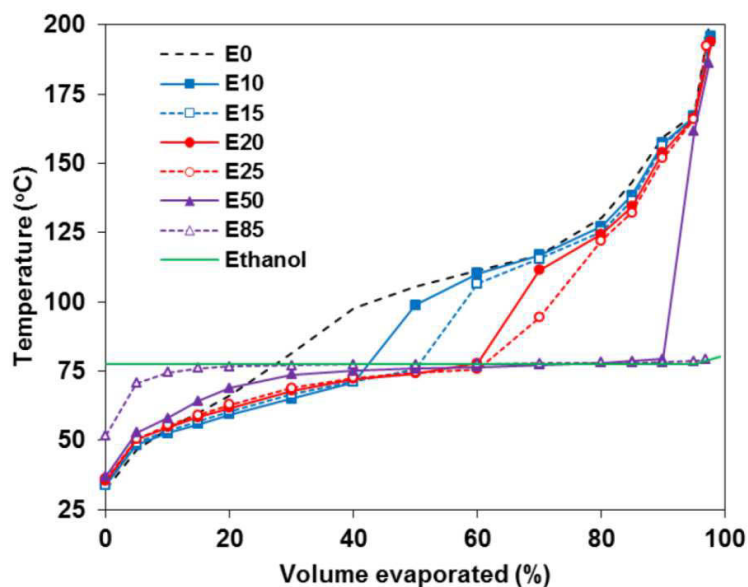


Figure 2.2–Distillation characteristics of ethanol blends [91]

The variation of the vaporisation characteristics of ethanol and gasoline with temperature, as shown in Figure 2.3, further confirms that ethanol is vaporised more quickly compared to gasoline in the ambient temperature of higher than 410 K. From the calculation of bulk gas temperature from the unfired in-cylinder mixture, the 410 K is a temperature that can be easily reached by modern engines during the compression process [92]. Thus, the volatility of ethanol is greater than that of gasoline.

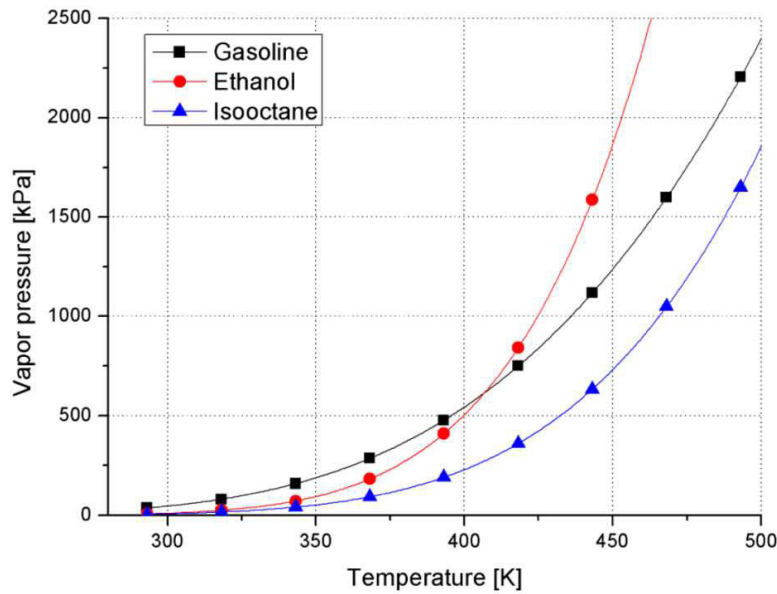


Figure 2.3–Vaporisation curve for ethanol, gasoline and Isooctane [92]

Because of ethanol’s high volatility, a homogeneous mixture can easily be formed in a short time period when injecting ethanol fuel. Thus, the SOI timing can be retarded to enhance the charge cooling effect. In stratified combustion, ignitable fuel mixture can be quickly formed adjacent to the spark plug and this may improve the combustion stability and ultimately increase engine efficiency [92][93][94]. However, it should be noted that although ethanol’s volatility is higher than that of gasoline, its great latent heat of vaporisation may play a negative role in affecting fuel vaporisation due to its reduction on the in-cylinder temperature. The low in-cylinder temperature caused by ethanol vaporisation sometimes may bring down the in-cylinder temperature to lower than 410 K which is a critical temperature in affecting ethanol vaporisation [95] [96]. Thus, the real effect of DI ethanol on mixture quality may depend on different engine operation conditions, and the in-cylinder temperature is a key factor that affects

the homogeneous quality of ethanol/air mixture.

2.2.4 Combustion process

Ethanol's high laminar flame velocity, high volatility, low adiabatic flame temperature and oxygen content properties can contribute to improving the combustion process. Ethanol has a faster laminar flame speed than gasoline does, 39cm/s compared to 33cm/s (measured at 393 K [95]). This 18% increment in laminar flame speed contributes to the short combustion duration which may reduce heat losses, release heat more intensively and advance the combustion phasing [97] [98]. The volatility of ethanol is higher than gasoline. High volatility of ethanol improves the mixture preparation by producing a more homogeneous mixture especially in the DISI engine. The improved mixture quality accelerates the combustion speed, reduces diffusion burning and results in more complete combustion. The ethanol flame adiabatic temperature is about 100 K lower than that of gasoline. This reduction in the adiabatic flame temperature coupled with ethanol's higher laminar flame speed may effectively reduce the auto-ignition of unburned gas and permits the engine to achieve high efficiency [99] [100]. The ethanol is an oxygenated fuel which contains about 34.7% oxygen in its total weight. Compared with combusting gasoline, the combusting ethanol can provide more readily available oxygen for the oxidation process and this results in a more complete combustion and reduces unburned combustion products [65] [66].

2.2.5 Lean burn

Lean burn technology has great potential in simultaneously increasing engine efficiency and reducing emissions [101] [102]. When mixture is leaned, the pumping losses, heat losses and endothermic dissociation losses are reduced. Engine thermal efficiency can therefore benefit from these improvements [102] [103]. Operating with excess oxygen can shift the combustion reaction closer to completion, thus releasing more energy per mole of fuel and adding to the increase of thermal efficiency [103] [104]. Additionally, the mixture's ratio of specific heats

increases with the increase of AFR. Theoretically this increase in the mixture's ratio of specific heats can lead to raises in engine thermal efficiency [104]. The emissions in lean combustion are different from their stoichiometrically fuelled counterparts. HC and CO emissions usually decrease by complete combustion. However, as the lean burn limit approaches misfires, combustion becomes unstable and the production of HC and CO emissions begins to increase [105] [106]. NO_x emissions normally reach a maximum in slightly lean conditions ($1.05 \cong \lambda \cong 1.1$). Further increases in the lean burn limit above this range can bring down the NO_x due to the low peak-cylinder temperature. In lean conditions, the three-way catalyst is no longer able to convert NO_x with high efficiencies. Consequently, the NO_x emissions should be low enough to offset this disadvantage (less than 100ppm is regarded as optimum) [107] [108].

Lean burn can be generally divided into two categories: homogeneous lean burn and stratified combustion. Ethanol has been studied and proven that it could improve homogeneous lean burn stability and extend the limit due to its wider flammability limit (lambda of 0.4~1.7 in ethanol compared to lambda of 0.5~1.3 in gasoline), higher laminar flame speed (39 cm/s compares to 33 cm/s of gasoline) and stable in low temperature combustion. It was found that by adding a small amount of ethanol fuel such as 10% into gasoline, the laminar flame speed of the blend did not decrease until it reached a lambda (λ) value of 1.2. However, for pure gasoline the laminar flame speed started to decrease when the λ was just over 1.1 [109] [110]. It was found from the investigation to PFI engines that that using ethanol/gasoline blends can largely extend lean burn limit as opposed to using pure gasoline. As found by Wu et al. and Alexandrian et al., the maximum lean burn limit in pure gasoline conditions was 1.2. This value can be extended to 1.48 when using ethanol/gasoline blends. It was also found that light engine load and low engine speed were more suitable for lean burn, as the lean burn limit in these conditions was higher than that in heavy load and high speed conditions [111] [112]. The combustion stability represented by the coefficient of variation of IMEP (COV_{IMEP}) was reduced when the ethanol/gasoline blends were used. Generally, about 20% improvement in COV_{IMEP} was achieved and the improvement increased with the increase of the ethanol/gasoline ratio [113] [114].

The advent of DI technology has made lean burn possible in stratified combustion in SI engines by creating a very rich local mixture around the spark plug late in the compression stroke whilst maintaining a very lean global AFR ($\lambda \gg 1$) [115]. The engine load in this method is controlled by the fuel quantity and SOI timing. The latest stratified lean combustion engine has realised a stable operation at AFR $\approx 40:1$ which is far more than the homogenous lean burn limit of AFR $\approx 18:1$ [116]. Nevertheless, stratified combustion is not easy to achieve. In order to ensure stable combustion, it requires careful optimisation of the end of injection timing relative to spark timing, where a small variation can lead to misfires [117]. The late injection with stratification also leads to significant fuel impingement on the piston crown. If the fuel is not well vaporised prior to the onset of discharge, the engine combustion will be negatively affected and lean burn limit will be reduced. For ethanol, its volatility is higher than gasoline when the ambient temperature is over 410 K [92]. This may help to reduce the time for fuel evaporation and produce a homogeneous mixture in lean conditions. However, as the latent heat of vaporisation of ethanol is about three times that of gasoline (Table 1.1), the stronger charge cooling effect of ethanol vaporisation may substantially reduce the in-cylinder mixture temperature which is regarded as an important parameter in influencing the lean burn stability and limit [118] [119]. Normally, the unburned mixture temperature below 1000 K is regarded as leading to a significant reduction in lean mixture burning velocity and this can cause unstable combustion [120]. Thus the stratified combustion may be negatively affected by the ethanol fuel, especially when the DI ethanol amount is great enough to substantially bring down the unburned mixture temperature. EDI+GPI engine, on the other hand, has the potential to avoid this disadvantage of ethanol in stratified combustion. In the EDI+GPI mode, the EDI amount can be reduced and adjusted to a level that will not significantly bring down the unburned mixture temperature, and this will still maintain the quick formation of enough locally rich mixture adjacent to the spark plug. The engine total energy input will not be affected by the reduced EDI amount during this process, because the GPI can be adjusted to maintain the total energy flow rate. Thus the lean burn operation load window will not be affected by the reduced DI amount. Moreover, the homogeneous mixture provided by GPI may further improve the

flame propagation in stratified combustion and offset the influence of inhomogeneous mixture formation caused by DI [121] [122]. Therefore, the EDI+GPI engine has the potential to improve the stratified combustion.

2.2.6 Pollutant emissions

The potential of ethanol in reducing SI engine emissions has been investigated by many previous scholars. Subramanian et al. [123], Sementa et al. [124] and Delgado et al. [125] tested different ethanol/gasoline blends in different types of SI engines (including PFI, SIDI and the small SI engine*). It was reported that by adding ethanol into gasoline, emissions of HC, CO and NO_x were effectively reduced by up to 33%. CO₂ emissions also decreased. The wide flammability and oxygenated characteristics of ethanol were regarded to contribute towards HC, CO and CO₂ emissions' reduction. The charge cooling effect and low adiabatic flame temperature of ethanol were considered to be the factors leading to the decrease of NO_x emissions.

In contrast with those studies, more recent research found that increasing ethanol concentration in ethanol/gasoline blends does not always show a positive effect on pollutant emissions. Wallner et al. [126] and Tanaka et al. [127] tested ethanol/gasoline blends in a DISI engine. It was reported that at high engine loads, CO and HC emissions decreased with the increase of ethanol concentration. However, at light engine loads, high ethanol concentration led to an increase in HC and CO emissions. Ethanol/gasoline ratio of 30% was the best ratio for HC and CO emission reduction at all engine speeds and loads. Martínez et al. [128] and Li et al. [129] tested the high percentage ethanol/gasoline blends in PFI engines. They found that high percentage ethanol/gasoline blends (over 60%) led to an increase in HC emissions at light and medium engine load. 20% of ethanol/gasoline blend demonstrated the best effect on reducing HC and CO emissions at light engine load. Similarly, Celik et al. [130] and Bresenham et al. [131] found that when the ethanol concentration was over 50%, the HC emissions from the small SI engine began to increase in full load engine conditions. NO_x emissions increased when

low ethanol/gasoline blends, such as 10% and 20%, were used in medium and high load conditions. The report from Orbital found that in high engine load conditions and in both PFI and DISI engines, the NO_x emissions increased when the concentrate of ethanol/gasoline blends was less than 20%. Further increasing the ethanol percentage above 20% led to a decrease in NO_x emissions [132]. Thus, for different engine loads and speeds, different ethanol/gasoline blending ratios may be required to achieve the best effect on emissions reduction. To realise the real-time adjustment of the ethanol/gasoline blending ratio, the dual-fuel injection technology is an appropriate choice.

*Small engine refers to those engines with displacements in the range of 20cm³ to 225cm³

2.3 Research up to date

Currently, the research on the dual-injection engine is incomprehensive. Most papers published have focused on the effect of dual-fuel injection on knock mitigation, or the engine performance and emissions of a dual-injection engine fueled with different fuels such as ethanol, methanol, and 2,5-dimethylfuran. The effects of engine control parameters, for example the DI/PFI ratio, spark timing, SOI timing and AFR on engine performance, combustion characteristics and emissions were seldom reported in these papers.

The potential of dual-fuel injection was first assessed by Cohen et al. with the original idea to build a half-size, high compression ratio gasoline engine which used ethanol direct injection (hydrous and anhydrous) to boost PFI engine performance [82]. As they proposed, ethanol was directly injected into the cylinders (and the gasoline injection was simultaneously reduced) only when necessary to suppress 'knock' e.g. when there was significant acceleration and great engine load. The direct ethanol injection could raise the already high octane rating of ethanol up to an effective 130 [80]. A self-developed numerical simulation code (Chemkin) was used to assess the knock suppressing effect when directly injecting ethanol at different manifold pressures, compression ratios and speeds. The results indicated that the cooling effect due to ethanol's high latent heat of vaporisation in suppressing knock was more significant than that which was due to ethanol's high octane number. Later injection of ethanol after inlet valve

closure and stratified injection could enhance this effect rather than injecting ethanol before the inlet valve closed. The enhanced knock resistance could be used to increase the manifold pressure by more than a factor of two [81]. Compression ratio could also be substantially increased by about 2-4 units. Thus high engine torque, power output and efficiency would be possible. The engines could be potentially downsized by a factor of two and the fuel efficiency could thereby be increased by approximately 30%. The leveraging effect of increasing the efficiency of gasoline usage could substantially enhance the energy value of ethanol. The amount of ethanol that was required would be less than 1 gallon for every 20 gallons of gasoline [133]. Other alcohols, like methanol and methanol with 50% cosolvent, were also assessed by Cohen et al. in their later works. They found that DI methanol allows more than a 30% increase in knock free turbocharging pressure at a given compression ratio, as compared to DI ethanol. Thus, this increased the turbocharging pressure allowed for a possible downsizing by a factor of 3-3.5 [134].

Following the work of Cohen et al., Stein et al. [135] and Daniel et al. [136], the knock mitigation effect of dual-fuel injection was tested experimentally. Stein et al. conducted the test on a 3.5 L “EcoBoost” gasoline turbocharged direct injection engine equipped with PFI for gasoline and DI for E85. The gasoline PFI was used for providing main combustion fuel and the amount of directly injected E85 was used only in the conditions that were required to prevent knock. The experimental results showed that DI E85 demonstrated great potential in increasing the engine’s anti-knock ability. By applying DI E85, the engine could be kept working at MBT timing even at BMEP of 21 Bar. Nevertheless, in DI gasoline conditions, the spark timing had to be progressively retarded to avoid knocking when BMEP was above 7.0 Bar. It also showed that through the synergetic use of spark retard and a different E85/gasoline ratio, a minimum combined BSFC and best thermal efficiency point could be found. It was suggested that in optimal conditions, normally in heavy load or full load conditions, the E85 DI plus gasoline PFI engine could use 0.5 gallon of E85 to yield the same power output that was equivalent to using 2.5 gallons of gasoline in baseline gasoline PFI engine. Thus, 0.5 gallons of E85 can replace 2.5 gallons of gasoline, which is a leveraging of 5:1 ($2.5/0.5$). This result verified Cohen’s

estimation that the leveraging effect of using DI ethanol could reduce the gasoline fuel consumption in the PFI engine [135]. Daniel et al. compared the effects of ethanol and methanol direct injection on knock suppression and emissions reduction in a single cylinder research engine. The engine speed was fixed at 1500rpm and the DI pressure and SOI timing were set at 150 Bar and 280 CAD BTDC, respectively. The results indicated that the high latent heat of vaporisation of ethanol and methanol dramatically mitigated the knock tendency which was found in PFI conditions. The decrease of combustion duration and emissions of HC, CO and CO₂ were also found at almost all engine loads when the engine was at dual-fuel injection mode [136].

The potential of dual-fuel injection for improving engine performance was also assessed by Ikoma et al. [137] and Wurms et al. [138]. Ikoma et al. conducted the experiments on a 3.5 L V6 2GR-FSE engine with the purpose of improving engine full load performance. In their tests, it was found that the dual-injection method could reduce the dependence of the high tumble ratio on forming a homogeneous mixture at high engine speed and therefore improving the volumetric efficiency and consequent engine performance. There was an optimal gasoline PFI/DI ratio which existed for every load at which the engine torque output and fuel consumption could best be achieved. A balance point between HC emissions and torque fluctuations during idling condition could also be found by adjusting the gasoline PFI/DI ratio. Finally, after the optimisation of engine parameters with the dual-injection system, the engine power output could be increased by 7% and fuel consumption could be reduced by 10g/kWh compared to the baseline gasoline PFI engine [83]. The work by Wurms et al. was carried out on a 1.8L EA888 Gen 3 turbo fuel stratified injection (TFSI) engine which incorporated both (multipoint injection) MPI and DI systems. The experimental results indicated that with the help of the dual-injection system and modified turbocharger, the engine torque and power output was comparable with that of a larger-capacity 2.0 L TFSI engine and CO₂ emissions were reduced about 7g/km, additionally. Therefore, the 1.8 L EA888 Gen 3 TFSI engine was able to meet the latest EURO 6 emission standard.

Daniel et al.[139] investigated the dual-fuel injection of gasoline, ethanol and 2,5-dimethylfuran at different PFI/DI ratios in a single cylinder research engine. The test engine they used was a 500cc single cylinder engine. The engine speed was fixed at 1500rpm. DI pressure and SOI timing were set at 150 Bar and 280 CAD BTDC. The results indicated that IMEP increased and combustion duration decreased with the increase of DI fraction. HC, NO_x and CO₂ were reduced under the dual-injection strategy. Ethanol was effective in improving volumetric efficiency and reducing combustion duration. The use of ethanol produced the highest indicated efficiency among all tested conditions.

Finally, the combustion characteristics of dual-injection were evaluated by Zhu et al. [140] and Daniel et al. [141]. Both experiments were carried out on single cylinder engine with a constant speed of 1500rpm. The direct injection SOI timing at both tests was before the inlet valve closing (300 CAD BTDC for Zhu et al. and 280 CAD BTDC for Daniel et al.). In the tests in [140], the DI pressure was fixed at 150 Bar and 20 Bar in [141]. Their experimental results showed that when port injecting gasoline, the engine produced a higher indicated thermal efficiency at light loads but a lower indicated thermal efficiency at heavy loads. DI gasoline could result in higher indicated thermal efficiency at heavy loads, but lower indicated thermal efficiency at light loads. Dual-injection combined the merits of both DI and PFI, high efficiency was achieved at both light and heavy loads. It was also found that the engine efficiency of the dual-fuel and dual-injection mode exceeded the sole fuel dual-injection mode because the advantages of both fuels could be incorporated. Using oxygen content fuel could lead to low combustion duration and less unburned emissions.

2.4 Existing problems and research objectives

From the above review, it can be seen that although various engine parameters have been tested extensively by previous researchers, the dual-fuel injection technology is still in its early stages. Only seven papers, excluding the author's, regarding this technology have been presented so far. Among these papers, only four of them ([135][136][139][140]) are directly related to this

dissertation's research topic, EDI+GPI. Therefore, more details and further optimisation are needed to be done based on previous work.

1. Previous works on the dual-injection engine mainly focused on utilising ethanol or other alcohol fuels to enhance the engine anti-knock property. The usage of ethanol in these studies was mainly based on the requirement of knock suppression. Other studies showed that ethanol had the potential to optimise combustion and reduce emissions, and different engine conditions required different EDI/GPI ratios to achieve the best efficiency. These indicated that the ethanol usage is not limited to heavy load conditions to suppress knock, it can be used in all engine operating conditions to improve engine performance and decrease emissions. In different engine conditions, a best ethanol/gasoline ratio may exist for low emissions and high performance.
2. As reviewed in section 2.1, in an engine equipped with the EDI+GPI system, the mixture physicochemical properties vary with the ethanol/gasoline blending ratio. In order to reach the best engine efficiency, it is necessary to understand how the spark timing should be adjusted to adapt to the changed properties. However, this part of information is missing in previous studies. Therefore, the combustion performance at different spark timing and ethanol/gasoline blending ratios should be studied.
3. Although the effect of dual-injection on knock mitigation has been investigated by Stein et al. [135] and Daniel et al. [136], their tests were all carried out at fixed SOI timing where the ethanol was injected before inlet valve closing. As suggested by Cohen et al. [80], the SOI timing had a significant influence to mixture formation and in-cylinder temperature reduction. Thus, the effect of SOI timing on dual-injection engine knock propensity and combustion needs to be investigated.
4. Lean burn technology has great potential in increasing engine efficiency and reducing emissions. The review in section 2.2.5 shows that the EDI+GPI engine has great

potential in substantially improving stratified lean burn performance. Little investigation into this kind has been reported yet. Therefore the investigations on lean burn in the EDI+GPI engine can supplement the knowledge about the dual-injection engine.

Based on the literature review and the existing problems, the objectives of this project are as follows:

1. To exam the effect of the EDI/GPI ratio on engine performance, combustion and emissions, and to try to find out the best ratio for low emissions and high efficiency;
2. To exploit the potential of the EDI+GPI on knock mitigation and investigate the combustion performance at different spark timings and EDI/GPI ratios;
3. To investigate the effect of SOI timing on the EDI+GPI engine knock propensity;
4. To preliminarily evaluate the potential of the EDI+GPI on lean burn.

2.5 Outlines

Chapter Two reviews the essential background information drawn from previously published work on ethanol fuel and dual-injection. The potential benefits of EDI+GPI on mixture formation, combustion, engine performance and emissions are concluded. Details of relevant works about dual-injection are reviewed

Chapter Three gives the details of the experimental apparatus used, including the specifications of the single cylinder engine, engine control system, dual-injection system, gas analyser and data acquisition system. The engine control methods are described along with details on the

important data processing techniques and calculations used in the study.

Chapter Four presents the variation of engine performance, combustion and emissions caused by EER* only. Test results of GDI+GPI are also presented for comparison. Possible reasons that lead to an increase of indicated thermal efficiency with EDI/GPI ratio are discussed.

Chapter Five focuses on the combustion characteristics at different EERs with the advance of spark timing and the knock mitigation effect of EDI+GPI at different engine loads and inlet air pressure levels.

Chapter Six explains the effect of DI ethanol fuel SOI timing on engine, combustion, emissions and knock mitigation. The effect of DI gasoline fuel SOI timing on engine performance is also presented for comparison. The EDI+GPI lean burn performance at different DI timings is included in this chapter.

Chapter Seven concludes the thesis by summarising the contents of each chapter and proposing future works.

*Ethanol energy ratio (EER), defined in Section 3.4.4.

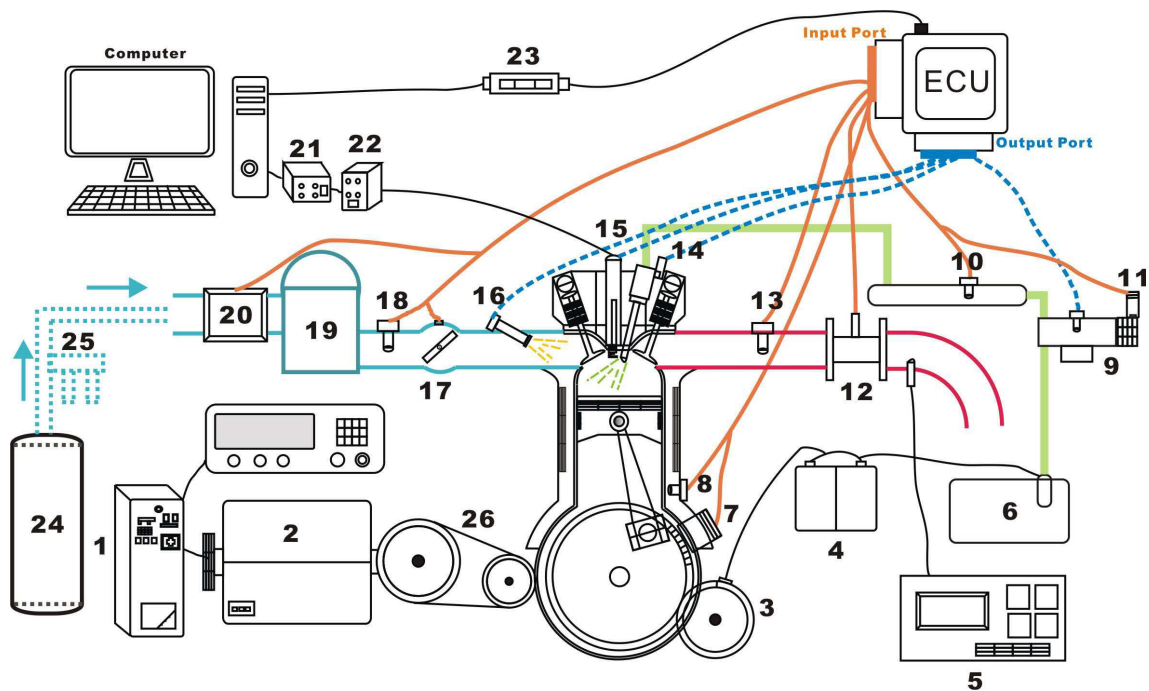
Chapter Three

3. Experimental setup and test facilities

One of the tasks in this project was to design and build up a testing rig which can meet the requirements of experimental study. The details of the engine testing rig will be presented in this chapter. The major control methodology and data acquisition and analysis processes will be introduced.

3.1 General description

All the experiments were conducted on a single cylinder four-stroke engine which was modified to be equipped with a new control system, an ethanol fuel direct injection system, sensors and actuators. Figure 3.1 is the schematic description of the entire experimental setup.



1. Dynamometer controller 2. Dynamometer 3. Start motor 4. Battery 5. Horiba MXEA-584L gas analyzer 6. Ethanol fuel tank 7. Encoder on crankshaft 8. Temperature sensor 9. High pressure fuel pump 10. Common rail pressure sensor 11. Encoder on high pressure pump shaft 12. Bosch wide-band lambda sensor 13. Temperature Sensor 14. Direct fuel injector 15. Kistler spark plug pressure transducer 16. Port fuel injector 17. Throttle valve position sensor and driving motor 18. Temperature sensor 19. Inlet air regulator 20. Air flow meter 21. Combustion analyzer 22. Charge amplifier 23. CAN Communication module 24. Compress air tank 25. Air pressure regulator and water & oil separator 26. Flywheel system

Figure 3.1–Schematic description of the entire experimental setup

The experimental system is constituted by three major parts: data acquisition and monitoring panel, engine and ECU. Figure 3.2 illustrates the composition and functional links between them. The following section explains the apparatus and experimental procedures in detail.

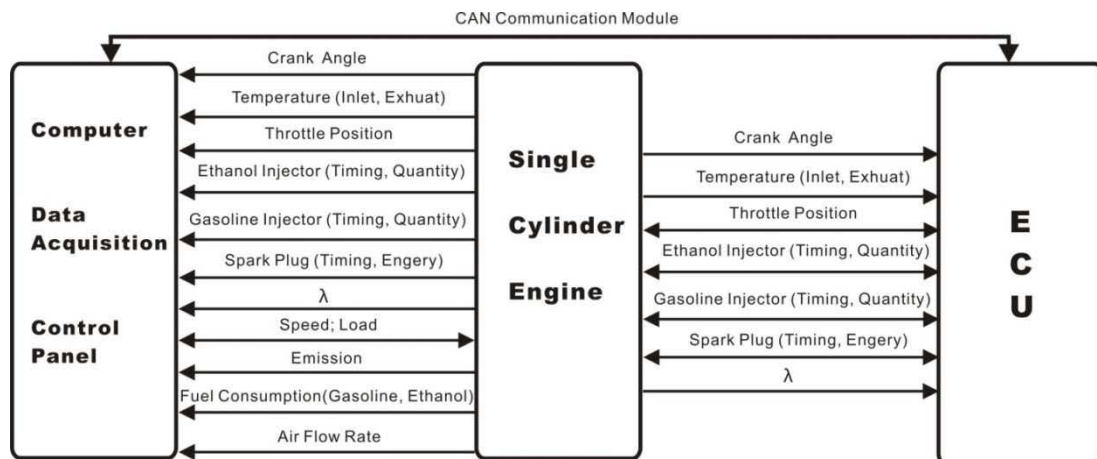


Figure 3.2–Components and links of the control system

3.2 Research engine system

3.2.1 Research engine

A four stroke single cylinder air cool gasoline engine which was originally part of a Yamaha YBR250 Motorcycle was selected as the baseline engine for this study. The original engine was equipped with port injection and three way catalyst and controlled by an on board ECU. It was selected because its cylinder capacity and compression ratio were representative for a down sized light duty passenger vehicle. Table 3.1 lists the specifications of the Yamaha YBR250 Engine.

Table 3. 1 Specifications of Yamaha YBR250 engine

Engine type	Air cooled 4-stroke, SOHC
Cylinder arrangement	Forward-inclined single cylinder
Displacement	249.0 cm ³ (15.2 cu.in)
Bore × stroke	74.0 x 58.0 mm (2.91 x 2.28 in)
Compression ratio	9.80:1
Lubrication system	Wet sump
Maximum horse power	15.7kW (8000r/min)
Maximum Torque	20.5Nm (6500r/min)
Intake valve opening	45 CAD BTDC
Intake valve closing	60 CAD ABDC
Exhaust valve opening	58 CAD ATDC
Exhaust valve closing	21 CAD ATDC
Exhaust Valve Peak lift@park	-6.78mm
Intake Valve Peak lift@park	-6.80mm

The original engine was modified to an EDI+GPI one by adding a direct fuel injection system. Figures 3.3 and 3.4 illustrate the relative position of the DI injector on the cylinder head.

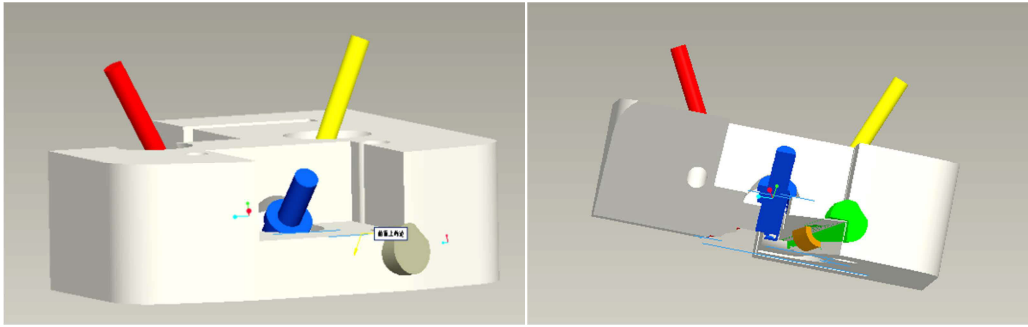


Figure 3.3–Relative position of direction injector on cylinder head (External View)

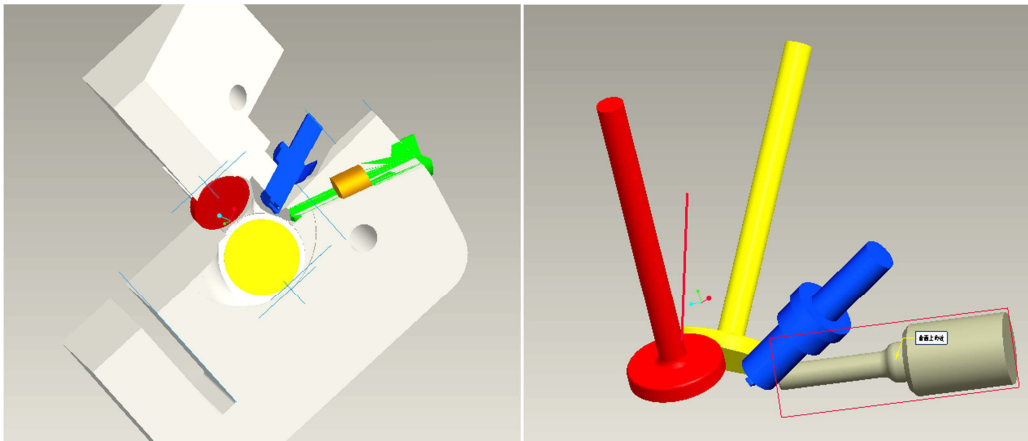


Figure 3.4–Relative position of direction injector on cylinder head (Internal View)

The injector was mounted at the same side of the spark plug, opposite to the sprocket of the camshaft to avoid any interference with the timing chain which was used to drive the camshaft. There is a slop angle of 15° between the axis of the injector and horizontal surface which is the interior surface of the cylinder head and a 12° between the axis of the injector and the vertical surface. The tip of the injector was placed between the intake valve seat and the spark plug. In this way, the tumble flow could be partially used to facilitate the vaporisation of DI fuel and a richer mixture could be formed adjacent to the spark plug. Figure 3.5 shows the images of the DI injector on the cylinder head.



Figure 3.5–Images of injector in combustion chamber and external cylinder

3.2.2 High pressure ethanol fuel supply system

A high pressure fuel supply system was developed to deliver high pressure ethanol fuel. The system was composed by an injector, a common rail, a pressure sensor, decompression valves, a low pressure fuel pump, a high pressure fuel pump, electrical drive motor and an encoder. The whole system was controlled by the ECU which was also used to control the engine operation.

Figure 3.6 is the schematic diagram of the high pressure fuel system for ethanol.

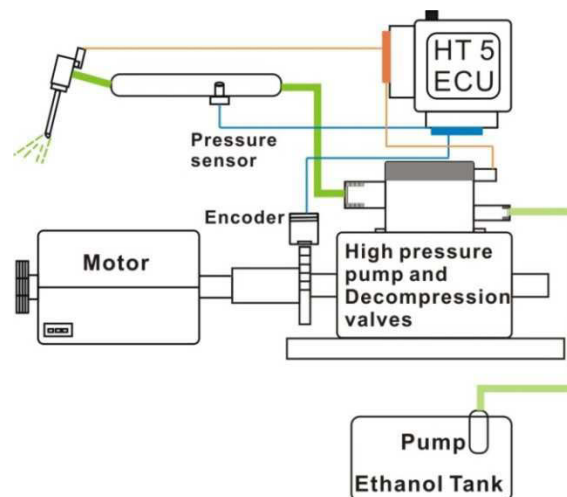


Figure 3.6–Schematic diagram of high pressure ethanol fuel system

The high pressure pump and the injector used in this research were originally adopted from Volkswagen EA888 turbo charged direct injection engine. The pump was a single cylinder electronically controlled pump with a safety valve setting at an opening pressure of 140 Bar. It could provide fuel pressure at a steady range from 30 Bar to 130 Bar. The common rail pressure

was controlled by a high speed electronic on/off valve which allowed a certain amount of fuel into the rail. An encoder was used in this system to decide an appropriate timing to open and close the on/off valve, so that the amount of fuel in the common rail could be kept at a designated range in order to maintain a certain fuel pressure. In the EA888 engine the pump was driven by a quadrilateral cam on the overhead camshaft. In this system, it was driven by an electrical motor at a constant speed of 1500rpm/min.

The multi-hole injector can produce six spray plumes or jets in a $\frac{3}{4}$ moon pattern as shown in Figure 3.7. It was side-mounted and aimed to form a rich mixture around the spark plug with the aid of engine crossflow. The six nozzle holes have different angles to direct fuel to different areas of the combustion chamber. It has a spray cone angle of 34° with a 17° bent axis. In the present work, the injector was installed with the angle that some of fuel spray plumes (spray plumes 1 and 6) could direct fuel towards the area adjacent to the spark plug.

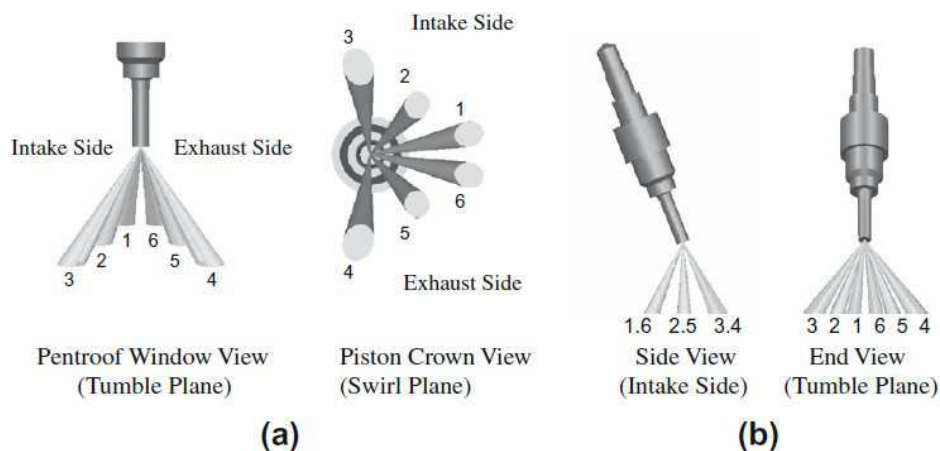


Figure 3.7–Nominal spray pattern of the injector used: (a) engine views and (b) pressure chamber views [142]

3.2.3 Control unit

The ECU which was a commercial product provided by Hents Technology was the center of the whole testing system. It was used to replace the original ECU on the YBR250 engine and to ensure stable operation. It was also used to control the high pressure fuel supply system and monitor some important operating data during the tests. Figure 3.8 illustrates the function of the

ECU in the testing rig.

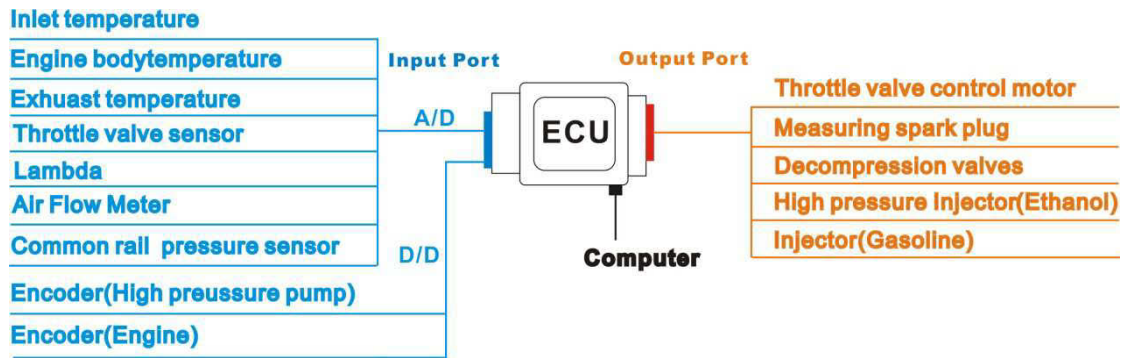


Figure 3.8–Function of ECU

The ECU was based on Freescale’s MC9S12XPE100 16-bit high performance micro computer unit (MCU) which is specifically designed for automotive electronics. The core of the system was the XPE100 microprocessor which featured sufficient inputs and outputs to provide great flexibility in the control and monitoring testing rig system.

3.2.4 Engine control strategy

Basic engine control strategies were developed and implemented in the operation of the research engine to minimise the time and other resources for conducting the experiments. Figure 3.13 shows the basic engine control strategy.

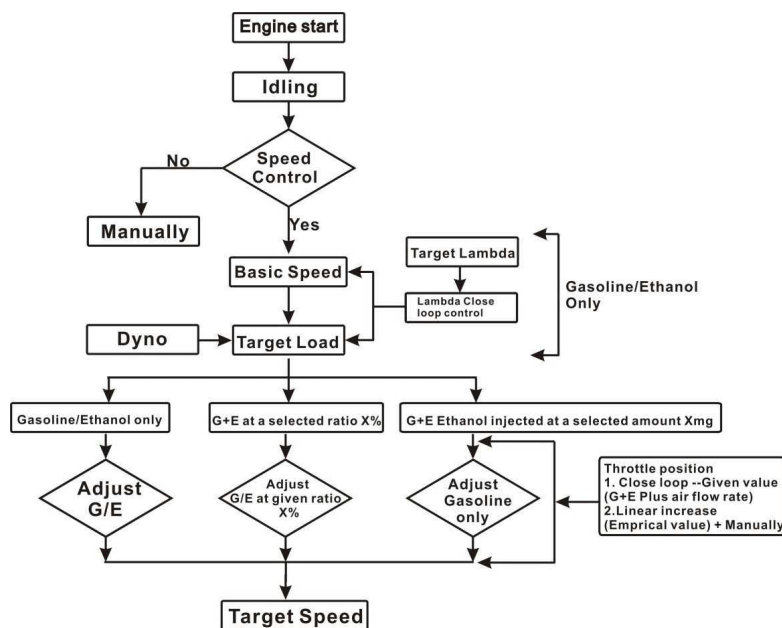


Figure 3.9–Roadmap of control strategy

During the experiments, the engine load was provided by a dynamometer and the engine speed was controlled by the dynamometer control system. The engine was started with gasoline fuel only. After the engine was started, the controller ran the 'Idling' program to set the engine speed at around 2000rpm to warm up the engine. Once the engine oil temperature was in the designated range (398 ± 5 K for the tests about engine knock and 368 ± 5 K for the rest of the tests), the engine load and speed were increased to target conditions. The engine conditions were stabilised at target speed and load for several minutes, then the quantity of the PFI fuel was decreased and the DI fuel with equivalent energy was injected directly into the combustion chamber to maintain the constant engine conditions. The DI and PFI fuel can be adjusted separately or together with a fixed DI/PFI ratio. The AFR was kept constant during the tests by adjusting the throttle position or DI and PFI fuel injector pulses, the adjustment of which was based on the purpose of the tests.

3.2.5 Dynamometer

An eddy-current dynamometer produced by Land & Sea was used for motoring, measuring engine torque and speed. It was mounted on the same steel frame where the engine was installed. A Kistler 2614B crank angle encode with a resolution of 0.1 degrees was directly connected to the engine crank angle for the measurement of piston phasing when acquiring the cylinder pressure data. Engine speed was monitored using another optical RPM sensor installed on the dynamometer. The sensor worked by detecting the light pulses bounced back from a strip of reflective tape on the rotating connector between the engine and dynamometer.

3.3 Instruments and measurements

3.3.1 In-cylinder pressure measurement

A Kistler's 6115B piezoelectric measuring spark plug pressure transducer was used for measuring the in-cylinder pressure. It was a small piezoelectric high-temperature cylinder pressure sensor incorporated in a M12*15 spark plug. Figure 3.10 is the schematic of the Kistler

6115B pressure transducer. The in-cylinder pressure data were used to calculate the IMEP, heat release rate and mass fraction burnt (MBF). They were also be used for analysing cycle-by-cycle variation and identifying knocking combustion and misfire regions.

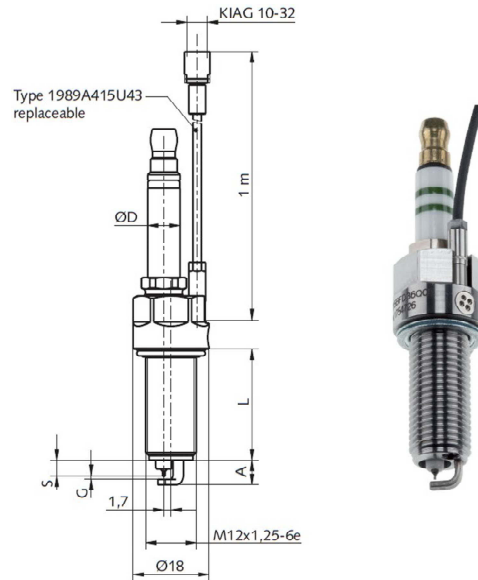


Figure 3.10–Schematic of Kistler 6115B pressure transducer [143]

The charge output generated by the pressure transducer was supplied to the charge amplified (Kistler type 5018a) via a high impedance shield cable due to minimal level of signal output. The transducer output was converted to voltage and then amplified by the charge amplifier.

3.3.2 Data acquisition system

The data were acquired by two systems, the ECU and the MP421 combustion analyser. The parameters that were relevant to engine operation such as engine speed, AFR, inlet air pressure, and temperatures were acquired through the ECU built-in program and were real-time displayed on the computer screen through the interface. The signals from the rotary encoder and cylinder pressure transducer were acquired by the MP421 data acquisition card. The data acquisition system sampled simultaneously 16 channels at 24-bit resolution and 100 kHz rate. It was able to synchronously process the cylinder pressure to the corresponding heat release curve, accumulative heat release curve and average temperature. IMEP, PIR Max (Maximum pressure increase rate), coefficient of variation of indicated mean effective pressure (COV_{IMEP}) and

Maximum cylinder pressure were also calculated and recorded. The system was capable of acquiring and averaging 100 consecutive cycles with a resolution of 0.1 crank angle and it saved the data in an Excel file.

3.3.3 Exhaust gas emission measurement

Concentrations of CO, CO₂, HC, NO and O₂ level in the exhaust gas were measured by a Horiba Mexa-584L gas analyser (Figure 3.11), which was a typical type used for regulatory tests of privately owned Light Goods Vehicles (LGV) and motorcycles. The exhaust gas was picked up in the middle of the exhaust gas pipe (0.4 m from the exhaust valve) and delivered via a silicon rubber sample line, a water trap and a combined concentrate and particulate removal filter.



Figure 3.11–Photo of MEXA-584L Gas analyser [144]

Cooled exhaust gas from the exhaust pipe was drawn into the Horiba gas analyser by an integral vacuum pump and the gas was divided by an infrared absorption cell and a galvanic cell. A non-dispersive infrared (NDIR) absorption cell measured CO and CO₂ and a galvanic cell measured the oxygen content of the exhaust gas to determine the AFR. The NDIR absorption cell also measured the concentration of HC in the exhaust gas. NO emissions were measured via A Chemi-luminescence (CLD) sensor. The resolutions of the gas analyser are listed in Table 3.2

Table 3. 2 Resolution of the gas analyser

CO:	0.01 %vol
HC:	1 ppmvol (within the range of 0 ppmvol to 2000 ppmvol), 10 ppmvol (within the range of 2000 ppmvol to 10000 ppmvol)
CO ₂ :	0.02 %vol
AFR:	0.1
LAMBDA:	0.001
O ₂ :	0.02 %vol
NO:	1 ppmvol

The exhaust gas emissions measured by the gas analyser were used to calculate the specific exhaust gas emissions according to the methods and procedures specified in the EU directive 2002/88/EC. The output of HC provided by the gas analyser was on a Carbon 6 (C6) basis. Since the EU directive specifies that the HC emissions should be measured on a C1 basis, the HC results obtained from the gas analyser had to be converted from C6 to C1. This conversion was performed according to the relationship of HC readings from NDIR (C6) and FID (C1) presented by Heywood and Sher, as shown in Figure 3.12.

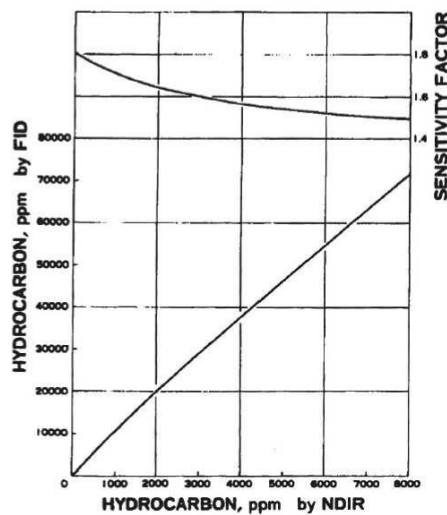


Figure 3.12–HC concentrations from NDIR and FID analysis [145]

3.3.4 Fuel mass flow, air mass flow and other measurement

Ethanol and gasoline fuel were supplied from two separate fuel tanks. The ethanol fuel was first pumped by a production 2.5 Bar fuel pump and then supplied to the high pressure pump. The gasoline was pressured to 3.0 Bar by a fuel pump and directly delivered to the PFI injector. The quantities of both ethanol and gasoline fuels were measured through metering the injection pulse width of corresponding injectors. The calibrations of injection pulses vs. gravimetric fuel injection amount of both injectors are shown in Figure 3.13.

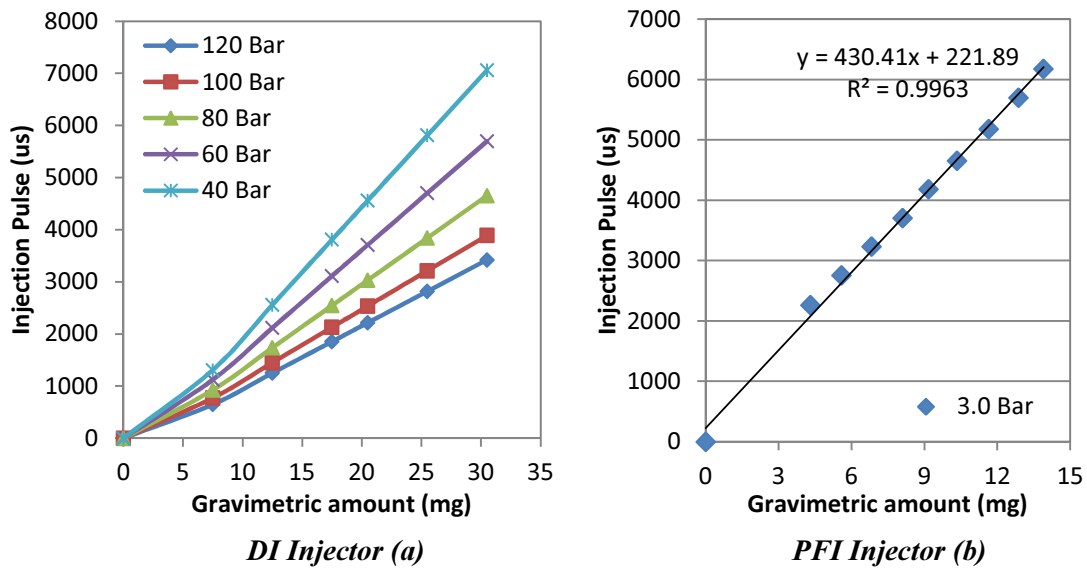


Figure 3.13–Gravimetric calibration of DI and PFI injectors

Air mass flow rate was measured through a ToCeil20N hot-wire thermal air-mass flow meter. A 80L intake buffer tank (approximately 320 times the engine’s displacement volume) was used to stabilise the intake flow. Engine body temperature, lubricant oil temperature, intake and exhaust air temperature were measured through K-type thermal couples with a resolution of 0.1 K.

3.4 Data processing and analysis

3.4.1 Indicate mean effect pressure

The Indicated Mean Effective Pressure (IMEP) is a key parameter to measure the engine load. It helps us to know how the cylinder pressure behaves in relation to cylinder volume which is determined by the engine geometry. The IMEP is numerically determined by the ratio of the area enclosed by the pressure curve and cylinder displacement volume. It represents the specific

work done on the piston over a four stroke cycle.

The IMEP is a net one, rather than Gross IMEP, which is worked over the compression and expansion strokes. It should present work delivered for entire 4-stroke cycle. Pumping work per cycle is considered as an engine operating loss and is calculated by subtracting the Gross IMEP from net IMEP [146].

$$\text{IMEP} = \frac{1}{V} \oint P dV \quad \text{Equation 3.1}$$

3.4.2 Heat release rate

Heat release rate was calculated and compared to characterize the combustion process in terms of combustion phase, speed, peak rate. It gives a straight view of the impact of different factors on the engine combustion process. The heat release rate was obtained from the measured pressure trace and calculated with cylinder volume with respect to crank angle and with the estimated average ratio of the specific heats value [146].

The calculation of the heat release rate was based on the first law of thermodynamics in which the cylinder is considered as a closed system for the combustion event. The combustion chamber was considered as a single zone, where no temperature gradients exist and the reactants and products were completely mixed. The reactants and products were also assumed to have the same properties.

$$\delta Q_T = dU + \delta W + \delta Q_L \quad \text{Equation 3.2}$$

Where δQ_T is the total heat released in a time interval of δT during the combustion process. dU is the change in internal energy, δW is the work done on the piston and δQ_L is the change in heat loss [146].

Each of the terms is:

$$\delta W = p dV \quad \text{Equation 3.3}$$

$$dU = mc_v dT \quad \text{Equation 3.4}$$

Consider the mixture in cylinder as an ideal gas

$$mdT = \frac{1}{R} [pdv + Vdp] \quad \text{Equation 3.5}$$

The net heat release now can be presented on an angle incremental basis [147]

$$\frac{dQ_{net}}{d\theta} = \frac{\gamma}{\gamma-1} p \frac{dv}{d\theta} + \frac{1}{\gamma-1} V \frac{dp}{d\theta} \quad \text{Equation 3.6}$$

Where γ (the ratio of specific heats) = C_p / C_v and Θ is the crank angle. It should be noted that a fixed $\gamma=1.3$ was chosen according to the suggested value for direct injection engine provided in [146].

3.4.3 Coefficient of variation

The coefficient of variation of indicated mean effective pressure (COV_{IMEP}) is defined as [148]

$$COV_{imep} = \frac{\sigma_{imep}}{imep} \times 100\% \quad \text{Equation 3.7}$$

It is used to indicate the cyclic variability for the combustion engine. In this study the IMEP value is averaged from the completion of 100 engine cycle. σ_{imep} is the standard deviation in IMEP. The maximum acceptable deviation in this study is 10%.

3.4.4 Fuel efficiency

In this study, the EER is defined as the rate of the heating energy (HE) of the ethanol fuel divided by the rate of the total heating energy of ethanol and gasoline fuels. The rate of heating energy is equal to the fuel mass flow rate multiplied by the lower heating value (LHV) of the fuel.

$$EER = \frac{\dot{H}E_{Ethanol}}{\dot{H}E_{Ethanol} + \dot{H}E_{Gasoline}} \quad \text{Equation 3.8}$$

Where $\dot{H}E$ (rate of heating energy, kJ/s) = fuel mass flow rate (g/s) \times LHV. The denominator

in Equation 3.8 is the rate of the total heating energy of the two fuels. This total heating energy rate was kept unchanged in most of the tests, and the EER was varied by changing the mass flow rates of both ethanol and gasoline fuels.

Similar to Equation 3.8, the DI/PFI ratio (Equation 3.9) is used in to define the energy flow ratio between direct injection fuel and port injection fuel.

$$\text{DI/PFI ratio} = \frac{\dot{H}E_{DI}}{\dot{H}E_{DI} + \dot{H}E_{PFI}} \quad \text{Equation 3.9}$$

Where $\dot{H}E_{DI}$ and $\dot{H}E_{PFI}$ are the energy flow rates of direct injection fuel and port injection fuel.

To evaluate the leveraging effect of ethanol fuel on saving energy consumption, the indicated specific energy consumption (ISEC) is used to measure the integrated fuel energy of both fuels. ISEC is defined by Equation 3.10.

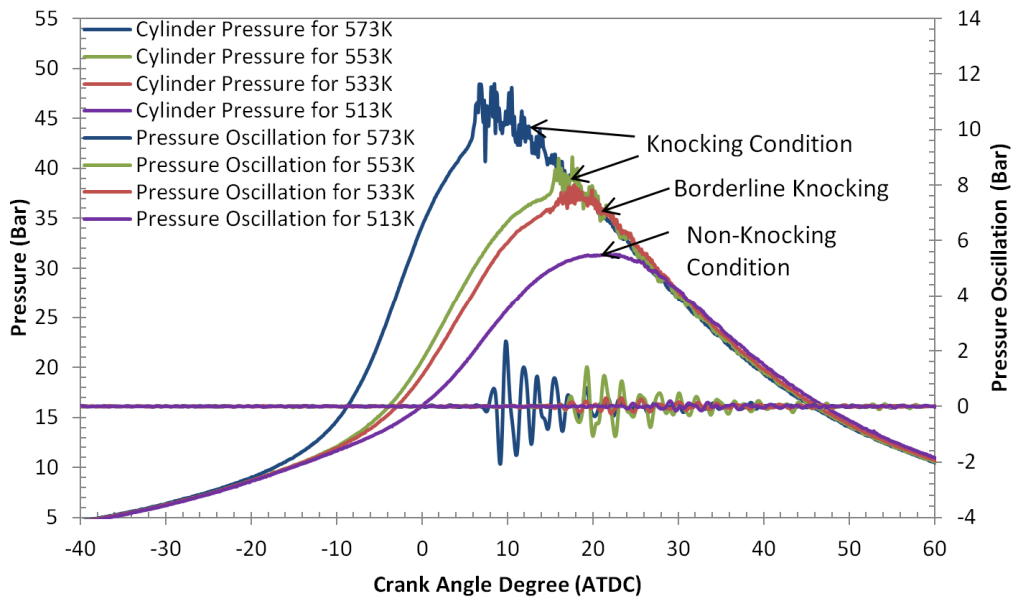
$$\begin{aligned} \text{ISEC} &= \frac{\dot{H}E_{Ethanol} + \dot{H}E_{Gasoline}}{P_i} \\ &= \frac{\dot{m}_{Ethanol} \times LHV_{Ethanol} + \dot{m}_{Gasoline} \times LHV_{Gasoline}}{P_i} \end{aligned} \quad \text{Equation 3.10}$$

Where $\dot{H}E_{Ethanol}$ and $\dot{H}E_{Gasoline}$ are the rates of heating energy (kJ/s) of the ethanol fuel and gasoline fuels respectively, as defined in Equation 3.10. $\dot{m}_{Ethanol}$ and $\dot{m}_{Gasoline}$ are the mass flow rates (g/s) of the ethanol and gasoline fuels. $LHV_{Ethanol}$ and $LHV_{Gasoline}$ are the lower heating values of the ethanol and gasoline fuels. P_i is the engine indicative power (kW·hr).

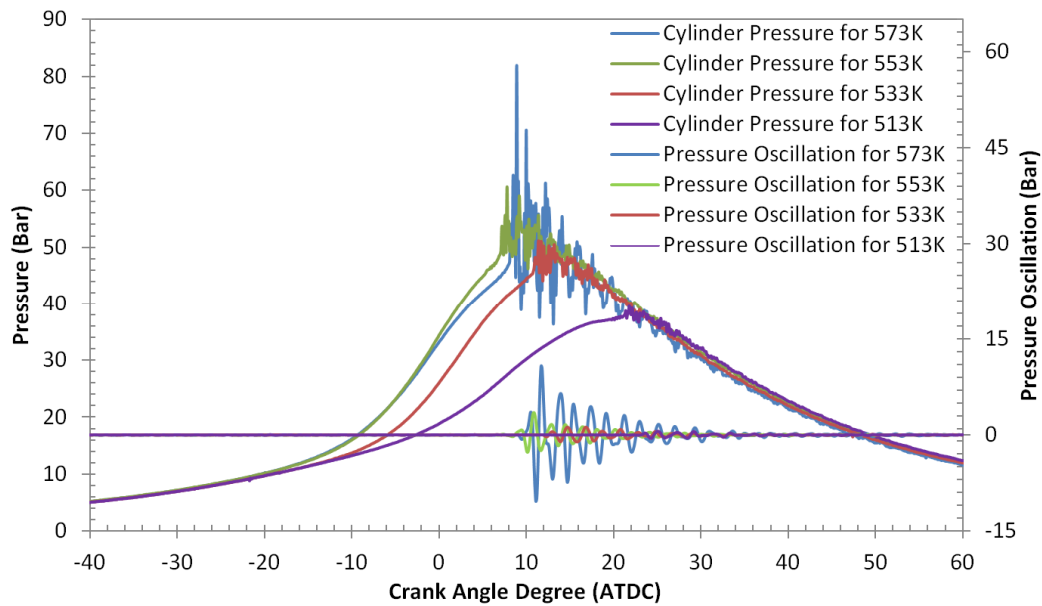
3.4.5 Knock detection

One of the major purposes of using ethanol in this study was to mitigate engine knock. The engine knock in this study was detected by monitoring the cylinder pressure trace. If at least 10 of 100 consecutive cycles were detected with noticeable pressure wave oscillations (peak to

peak oscillation over 1.0 Bar) around the peak cylinder pressure, the engine condition was regarded as knock condition. A MATLAB high band pass filter program was developed to detect the pressure wave oscillation. In the experiments, the engine body temperature was stabilised at 573 ± 5 K which corresponded to the lubricant oil temperature around 398 K. Keeping the engine temperature at this level was for increasing the propensity of knock in such an engine with a compression ratio of only 9.8:1 and late inlet valve closing. Thus the knock could occur at medium load, and the investigation could be performed in a certain load range. Another reason for doing so was because of the peak pressure limited by the strength of the cylinder head. The cylinder head of the engine was modified to accommodate the ethanol DI injector. The strength of the cylinder head might have been weakened by this modification. Therefore, the peak cylinder pressure was limited to no more than 100 Bar to protect the prototype engine. Increasing the engine temperature was an effective way to realise knock with low peak cylinder pressure. Figures 3.14 (a) and 3.14 (b) illustrate the relation between knock intensity and engine body temperature at two different engine loads. In these Figures the engine body temperature of 513 K corresponded to the lubricant oil temperature of 368 K. It can be clearly seen that the knock propensity in each load increases with the increase of engine body temperature. In Figure 3.13 (a), the cylinder pressure trace for engine body temperature of 553 K was regarded as knock borderline because the pressure oscillation was less than 1.0 Bar which was according to the definition presented in [149]. The used oil temperature range was within the safety range according to the manuals of the YBR250 air cooled motorcycle engine and the SAE 20w-50 synthetic lubricant oil [150]. Once the knock condition was found, the spark timing was then retarded 2 CAD and marked as KLSA by adopting the method reported in [136].



(a) Throttle=25%, Spark timing=35 CAD BTDC, Gasoline fuel only



(b) Throttle=32%, Spark timing=35 CAD BTDC, Gasoline fuel only

Figure 3.14– Original cylinder pressure trace and 3–20 kHz band pass filtered pressure for different engine body temperature conditions

3.4.6 Mass burnt fraction

The MBF was calculated based on the techniques developed by Rassweiler and Withrow. This method is based on the idea that the total cylinder pressure rise during a crank rotation interval is equal to the sum of the pressure rise due to the piston movements and the pressure rise due to

combustion [151] [152].

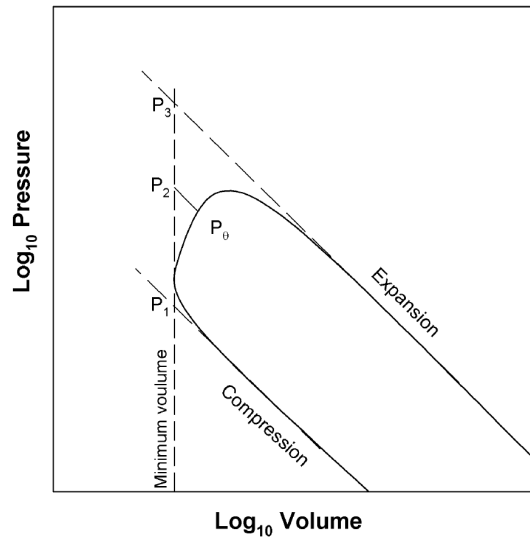


Figure 3.15–Pressure-Volume diagram to show the pressure values in calculating MBF [152]

This method is based on the assumptions that 1. The cylinder volume is considered as a homogeneous reactor; 2. There is no heat transfer; 3. There are no crevice volumes and blow-by leakages.

In Figure 3.15, P_1 and P_3 are the points where the extended compression and expansion lines intersect with the minimum volume line. P_θ in Equation 3.11 is the instantaneous pressure at crank angle θ . Point P_2 is the projection of P_θ on the minimum volume line, defined by Equation 3.10.

$$P_2 = P_\theta \times \left(\frac{V}{V_c}\right)^n \quad \text{Equation 3.11}$$

Where V is the instantaneous cylinder volume, V_c is the minimum volume or the clearance volume of the cylinder and n is the polytropic index [152]. Thus, the MBF (denoted by X_θ) at a given crank angle can be calculated from Equation 3.12.

$$X_\theta = \frac{P_2 - P_1}{P_3 - P_2} \quad \text{Equation 3.12}$$

3.4.7 Calculation of lambda

In a conventional way, the lambda of a known fuel composition was measured using an appropriate lambda meter or oxygen sensor, which requires the presetting of fuel properties. However, in dual-injection the exact mixing ratio between ethanol and gasoline varied during the tests. Therefore, the fuel's chemical composition such as hydrogen to carbon (H/C) and oxygen to carbon (O/C) ratios, as well as stoichiometric AFR cannot be real-time inputted into the lambda sensor or gas analyser which requires manually entering. Thus, real-time lambda control was impossible. In this investigation, the lambda in dual-fuel injection conditions was calculated from gasoline and ethanol fuel flow rates and inlet air flow rate, as it is shown in Equation 3.13.

$$\lambda = \frac{\dot{m}_{air}}{(\dot{m}_{Ethanol} \times AFR_{StoicEthanol} + \dot{m}_{Gasoline} \times AFR_{StoicGasoline})} \quad \text{Equation 3.13}$$

It should be noted that when the engine was running with gasoline fuel only, a Bosch wide-band lambda sensor which was mounted on the exhaust pipe which was used to monitor the lambda and for close-loop control.

In order to ensure the conformity, the two lambda measurement methods were compared compared at gasoline only condition, pure ethanol condition and two selected dual-fuel conditions (EERs of 24% and 48%). In the comparison, the H/C and O/C ratios were first first calculated according to the ratio of gasoline/ethanol and directly input into the gas analyser. Then the lambda reading from the gas analyser and the lambda calculated from from air flow and fuel flow rates were compared. The results were equivalent. Moreover, in order to further verify the conformity of the two methods, the quantity of fuel injected injected per cycle calculated with the output of the lambda sensor in the gas analyser and and air flow meter was compared with the data measured on the injector testing bench. In In the injector testing bench the fuel injection amount per cycle for a given width of driven pulse can be directly measured. This test was conducted in pure gasoline port

injection condition and pure ethanol direct injection condition where the stoichiometric AFR of both fuels were known. The fuel injection amount for a given width of pulse was measured. The results were also equivalent.

3.4.8 Combustion efficiency

In order to further analyse some of the experimental results, the combustion efficiency ($n_{Combustion}$) which is calculated from CO and HC in the exhaust stream, is used to assist in analysing some of the results. The combustion efficiency is defined by Equation 3.13 which is a simple version that is used by Christensen et al. [153].

$$n_{Combustion} = 1 - \frac{x_{CO}Q_{LHV_{CO}} + x_{HC}Q_{LHV_{fuel}}}{\left[\frac{\dot{m}_{fuel}}{(\dot{m}_{air} + \dot{m}_{fuel})} \right] Q_{LHV_{fuel}}} \quad \text{Equation 3.14}$$

Where χ_{CO} and χ_{HC} represent the mass fraction of CO and HC. $Q_{LHV_{CO}}$ and $Q_{LHV_{fuel}}$ are the lower heating values of fuels and CO. \dot{m}_{fuel} and \dot{m}_{air} are the mass flow rate of fuels and air (g/s).

3.5 Tested fuels

The gasoline fuel used in this study was BP Australia premium No. 91 gasoline with an octane number of 91. It was used to provide a benchmark for the ethanol fuel. The ethanol fuel was provided by Manildra. Properties of ethanol and gasoline fuels are listed in table 3.3.

Table 3.3 Test fuel properties

	Ethanol	Gasoline
Chemical formula	C ₂ H ₆ O	C ₂ -C ₁₄ [‡]
H/C ratio	3	1.90 [‡]
O/C ratio	0.5	0
Gravimetric oxygen content (%)	34.78 [*]	0
Density@293 K (Kg/m ³)	790.0 [*]	744.6 [†]
Research Octane Number	106	91 [‡]
Stoichiometric air/fuel ratio	9.0:1	14.79:1 [‡]
LHV(MJ/kg)	26.9	43.9 [‡]
LHV(MJ/L)	21.3	31.9
Enthalpy of vaporization (kJ/kg)	854 [*]	373 [†]
Temperature at boiling point (K)	78.4 [*]	32.8 [†]

* Provided by Manildra Group

‡ <http://www.environment.gov.au/atmosphere/fuelquality/publications/pubs/paper2.pdf>

† Heywood, J.B., Internal Combustion Engine Fundamentals. 1988: McGraw-Hill

Chapter Four

4. Leveraging effect of EDI

4.1 Influence of EER

In this section the experimental results about the effect of EER on engine performance, combustion characteristics and emissions will be presented and discussed. Possible reasons for the increase of IMEP due to the use of EDI will be analysed. Experiments were conducted in two engine load (light and medium) conditions with engine speed varying from 3500rpm to 5000rpm (500rpm interval). Spark timing and SOI timing of ethanol fuel were fixed at 15 CAD BTDC and 300 CAD BTDC. 15 CAD BTDC was the spark timing in the original engine control system. The SOI timing of 300 CAD BTDC was for the purposes of providing sufficient time for charge mixing, so that the cooling effect of ethanol fuel on improving the volumetric efficiency could be investigated. In each engine load condition, the throttle position was set at a fixed position and the EER was varied from 0% (gasoline only) to 60%. The AFR was set at stoichiometric value through adjusting the injection pulse-widths of gasoline and ethanol. The ethanol direct injection fuel pressure was fixed at 40 Bar when EER was less than or equal to 48% and 60 Bar when EER was greater than 48%. Increasing the injection pressure at high EERs was to keep the ethanol fuel injection duration similar and to avoid the influence of the injection period on engine performance. The engine experimental conditions for this part of tests are listed in Table 4.1.

Table 4.1 Experimental conditions for Section 4.1

Engine speed	3500rpm
Engine load	Medium (IMEP~7.0 Bar, Throttle ~35%); Light (IMEP~5.0 Bar, Throttle ~25%)
EER	0%, 18%(Only in Medium load), 24%, 30%, 36%, 42%, 48%
Injection timing	300 CAD BTDC
Injection pressure	40 Bar (When EER<48%) 60 Bar (When EER≥48%)
Spark timing	15 CAD BTDC

4.1.1 Engine performance

Figure 4.1 shows the variation of IMEP with EER in light and medium engine load conditions with the speed varying from 3500rpm to 5000rpm. As shown in Figure 4.1, the engine IMEP increases with the increase of EER at all the tested conditions. This shows that with the increase of EDI energy percentage, the IMEP of a port-injection SI engine is increased. Therefore, the total fuel consumption is reduced by using the ethanol fuel without sacrificing the engine power. Several factors may contribute to the increase of IMEP. They include the charge cooling effect associated with ethanol fuel direct injection and ethanol's high latent heat of vaporisation [154], high energy content of stoichiometric mixture per unit mass of air, change in products moles [47] and ethanol's high flame propagation speed [136] [155]. Details of these possible reasons will be analysed and discussed later in this section.

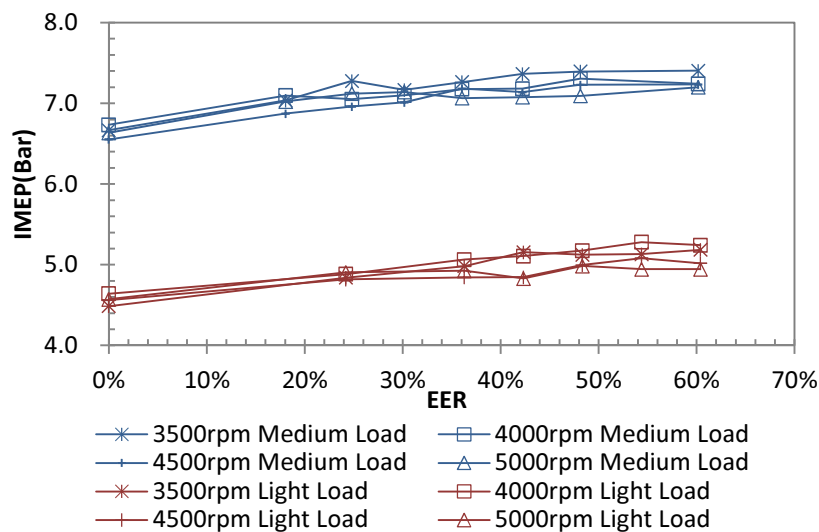


Figure 4.1–Variation of IMEP with EER

Directly linked to the charge cooling, volumetric efficiency is another parameter to evaluate the leveraging effect of using ethanol fuel direct injection in a SI engine. As shown in Figure 4.2, the volumetric efficiency is increased with an increase of EER from about 53.5% to 54.5% in light load conditions and 68.5% to 72.5% in medium conditions. The charge cooling effect and the reduced partial pressure of the port injected gasoline fuel may contribute to the improvement of volumetric efficiency. When the ethanol fuel is injected into the cylinder during the early stage of the intake stroke, the ethanol fuel evaporation may be more effective on cooling the

fresh charge and increasing its density than the gasoline fuel. On the other hand, the quantity of the port injected gasoline fuel decreases with the increase of EER. The partial pressure of gasoline fuel decreases with reductions to the gasoline volume fraction, which also contributes to improving the volumetric efficiency.

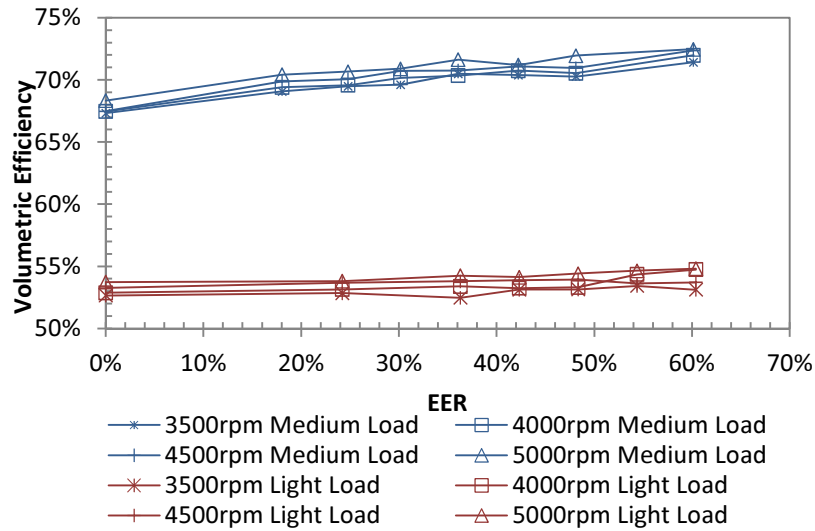


Figure 4.2–Variation of volumetric efficiency with EER

Figure 4.3 shows the variation of indicated specific fuel consumption (ISFC) with EER. As shown in the figure, the ISFC increases with the increase of EER except for a minor drop at EER of 24.2% in light load conditions. This result may be because the ethanol fuel's lower heating value is only about 66% of gasoline (See Table 3.3), so that more ethanol fuel is needed to maintain the same engine power.

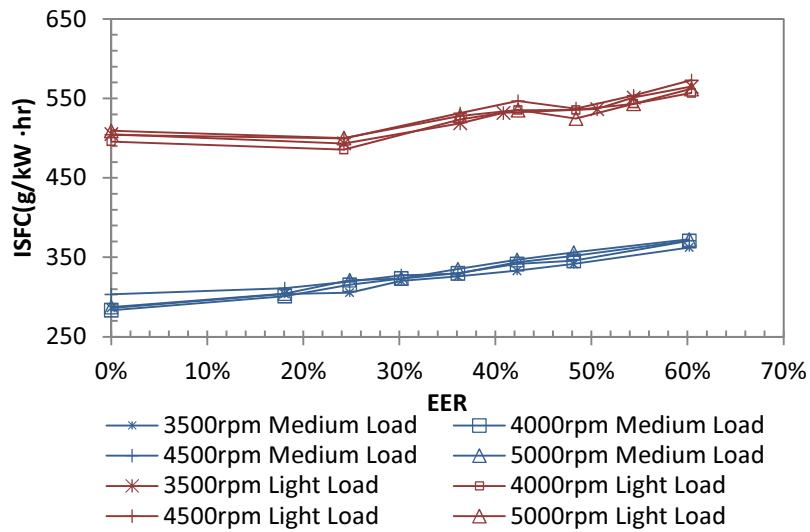


Figure 4.3–Variation of ISFC with EER

To evaluate the leveraging effect of ethanol fuel on saving energy consumption, ISEC is also used to measure the integrated fuel energy of both fuels. As shown in Figure 4.4, the ISEC decreases with the increase of EER. This means that less energy input is required to achieve the same IMEP than through gasoline fuel only. Therefore, the engine energy consumption is reduced by using ethanol fuel direct injection.

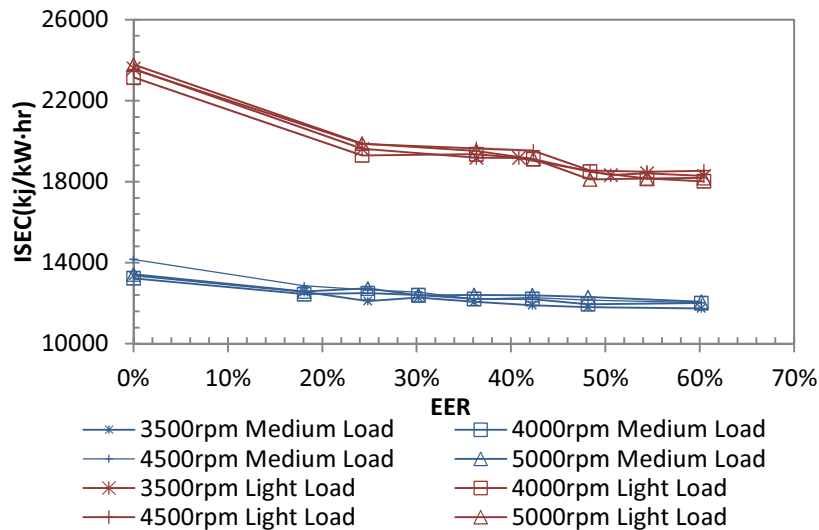


Figure 4.4–Variation of BSEC with EER

4.1.2 Possible reasons for the increase of IMEP

When comparing the IEMP at EER of 0% with that at EER of 60%, an average 10% increase can be noticed in medium load conditions and 11% in light load conditions as shown in Figure

4.1. The increased volumetric efficiency (4.5% increase in medium load and 1.3% increase in light load) may partially explain the IMEP increment. However, the decreased ISEC (Figure 4.4) indicates that the increased volumetric efficiency does not provide a substantial explanation for the results. The following section will discuss the possible reasons for the IMEP increment when using EDI.

Charge cooling effect

During the experiments, the ethanol was directly injected into the cylinder at an injection timing of 300 CAD BTDC. Because the fuel is delivered at an early stage of the intake stroke, its vaporization needs to extract heat, at least partially, from fresh air charge which decreases the in-cylinder temperature, increases the specific volume of the intake charge and improves the volumetric efficiency. The latent heat of vaporisation of ethanol used in this test is 854 kJ/Kg which is about three times that of gasoline (373 kJ/Kg). Greater latent heat of vaporisation means that the ethanol is more potentially efficient than gasoline in decreasing the in-cylinder temperature. In order to specify the variation of EDI percentage on the latent heat of vaporisation and consequently in-cylinder temperature reduction, the variation of heat of vaporisation for a stoichiometric mixture and maximum thermodynamic charge cooling are calculated and shown in Figure 4.5 and Figure 4.6. It is noted that the Figure 4.5 is expressed as kJ per kg of air of a stoichiometric mixture, because this expression directly relates to the amount of charge cooling provided by the vaporisation of the ethanol. As shown in Figure 4.5, the latent heat of vaporisation of the stoichiometric mixture increases with the ethanol volumetric percentage. When compared with the gasoline only condition (EER of 0%), the latent heat of vaporisation of the stoichiometric mixture increases to about 80 kJ/kg which leads to a maximum of 80 K in-cylinder temperature reduction in most ideal conditions. This in-cylinder temperature reduction results in about 24% volumetric efficiency improvement, theoretically (Figure 4.6).

However in real engine operation, the wall-wetting effect, fuel atomisation quality, heater

transfer to the charge and other factors may affect the effective charge cooling. Figure 4.7 illustrates the in-cylinder temperature trace after the inlet valve is closed and before the ignition. This in-cylinder temperature was calculated from the cylinder gas pressure based on first law of thermodynamics. As shown in Figure 4.7, the in-cylinder temperature in EDI conditions (EER of 35% and EER of 60%) is less than that in the gasoline only condition (EER of 0%). At the crank angle position of 20 CAD BTDC, the in-cylinder temperature at EER of 60% is 28.5 K lower than that at EER of 0%. This reduction corresponds to 4.5% volumetric increment as that measured in the real engine test. However, the in-cylinder temperature change between EER of 35% and EER of 60% is not significant. This may indicate that wall wetting occurs at EER of 60%, which leads to the vaporisation of ethanol absorbing heat from the cylinder wall. Thus, the effect of EDI on in-cylinder temperature reduction becomes less significant.

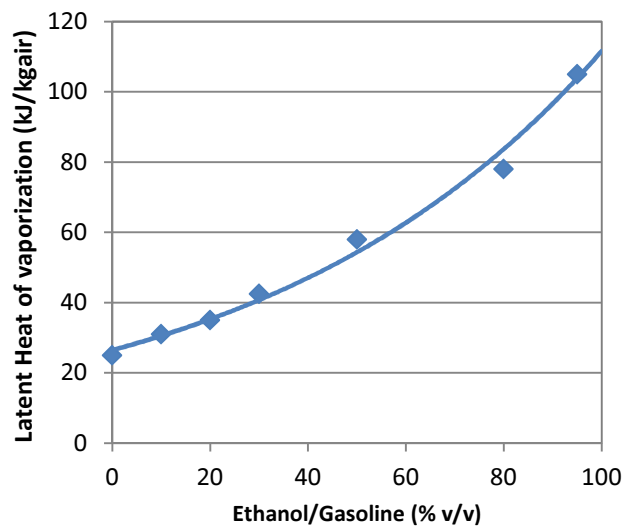


Figure 4.5–Variation of heat of vaporisation of stoichiometric mixture (data from [46])

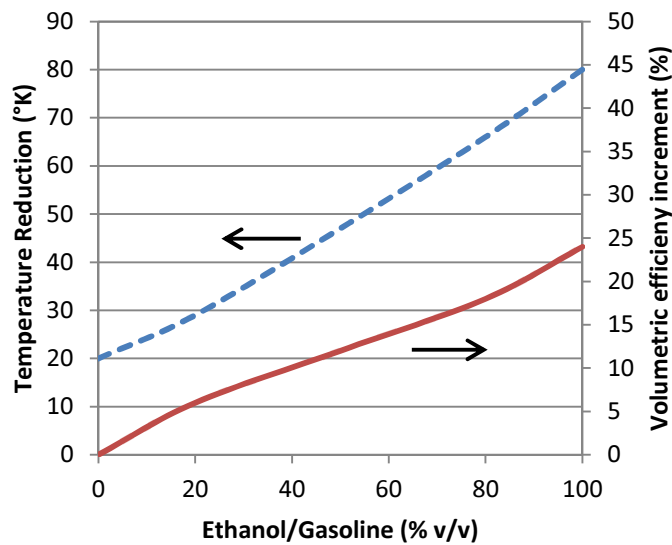


Figure 4.6- Variation of in-cylinder temperature reduction and volumetric efficiency increment with volume based ethanol/gasoline ratio. It was assumed that there was no fuel wall wetting and instantaneous evaporation at intake air conditions (constant pressure, 50° C Temperature, data from[86])

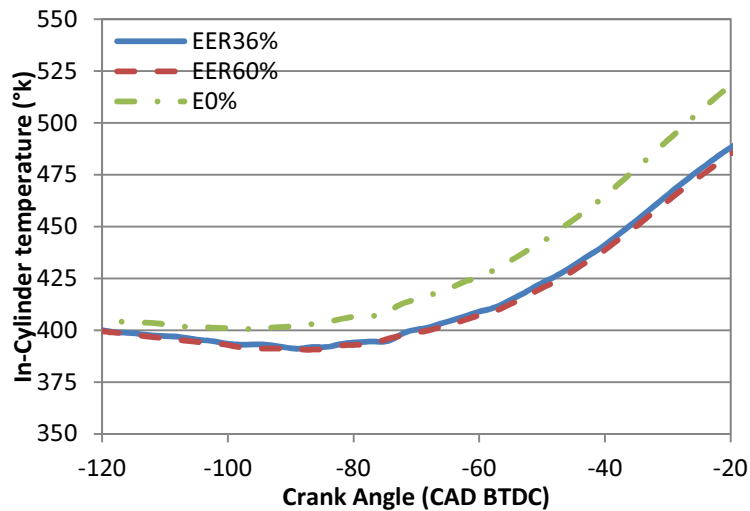


Figure 4.7–In-cylinder temperature before combustion (3500rpm, Spark timing 15 CAD BTDC, light load)

The increased volumetric efficiency means that the mass of air per engine cycle increases, which enables far more fuel to be burned and more work to be done per cycle, thus allowing for the increase of power produced by the engine. In fact, not only more fresh charge enters into the cylinder, but also the energy content of the mixture increases when using ethanol fuel. Although the energy content of ethanol/gasoline fuel blends decreases with the increase of the ethanol percentage due to the low lower heating value of ethanol (Table 3.3), the energy content of

ethanol/gasoline stoichiometric air mixture actually increases as the ethanol content increases. Figure 4.8 shows the LHV of stoichiometric per unit mass of air and LHV of ethanol/gasoline air mixture. As shown in Figure 4.8, the LHV of ethanol/gasoline mixture per volumetric of air actually increases with the increase in ethanol content. When it converts to per unit mass of air, it can be seen that at 60% of ethanol/gasoline, the LHV of stoichiometric per unit mass of air is about 3.0% higher than that of pure gasoline. This 3.0% increment in the stoichiometric mixture energy content works together with the 4.5% increment in volumetric efficiency and in such a way contributes to a total energy flux increase of around 7.6%.

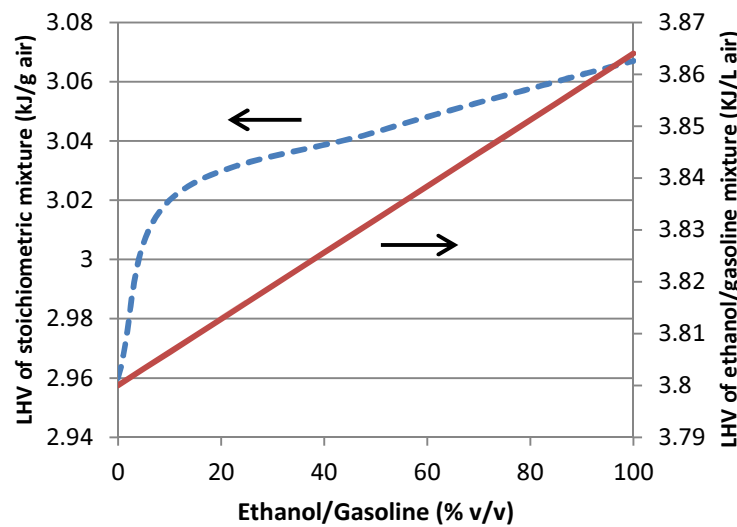


Figure 4.8—Variation of LHV per unit mass of air and LHV of ethanol/gasoline air mixture with volume based ethanol/gasoline ratio (data from [47])

Differences in the ratio of constant pressure to constant volume heat capacity

As stated in the last section that the 7.6% of IMEP improvement accounts for the increased volumetric efficiency and the energy content of per unit mass of air, the rest of the increases in IMEP can be attributed to the higher efficiency of ethanol fuel combustion. The factors that contribute to the increase in combustion efficiency include the ratio of constant pressure heat capacity to constant volume heat capacity (γ) and the change in the number of moles during the combustion process (mole multiplier effect).

For the change of γ , the first law of thermodynamics is used for further explanation [146].

$$\frac{W}{n} = -\frac{R \cdot T_1}{\gamma - 1} \times \left[\left(\frac{P_2}{P_1} \right)^{(\gamma-1)/\gamma} - 1 \right]$$

Equation 4.1

Here R is the universal gas constant, n is the number of moles, T_1 is the initial temperature, and P_1 and P_2 are the initial and final pressures. The equation 4.1 can be further written as equation 4.2 by substituting the pressure terms in equation 4.1 with volume terms in equation 4.2. Here V_1 and V_2 are the initial and final volumes in a process 1-2. In this way, the equation is more applicable to describe engine expansion and compression work which have a fixed displacement and clearance volumes. It is noted that the thermodynamic work discussed in this section is in a reversible and adiabatic gas system.

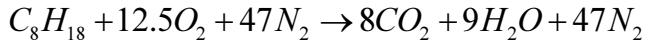
$$W = -\frac{n \cdot R \cdot T_1}{\gamma - 1} \times \left[\left(\frac{V_2}{V_1} \right)^{\gamma-1} - 1 \right]$$

Equation 4.2

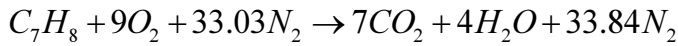
γ relates to the amount of work for the compression process and the amount of work that can be extracted from the expansion process. From an efficiency standpoint, high γ can improve the Otto cycle efficiency, as described in equation 4.1. When more work is done on the work fluid during the compression process, the temperature and pressure at the end of compression process are higher. This results in a greater ΔP and more net work is done. If the compression and expansion process are treated separately, things become a little different. For the compression process, if the γ is decreased, less work will be required for a specific ΔV . For an expansion process, a low γ reduces the work output from a given initial temperature and pressure, as it is described in equation 4.2.

To qualify the γ , fuels (Iso-octane, toluene) with known molecular weights are used instead of the real gasoline. Thus the composition in both the compression and expansion process are

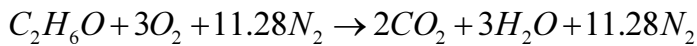
known by balancing the stoichiometric equation for these fuels, as they are described in Equations 4.3 to 4.5.



Equation 4.3



Equation 4.4



Equation 4.5

Using the thermodynamic data from reference [156] [157], γ is calculated as a function of temperature and a function of the ethanol/gasoline ratio and this is shown in Figures 4.9 and 4.10.

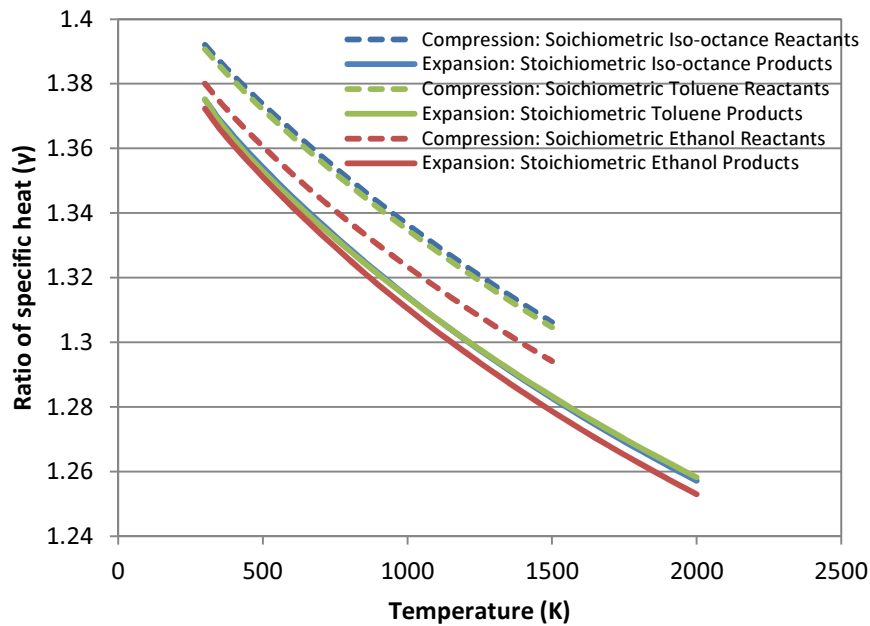


Figure 4.9–Variation of γ with temperature at stoichiometric air/fuel reactants and complete stoichiometric products (data from [156] and [157])

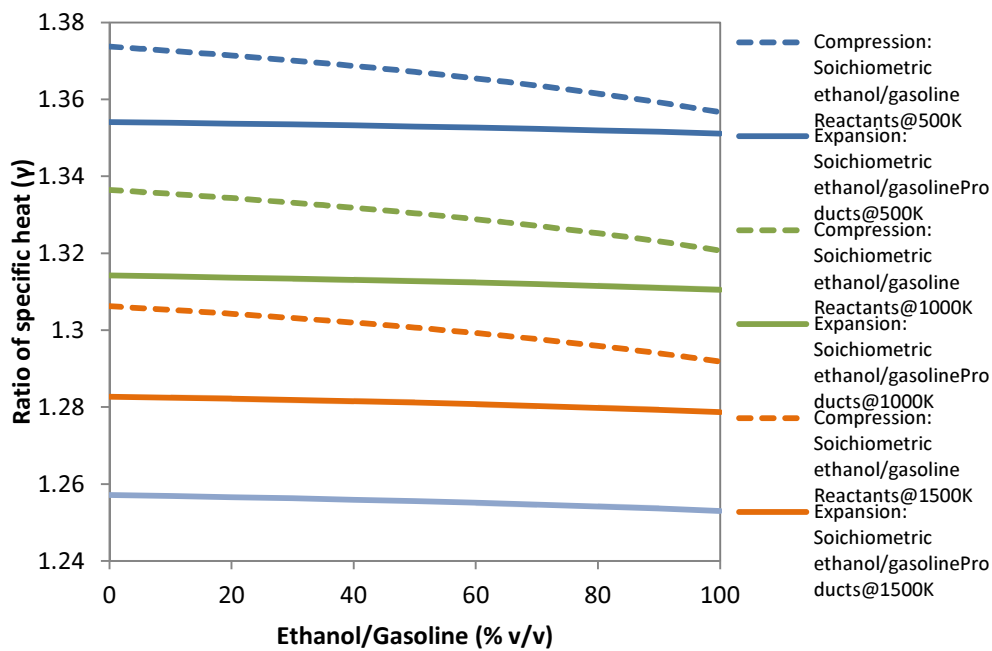


Figure 4.10–Variation of γ with ethanol/gasoline ratio (data from [156] and [157])

From Figures 4.9 and 4.10 it can be seen that, the γ of the ethanol stoichiometric mixtures is on average 1% lower than the Iso-octane in the compression process and it is about 0.33% lower during the expansion process. As mentioned previously, the lower γ is favourable in terms of improving the efficiency of the compression process but it can negatively affect the expansion process. The engine combustion process may benefit from the differences of γ when using ethanol fuel. However, the specific changes that the γ may exert on the engine efficiency are hard to qualify in this research due to the lack of many boundary conditions.

Change in combustion products moles

The change in combustion products moles, denoted as mole multiplier effect, is defined as the ratio of the number of product moles (n_{products}) to the number of reactant moles ($n_{\text{reactants}}$). It accounts for the change in the number of moles during the combustion and directly affects the n term in equation 4.2. It should be noted that the fresh air and mixture are assumed as an ideal gas in the whole process. From the stoichiometric equation of ethanol ($\text{C}_2\text{H}_6\text{O}$) and gasoline ($\text{C}_7\text{H}_{13.3}$), the variation of the mole multiplier with the ethanol content can be easily calculated, and this is displayed in Figure 4.11. As it is shown, the mole multiplier of the blends gradually increases as there is an increase in ethanol content. So the final cylinder pressure may increase

due to this change. At an ethanol/gasoline ratio of 60%, the mole multiplier is 1.061. So the final cylinder pressure of combusting E60 should be 1.4% (1.061/1.046) higher than using pure gasoline. It should be noted that conventional combustion analysis methodologies do not account for any increase in the number of the in-cylinder moles. As a result, there is an inherent error in the calculation of the in-cylinder temperature that is calculated from the pressure trace.

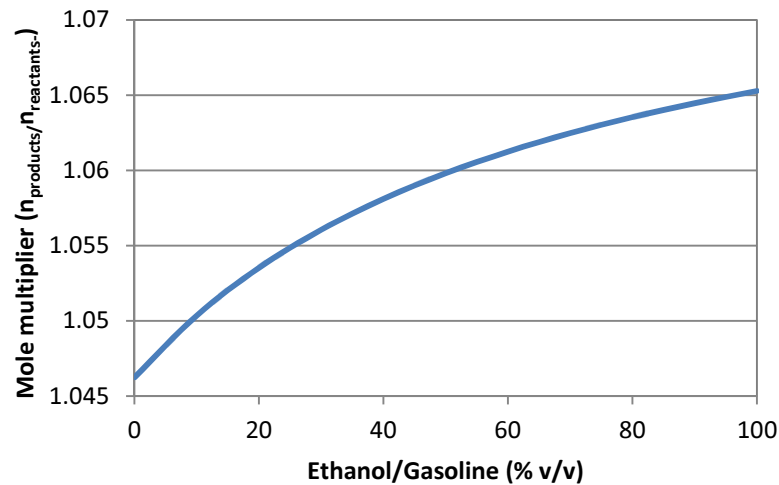


Figure 4.11–Variation of mole multiplier with ethanol/gasoline ratio

Reduced heat losses

The laminar flame speed of ethanol is 39 cm/s which is about 18% higher than that of gasoline (33 cm/s). This 18% increase in laminar flame speed contributes to the short combustion duration of mixtures containing ethanol. As it was reported by Ormman et al. [158] and Charoenphonphanich et al. [159], who conducted their experiments in constant volume bombs, the combustion duration of ethanol/gasoline blends gradually decreased with the increase in ethanol content. In pure ethanol conditions, the combustion duration was about 5ms shorter than that in gasoline conditions. The decreased combustion duration indicates that the ethanol content mixtures can release their heat more intensively and this results in less heat losses through the cylinder-wall. However, it should be noted that in an engine, the effective flame speed is a function of both the laminar flame speed and the turbulent combustion speed the latter of which is also dependent on different engine configurations and working conditions. So the effective flame speed could be up to two orders of magnitude faster.

The combustion of ethanol fuel results in around 30% more triatomic molecules than gasoline, as is illustrated by the chemical reaction formulae of equations 4.6 and 4.7.



Equation 4.6



Equation 4.7

This increased triatomic molecules means that the ethanol's combustion gas heat capacity is larger than that of gasoline and the combustion gas temperature is low.

Similar results can also be drawn by analysing the ideal gas law which is described as $P=nRT/V$. If assuming P, R and V are constant, then the term n and T have an inverse relationship. The term n of ethanol containing mixtures is higher than gasoline. So the temperature required for a given cylinder pressure is lower. The lower temperature of ethanol combustion can result in less heat loss through the combustion chamber walls and engine efficiency is therefore increased. Sezer et al. [160] and Marriot et al. [161] studied the effect of mixtures containing ethanol on heat losses numerically and experimentally. Their results of their studies supported this analysis.

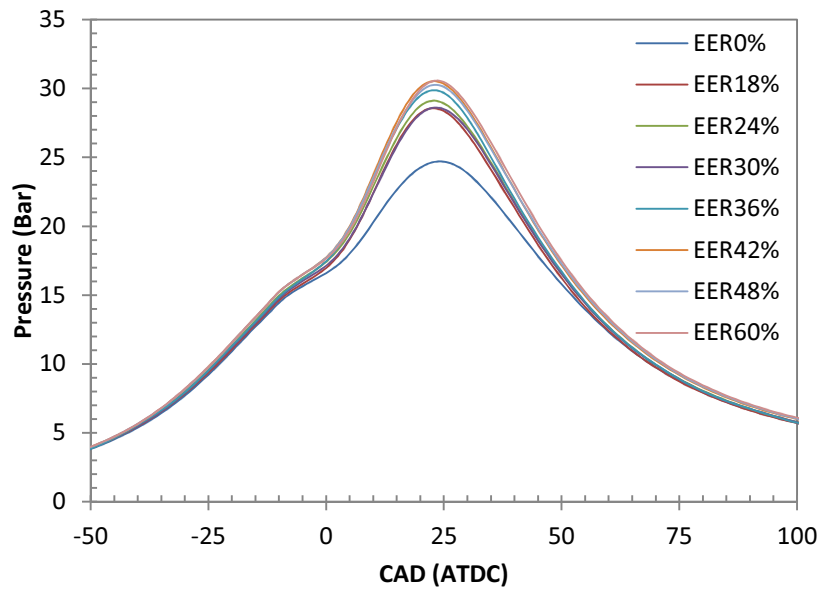
The above theoretical analysis of the fuel properties shows that the low γ at compression stroke and mole multiplier effects of ethanol fuel may contribute to the improvement of engine thermal efficiency.

4.1.3 Combustion characteristics

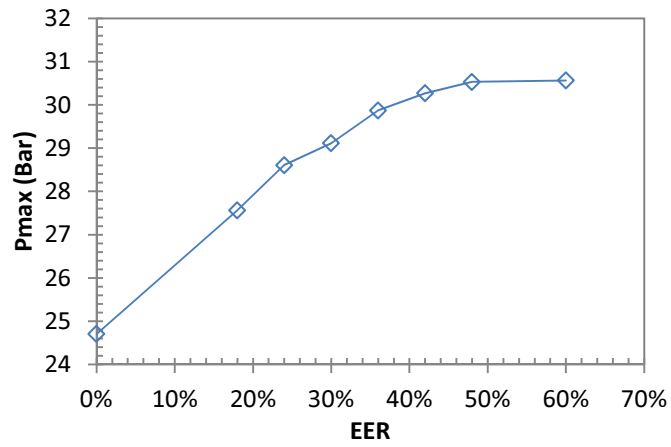
To understand the leveraging effect of using ethanol fuel on engine performance and emissions, combustion characteristics and emission results are presented and analysed in this subsection.

Figure 4.12 (a) shows the variation of cylinder pressure with the crank angle for eight different EER values varying from 0% to 60%. The corresponding peak cylinder pressure varying with EER is shown in Figure 4.12 (b). As shown in both Figures, the increase of EER results in the peak pressure increased from 24.7 Bar to 30.5 Bar. The occurrence of the peak pressure is slightly more advanced with the increase of EER (0% at 24 CAD BTDC, 24% at 23 CAD BTDC, 48% at 23 CAD BTDC and 60% at 18 CAD BTDC). When compared to gasoline fuel's combustion velocity, this can be attributed to the increase of volumetric efficiency and the mole multiplier effect plus ethanol fuel's higher flame propagation speed.

Figures 4.13 (a) and 4.13 (b) illustrate the heat release rate and central combustion phasing, CA50 derived from the same pressure data as that for the results shown in Figures 4.12 (a) and 4.12 (b). As shown in Figure 4.13 (a), the heat release rate at the beginning of the combustion process is almost independent of the EER. However, after that, the heat release rate increases rapidly with the increase of EER. The peak value of the heat release rate also increases with the increased EER. CA50 describes the crank angle position where the accumulated heat release reaches 50% of the total released heat. The CA50 of an effective engine should occur after the TDC. Smaller CA50 means that work is done more effectively by the combustion product on the piston which is at a position close to but just after the TDC. As shown in Figure 4.13 (b), the CA50 degree is 24 CAD after the TDC with 0% ethanol fuel and it reduces to 20 CAD when the EER is increased to 24%. It is further reduced to 17 CAD when the EER is 60%. The reduced CA50 with the increased EER indicates that the timing for 50% of the fuel burnt is gets closer to the TDC, so that the work done by the combustion product on the piston increases with the increased EER.

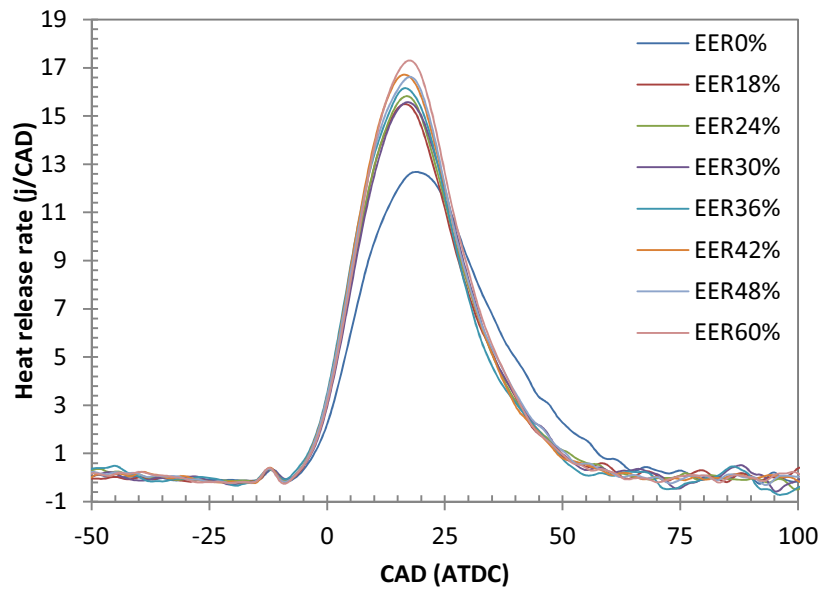


(a) In-cylinder pressure trace

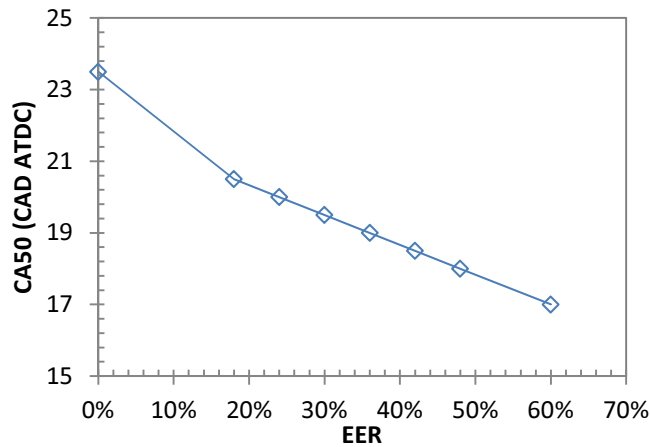


(b) Maximum In-cylinder pressure

Figure 4.12– In-cylinder pressure trace and maximum in-cylinder pressure at different EERs at 3500rpm



(a) Heat release rate



(b) CA50

Figure 4.13– Heat release rate and CA50 at different EERs at 3500rpm

The combustion initiation duration (CA0-5%) is defined by the crank angle degrees starting from the spark timing and ending when 5% of the fuel mass is burnt. It is one of the parameters characterising the combustion quality. CA0-5% is affected by the in-cylinder temperature and pressure, mixture quality and fuel properties. Normally, short CA0-5% means better combustion stability and quality. Figure 4.14 illustrates the variation of CA0-5% with EER at two engine loads and 3500rpm. It can be seen that the CA0-5% first decreases with the increase of EER until it reaches 42% at light load and 36% at medium load. It then gradually increases with a further increase of EER. The decrease of CA0-5% may be attributed to the low ignition energy required and higher flame velocity of ethanol fuel, which permits the ethanol/gasoline fuel

mixture to be more easily ignited and to burn faster. The increase of CA0-5% with the further increase of EER may be because of ethanol's greater latent heat of vaporisation which decreases the in-cylinder temperature and offsets the speed of flame growth.

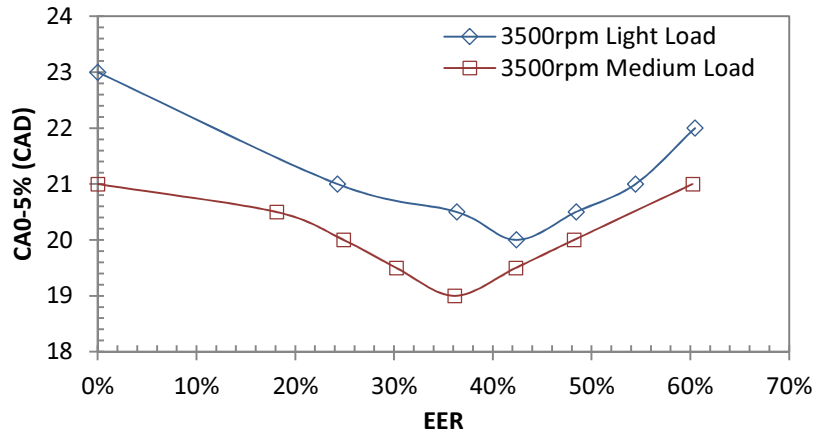


Figure 4.14–Variation of CA0-5% with EER

The early combustion duration, CA5-50%, is defined as the time period for 5-50% of the fuel mass to be burnt and it is often used to locate the combustion phase and evaluate the combustion efficiency. The variation of CA5-50% with EER is shown in Figure 4.15. As illustrated in Figure 4.15, the CA5-50% first decreases with the increase of EER. When EER is greater than 42% at light load and 36% at medium load, CA5-50% starts to increase with the increase of EER. As previously stated, the ethanol fuel has a faster laminar flame speed than gasoline fuel does, so a decrease of CA5-50% with EER is expected. However, due to the increased cooling effect of ethanol fuel, further increases of EER (greater than 42% at light load and 36% at medium load) may result in a lower in-cylinder temperature which reduces the flame speed and leads to an increase of CA5-50%. As the CA5-50% is reduced or prolonged, the location of the center of combustion phasing varies and this may have a major effect on the variation of the engine indicated thermal efficiency especially in the stage where engine tests have a fixed spark timing of 15 CAD BTDC.

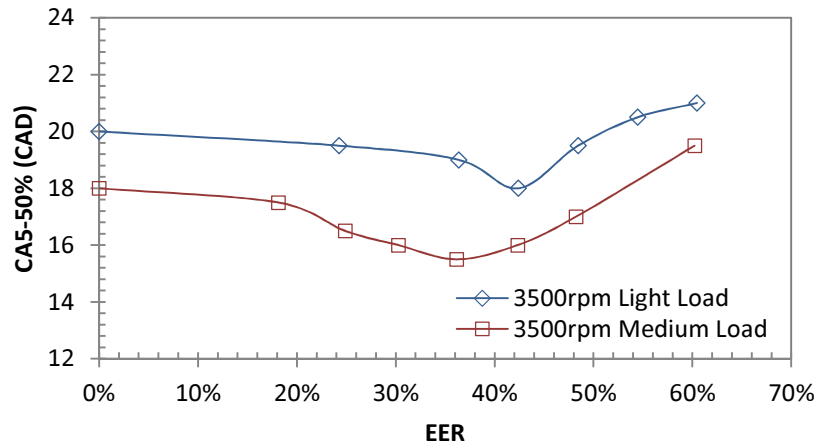


Figure 4.15–Variation of CA5-50% with EER

The major combustion duration, CA5-90%, is defined by the crank angles starting with 5% of the fuel mass burnt and ending with 90% of the fuel mass burnt as shown in Figure 4.16. It directly affects the engine thermal efficiency. The longer the combustion duration is, more heat will be lost through the cylinder wall. Consistent with the trends in Figures 4.12 (a) and 4.12 (b), the CA5-90% first decreases with the increase of EER when the EER is less than 42% at light load and 36% at medium load. When EER is greater than 42% at light load and 36% at medium load, the CA5-90% increases with the EER.

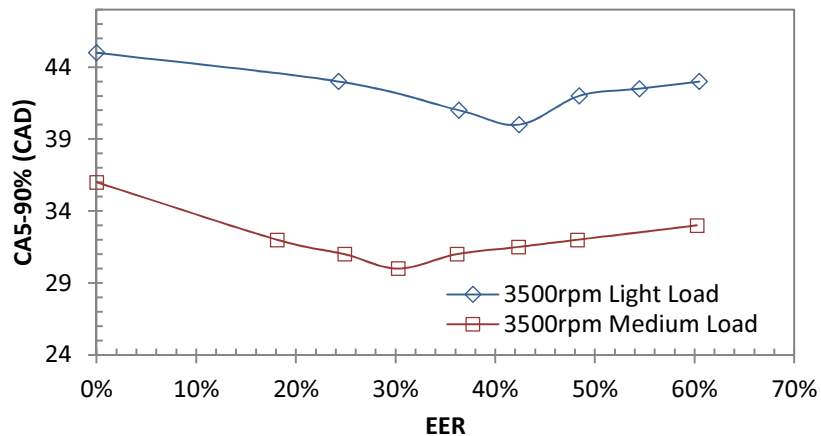


Figure 4.16–Variation of indicated CA5-90% with EER

To examine the stability of the combustion, the cycle-by-cycle variation is presented by the coefficient of variation (COV_{IMEP}). Figure 4.17 shows the COV_{IMEP} . As shown in Figure 4.17, the COV_{IMEP} decreases with the increase in EER. However, in a light engine load, the COV_{IMEP} drops more quickly from 9.1% at an EER of 0% to 4.0% at an EER of 60%. In the medium

engine load, the COV_{IMEP} reduces relatively slowly from 7.1% at an EER of 0% to 5.4% at an EER of 48% and then it becomes quite stable until it is 4.9% at an EER of 60%. It is assumed that the reduced combustion duration (Figure 4.16) contributes to the decreased cyclic variation. The higher laminar flame propagation speed and better low temperature combustion stability of ethanol fuel may also contribute to the decrease of COV_{IMEP} in this study.

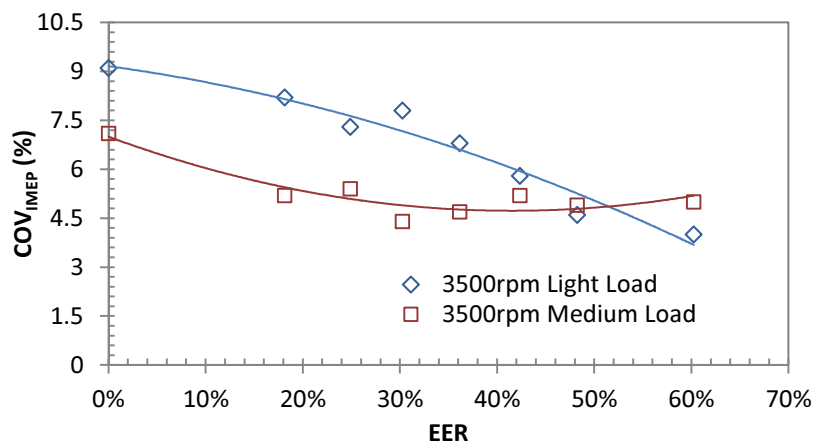


Figure 4.17–Variation of COV_{IMEP} with EER

The variation of indicated thermal efficiency with EER in Figure 4.18 is consistent with and can be well explained by the results of the combustion characteristics shown in Figures 4.14, 4.15 and 4.16. As shown in Figure 4.18, the indicated thermal efficiency increases with the increase of EER. When the EER is greater than 42% at light load or 36% at medium load, the increase of indicated thermal efficiency begins to slow down. EER of 42% at light load and 36% at medium load are critical values. When EER is less than the critical value the combustion characterised by CA0-5%, CA5-50% and CA5-90% is improved with the increase of EER. In combination with other factors such as ethanol’s high energy content of stoichiometric mixture per unit mass of air and mole multiplier effect, improved combustion results in the increase of indicated thermal efficiency. When EER is greater than the critical value, the combustion duration is prolonged (Figure 4.16). Fortunately, this negative effect is not dominating. Therefore, the indicated thermal efficiency is maintained without reduction and it continues to increase but slowly.

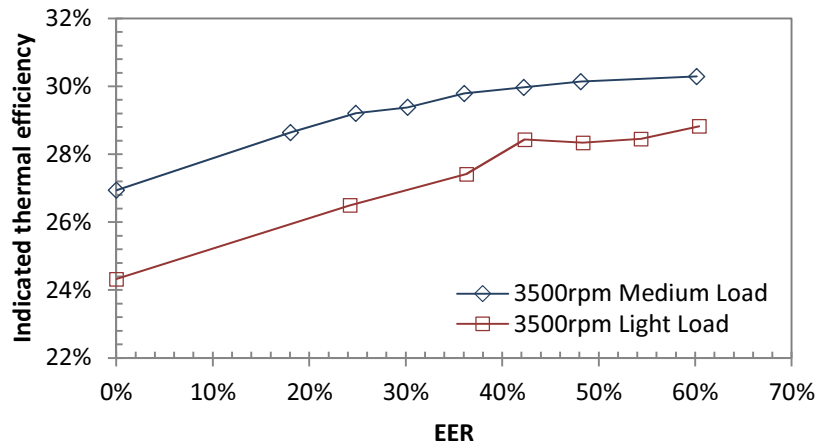


Figure 4.18–Variation of indicated thermal efficiency with EER

4.1.4 Emissions

Figure 4.19 shows the variation of indicated specific hydrocarbon (ISHC) emission with EER at light and medium load and speed from 3500rpm to 5000rpm. As shown in Figure 4.19, the ISHC in light engine load conditions first slightly decreases with the increase of EER. When the EER is larger than 24%, the ISHC begins to increase with the increase in EER. Note that there is a leap of ISHC at light load conditions when the EER is over 42%. The ISHC in medium load conditions almost stays stable until EER reaches 36%. Then it begins to increase with further increases of EER. The decrease of ISHC when the EER is less than 18% at medium load and 24% at light load may be due to the combustion improved by the ethanol fuel’s high flame speed and oxygen content property. The increase of ISHC with the increase of EER may be caused by three factors. The first one is the poor mixture quality and wall-wetting effect caused by ethanol fuel direct injection. The second one is that the increased cylinder pressure may result in more hydrocarbons being trapped in the crevice volumes. The third factor is that the lower in-cylinder temperature caused by ethanol direct injection results in less oxidation taking place when the trapped hydrocarbons get released (in the exhaust stroke) from the crevices. When EER is larger than 42% at medium load, the increased ethanol direct injection amount may lead to the fuel’s incomplete vaporization before ignition and sever wall-wetting, thus resulting in incomplete combustion and substantially increase of ISHC. Low in-cylinder temperature at high EERs (EER.>42%) may also be one of the factors as it is evident in Figures 4.16 that the major combustion duration is elongated owing to the reduced in-cylinder temperature.

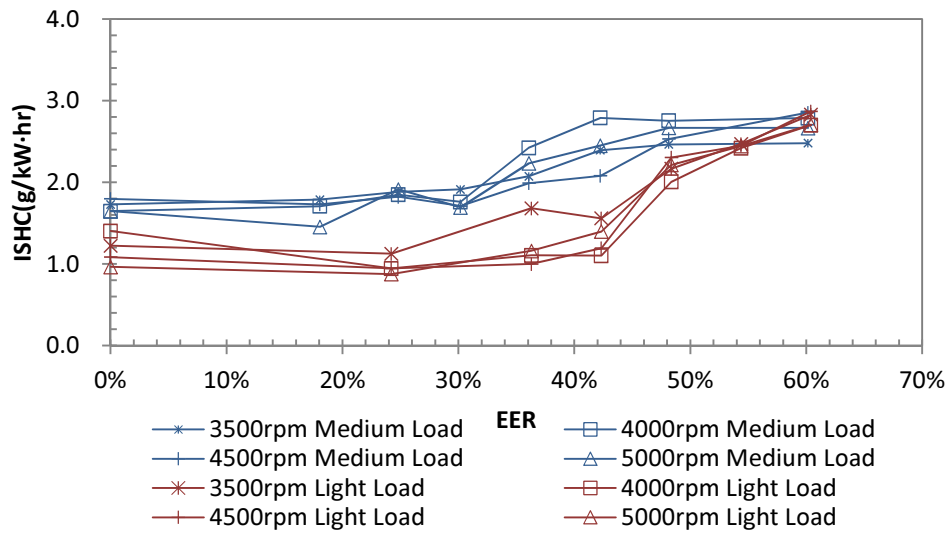


Figure 4.19–Variation of ISHC with EER

The variation of indicated carbon monoxide (ISCO) emission with the EER is shown in Figure 4.20. As shown in the figure, the ISCO first decreases with the increase of EER. When the EER is greater than 18% at medium load and 24% at light load, the ISCO begins to increase. There is also a leap of ISCO when the EER is over 42% in light load conditions. As CO is a product of incomplete combustion, the decrease of ISCO may also be due to the ethanol fuel’s fast laminar flame speed and oxygen content property. The increase of ISCO may be caused by poor ethanol fuel mixture quality, wall-wetting effect and a low in-cylinder temperature when the percentage of ethanol fuel is great. This is because the formation of CO emissions is mainly controlled by local AFR, and mixture inhomogeneous and wall-wetting may easily lead to high CO [146].

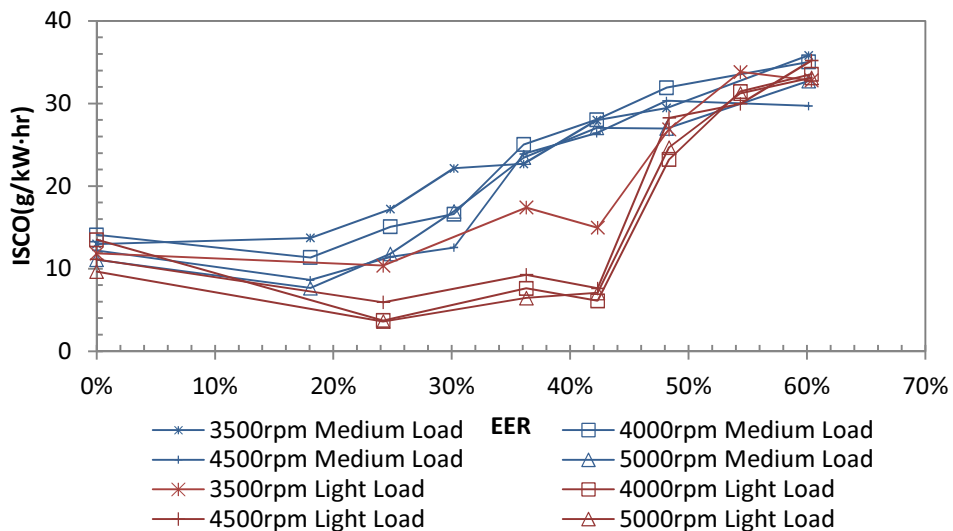


Figure 4.20–Variation of ISCO with EER

The variation of indicated specific nitrogen oxides (ISNO) emission with EER is shown in Figure 4.21. As shown in Figure 4.21, the ISNO first increases with the increase of EER when the EER is less than 18% at medium load and 24% at light load. When the EER is greater than those two percentages, the ISNO begins to decrease with further increases of EER. It is well known that NO emissions increase with the increase of the in-cylinder temperature. As discussed above, at low EER (lower than 18% at medium load and 24% at light load), the increase of EER may accelerate the combustion speed as well as the combustion temperature which is the necessary condition to form NO emissions. Therefore, the ISNO increases. However, further increase of EER would decrease the in-cylinder temperature due to the charge cooling effect. Thus the ISNO decreases.

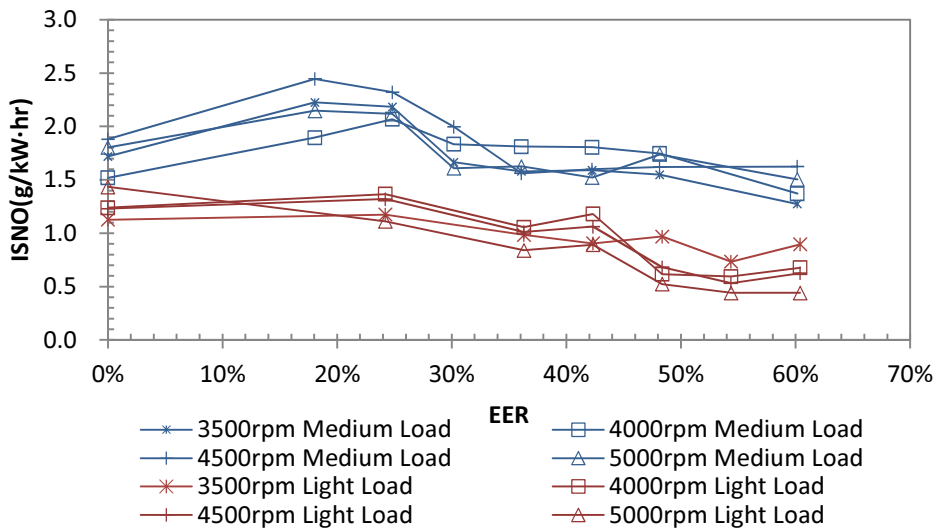


Figure 4.21–Variation of ISNO with EER

4.2 Comparison of EDI+GPI with GDI+GPI

4.2.1 Engine performance

In order to further identify the effect of EDI+GPI on improving engine performance, the comparison of EDI+GPI and GDI+GPI will be made and presented in this section. The experimental procedures in this study were similar to that presented in Section 4.1. The engine was first warmed up with gasoline fuel only. When the lubricant oil temperature reached the designated range of 398 ± 5 K, the PFI fuel was reduced and the DI fuel was increased to maintain the engine load unchanged in each test condition. For each engine load, the throttle position was set at a fixed position. The injection pulse-widths of gasoline and ethanol were

adjusted to keep stoichiometric AFR. All of the experiments were carried out at fixed injection timing of 300 CAD BTDC, spark timing of 15 CAD BTDC and engine speed of 3500rpm. The DI pressure was fixed at 40 Bar when the DI/PFI energy ratio was less than 48% for ethanol and 36% for gasoline. It was increased to 60 Bar at greater DI/PFI energy ratio. The engine experimental conditions for the results discussed in this section are listed in Table 4.2.

Table 4. 2 Experimental conditions for Section 4.2

Engine speed	3500rpm
Engine load	Medium (IMEP~7.0 Bar, Throttle ~35%); Light (IMEP~5.0 Bar, Throttle ~25%)
DI/PFI ratio	0%, 18% ^{#*} , 24% [#] , 30% [#] , 33% ^{&} , 36%, 42%, 48%
Injection timing	300 CAD BTDC
Injection pressure	40 Bar (When EER<48%) 60 Bar (When EER≥48%)
Spark timing	15 CAD BTDC

[#] Only for ethanol/gasoline dual fuel conditions; ^{*} Only for ethanol/gasoline dual fuel medium load conditions; [&] Only for gasoline/gasoline dual fuel medium load conditions

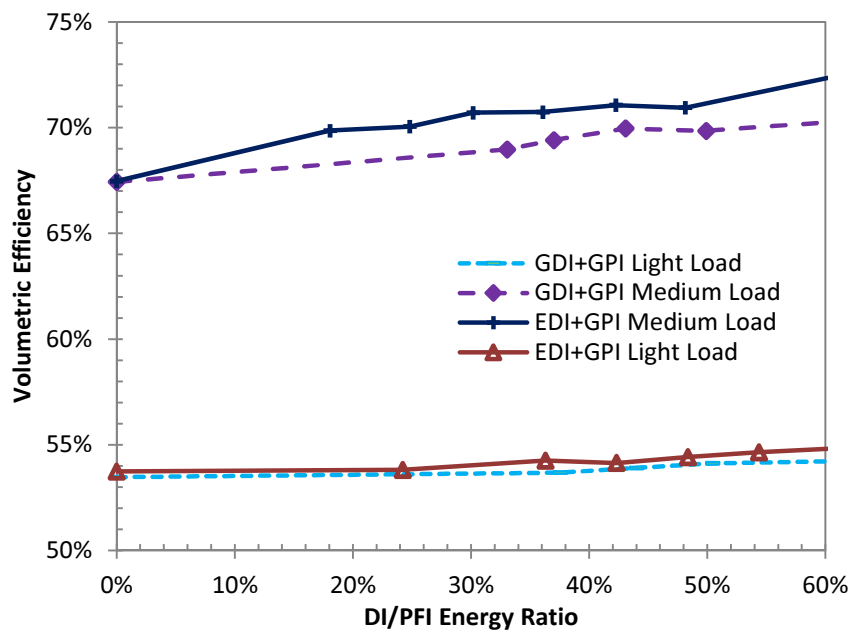


Figure 4.22–Variation of volumetric efficiency with DI/PFI energy ratio at 3500rpm

The variation of volumetric efficiency with the DI/PFI energy ratio at 3500rpm is shown in Figure 4.22. As shown in the figure, the volumetric efficiency in both EDI+GPI and GDI+GPI

conditions increases with the raise of the DI/PFI energy ratio. Since the latent heat of vaporisation of gasoline is only about 33% of ethanol (Table 3.3), the charge cooling effect of DI gasoline is less obvious than that of DI ethanol. As shown in Figure 4.22, volumetric efficiency in EDI+GPI conditions increases faster than that in GDI+GPI conditions at both light and medium engine loads. At light load, the volumetric efficiency in GDI+GPI conditions increases only by about 0.6% when the GDI/GPI ratio is increased from 0% to 60%, whereas in the EDI+GPI condition, the volumetric efficiency increases 1.2%. At medium load, the volumetric efficiency in the GDI+GPI condition increases about 2% and in the EDI+GPI condition, it raises 4.5%. This result well demonstrates the great effect of EDI on cooling the fresh charge and increasing its density, which finally results in the improved volumetric efficiency. It should be noted that although the charge cooling of fuel vaporisation plays an important role in improving volumetric efficiency, the reduced partial pressure of port injected fuel may also contribute to the increase of volumetric efficiency in both the EDI+GPI and GDI+GPI conditions. The details of this phenomenon are provided in the discussion for Figure 4.2.

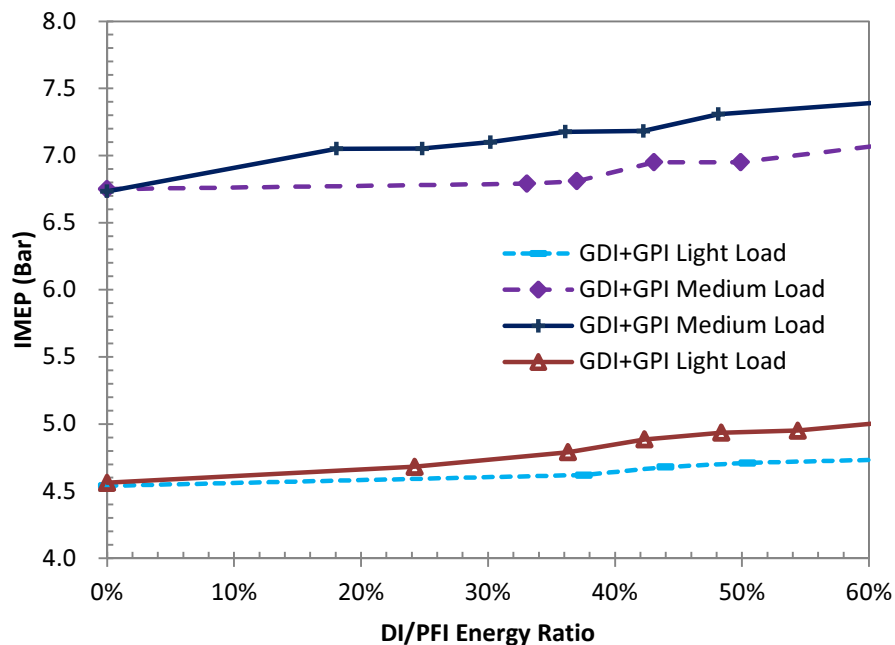


Figure 4.23–Variation of IMEP with DI/PFI energy ratio at 3500rpm

As the increment of volumetric efficiency in the GDI+GPI condition is less than that in the EDI+GPI condition, the IMEP is subsequently affected. It can be seen in Figure 4.23 that when

the DI/PFI energy ratio is increased from 0% to 60%, the increase of IMEP in the EDI+GPI condition is quicker than that in the GDI+GPI condition at both loads. This result is mainly because the engine tests were conducted at fixed throttle position. When the volumetric efficiency is increased, more fresh charge will flow into the cylinder, enabling far more fuel to be burned and more work to be done per cycle. Therefore, the IMEP increases with the increased volumetric efficiency. Additionally, for the EDI+GPI conditions, the aforementioned (Section 4.1.2) high energy content of the stoichiometric mixture per unit mass of air, mole multiplier effect and ethanol's high flame propagation speed may also contribute to the IMEP increment. For the GDI+GPI condition, the change of constant volume heat capacity (γ) makes a contribution to the increase of IMEP.

4.2.2 Combustion characteristics

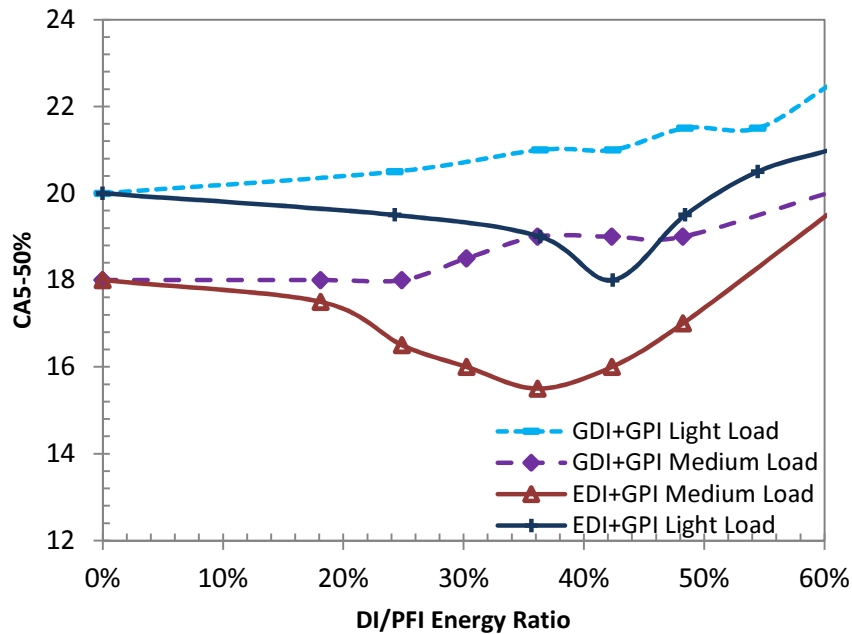


Figure 4.24–Variation of CA5-50% with DI/PFI energy ratio at 3500rpm

The early combustion duration (CA5-50%) and major combustion duration (CA5-90%) are presented in Figures 4.24 and 4.25 in order to compare the combustion characteristics of EDI+GPI and GDI+GPI. Here, a clear difference between EDI+GPI and GDI+GPI can be seen. As shown in Figures 4.24 and 4.25, the early combustion duration and major combustion duration in the GDI+GPI condition almost linearly increases with the increase of the DI/PFI

energy ratio, whereas in the EDI+GPI condition, it first decreases with the increase of the DI/PFI energy ratio and then it increases progressively with the further increase of the DI/PFI energy ratio. The CA5-50% in the GDI+GPI condition increases about 2.5 CAD for light load and 2 CAD for medium load when the DI/PFI energy ratio is increased from 0% to 60%. While in the EDI+GPI condition, the CA5-50% first reaches the minimum of 15.5 CAD at medium load and 18 CAD at light load. Then it gradually increases to 19.5 CAD and 21 CAD, respectively when the DI/PFI energy ratio reaches 60%. Similarly, CA5-90% in the GDI+GPI condition increases from 45 CAD to 48.5 CAD at light load and 36 CAD to 39 CAD at medium load when the DI/PFI energy ratio is raised from 0% to 60%. In the EDI+GPI condition, it first decreases to 39 CAD at light load and 30 CAD at medium load, then it gradually increases to 43 CAD and 33 CAD, respectively.

This difference in combustion characteristics further confirms that in certain DI/PFI energy ratio ranges (less than 36% for light load and 42% for medium load in this study), the EDI+GPI could result in better combustion performance than the GDI+GPI does due to ethanol's high volatility and fast laminar flame speed. The mechanism of this phenomenon has been discussed in Section 4.1.3. It will not be detailed in this part.

In the pure gasoline mode (GDI+GPI), the increase of combustion duration when EER is higher than 36% may be due to the deterioration of mixture quality because the gasoline contains more heavy fractions than ethanol, which make its vaporisation more difficult and incomplete than ethanol. Therefore, when the DI/PFI energy ratio increases, the mixture quality may exacerbate and combustion may be negatively affected. Additionally, the enhanced wall-wetting effect caused by the increased DI fraction may also contribute to the deterioration of mixture quality.

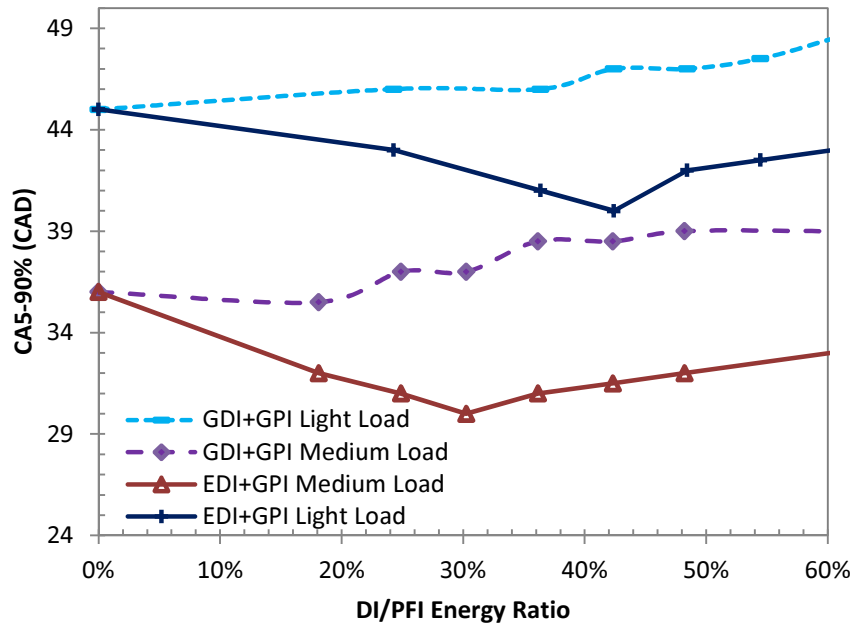


Figure 4.25–Variation of CA5-90% with DI/PFI energy ratio at 3500rpm

The differences in combustion characteristics and volumetric efficiency result in the difference in indicated thermal efficiency. As it can be seen in Figure 4.26, the indicated thermal efficiency in the EDI+GPI condition is increased faster than that in the GDI+GPI condition. Higher volumetric efficiency (Figure 4.22) and higher combustion conversion efficiency of ethanol fuel [65] should be the main reasons that lead to the higher indicated thermal efficiency. It can also be seen that the gap of indicated thermal efficiency between the EDI+GPI condition and the GDI+GPI condition reaches the maximum when the DI/PFI energy ratio is in the range between 30% and 45%. This large gap should be due to the relatively short combustion duration (Figures 4.25 and 4.26) in this range which advances the combustion phasing and reduces the heat losses, thus resulting in a higher indicated thermal efficiency. From the results presented in Figure 4.26, the following conclusions can be drawn. 1), DI can increase the engine efficiency in both EDI+GPI and GDI+GPI conditions due to the improved volumetric efficiency and the change of constant volume heat capacity (γ); 2), EDI is more effective than GDI in improving engine efficiency because of the enhanced charge cooling and optimised thermodynamic process (change in combustion products moles, less heat losses and high energy content of stoichiometric mixture per unit mass of air).

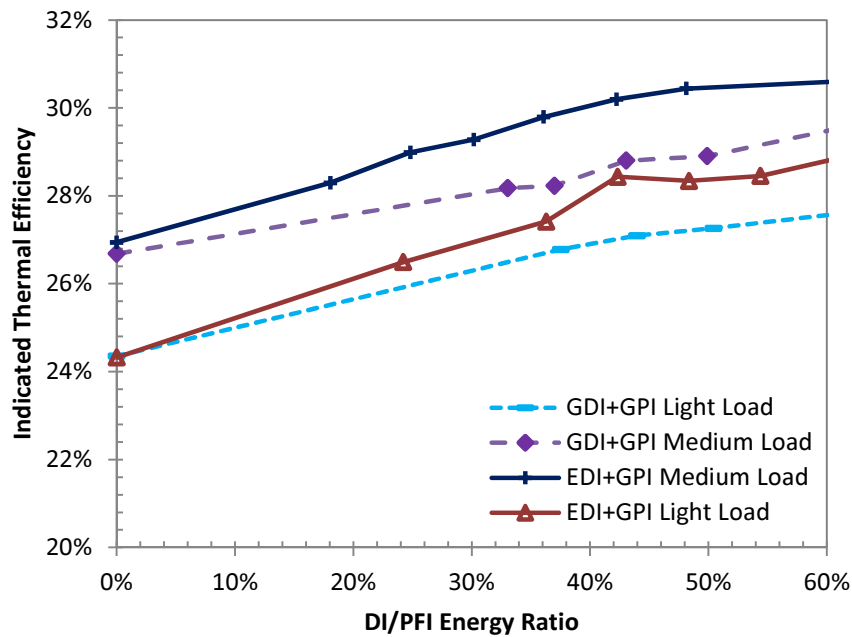


Figure 4.26–Variation of indicated thermal efficiency with DI/PFI energy ratio at 3500rpm

4.2.3 Emissions

The variations of ISCO and ISHC with the DI/PFI energy ratio at 3500rpm are shown in Figures 4.27 and 4.28. Compared with EDI+GPI condition, the variation of HC and CO emissions in the GDI+GPI condition is monotonous. Both ISCO and ISHC increase progressively with the increase in the DI/PFI energy ratio. The reduced mixture quality and increased wall-wetting should be the main reasons that cause the increase of CO and HC emissions.

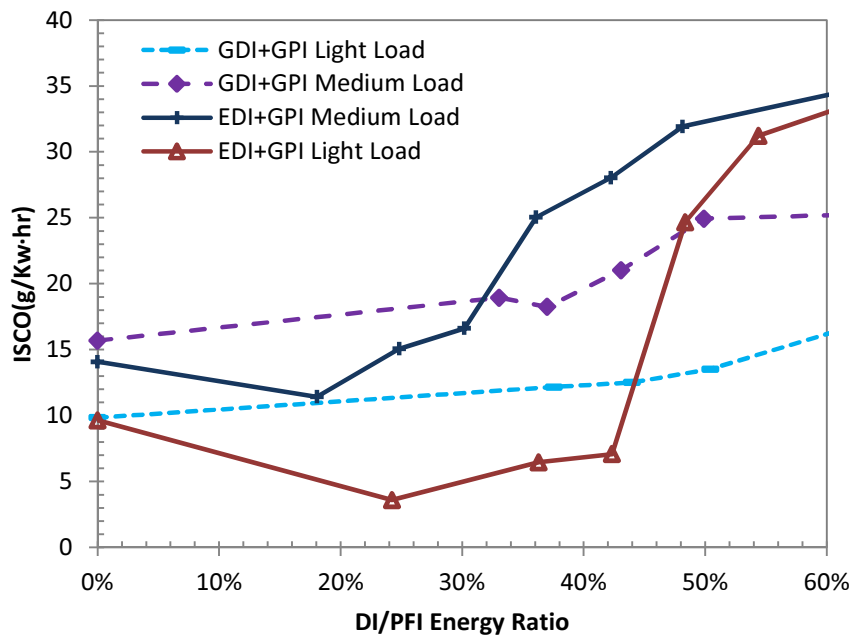


Figure 4.27–Variation of ISCO with DI/PFI energy ratio at 3500rpm

The variation of exhaust emissions in the EDI+GPI condition is different from that in the GDI+GPI conditions. The ISCO and ISHC first decrease with the increase in the DI/PFI energy ratio and reach the minimum. Then, both of these emissions increase sharply with a further increase in the DI/PFI energy ratio. The decrease of HC and CO emissions may be related to the high volatility of ethanol which improves the mixture quality, ethanol’s fast combustion speed which optimises the combustion process and ethanol’s oxygen content property which improves the oxidization process. The increase of ISCO and ISHC with the raise of DI/PFI energy ratio can be attributed to the over charge cooling of ethanol vaporisation and wall-wetting. When the DI/PFI energy ratio is greater than a certain range for example 45% at light load in both Figures 4.27 and 4.28, the great charge cooling of ethanol vaporisation may substantially reduce the in-cylinder temperature, which impedes the formation of the homogeneous mixture and therefore increases the CO and HC emissions. The ethanol’s low heat value is only about 60% of gasoline (Table 3.3). In order to main the same engine energy input, the quantity of DI fuel (ethanol) should be increased, thus causing severe wall-wetting, especially at high DI/PFI energy ratios. This wall-wetting effect may also contribute to the increase in CO and HC emissions.

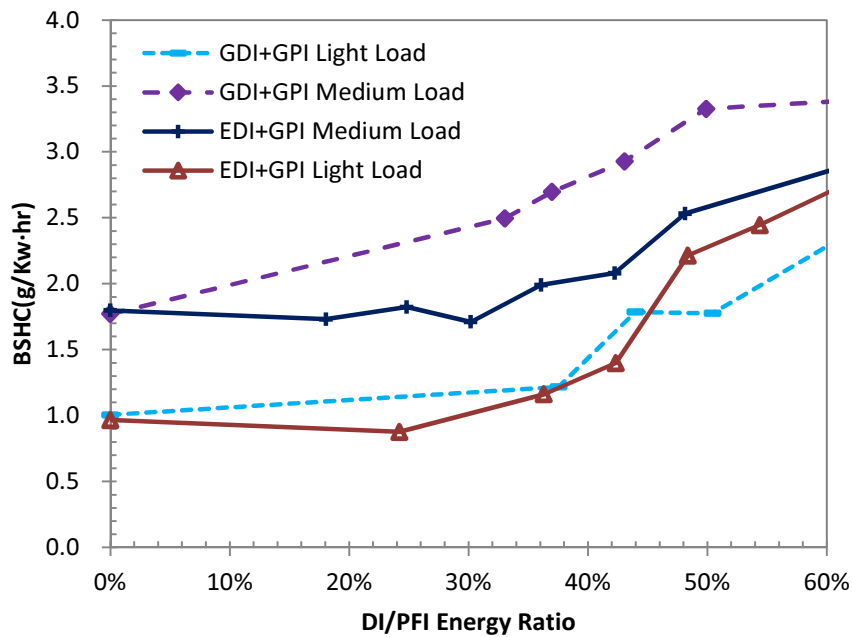


Figure 4.28–Variation of ISHC with DI/PFI energy ratio at 3500rpm

The variation of ISNO with the DI/PFI energy ratio is almost opposite to that of ISCO and ISHC. As shown in Figure 4.29, ISNO in GDI+GPI conditions slightly decreases with the increase in the DI/PFI energy ratio. ISNO in EDI+GPI conditions first increases with the increase in the DI/PFI energy ratio. When the DI/PFI energy ratio is greater than 25%, it begins to decline with further increases in the DI/PFI energy ratio. The increase of ISNO should be related to the decreased combustion duration around this ratio (Figures 4.24 and 4.25), which makes the mixture release its heat more intensively, and hence increases the in-cylinder temperature. Thus, the ISNO increases. Further increases in the DI/PFI energy ratio at greater than 25% in EDI+GPI conditions can lead to a great charge cooling effect and low adiabatic flame temperature, which decreases the cylinder temperature and combustion temperature and thereby results in a reduction of NO emissions. The linear decrease of ISNO in GDI+GPI conditions should be related to the charge cooling of gasoline vaporisation, however, this charge cooling effect is less obvious in GDI+GPI conditions than in EDI+GPI conditions. Therefore, NO emissions in GDI+GPI conditions are greater than those in EDI+GPI conditions when the EER is larger than 42%.

GDI+GPI can only change the ratio between DI gasoline fuel and PFI gasoline fuel, which is

unlike EDI+GPI that can change the mixture physicochemical properties due to the use of two different fuels. Increasing the DI ratio in the GDI+GPI condition only slightly enhances the charge cooling effect which increases the volumetric efficiency, and changes the mixture quality which influences the HC and CO emissions. However, in the EDI+GPI condition, the participation of ethanol in the combustion process directly affects the mixture burning rate, oxidization process and combustion temperature. Thus, in the EDI+GPI condition, the combustion and emissions show different trends at different DI/PFI energy ratios.

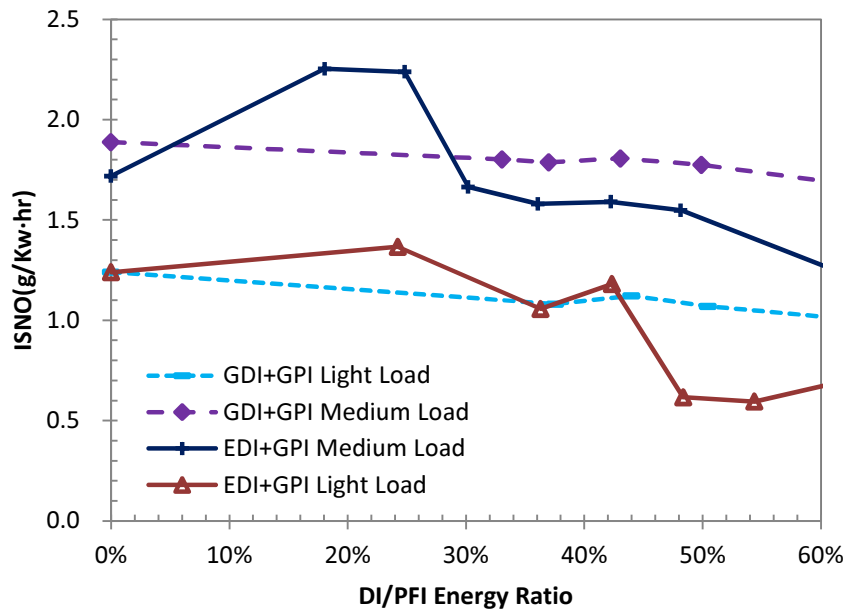


Figure 4.29–Variation of ISNO with DI/PFI energy ratio at 3500rpm

4.3 Summary

1. The IMEP increased with the increase of EER. Possible reasons that contributed to the IMEP increment include the charge cooling effect, high LHV per unit mass of air, an increase in the ratio of constant pressure to constant volume heat capacity, an increase in products moles, reduced heat loss and an improved combustion process. ISEC was decreased with the increase of EER. This indicates that to achieve the comparable engine IMEP, less energy input will be required in a SI engine equipped with EDI+GPI. Hence the total fuel consumption could be reduced by the leveraging use of ethanol fuel.

2. At 3500rpm, the initial combustion period (CA0-5%), early combustion period (CA5-50%) and major combustion period (CA5-90%) decreased with the increase of EER when the EER was less than 42.4% at light load and 36.3% at medium load. However, further increase of EER would deteriorate the combustion leading to the elongation of CA0-5%, CA5-50% and CA5-90%. The combustion temperature reduced by over cooling effect may be one of the major causes.

3. ISHC and ISCO first decreased with the increase of EER and then increased with further increases of EER when the EER was greater than 18.0% at medium load and 24.0% at light load. ISNO displayed an opposite trend with ISHC and ISCO. It first increased with the increase of EER when it reached 24.2%, then it decreased with the further increase of EER.

4. Compared with EDI+GPI conditions, the volumetric efficiency in GDI+GPI conditions only slightly increased with the increase in the DI/PFI energy ratio. Combustion characteristics of CA5-50% and CA5-90% elongated with the increase in the DI/PFI energy ratio and pollutant emissions of ISHC and ISCO increased with the increase in the DI/PFI energy ratio. These results indicate that GDI+GPI only leads to moderate improvements in engine performance and emissions. EDI+GPI, on the other hand, showed more obvious benefits in relation to combustion and emissions when the DI/PFI energy ratio was in a certain range (less than 36% for light load and 42% for medium load in this study).

Chapter Five

5. Leveraging effect of EDI enhanced by spark advance and inlet air pressure increment

5.1 Effect of spark timing on EDI+GPI engine

In a SI engine, spark timing is one of the main control parameters. It significantly affects the combustion which determines the fuel economy, torque output and engine emissions. In EDI+GPI engine, the change of the ethanol/gasoline ratio may lead to the change of the in-cylinder temperature, mixture homogeneous quality and the combustion characteristics. All these factors may alter the mixture combustion speed which requires the corresponding adjustment of spark timing to achieve higher efficiency and low emissions. The investigation on spark timing in the EDI+GPI engine is presented in this section.

The experiments were conducted at 3500rpm and light engine loads (IMEP was around 4.0 Bar) with spark timing swept from 25 CAD BTDC to 50 CAD BTDC (5 CAD intervals) at an EER range from 0% to 48% (0%, 29%, 34%, 39%, 41%, 48%). Ethanol SOI timing was fixed at 300 CAD BTDC for ensuring sufficient time to DI fuel evaporation. 29% was the minimum achievable EER in this part of the test due to the limitation of the injector's minimal opening pulse-width. When the engine lubricant oil temperature was stabilised at 368 K, the quantity of the gasoline fuel was reduced and the quantity of the ethanol fuel was increased until the designated EER was achieved. The rate of total fuel energy (ethanol and gasoline) was kept constant during the tests, while throttle position was adjusted to maintain AFR at stoichiometric value. The engine experimental conditions for this part of tests are listed in Table 5.1.

Table 5.1 Experimental conditions for Section 5.1

Engine speed	3500rpm
Engine load	Light (IMEP~4.0 Bar, Throttle=20%)
EER	0%, 29%, 34%, 39%, 41%, 48%
Injection timing	300 CAD BTDC
Injection pressure	40 Bar
Spark timing (CAD BTDC)	25, 30, 35, 40, 45, 50

5.1.1 Effect of spark timing on combustion at different EERs

In this section, the experimental results will be presented and discussed in three subsections: the effect of spark timing on combustion, emissions and efficiency. In each subsection, the same experimental result is plotted in two different figures. One has the spark timing as the horizontal axis and the other has EER as the horizontal axis. The reason for doing so is to show the variation of engine performance with spark timings and EERs separately. It should be noted that in the figures with EER as the horizontal axis, the EERs of 0% and 29% are connected with dash line because the engine performance in this EER span has not been tested, which is due to the limitation of the injector's minimal opening pulse-width that prohibits the investigation of lower EERs.

Figures 5.1 (a) and 5.1 (b) show the variation of IMEP with spark timing and EERs. As shown in Figure 5.1 (a), IMEP first increases with the advance of spark timing and reaches the maximum when the spark timing is in the range from 30 CAD BTDC to 35 CAD BTDC. After this spark timing range, it decreases gradually with further advances of spark timing. When the spark timing is later than 30 CAD BTDC, the ignition occurs too late, the expansion of combustion products take place at a relatively large cylinder volume and this leads to a reduction of work done on the piston and decreases the effective work (IMEP). When the spark timing is earlier than 35 CAD BTDC, the ignition is too early, the combustion of the mixture generates negative work which slows the piston speed and leads to the reduction of IMEP [80].

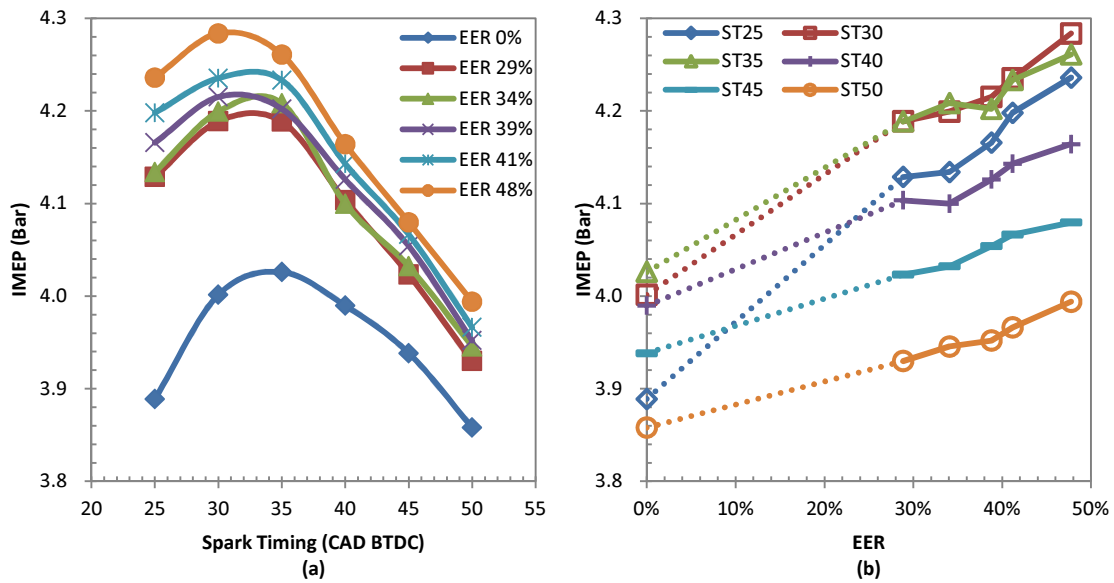


Figure 5.1–Variation of IMEP with spark timing (a) and EERs (b)

As shown in both Figures 5.1 (a) and 5.1 (b), IMEP reaches the maximum at the spark timing which ranges from 30 CAD BTDC to 35 CAD BTDC. This is also the spark timing range where the engine reaches the MBT. It should be noted that the MBT timing in this study is defined as the spark timing to produce the maximum IMEP for a fixed energy flow rate. Detailed analysis can be seen from Figure 5.1 (b) that the spark timing for the maximum IMEP changes with the increase of EER. When the EER is less than 29%, the IMEP at spark timing of 35 CAD BTDC is higher than that at 30 CAD BTDC. When the EER is in the range between 29% and 39%, the IMEP at these two spark timings (35 CAD BTDC and 30 CAD BTDC) is almost the same. With further increases of EER greater than 39%, the IMEP at spark timing of 30 CAD BTDC becomes greater than that at the spark timing of 35 CAD BTDC. Thus when EER is higher than 39%, later spark timing (30 CAD BTDC) is better than earlier spark timing (35 CAD BTDC) in maintaining the combustion phasing at its optimum level and this achieves the highest IMEP. Similar tests that found the use of ethanol could advance combustion phasing were reported in [162]. The result in Figure.5.1 (b) can be attributed to ethanol's higher laminar flame speed (39cm/s of ethanol vs. 33cm/s of gasoline) which decreases the combustion duration (Figure 5.4) and advances the combustion phasing (Figure 5.3). However, it should be noted that the effective flame speed is a function of both the laminar flame speed and the turbulent combustion speed of the gas mixture, which could be up to two orders of magnitude faster.

As shown in Figure 5.1 (b), when the spark timing is in the range between 25 CAD BTDC and 35 CAD BTDC, the gap between the IMEP at MBT timing (spark timing of 30 CAD BTDC or 35 CAD BTDC) and IMEP at spark timing of 25 CAD BTDC reduces with the increase of EER. This result indicates that with the increase of EER, the IMEP becomes less sensitive to the spark advance when it is around MBT timing. EER of 0% (GPI condition) is the condition which is the most sensitive to the advance of spark timing, as the gap between IMEP at 35 CAD BTDC (MBT timing at EER of 0%) and 25 CAD BTDC is greater than the gaps at other EER levels. When the EDI is used, the IMEP gap between spark timing at 25 CAD BTDC and MBT timing (spark timing at 30 CAD BTDC or 35 CAD BTDC) decreases gradually with the EER. This low spark timing sensitivity of IMEP in EDI conditions can be beneficial to the engine calibration by reducing HC and NO_x emissions [162]. In engine calibration, spark timing retard from MBT timing is often employed in order to reduce HC and NO_x emissions. If the spark timing sensitivity of a fuel to IMEP is low, the sacrifice for the engine power output will be less when the spark timing is retarded for reducing HC and NO_x emissions. Thus high efficiency and low emissions can be achieved simultaneously. Similar experimental results were also found by Daniel et al. [163]. They found that when the spark timing is around MBT timing, the IMEP in GPI conditions is more sensitive to the same spark timing advance or retard than that in gasoline plus ethanol dual-injection conditions.

From Figure 5.1 (b), it can also be seen that IMEP increases with EER at the fixed spark timing. However, at different spark timings, the IMEP shows different increments with the EER. At the spark timing of 25 CAD BTDC, the increase of IMEP with EER is quicker than that at other spark timings. At this timing, the IMEP increases from 3.89 Bar to 4.24 Bar when EER is raised from 0% to 48%. When spark timing is at 30 CAD BTDC and 35 CAD BTDC, the IMEP continues to increase with EER but slowly. The corresponding IMEP increment for 30 CAD BTDC and 35 CAD BTDC is 0.28 Bar and 0.23 Bar. When spark timing is earlier than 35 CAD BTDC, the increase of IMEP with EER is similar at the tested spark timings (40 CAD BTDC, 45 CAD BTDC and 50 CAD BTDC). About 0.15 Bar increment in IMEP is found when the

EER is increased from 0% to 48% at these spark timings. This difference in IMEP increment is resulted from different combustion performances at different spark timings as discussed later in Figures 5.2 to 5.5. This result also supports the discussion in Section 4.1.1 that at fixed spark timing the IMEP increases with the raise of EER. The possible mechanisms of the IMEP increment can be attributed to ethanol fuel’s high flame propagation speed, high energy content of stoichiometric mixture per unit mass of air, and the mole multiplier effect. Details can be referred to Section 4.1.3.

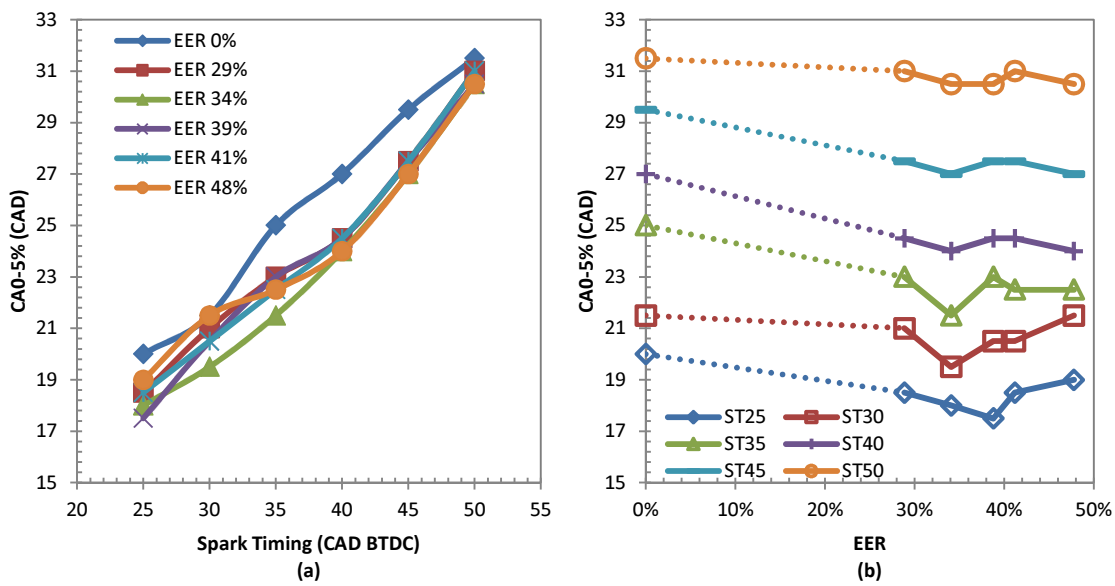


Figure 5.2–Variation of CA0-5% with spark timing (a) and EERs (b)

Figures 5.2 (a) and 5.2 (b) show the variation of CA0-5%. As shown in Figure 5.2 (a), CA0-5% decreases with the advance of spark timing. CA0-5% at spark timing of 50 CAD BTDC is on average 11 CAD longer than that at a spark timing of 25 CAD BTDC. The increase of CA0-5% with the advance of spark timing may be related to the time for mixture heat recovery. The earlier the spark timing is, the shorter the time available for heat recovery (heat transfer from cylinder chamber to fresh charge) will be [160]. Therefore, the in-cylinder temperature before combustion at early spark timing may be too low and then it will impede the flame propagation and prolong the combustion initiation duration.

In this work, the charge cooling effect and ethanol’s fast laminar flame speed may be the

important factors, apart from spark timing, to influence combustion. As shown in Figure 5.2 (b), the CA0-5% at all tested spark timings first decreases with the increase of EER and reaches the minimum when EER is in the range between 34% and 39%. The decrease of CA0-5% with the increase of EER may be caused by ethanol's fast laminar flame speed which leads to early laminar flame growth occurring at a faster rate. When the EER is greater than 39%, CA0-5% at different spark timings shows different trends. At spark timings of 25 CAD BTDC, 30 CAD BTDC and 35 CAD BTDC, the CA0-5% increases gradually with the raise in the EER level. In the spark timing range from 40 CAD BTDC to 50 CAD BTDC, the CA0-5% becomes almost stable with the increase of EER. The raise of CA0-5% at spark timings of 25 CAD BTDC, 30 CAD BTDC and 35 CAD BTDC when EER is greater than 39% may be due to the over charge cooling effect caused by the increased EDI amount. This over charge cooling may substantially reduce the in-cylinder temperature and hence lead to longer combustion initiation duration. The stable trend of CA0-5% at spark timing from 40 CAD BTDC to 50 CAD BTDC may be because a balance has been reached between the charge cooling effect and the faster laminar flame speed of ethanol. The effect of ethanol's fast laminar flame speed on reducing the combustion initiation duration is counterbalanced by the effect of charge cooling.

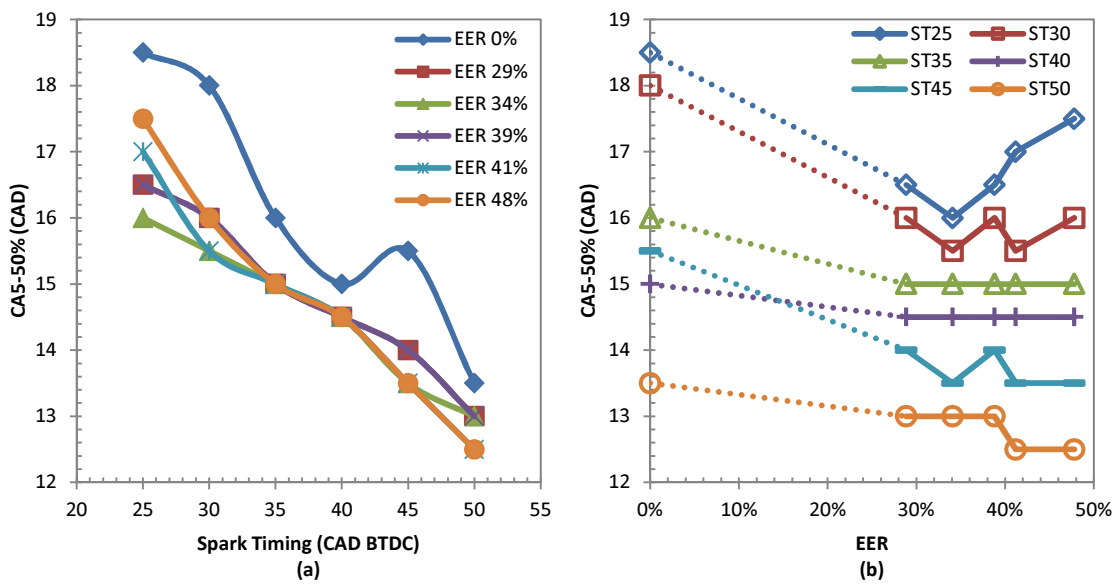


Figure 5.3–Variation of CA5-50% with spark timing (a) and EERs (b)

The variation of early combustion duration, CA5-50%, is shown in Figures 5.3 (a) and 5.3 (b).

This duration is presented here because the timing/crank angle for the 50 % mass burnt fraction is often used to locate the combustion phasing. It is also a period which is susceptible to combustion noise and combustion stability. From Figure 5.3 (a), it can be seen that when the spark timing is advanced from 25 CAD BTDC to 50 CAD BTDC, the CA5-50% decreases progressively. This is because when spark timing is advanced, more combustion occurs in a smaller in-cylinder volume (piston at or close to TDC) and hence the temperature rise is greater. This increase in temperature promotes combustion speed and reduces the combustion duration.

As mentioned in the discussion for Figure 5.2 (b), the charge cooling effect of ethanol vaporisation and ethanol's fast combustion speed are the two factors that influence the combustion initiation duration. Here, for CA5-50%, these two factors may also play an important role. From Figure 5.3 (b), it can be seen that when the EER is below 34%, the ethanol's fast combustion speed may dominate the trend as the CA5-50% decreases with the increase of EER. When the EER is greater than 34%, the charge cooling effect may become an important factor which works together with ethanol's fast combustion speed to affect the result. As shown in Figure 5.3 (b), when the EER is greater than 34%, CA5-50% begins to increase with the EER at the spark timings of 25 CAD BTDC and 30 CAD BTDC. In the spark timing range between 35 CAD BTDC and 40 CAD BTDC, the CA5-50% stays stable and is almost independent with the increase of EER. Finally, at spark timing of 45 CAD BTDC and 50 CAD BTDC, the CA5-50% slightly decreases with the increase of EER, which may be because the earlier spark timings have a more dominant effect than the charge cooling on the early combustion duration.

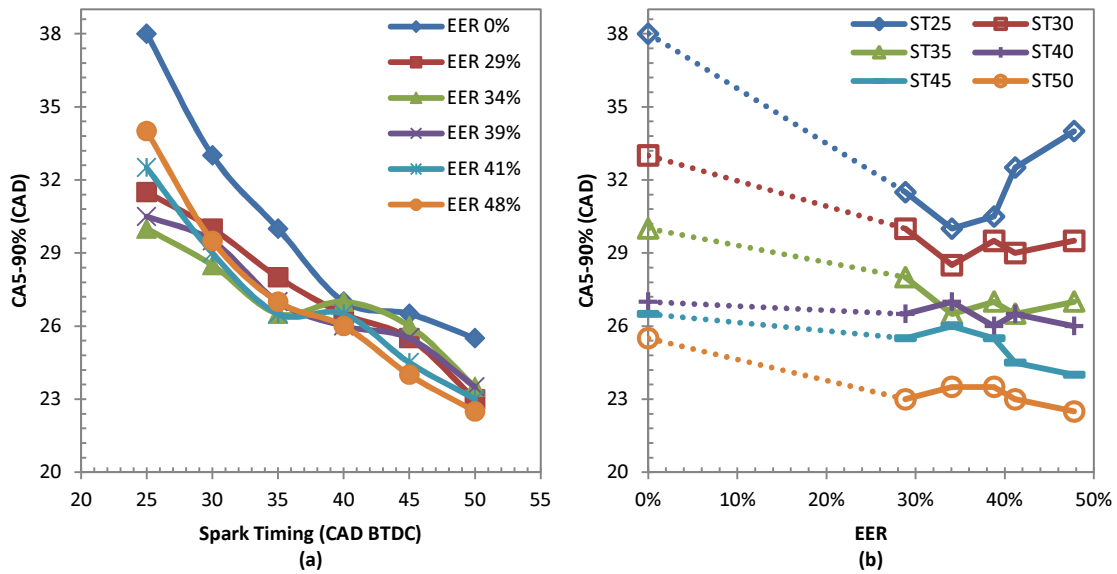


Figure 5.4–Variation of CA5-90% with spark timing (a) and EERs (b)

The variation of major combustion duration, CA5-90%, is shown in Figures 5.4 (a) and 5.4 (b). It can be seen from Figure 5.4 (a) that when the spark timing is advanced from 25 CAD BTDC to 50 CAD BTDC, the CA5-90% gradually decreases at all EER levels. This result can be attributed to the increased spark timing which advances the combustion phasing (CA5-50%, Figure 5.3 (a)) and makes more combustion processes occur at the small in-cylinder volume. Therefore, the combustion temperature increases, the distance of flame propagation shortens and the combustion duration reduces [80].

The variation of CA5-90% generally follows the same trend as that of CA5-50%. As shown in Figure 5.4 (b), at spark timings of 25 CAD BTDC and 30 CAD BTDC, the CA5-90% first decreases with the increase of EER and reaches the minimum at EER of 34%. Then, the CA5-90% begins to increase with further increases of EER. At spark timings of 35 CAD BTDC and 40 CAD BTDC, the CA5-90% first decreases until EER reaches 29%, then it becomes independent of the EER and stays at around 27 CAD. When the spark timing is further advanced to 45 CAD BTDC and 50 CAD BTDC, the CA5-90% generally decreases with an increase in the EER.

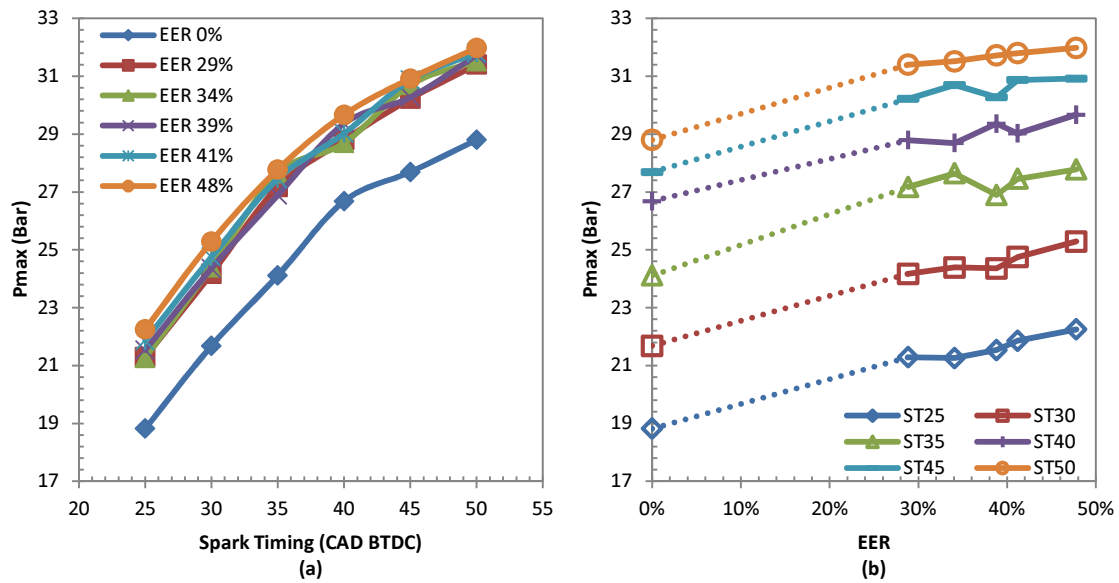


Figure 5.5–Variation of P_{max} with spark timing (a) and EERs (b)

Figure 5.5 shows the variation of peak cylinder pressure, P_{max} with spark timing. As shown in Figure 5.5 (a), the P_{max} gradually increases with the advance of spark timing. This is because when spark timing is advanced, more of a combustion process occurs at the lower in-cylinder volume and this generates higher combustion pressure. It should be noted that although the P_{max} increases with the advance of spark timing, the combustion phasing may be over advanced. This over advanced combustion phasing can result in negative work and it can therefore reduce the IMEP.

It can be seen from Figure 5.5 (b) that the P_{max} gradually increases with the increase of EER at all tested spark timings. It is believed that ethanol’s faster laminar flame speed, which advances combustion phasing, contributes to the increment of P_{max} . The P_{max} result in Figure 5.5 (b) is similar to the results of some recent investigations about using ethanol in DISI engines. In these studies, an increase of P_{max} with the increase of ethanol/gasoline ratio was found [162] [163].

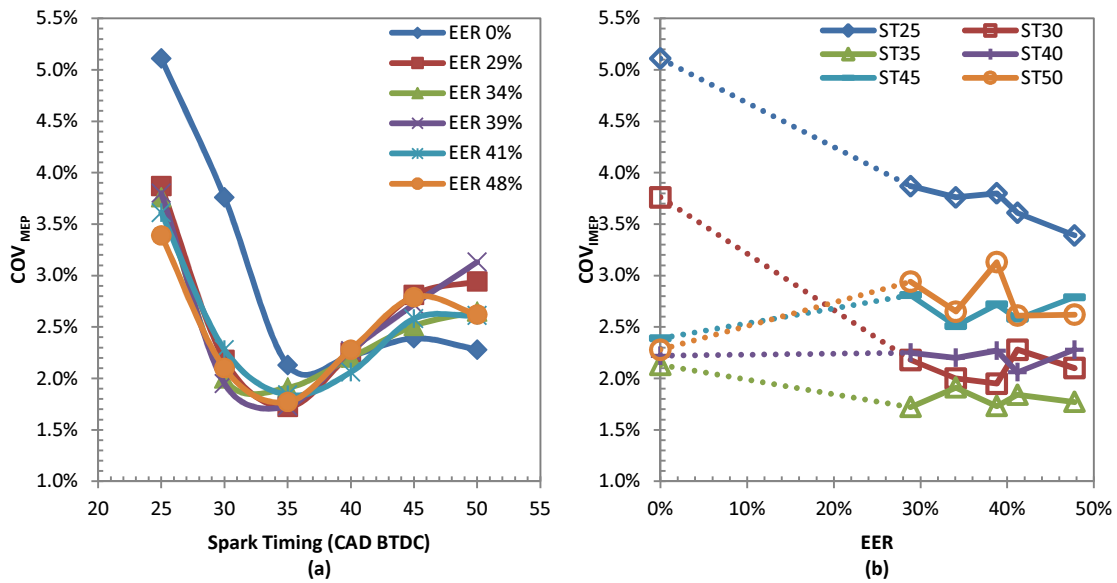


Figure 5.6–Variation of COV_{IMEP} with spark timing (a) and EERs (b)

To examine the stability of the combustion, COV_{IMEP} is calculated. As shown in Figure 5.6 (a), COV_{IMEP} first decreases with the advance of spark timing until it reaches 35 CAD BTDC where the COV_{IMEP} at all EER levels achieves the minimum. A further advance of spark timing earlier than 35 CAD BTDC leads to an increase of COV_{IMEP} as shown in the spark timing range from 45 CAD BTDC to 50 CAD BTDC. It is generally regarded that COV_{IMEP} is related to the in-cylinder flow and position movement. The faster the combustion is, the less time there is for the flame to be affected by the in-cylinder flow motion and gas expansion and this therefore results in better stability [164]. The major combustion duration decreases with the advance of spark timing (Figure 5.4 (a)). Thus, the COV_{IMEP} should theoretically decrease with an increase of spark timing. However, in this study, it can be seen that the COV_{IMEP} in the spark timing range from 40 CAD BTDC to 50 CAD BTDC does not follow this trend. One explanation for this result is the poor mixture quality which is caused by the advance of spark timing. The combustion stability is negatively affected by the poor mixture quality and the COV_{IMEP} increases.

From Figure 5.6 (b), it can be seen that COV_{IMEP} decreases gradually with the increase of EER when the spark timing is at 25 CAD BTDC and 30 CAD BTDC. Ethanol's higher laminar flame propagation speed and better low temperature combustion stability may be the factors that cause

the decrease of COV_{IMEP} [165]. In the spark timing range from 35 CAD BTDC to 40 CAD BTDC, the COV_{IMEP} is almost independent of the variation of EER, and in the spark timing range from 45 CAD BTDC to 50 CAD BTDC, it raises with the increase in EER. One possible explanation for this result is that the increased EER and advanced spark timing may substantially reduce the in-cylinder temperature before ignition, due to the increased charge cooling and reduced time for heat recovery. The low in-cylinder temperature negatively affects the combustion stability, causing the increase of COV_{IMEP} .

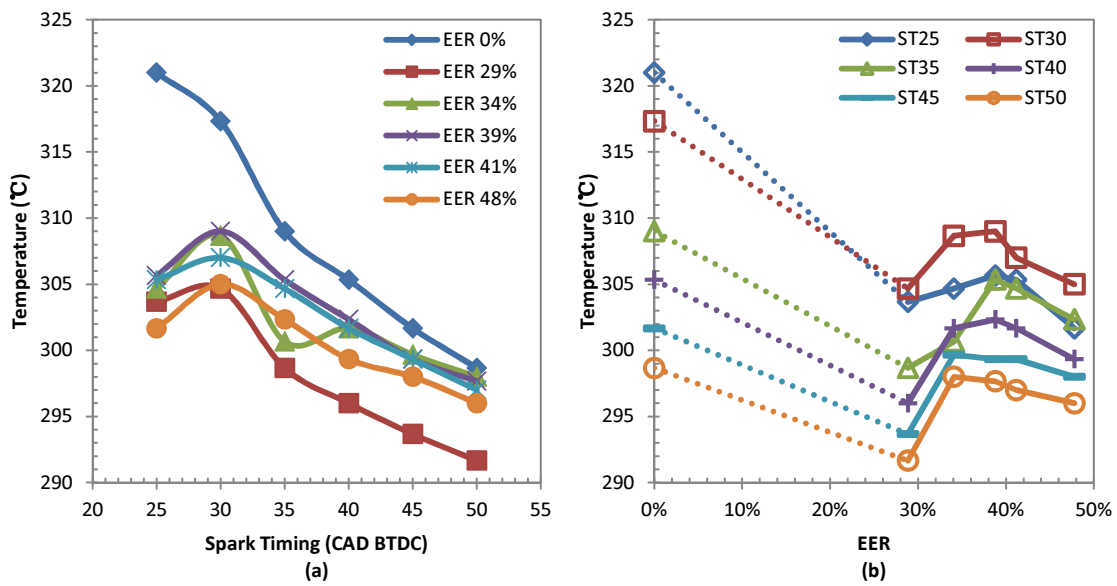


Figure 5.7–Variation of exhaust temperature with spark timing (a) and EERs (b)

Exhaust gas temperature is an important parameter which can indicate the late oxidation of HC and CO emissions and relate to the light-off and effectiveness of a three-way catalyst converter. Although in this study, the test was performed in warm conditions, the trends of the exhaust temperature in warm condition can still help us to understand the impact of advancing spark timing on the exhaust temperature in a cold engine. Figure 5.7(a) shows the variation of the exhaust gas temperature with spark timing at different EERs. As shown in Figure 5.7(a), at all tested EERs the advance of spark timing leads to a lower exhaust temperature. This is mainly because when the spark timing is increased, there is a longer gas expansion between the end of combustion and exhaust valve opening. Thus, the exhaust temperature reduces.

As for the effect of EER on the exhaust temperature (Figure 5.7 (b)), it can be seen that when the EER is increased from 0% to 48%, the exhaust temperature first decreases with EER until it reaches the minimum at EER around 29%, then it increases and reaches a peak in the EER range between 34% to 39%, after this range the exhaust temperature decreases again with further increases of EER. The ethanol has a lower adiabatic flame temperature than gasoline. So, the decrease of the exhaust temperature with the increase of EER between EERs of 0% and 29% can be attributed to the decreased flame temperature. In the EER range from 34% to 39%, short major combustion duration (CA5-90%) is observed in Figure 5.4 (b). This means the mixture can release its heat more intensely and the maximum in-cylinder temperature should be increased. Thus, the increase in the exhaust temperature may be due to the raised in-cylinder temperature [166]. Further increases of EER may lead to great charge cooling effect which can in turn reduce the in-cylinder temperature as well as the exhaust temperature.

5.1.2 Effect of spark timing on emissions and efficiency at different EERs

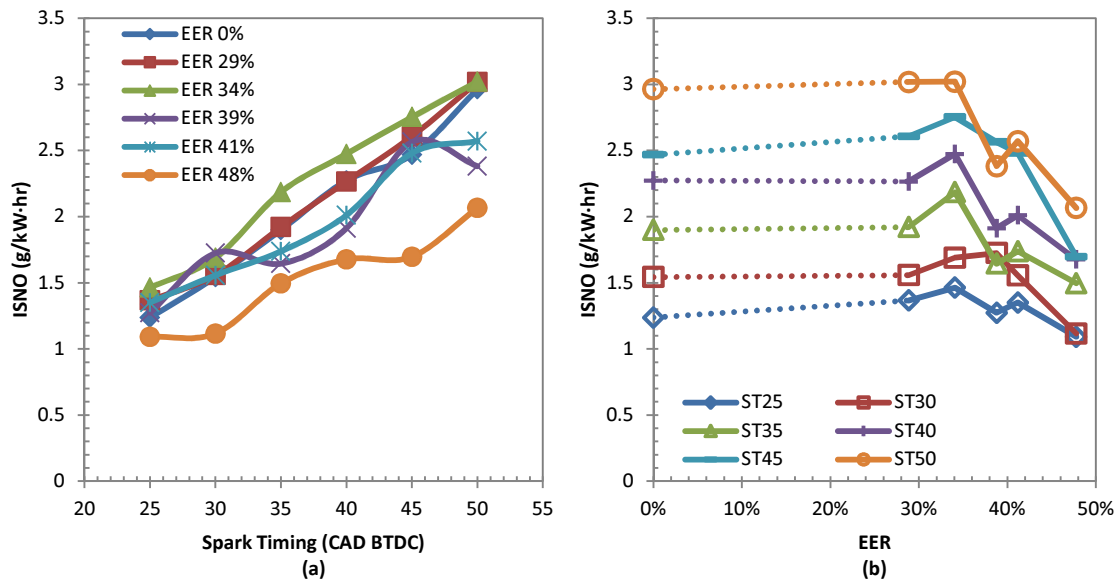


Figure 5.8–Variation of ISNO with spark timing (a) and EERs (b)

The effect of spark timing on ISNO is shown in Figures 5.8 (a) and 5.8 (b). As shown in Figure 5.8 (a), ISNO increases gradually with the advance of spark timing in all tested EERs. It is well

known that the formation of NO_x increases very strongly with combustion temperature, which itself is related to the combustion pressure. The combustion pressure increases with the advance of spark timing as shown in Figure 5.5 (a). Therefore, the ISNO increases when the spark timing is advanced. It can be seen from Figure 5.8 (b) that when EER is in the range from 0% to 34%, ISNO stays stable. When EER is greater than 34%, it decreases with further increases of EER. In the EER range from 0% to 34%, a reduction in CA5-90% can be seen in Figure 5.4 (b). This may lead to a more intense heat release and hence a higher in-cylinder temperature. However, this increased in-cylinder temperature may be counterbalanced by the charge cooling effect and low adiabatic flame temperature of ethanol. Thus, ISNO is almost independent with EER in the range from 0% to 34%. Further increases of EER when it is above 34% may lead to great charge cooling and lower adiabatic flame temperature. ISNO is therefore reduced.

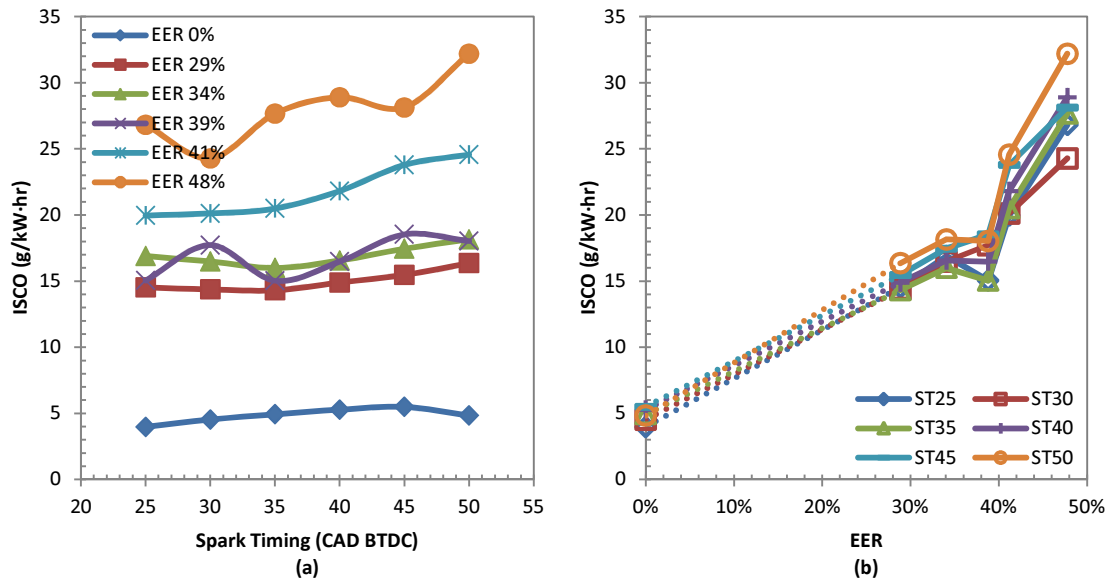


Figure 5.9–Variation of ISCO with spark timing (a) and EERs (b)

The variations of ISCO and ISHC are shown in Figures 5.9 and 5.10. As shown in Figure 5.9 (a), when the EER is below 34% (EERs of 0%, 29% and 34%), ISCO slightly increases with the advance of spark timing. When EER is greater than 39% (EERs of 41% and 48%), the increase of ISCO with spark timing becomes more obvious. This increase in ISCO can be attributed to the advanced spark timing which shortens the time for ethanol’s vaporisation, thus resulting in in-homogeneous mixture and higher CO emissions.

ISHC, as shown in Figure 5.10 (a), is close related to the spark timing. It gradually increases with the advance of spark timing at all EER levels. This increase in ISHC may be caused by two mechanisms. Firstly, the advance of spark timing increases in-cylinder pressure which leads to more hydrocarbons being trapped in the crevice volumes and a corresponding increase in HC emissions. Secondly, the exhaust temperature decreases with the advance of spark timing (Figure 5.7 (a)). The reduced exhaust temperature indicates that less oxidization happens as the trapped hydrocarbons get off from the crevice volumes. Therefore, ISHC increases with the advance of spark timing.

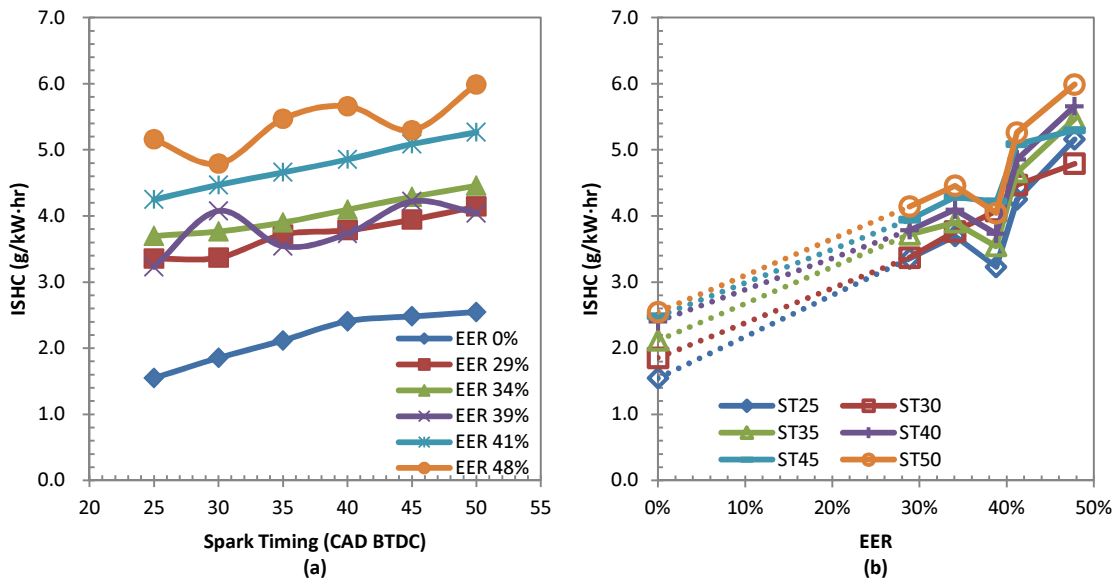


Figure 5.10–Variation of ISHC with spark timing (a) and EERs (b)

As shown in Figures 5.9 (b) and 5.10 (b), ISCO and ISHC increase linearly with the increase of EER, except at an EER of 39% at which both emissions drop. These results are different from the results reported in [167] whereby using ethanol reduced emissions of HC and CO. The explanations for this result are related to two mechanisms. Firstly, the engine was operated at a low load range (IMEP around 4.0 Bar) in order to realise that the spark timing could be swept in a wide range without knocking. This means that the in-cylinder temperature in this test may be not high enough for HC and CO to fully oxidate. The great charge cooling effect caused by EDI may further reduce the in-cylinder temperature and deteriorate the HC and CO oxidation

process. Secondly, the ethanol fuel may not be well vaporised at such a relatively low in-cylinder temperature. Therefore, poor mixture quality leads to more unburned products such as CO and HC, and this effect is fortified when the EER level is increased because more ethanol is direct injected. The drop of ISHC and ISCO at an EER of 39% indicates optimal EER level for less HC and CO emissions. This test has been repeated on a separate day to exam the repeatability of the results and similar trends were observed.

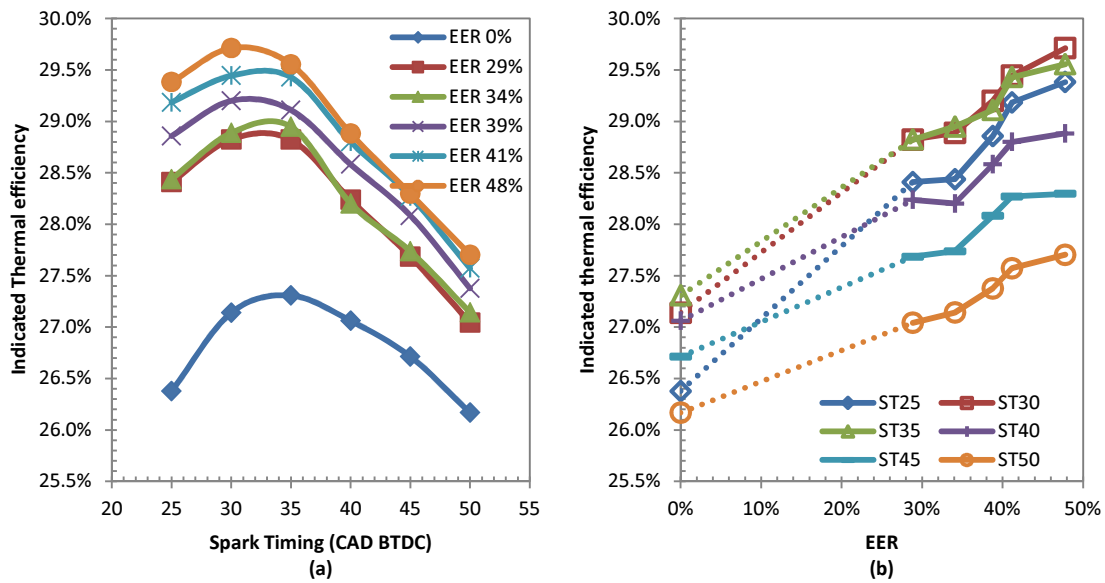


Figure 5.11–Variation of indicated thermal efficiency with spark timing (a) and EERs (b)

Figures 5.11 shows the variation of indicated thermal efficiency with spark timing at different EERs. As shown in Figure 5.11 (a), the indicated thermal efficiency at all EERs increases with the advance of spark timing until it reaches the maximum, then it decreases with further increases of spark timing. This change in indicated thermal efficiency should be related to the change of combustion phasing (caused by advancing spark timing) which alters the conversion efficiency of combustion products into effective work.

Figures 5.11 (b) shows that at all tested spark timings, indicated thermal efficiency increases with increases of EER. Indicated thermal efficiency at spark timings of 30 CAD BTDC and 35 CAD BTDC are higher than that at other spark timings. When the EER is low than 29%, the indicated thermal efficiency at spark timing of 35 CAD BTDC is higher that at 30 CAD BTDC,

however, when the EER is greater than 39%, the indicated thermal efficiency at spark timing of 30 CAD BTDC is the maximum.

Figure 5.11 (b) also shows that the gap between the maximum and minimum indicated thermal efficiency at the same EER increases with the advance of spark timing. In gasoline only conditions (EER of 0%), the gap between maximum (27.3%, at spark timing of 35 CAD BTDC) and minimum (26.2%, at spark timing of 50 CAD BTDC) indicated thermal efficiency is 1.1%. This gap gradually increases to 2.0% when the EER is 48%. As shown in Figure 5.11(b), when the EER is raised from 0% to 48% there is an average 2.0% increase in indicated thermal efficiency at all tested spark timings, except at the spark timing of 25 CAD BTDC where the indicated thermal efficiency increases 3.0%.

5.2 Leveraging effect enhanced by spark advance and inlet air pressure increment

In Section 4.1, the effect of ethanol on leveraging gasoline fuel usage was evaluated at spark advance (15 CAD BTDC) of the original engine. In order to enhance this leverage effect, the effect of spark timing advance and inlet air pressure increment will be presented and discussed in this section. In a SI engine, keeping the spark advance at MBT timing and increasing the boost pressure can lead to high engine efficiency and low fuel consumption. However, this may be prohibited by engine knock. Knocking is a major constraint that limits the improvement of SI engine efficiency. The EDI+GPI engine, on the other hand, provides great potential for mitigating engine knocking. Therefore, in this method, the spark timing can be greatly advanced and the boost pressure can be highly increased. The engine efficiency may reach a higher level and the leveraging effect of reducing fuel consumption may be further enhanced. In the following parts, the knock mitigation ability of the EDI+GPI engine, which permits the engine to operate at a more advanced spark timing and high inlet air pressure level, was experimentally investigated and discussed.

Experiments were started at the stoichiometric AFR, fixed injection timing of 300 CAD BTDC and engine speed of 3500rpm. In each tested load condition, the spark timing was first advanced

to reach KLSA with gasoline fuel only, then the quantity of the gasoline fuel was decreased and the ethanol fuel with equivalent energy was injected directly into the combustion chamber to maintain the total energy fuel unchanged. Meanwhile, the spark timing was advanced until the engine reached the new KLSA at that particular EER. During the test, the EER was gradually increased and the KLSA was progressively advanced until it was over optimal spark timing or MBT timing. In this way, the relation between the increase of EER and possible spark advance could be found. The method used for detecting engine knock was introduced in Section 3.4.5. The engine experimental conditions for this part of tests are listed in Table 5.2.

Table 5. 2 Experimental conditions for Section 5.2.1

Engine speed	3500rpm
IMEP (Bar)	7.2, 7.8, 8.5
Throttle Position	34%, 40%, 49%
Inlet air pressure	Ambient (~1.0 Bar)
Injection timing	300 CAD BTDC
Injection pressure	40 Bar (When ethanol flow rate < 0.6kg/h) 60 Bar (When ethanol flow rate ≥ 0.6kg/h)
Spark timing	KLSA

The experiments aimed to investigate the effect of EDI on knock due to increasing inlet air pressure were conducted at three fixed throttle openings (20%, 25%, 30%, denoted as T1, T2 and T3). The effect of turbocharging was simulated using compressed air supplied through a compressed air line from the campus power generation plant. The supplied compressed air was regulated through a pressure regulator and connected to the engine manifold. The pressure was initially set at an ambient air pressure of 1.0 Bar. Then, the inlet air pressure was progressively increased to 1.4 Bar with 0.1 Bar intervals. During the tests, the EER was adjusted to keep the KLSA at MBT timing. At IMEP 7.2 Bar, 7.8 Bar and 8.5 Bar, the minimum EERs were 15.4%, 17.2% and 18.5% respectively, which was due to the limitation of the minimum injector opening pulse. The ethanol fuel mass flow rate for these EERs was 0.38 kg/h, because the EER was the only ratio between ethanol and gasoline. More details of experimental conditions for this part of tests are listed in Table 5.3.

Table 5. 3 Experimental conditions for Section 5.2.2

Engine speed	3500rpm
Throttle opening	20%, 25%, 30%
Inlet air pressure (Bar)	1.0, 1.1, 1.2, 1.3, 1.4
Injection timing	300 CAD BTDC
Injection pressure	40 Bar (When ethanol flow rate < 0.6kg/h) 60 Bar (When ethanol flow rate \geq 0.6kg/h)
Spark timing	KLSA

5.2.1 Leveraging effect enhanced by spark advance

The variation of KLSA with EER in three load conditions is shown in Figure 5.12. As shown in the figure, GPI is the least effective in suppressing engine knock. In GPI conditions (EER of 0%), the KLSA at IMEP of 7.2 Bar, 7.8 Bar and 8.5 Bar is 21 CAD BTDC, 19 CAD BTDC and 15 CAD BTDC, respectively. GDI slightly advances the KLSA for about 1 CAD at each tested load due to the charge cooling effect of gasoline evaporation inside the combustion chamber. When ethanol is used, the effect of DI on knock mitigation and KLSA advancement is significant. At 7.2 Bar IMEP, the KLSA can be advanced from 21 CAD BTDC to 25 CAD BTDC when EER is increased from 0% to 18.5%. At 7.8 Bar IMEP, the KLSA is advanced from 19 CAD BTDC to 23 CAD BTDC when the EER is raised from 0% to 17.2%. At IMEP of 8.5 Bar, the increase of EER from 0% to 15.4% results in about 3 CAD KLSA advancement and the KLSA is advanced to 18 CAD BTDC. When the EER is increased from 15% to 35%, the results in Figure 5.12 show that every 2.0% or 3.0% of EER increment can lead to an advance of around 2 CAD of KLSA. For instance, at 7.2 Bar IMEP, when the EER is increased from 18.5% to 21.5%, the KLSA increases for about 2 CAD. At 8.5 Bar IMEP, when the EER is raised from 23.0% to 25.9%, the KLSA increases from 22 CAD BTDC to 24 CAD BTDC.

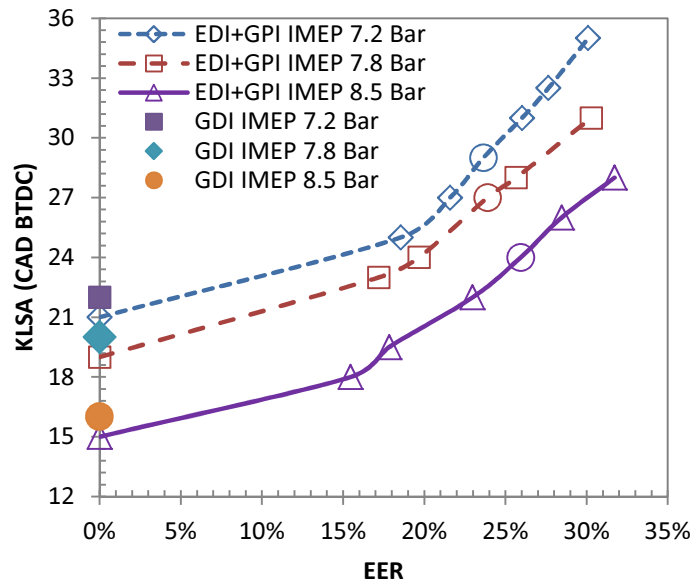


Figure 5.12–Variation of KLSA with EER

As also shown in Figure 5.12, the KLSA is advanced with the increase of EER and achieves the optimal spark timing or MBT timing at EER of 23.6% for 7.2 Bar IMEP, EER of 23.8% for 7.8 IMEP and EER of 25.9% for 8.5 IMEP, respectively. The MBT timing is marked with “O” in Figure 5.12. At 7.2 Bar IMEP, the MBT timing is at 29 CAD BTDC. At 7.8 Bar IMEP, it is at 27 CAD BTDC. At 8.5 Bar IMEP, the MBT timing is 22 CAD BTDC.

It should be noted that the SOI timing in this test was set at 300 CAD BTDC which was not a timing that can fully exploit DI’s potential in knock mitigation. If the SOI timing was set at a timing which is after the inlet valve closing, the effect of DI on knock suppression may be more significant due to the reduced time for heat transfer from wall to the fresh charge [168]. However, according to the tests on SOI timing, the engine efficiency and emissions were degraded at the SOI timing which was after the inlet valve closing, and the SOI timing of 300 CAD was an optimal timing for both high efficiency and low emissions. Details of the effect of SOI timing on engine performance and knock tendency will be presented in Chapter 6.

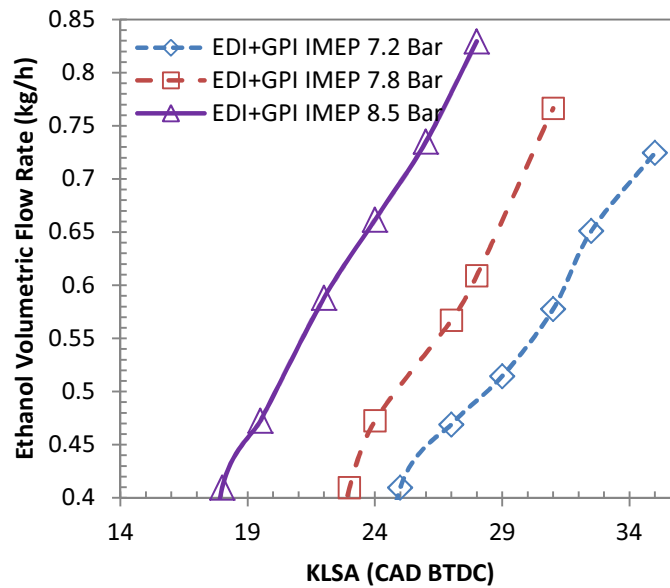


Figure 5.13–Variation of ethanol volumetric flow rate with KLSA

In order to further analyse the effect of EDI on mitigating knock, the variation of ethanol mass flow rate (kg/h) with KLSA is shown in Figure 5.13. The result with EER less than 15.4% is excluded in Figure 5.13 because there is no tested point between EER of 0% and EER of 15.4%. As shown in Figure 5.13, with the advance of spark timing, the ethanol amount required for mitigating knock increases. For example, at 8.5 Bar IMEP, 0.41 kg/h of ethanol is needed to ensure that the engine works at a spark timing of 18 CAD without knocking. When the spark timing is advanced to 28 CAD BTDC, this value increases to 0.83 kg/h. Similarly, at 7.2 Bar IMEP, 0.41 kg/h of ethanol is enough to keep the spark timing at 25 CAD BTDC without knock happening. When the spark timing reaches 35 CAD BTDC, the ethanol fuel mass flow rate is raised to 0.72 kg/h. Normally, when spark timing is increased, the combustion phasing is advanced, therefore more of the combustion process is occurring in a smaller volume (piston at or close to TDC) which results in great pressure and temperature rises. Thus more knock mitigate agent (ethanol) is needed to reduce the in-cylinder temperature and improve the chemical reaction (higher octane number) with the purpose of keeping the unburned mixture from auto-ignition. This should be the main reason for the increase of the ethanol mass flow rate with the advance of spark timing.

The mechanisms that determine the ethanol quantity requirement for knock mitigation are

complex. Several factors may influence the result. Firstly and most importantly, the advance of spark timing can substantially influence the in-cylinder temperature and pressure as well as the amount of ethanol required for knock suppression. Secondly, adding ethanol fuel can accelerate the burning rate due to its fast laminar flame speed, which may also advance the combustion phasing [162] and result in a higher in-cylinder pressure and temperature. Thirdly, the octane number of the dual fuel increases with the increase of EER. However, this increase is not linear. Normally, the initial octane number increases when the first 10% ethanol (volumetric based) added is greater than that for each subsequent 10% increase [60]. Therefore, the effect of using EDI on knock mitigation may slightly decrease with the increase of EER. The knock suppressing effect of EDI may be reduced at high EER levels. In addition, the ethanol evaporation speed and ethanol water content may also affect the quantity of ethanol fuel required for knock mitigation [169]. The understanding of the influence for each factor requires detailed engine testing and numerical study. These will be examined in the forthcoming work of another fellow student.

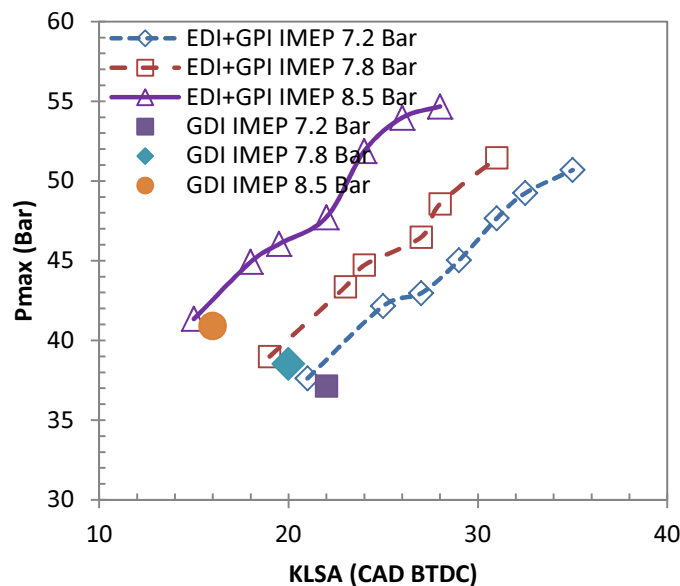


Figure 5.14–Variation of P_{max} with KLSA

Figure 5.14 shows the variation of peak cylinder pressure, P_{max} with KLSA. It should be noted that the P_{max} is calculated from the cylinder pressure data averaged from 100 consecutive cycles. As shown in the figure, the P_{max} increases monotonously with the increase of spark timing at

each load. At 7.2 Bar IMEP, P_{max} increases from 37.6 Bar to 50.7 Bar. At 7.8 Bar IMEP, it increases from 39.0 Bar to 51.5 Bar. At 8.5 Bar IMEP, the P_{max} raised from 41.3 Bar to 51.6 Bar. As the knock is suppressed by EDI, the spark timing is advanced progressively (Figure 5.12) and the combustion process initiates closer to TDC. Therefore, more of the combustion process occurs at a lower in-cylinder volume, resulting in higher combustion pressure. Additionally, the faster laminar flame speed of ethanol may also contribute to the increased in-cylinder pressure. The high burning rate can lead to the mixture releasing its heat more intensively, thus generating higher in-cylinder pressure. Generally, the increase of P_{max} can improve the combustion rate and increase the expansion of the combustion products into useful energy [136].

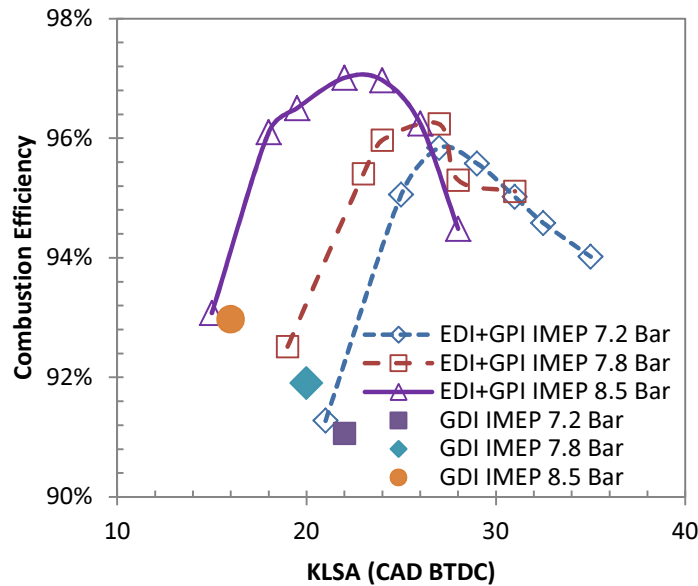


Figure 5.15–Variation of combustion efficiency with KLSA

The variation of combustion efficiency, calculated from CO and HC in the exhaust stream, is shown in Figure 5.15, it can be seen that the combustion efficiency first increases with the advance of spark timing until it reaches the range between 24 CAD BTDC and 29 CAD BTDC where the combustion efficiency in each load reaches the maximum. This is also the range where the MBT timing is achieved, as shown in Figure 5.12. With spark timing further advanced, the combustion efficiency begins to decrease. This result may be caused by the synergic effect of EER and spark timing. In the first place, the EER increases with the advance of spark timing (Figure 5.12) due to raised knock propensity. The ethanol fuel can improve the

combustion because of its oxygen content properties and high laminar flame speed. Therefore, the combustion efficiency increases. However, further increasing the EER (spark timing is advanced with the EER, see Figure 5.12) over a certain level may lead to serious fuel impingement on the piston and cylinder wall [23]. This fuel impingement should be mainly due to the injection of a large quantity of ethanol, which is caused by ethanol's low heating value. Thus the mixture quality reduces with further increases of EER or spark timing, which decreases the combustion efficiency. Secondly, the advance of spark timing advances the combustion phasing (Figure 5.16) which leads to more combustion occurring in a smaller volume (piston close to TDC) and hence resulting in a higher combustion temperature. This increase in the combustion temperature and pressure may assist the fuel oxidization process and therefore increase its combustion efficiency. However, the fuel/air mixing time also reduces with the advance of spark timing. When the spark timing is advanced earlier than a certain range, the mixture quality may be seriously affected which can lead to a decrease of combustion efficiency. The result in Figure 5.15 indicates that the ethanol quantity used for knock mitigation should be adjusted in order to keep it in a range where the high combustion efficiency can be achieved.

Figure 5.15 also shows that the combustion efficiency in GPI conditions is slightly higher than that in GDI conditions. This result should be related to the degradation of mixture quality when the injection strategy shifts from the GPI mode to the GDI mode.

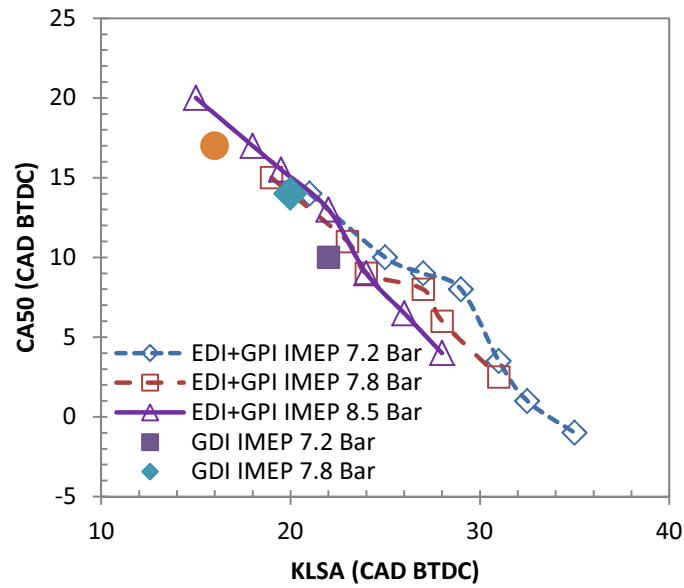


Figure 5.16–Variation of CA50 with KLSA

Figure 5.16 shows the variation of central combustion phasing (CA50) with KLSA. This result is presented because it directly relates to the engine power and thermal efficiency. Normally, keeping the CA50 between 8 CAD ATDC and 10 CAD ATDC is regarded as the optimum [170]. As shown in Figure 5.16, CA50 decreases with the advance of spark timing in all three tested loads. This is because the EDI suppresses the knock and permits the advance of spark timing, which advances the combustion phasing. It can also be seen that the CA50 reaches the optimal location (8 CAD ATDC~10 CAD ATDC) when the spark timing is in the range from 24 CAD BTDC to 29 CAD BTDC. The corresponding EER range for this spark timing range is from 22% to 26% (Figure 5.12). This means that at the three tested loads, the EER between 22% and 26% is enough to keep the combustion phasing at optimum without knocking. As shown in Figure 5.16, the CA50 in GDI conditions is slightly more advanced than that in GPI conditions. The result may be because the spark timing in the GDI conditions is about 1 CAD earlier than that in GPI conditions.

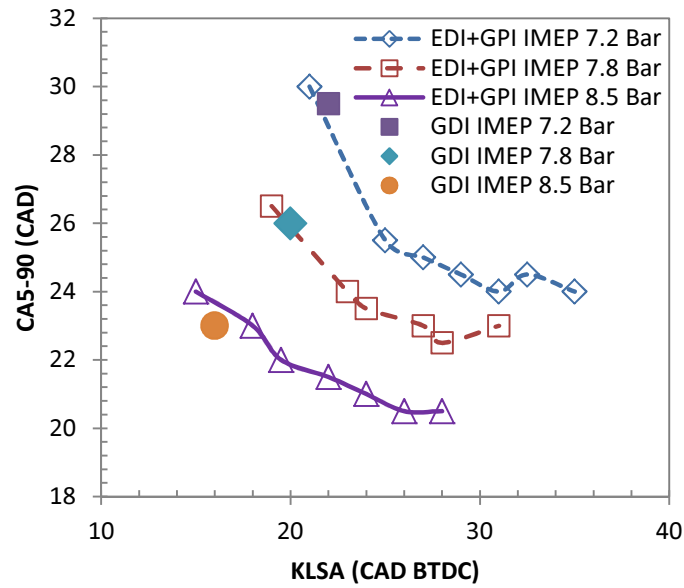


Figure 5.17–Variation of CA5-90% with KLSA

The major combustion duration, CA5-90%, is shown in Figure 5.17. As shown in Figure 5.17, the CA5-90% decreases with the advance of spark timing in all tested loads. The decrease of CA5-90% with the advance of spark timing can be attributed to the raised combustion temperature and pressure as the combustion initiates closer to TDC. The raised combustion temperature and pressure may accelerate the combustion speed, thus reducing the CA5-90%. Additionally, the EER level increases with the advance of spark timing. Ethanol’s high combustion speed may also contribute to the decrease of CA5-90%.

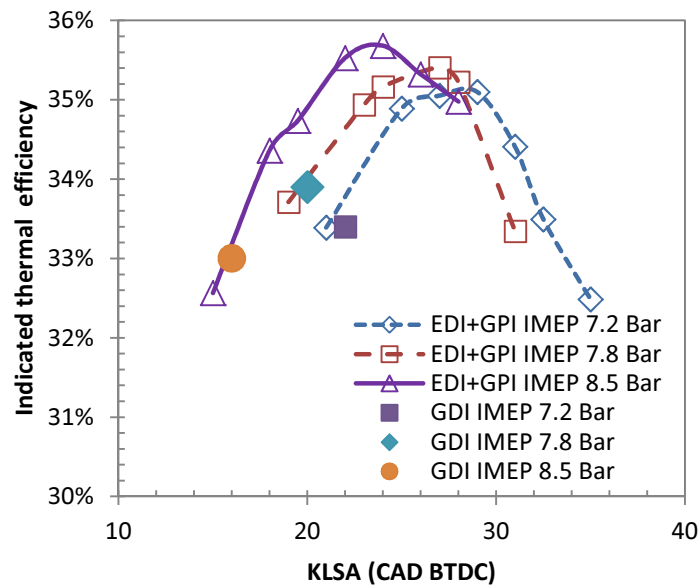


Figure 5.18–Variation of indicated thermal efficiency at KLSA

Figure 5.18 shows the variation of indicated thermal efficiency with spark timing. The benefit of knock mitigation on engine efficiency can be clearly seen from this result. As shown in Figure 5.18, the indicated thermal efficiency increases with the advance of spark timing and reaches the maximum when spark timing is in the range between 24 CAD BTDC and 29 CAD BTDC. The maximum indicated thermal efficiency at 8.5 Bar IMEP, 7.8 Bar IMEP and 7.2 Bar IMEP is 35.7%, 35.5% and 35.1%, respectively. In GPI conditions, where the spark timing is retarded in order to avoid knocking, the indicated thermal efficiency for 8.5 Bar IMEP, 7.8 Bar IMEP and 7.2 Bar IMEP is 33.4%, 33.6% and 32.6%, respectively.

The advance of central combustion phasing (CA50) should be one of the main factors that lead to the increase of indicated thermal efficiency. As shown in Figure 5.16, the combustion phasing advances with the spark timing. When the spark timing is in the range between 24 CAD BTDC and 29 CAD BTDC, the CA50 at three tested loads is located between 8 CAD ATDC and 10 CAD ATDC, which is normally regarded as optimum. The conversion efficiency of combustion products into useful energy may reach the highest at this timing range [24]. Therefore the indicated thermal efficiency increases. This result signifies that suppressing knock which allows the advance of spark timing and subsequently the advance of combustion phasing should be the main benefit of EDI to engine efficiency. Additionally, factors contributing to the increase of

indicated thermal efficiency may also include ethanol fuel's high flame propagation speed, high energy content of stoichiometric mixture per unit mass of air, and mole multiplier effect as explained in Chapter 4.

It can also be seen from Figure 5.18 that when the spark timing is over 29 CAD BTDC, the indicated thermal efficiency begins to decrease rapidly with the increase of spark timing. This is attributed to the over advanced CA50 which results in the combustion of the mixture generating negative work and slowing the piston speed when it is in the upward movements stage. Hence the effective work of the gases on the piston reduces. Indicated thermal efficiency in GDI conditions is slightly higher than that in GPI conditions. The earlier spark timing (1 CAD) in GDI condition may be the main cause to the slightly increased indicated thermal efficiency.

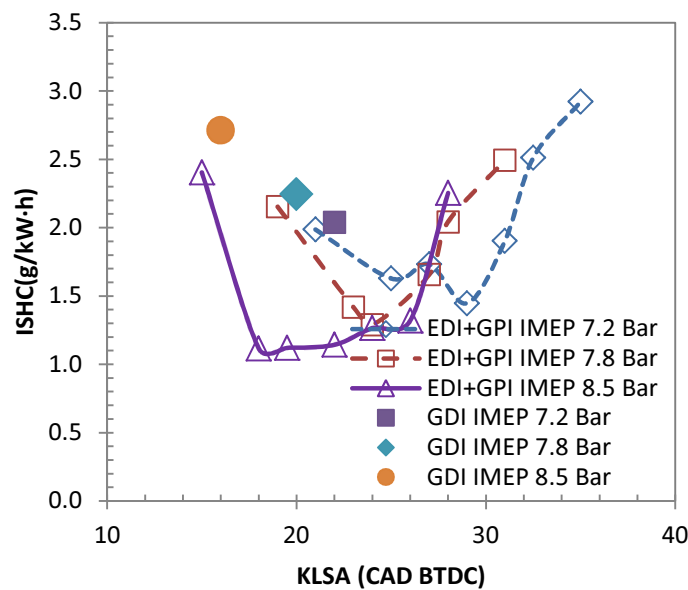


Figure 5.19–Variation of ISHC with KLSA

The variation of ISHC with KLSA is shown in Figure 5.19. As it is evident that the ISHC first decreases with the advance of spark timing and reaches the minimum in the spark timing range from 18 CAD BTDC to 29 CAD BTDC. The corresponding EER for the minimal ISHC is 15.5% at 8.5 Bar IMEP, 19.7% at 7.8 Bar IMEP and 23.7% at 7.2 Bar IMEP, respectively. Earlier than this spark timing range, the ISHC increases with the further advance of spark timing. High cylinder pressure may increase the HC emissions as more hydrocarbons may be trapped in

crevice volumes during the combustion [162]. Advancing spark timing and increasing engine load can raise the cylinder pressure. Therefore, HC emissions should theoretically increase with the advance of spark timing. However, in this study, the ISHC first decreases with the advance of spark timing. This decrease in HC emissions may be due to the high combustion speed and oxygen content of ethanol, which improves the combustion process and optimises the oxidization process of HC emissions. With a further advance of spark timing when it is earlier than the range between 24 CAD BTDC and 29 CAD BTDC, the time for fuel evaporation reduces and this may result in poor mixture quality. Thus ISHC increases with the advance of spark timing. From Figure 5.19, it can also be seen that the ISHC in GDI conditions is higher than that in GPI conditions. The degradation of mixture quality caused by DI fuel impingement may be the main reason for high HC emissions.

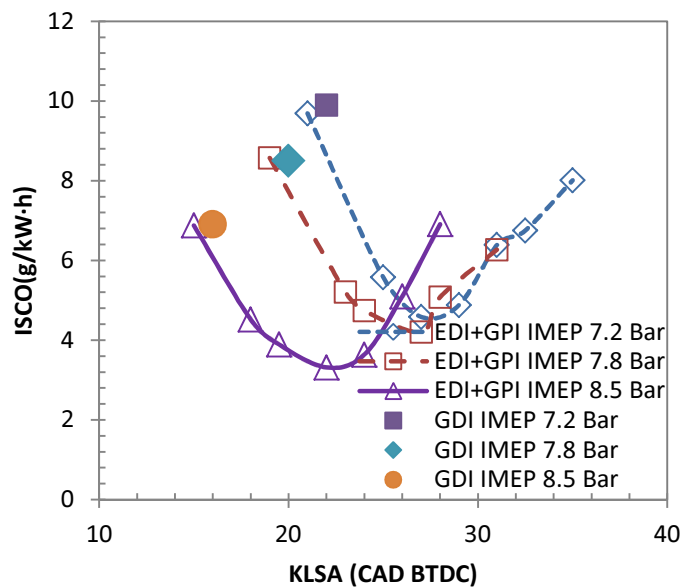


Figure 5.20–Variation of ISCO with KLSA

Figure 5.20 shows the variation of ISCO emission with KLSA. Similar to the ISHC, the ISCO at three tested loads first decreases with the advance of spark timing and reaches the minimum when the spark timing reaches the range between 24 CAD BTDC and 29 CAD BTDC, earlier than this range ISCO increases with the further advance of spark timing. The decrease of ISCO with spark timing may be related to the use of ethanol and the increased in-cylinder pressure (Figure 5.14) and temperature (by advanced spark timing) which facilitate the fuel oxidization

process. The increase of ISCO with further increases of spark timing can be attributed to the reduced time for fuel evaporation and DI fuel impingement which can lead to an in-homogeneous mixture.

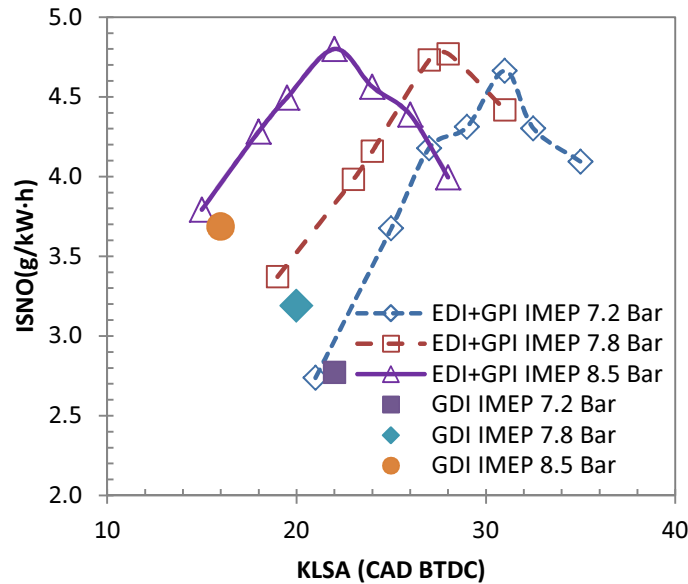


Figure 5.21–Variation of ISNO with KLSA

The emission of ISNO is shown in Figure 5.21. As the experiments were performed at KLSA where the in-cylinder temperature and pressure were at the borderline of causing unburned mixture auto-ignition, the ISNO should be closely related to the variation of KLSA. It can be seen that the ISNO first increases with the advance of spark timing and achieves the highest when the spark timing is in the range between 24 CAD BTDC and 29 CAD BTDC, then it decreases gradually with further advances in spark timing. The formation of NO_x emissions is related to the in-cylinder temperature which itself can be raised by advances in spark timing. Thus, when spark timing is advanced, NO emissions should increase with it. On the other hand, the EER increases with the advance of spark timing in order to suppress knocking. When the EER (spark timing) is over a certain range, the charge cooling effect caused by ethanol evaporation, and low adiabatic flame temperature of ethanol combustion may significantly bring down the in-cylinder temperature, resulting in a reduction of NO emissions.

5.2.2 Leveraging effect enhanced by inlet air pressure increment

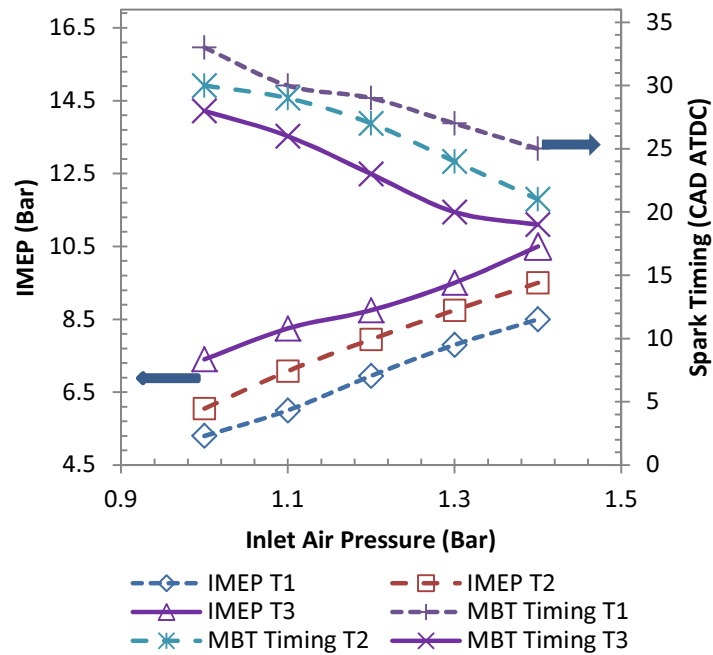


Figure 5.22– Variation of IMEP and MBT Spark timing with inlet air pressure

When the inlet air pressure is raised, the mass of air per engine cycle increases, enabling more fuel to be burned and allowing the increase of engine IMEP. From Figure 5.22, it can be seen that when the inlet air pressure increases from 1.0 Bar to 1.4 Bar, the IMEP in all tested conditions increases progressively. In the T1 condition, it increases from 5.3 Bar to 8.5 Bar and in the T3 condition it increases from 7.4 Bar to 10.5 Bar. Correspondingly, the MBT timing decreases gradually to adapt to the increased engine load (reduced combustion duration, Figure 5.25) and maintains combustion at ideal phasing. In the T1 condition, the MBT timing for 5.3 Bar IMEP is 33 CAD BTDC and it decreases to 25 CAD BTDC when the load reaches 8.5 Bar IMEP. In the T3 condition, the MBT timing reduces from 28 CAD BTDC to 19 CAD BTDC when the IMEP increases from 7.4 Bar to 10.5 Bar.

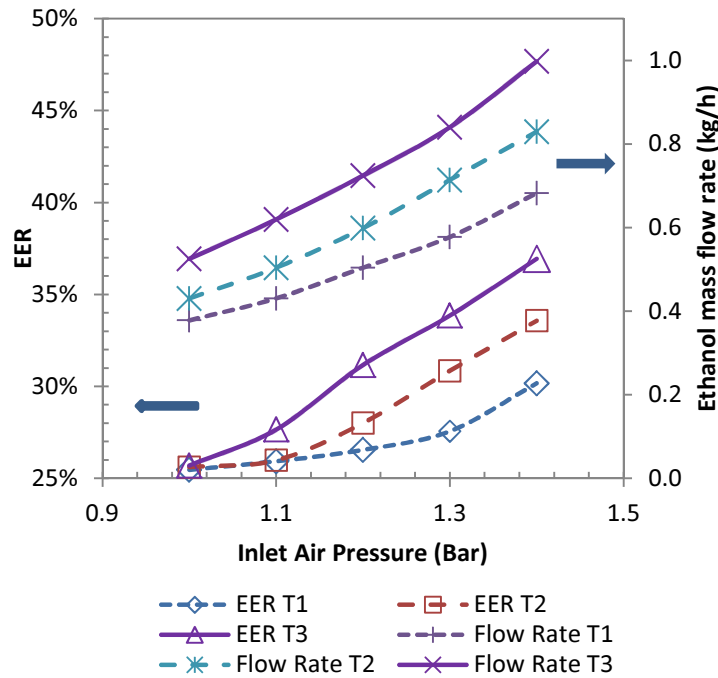


Figure 5.23–Variation of EER and ethanol volumetric flow rate with inlet air pressure

In order to maintain the engine at MBT timing while increasing the inlet air pressure, the knock must be suppressed by means of raising the EDI amount. Figure 5.23 shows the variations of EER and ethanol fuel mass flow rate with inlet air pressure. It can be seen that the amount of ethanol fuel for mitigating knock needs to be increased with the increase of inlet air pressure. At inlet air pressure of 1.0 Bar, the EER around 25% is enough to mitigate knock tendency for the tested conditions. When the inlet air pressure is raised to 1.4 Bar, the EER for T1, T2 and T3 increases to 31.2%, 33.6% and 36.9%, respectively. The EER is a ratio between ethanol and gasoline. Thus a similar EER for different engine conditions is possible if the energy ratios between gasoline and ethanol fuels at these conditions are similar. In order to investigate the real ethanol fuel consumption, the ethanol mass flow rate has also been plotted and is shown in Figure 5.23. From this result, the actual ethanol fuel consumption in different conditions can be clearly seen. As is evident, at inlet air pressure of 1.0 Bar, where the EER level in three tested conditions is almost the same, the flow rates for T1, T2 and T3 are 0.38 kg/h, 0.43 kg/h and 0.53 kg/h, respectively. These values increase to 0.68 kg/h, 0.83 kg/h and 1.0 kg/h when the inlet air pressure is raised to 1.4 Bar.

In the conditions where the inlet pressure is greater than 1.0 Bar, the ethanol used for knock

suppression actually needs to overcome three factors that may result in knocking. The first factor is that the engine load increases with the raise of inlet air pressure due to more air and fuel being inducted into the engine. In-cylinder pressure and temperature normally increase with the increase of engine load, therefore the knock propensity increases. The second factor is that increasing the inlet air pressure can result in a higher initial in-cylinder pressure which may enhance the tendency of mixture auto-ignition before spark discharge. The third factor is the knock tendency caused by the advance of spark timing. The spark timing is kept at MBT timing in order to maintain optimum combustion phasing during this test. This advanced spark timing also contributes to the occurrence of knocking. As shown in Figure 5.22, 10.5 Bar IMEP is the maximum load reached in this test. The EER for this condition is 36.9%. This relatively high EER level should be due to the synthetic effect of the three aforementioned factors.

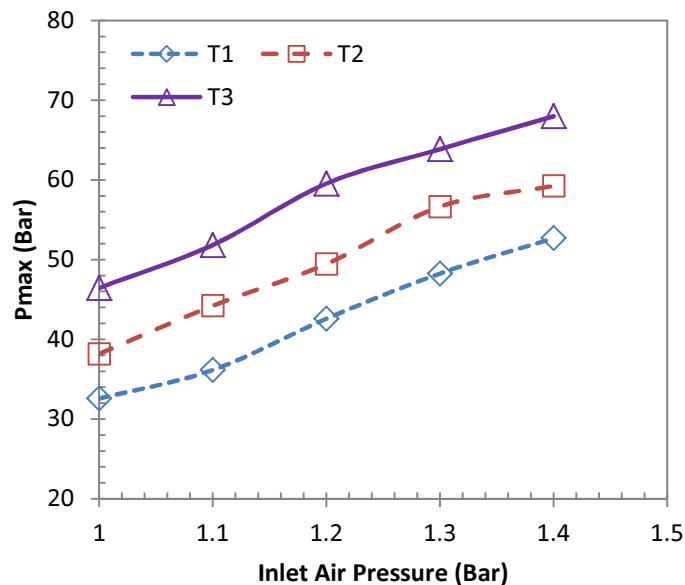


Figure 5.24– Variation of P_{max} with inlet air pressure

The variations of P_{max} and CA5-90% with inlet air pressure are shown in Figures 5.24 and 5.25, respectively. It can be seen from Figure 5.24 that the P_{max} increases progressively with the increase of inlet air pressure in all tested conditions. At an inlet air pressure of 1.0 Bar, the P_{max} for T1, T2 and T3 are 32.6 Bar, 38.2 Bar and 46.5 Bar, respectively. When the inlet air pressure is at 1.4 Bar, the pressure increases to 52.7 Bar, 59.3 Bar and 68.0 Bar. The increase of P_{max} is mainly due to two mechanisms. Firstly, the increased inlet air pressure results in a higher initial

cylinder pressure before ignition, which leads to higher maximum cylinder pressure during combustion. Secondly, when the inlet air pressure is raised, the engine load increases (Figure 5.22) thus more fuel is combusted and the combustion pressure increases as a consequence.

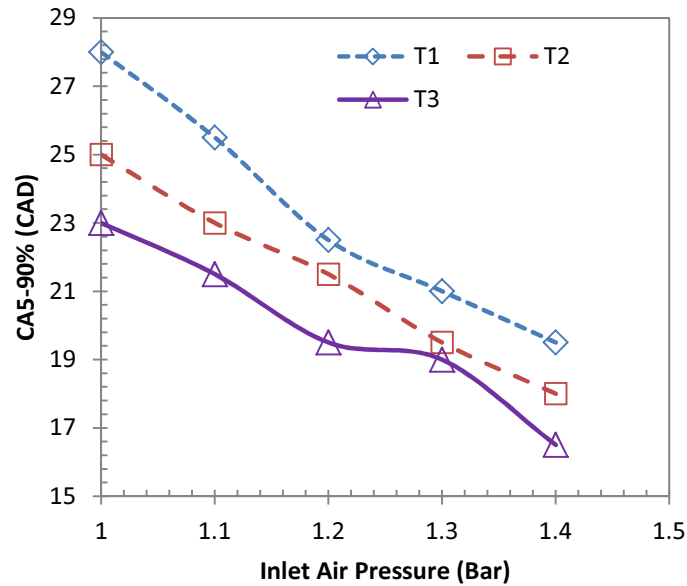


Figure 5.25– Variation of CA5-90% with inlet air pressure

When the P_{max} increases, the combustion process benefits from faster flame propagation speed. As shown in Figure 5.25, the major combustion duration (CA5-90%) decreases with the increase of inlet air pressure in all three test conditions. In the T1 condition, the CA5-90% decreases from 28 CAD to 19.5 CAD, in the T2 condition, it reduces from 25 CAD to 18 CAD and in the T3 condition, the CA5-90% drops from 23 CAD at inlet air pressure of 1.0 Bar to 16.5 CAD at inlet air pressure of 1.4 Bar. In addition to the increased maximum cylinder pressure, ethanol’s fast combustion speed may also add to the reduction of CA5-90%.

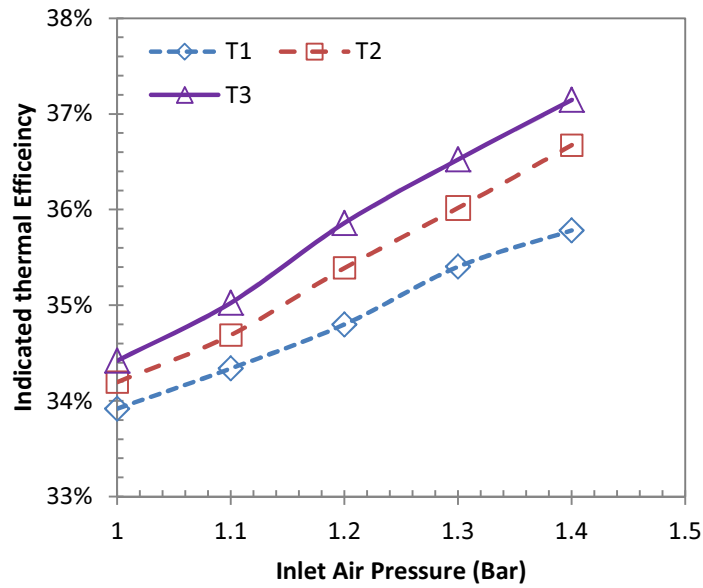


Figure 5.26– Variation of Indicated thermal efficiency with inlet air pressure

The indicated thermal efficiency also benefits from the increment of inlet air pressure as shown in Figure 5.26. When the inlet air pressure increases from 1.0 Bar to 1.4 Bar, the indicated thermal efficiency in all three tested conditions increases. The highest indicated thermal efficiency is 37.2% at 10.5 Bar IMEP and inlet air pressure of 1.4 Bar. This is about 1.5% higher than the highest indicated thermal efficiency (35.7%) obtained from the tests presented in Section 5.2.1. This increment in indicated thermal efficiency may be mainly attributed to the engine boost which reduces the pumping losses [80]. However, it should be noted that the relatively large (66 CAD, Table 3.1) overlap of the inlet and exhaust valve in this engine may blow part of the fresh charge directly into the exhaust pipe during scavenging, which can affect the real in-cylinder AFR and play a negative impact upon engine efficiency. Actually, it was found in the pre-test that the fuel consumption in boost conditions (inlet air pressure ≥ 1.4 Bar) was slightly higher than that in natural aspiration conditions when the engine load was at the same level. For this reason, the maximum inlet air pressure was limited to 1.4 Bar and the lambda was kept a little richer ($0.99 \leq \lambda \leq 1.0$) than the stoichiometry during the tests. Further investigation of the engine boost requires a modification of valve timing.

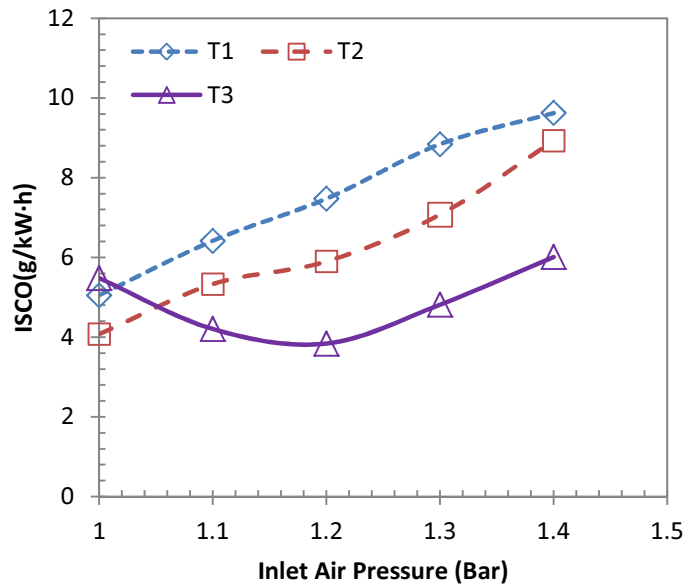


Figure 5.27– Variation of ISCO with inlet air pressure

The exhaust emissions of ISCO, ISNO and ISHC are shown in Figures 5.27, 5.28 and 5.29, respectively. As shown in Figure 5.27, the ISCO increases monotonously with the increase of inlet air pressure in the T2 and T3 conditions. In the T1 condition, it first decreases until the inlet air pressure reaches 1.2 Bar, then it increases with further increases of inlet air pressure. The increase of ISCO in the T1 and T2 conditions may be caused by poor mixture quality and over scavenging. When the inlet air pressure increases, the EER is raised in order to suppress the knock. Therefore, more ethanol fuel is directly injected into the combustion chamber, causing wall-wetting which may negatively affect the mixture quality and result in higher CO emissions. Moreover, the increased inlet air pressure may lead to more fresh charge directly entering the exhaust pipe line during the scavenging, thus causing an increase in CO emissions. The decrease of ISCO at inlet air pressure from 1.0 Bar to 1.2 Bar in the T3 condition may be because of the use of ethanol which optimises the fuel oxidation process.

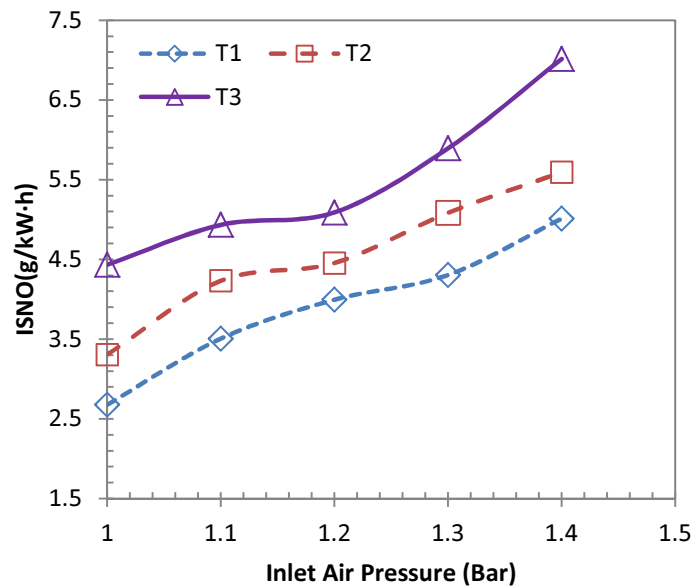


Figure 5.28– Variation of ISNO with inlet air pressure

As mentioned in section 5.1.2, the formation of NO_x emissions are strongly related to the combustion temperature, which itself depends on the combustion pressure. The combustion pressure increases with the increase of inlet air pressure as shown in Figure 5.24. Therefore, the ISNO increases with the increase of inlet air pressure as shown in Figure 5.28. The formation of HC emissions also partly relates to the cylinder pressure because the higher the cylinder pressure is, the more hydrocarbons will be trapped in the crevice volumes. Thus, the ISHC increases with the increase of inlet air pressure (Figure 5.29). Moreover, when the inlet air pressure increases, more ethanol is needed to mitigate knock. The mixture quality may decrease with the increase of the direct injecting ethanol fraction, primarily due to the wall-wetting effect. HC emissions are therefore increased. Finally, over scavenging in this engine may also contribute to the increase of ISHC.

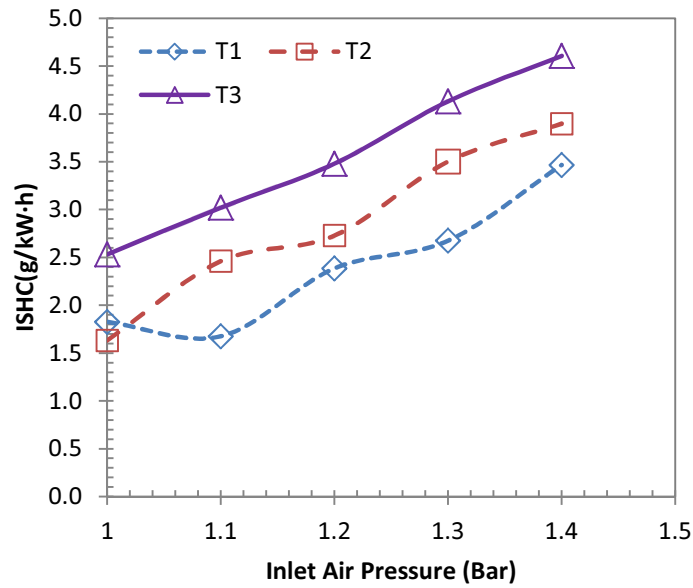


Figure 5.29– Variation of ISHC with inlet air pressure

5.3 Summary

1. When the spark timing was in the range from 25 CAD BTDC to 35 CAD BTDC, the effect of spark timing on the gasoline only condition (EER of 0%) was stronger than that on the EDI conditions. For the same spark advance in this spark timing range, IMEP in the GPI condition increased more quickly than that in the EDI condition. However, when the spark timing was earlier than 35 CAD BTDC, the effect of spark timing on the IMEP was similar at both the EDI and GPI conditions. The indicated thermal efficiency increased with the increase of EER at all tested spark timings.

2. CA_{0-5%} decreased, CA_{5-90%} and CA_{5-50%} increased with the advance of spark timing. COV_{IMEP} first decreased with the advance of spark timing until 35 CAD BTDC was reached, then it increased with further advances of spark timing. When the EER was less than 34%, the CA_{5-50%}, CA_{5-90%} and COV_{IMEP} decreased with the increase of EER in all tested spark timings. When the EER was greater than 34%, the CA_{5-50%}, CA_{5-90%} and COV_{IMEP} increased with the increase of EER in the spark timing range between 25 CAD BTDC and 30 CAD BTDC. In the spark timing range from 35 CAD BTDC to 40 CAD BTDC, these parameters were independent of the EER. Finally, when the spark timing was earlier than 45 CAD BTDC, the

CA5-50%, CA5-90% and COV_{IMEP} decreased with the further increase of EER.

3. ISNO, ISCO and ISHC increased and exhaust temperature decreased with the advance of spark timing. When the EER was raised from 0% to 48%, the ISCO and ISHC increased and the exhaust temperature first decreased then increased with the increase of EER. ISNO first slightly increased then decreased with the increase of EER at all tested spark timings.

4. The leveraging effect of EDI was enhanced by spark advance. The engine thermal efficiency increased on average by 2.0% in the three tested conditions. The engine knock caused by advancing spark timing could be effectively suppressed by EDI due to ethanol's great latent heat of vaporisation and high octane number. GDI, on the other hand, was less effective than EDI in mitigating engine knock. The KLSA in GDI conditions was only slightly earlier than that in GPI conditions. In the EER range from 15% to 35%, almost every 2.0% or 3.0% increment of EER could approximately permit a 2 CAD advance of KLSA.

5. When spark timing was advanced, EER was increased in order to suppress knock. This advanced spark timing and corresponding increase in EER led to a reduced major combustion duration (CA5-90%), an advanced the central combustion phasing (CA50) and a raised the maximum cylinder pressure (P_{max}). HC and CO emissions first decreased with the increase of spark timing, then increased with further advances of spark timing. The raised EER level with the advance of spark timing may contribute to the decrease of HC and CO emissions. NO emissions showed an opposite trend with those of HC and CO emissions. It first increased then decreased with the advance of spark timing. A high EER level at a more advanced spark timing may be the factor causing the decrease in ISNO.

6. With the increase of inlet air pressure, the EER level was increased due to the enhanced propensity of engine knocking. The engine load and efficiency increased with the increase of inlet air pressure. The highest load achieved in the tests was 10.5 Bar IMEP at inlet air pressure of 1.4 Bar. At this condition, the EER level of 36.9% was required to overcome the knocking

caused by both the spark advance and high inlet air pressure. The indicated thermal efficiency at 10.5 Bar IMEP was 37.2% which was the greatest in this study. Over scavenging which could blow part of the fresh charge directly into the exhaust pipe at boosted conditions may negatively affect the indicated thermal efficiency.

7. The exhaust emissions in terms of ISCO, ISNO and ISHC increased with the increment of inlet air pressure. Decreased mixture quality and over scavenging may contribute to the increase of HC and CO emissions. CA5-90% decreased with the increase in inlet air pressure and P_{\max} increased with increase in inlet air pressure.

Chapter Six

6. Influence of SOI timing and injection pressure on dual-injection engine performance

6.1 Effect of SOI timing and injection pressure on engine performance and comparison to GDI+GPI conditions

For an engine equipped with the DI system, SOI timing is one of the primary control parameters that can substantially influence engine performance, as it directly affects the heat transfer and mixture temperature. The variation in SOI timing may lead to changes in engine volumetric efficiency, anti-knock ability as well as mixture quality which will ultimately affect the emissions and power output. In this section the effects of SOI timing and injection pressure are experimentally investigated. Results of engine performance, combustion characteristics and emissions will be presented. Possible reasons will be discussed.

The experiments were conducted at three injection pressure levels of 40 Bar, 60 Bar and 90 Bar and a fixed DI/PFI energy ratio of 48% at 4000rpm. Spark timing was fixed at the original engine setting of 15 CAD BTDC. In each of the tested conditions, direct injection SOI timing was swept from 50 CAD BTDC to 110 CAD BTDC (late ethanol/gasoline fuel injection, defined as LEDI for ethanol and LGDI for gasoline) and 270 CAD BTDC to 330 CAD BTDC (early ethanol/gasoline fuel injection, defined as EEDI for ethanol and EGDI for gasoline) with 20 CAD intervals to investigate the effect of SOI timing on engine performance before and after the inlet valve was closed. The direct injection SOI timing from 120 CAD BTDC to 250 CAD BTDC was avoided due to the fluctuation of the IMEP as shown by the experimental results in Figure 6.1. The fluctuation in IMEP might be due to the turbulent flow passing the inlet port when the inlet valve was closing. 110 CAD BTDC was selected as the initial timing for LEDI/LGDI, because the inlet valve was closed at 120 CAD BTDC. 50 CAD BTDC was

chosen as the end point of LEDI/LGDI to give enough time for fuel vaporisation before the ignition. More details of the experimental conditions are listed in Table 6.1.

Table 6.1 Experimental conditions for Section 6.1

Engine speed	4000rpm
Throttle Position	40%
DI/PFI ratio	48%
Injection timing (CAD BTDC)	50, 70, 90, 110; 270, 290, 310, 330
Injection pressure	60 Bar
Spark timing	15 CAD BTDC

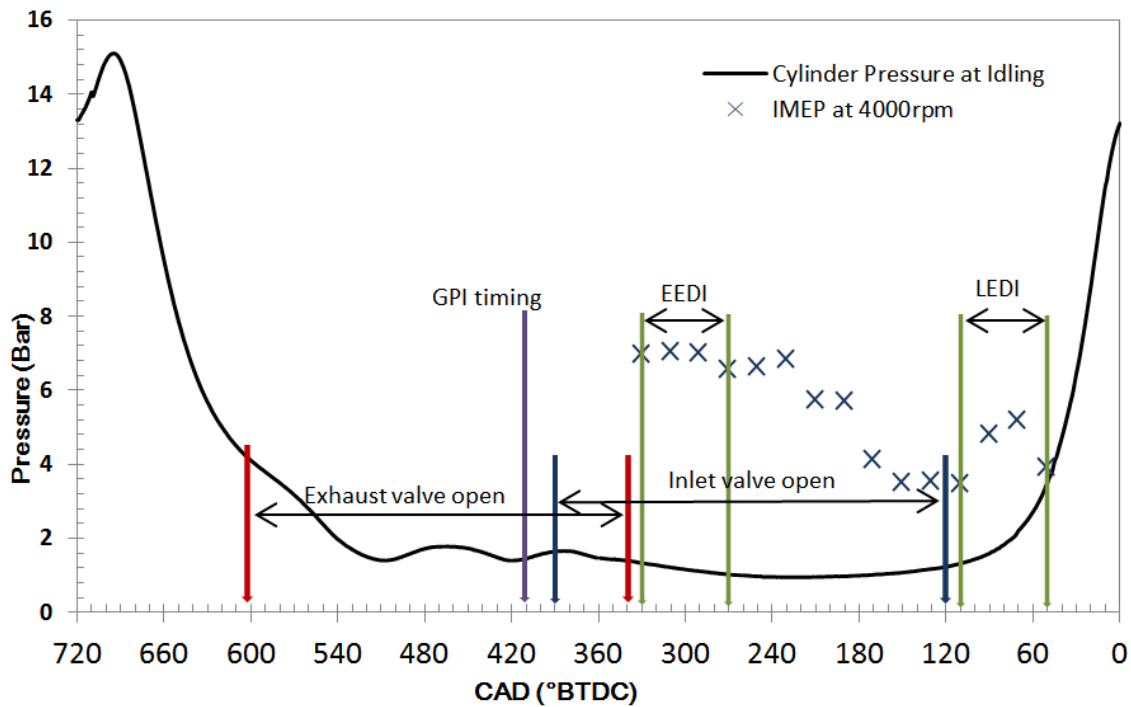


Figure 6.1–Experimental engine SOI timing windows

6.1.1 Engine performance

Figure 6.2 (a) shows the variation of IMEP with SOI timing at 4000rpm and three EDI pressure levels of 40 Bar, 60 Bar and 90 Bar. As shown, the IMEP in EEDI conditions is greater than that in LEDI conditions. The effect of injection timing and pressure is insignificant on IMEP in EEDI conditions. This means that in EEDI conditions the ethanol injection pressure may be kept to a minimum level such as the 40 Bar in this study to save the energy for driving the high pressure fuel pump.

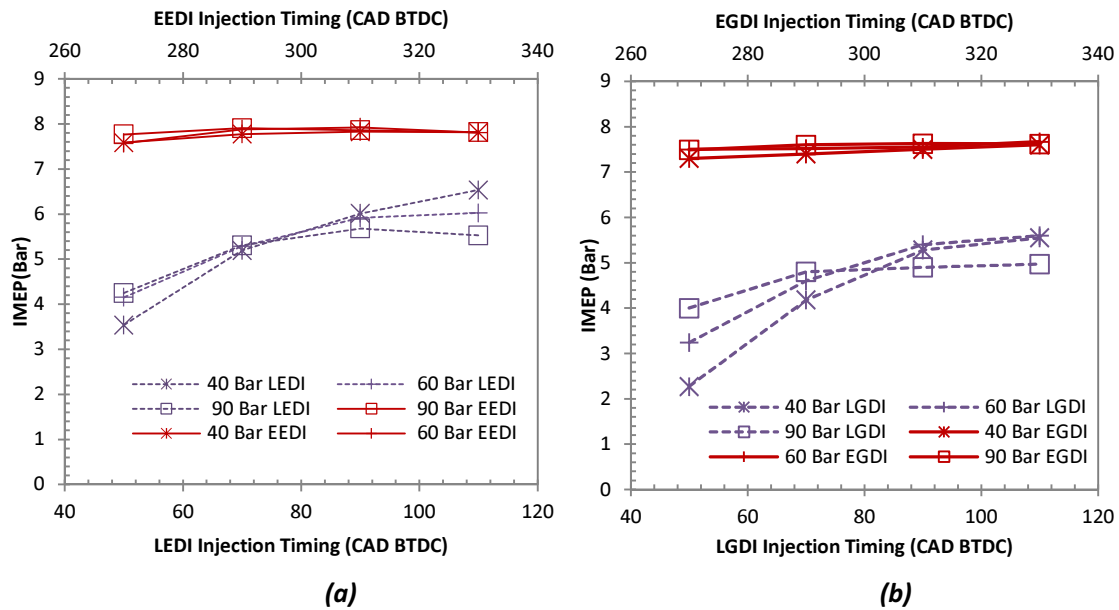


Figure 6.2–Variation of IMEP with SOI timing and pressure in EDI+GPI (a) and EDI+GPI (b) conditions

The results in LEDI conditions show that the effect of SOI timing on IMEP is stronger at lower injection pressure. At injection pressure of 40 Bar, the IMEP is increased from 3.54 Bar at SOI timing of 50 CAD BTDC to 6.53 Bar at SOI timing of 110 CAD BTDC. When the injection pressure is 60 Bar, the IMEP is increased from 4.25 Bar to 6.04 Bar. However, when the injection pressure is further increased to 90 Bar, the increase of IMEP becomes less dependent on the variation of SOI timing. It only increases from 4.35 Bar to 5.53 Bar.

Early ethanol injection (EEDI) may help to produce a more homogenous mixture due to a relatively long time for fuel to evaporate and increase the volumetric efficiency due to the charge cooling. Accordingly, the IMEP in EEDI conditions is in general greater than that in LEDI conditions. The increase of IMEP with the advance of SOI timing in LEDI conditions may also be because of the advanced SOI timing which increases the time for the ethanol fuel to vaporise and results in better combustion. Increasing the EDI pressure may enhance the fuel atomization. This may explain why the IMEP increases with the increase of EDI pressure at a SOI timing of 50 CAD BTDC. However, the high injection pressure may lead to a severe wall-wetting effect especially when the piston just passes the bottom dead center (BTD) at which the in-cylinder flow is weak and the ambient temperature and pressure are not high.

Wall-wetting can deteriorate combustion if the fuel on the wall cannot well evaporate. The decrease of IMEP with the increase of EDI pressure at a SOI timing of 110 CAD BTDC may be because of the wall-wetting effect.

Figure 6.2 (b) shows the variation of IMEP with SOI timing at 4000rpm and three GDI pressure levels of 40 Bar, 60 Bar and 90 Bar. Similar to the results presented in Figure 5.2 (a), IMEP in EGDI conditions is greater than that in LGDI conditions at three GDI pressure levels. However, in EGDI conditions, IMEP slightly increases with the advance of SOI timing, which is different from that in EEDI conditions where the IMEP stays stable and is almost independent with the variation of SOI timing. The stable trend of IMEP in the EEDI condition can be attributed to the removal of heavy fuel fractions and can thus lead to shorter ethanol fuel evaporation durations. When the SOI timing is in the range from 270 CAD BTDC to 330 CAD BTDC, the time period between fuel injection and spark discharge is long enough for ethanol fuel to fully evaporate. Therefore, the variation of IMEP in this SOI timing range becomes stable, which is unaffected by the SOI timing. Nevertheless, for gasoline fuel, its volatility is less than that of ethanol. Its full evaporation requires a higher temperature, stronger in-cylinder turbulence level (high speed) and a longer time period. Thus, with the advance of SOI timing, which provides more time for fuel vaporisation, the mixture quality is improved and the IMEP increases.

Compared with that in the LEDI condition as shown in Figure 6.2 (a), the variation of IMEP in the LGDI condition is more significant than that in the LEDI conditions. For example, at SOI timing of 50 CAD BTDC, the IMEP rises from 2.3 Bar to 4.0 Bar when the GDI pressure is increased from 40 Bar to 90 Bar. At GDI pressure of 40 Bar, the IMEP starts from 2.3 Bar and reaches 5.6 Bar when the SOI timing advances from 50 CAD BTDC to 110 CAD BTDC. Whereas, in the EEDI condition at SOI timing of 50 CAD BTDC, the IMEP increases only by about 0.7 Bar when the EDI pressure is increased from 40 Bar to 90 Bar. At a GDI pressure of 40 Bar, when the SOI timing is advanced from 50 CAD BTDC to 110 CAD BTDC, the IMEP increment is about 3.0 Bar which is 0.3 Bar less than that in the LGDI condition. This difference indicates that the gasoline fuel is more sensitive to the variation of SOI timing and DI pressure than ethanol fuel is. The different volatilities of gasoline and ethanol should be the main reason

that leads to this result.

Apart from the differences, there are still some similarities between Figures 6.2 (a) and (b). In LGDI condition, IMEP at SOI timing of 50 CAD BTDC increases with the increase of GDI pressure, which is similar to that at the same SOI timing in the EEDI condition where the IMEP augments with the raise in EDI pressure. In both the LEDI and LGDI conditions, IMEP at three tested pressure levels increases with advances in SOI timing, and at an SOI timing of 110 CAD BTDC, higher DI pressure results in lower IMEP. This result illustrates that the similarities of the testing results may be caused by the engine configuration (such as the relative position of the injector on the cylinder head, spray angle, cylinder geometries) and operation conditions, but not by the use of different fuels. Using ethanol fuel can ameliorate the IMEP losses at some conditions for example at an SOI timing of 110 CAD BTDC and 90 BTDC. This result also indicates that future engine tests should avoid these low engine performance conditions.

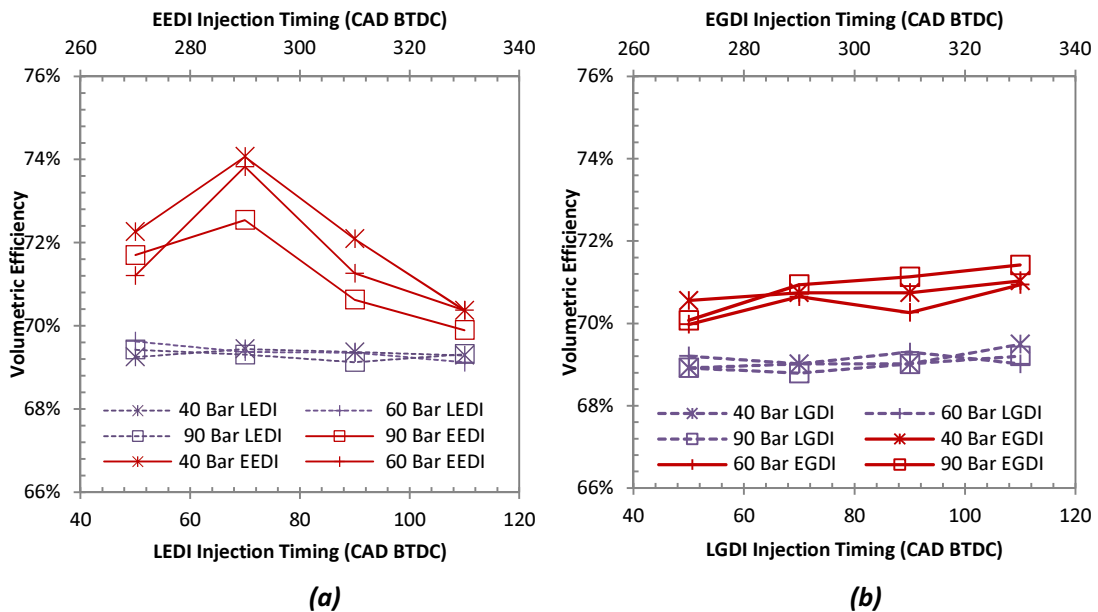


Figure 6.3–Variation of Volumetric efficiency with SOI timing and pressure in EDI+GPI (a) and EDI+GPI (b) conditions

The effect of SOI timing and pressure on the volumetric efficiency in EDI+GPI conditions is shown in Figure 6.3(a). As shown in Figure 6.3(a), the volumetric efficiency in EEDI conditions is higher than in LEDI conditions. The highest volumetric efficiency is 74% when the SOI timing is 290 CAD BTDC and the EDI pressure is 40 Bar. The volumetric efficiency in EEDI

conditions first increases and reaches its peak, then it decreases with further advances in SOI timing. The peak volumetric efficiency at 290 CAD BTDC corresponds to the peak IMEP in EEDI conditions as shown in Figure 6.2 (a). This indicates that the increased IMEP at this point may be because of the increased volumetric efficiency. Figure 6.3 (a) also shows that the volumetric efficiency in EEDI conditions decreases with the increase of the EDI pressure. As stated previously, high EDI pressure may result in a wall-wetting effect, leading to more ethanol fuel impinging on the piston surface and cylinder wall. Thus the evaporation of this fuel relies mainly on heat transfer from the piston surface and cylinder wall but not from the fresh charge. So the volumetric efficiency may decrease with the increase of EDI pressure. The decrease of volumetric efficiency with the advance of SOI timing before 290 CAD BTDC can also be attributed to the fuel impingement on the piston surface. At these timings (310CAD BTDC and 330 CAD BTDC), the piston just passes the TDC. The short distance between the piston surface and the injector tip may easily lead to fuel impingement. The drop of the volumetric efficiency at 270 CAD BTDC, when the inlet valve is fully opened, may be due to the reduced inlet air flow speed which affects fuel evaporation and reduces the time for fuel evaporation, which results in less effective charge cooling.

The volumetric efficiency in LEDI conditions is around 69%. It is almost independent from the variation of SOI timing and EDI pressure. This is because the ethanol fuel is injected after the inlet valve is closed and it has no effect on the fresh charge. Therefore, the volumetric efficiency stays stable in LEDI conditions.

The variation of volumetric efficiency with SOI timing and DI pressure in GDI+GPI conditions is shown in Figure 6.3 (b). Unlike in EEDI conditions where the volumetric efficiency first increases with the advance of SOI timing and then decreases linearly after it reaches the maximum at SOI timing of 290 CAD BTDC, the volumetric efficiency in EGDI conditions slightly increases with the advances in SOI timing and reaches its highest point at 330 CAD BTDC where the volumetric efficiency is around 71%. This difference in the volumetric efficiency result can also be attributed to the low volatility of gasoline which contains more heavy fractions, and the evaporation of these heavy fractions requires more time than ethanol

fuel which contains only a single component. Therefore, the earlier the SOI timing is, the more time will be available for gasoline vaporisation and the lower the charge temperature will be. Thus, the volumetric efficiency increases. This result also indicates that the mixture heat recovery resulting from advancing the SOI timing does not dominate the trends because otherwise the result will be reversed that volumetric efficiency decreases with the advance of SOI timing [171].

The volumetric efficiency in LGDI conditions is similar to that in LEDI conditions. It is almost independent of SOI timing and DI pressure because the inlet valve is already closed. The volumetric efficiency in the LGDI condition is around 68% which is very close to that in LEDI conditions. This result reveals that the influence of DI on volumetric efficiency is only effective in early fuel direct injection conditions.

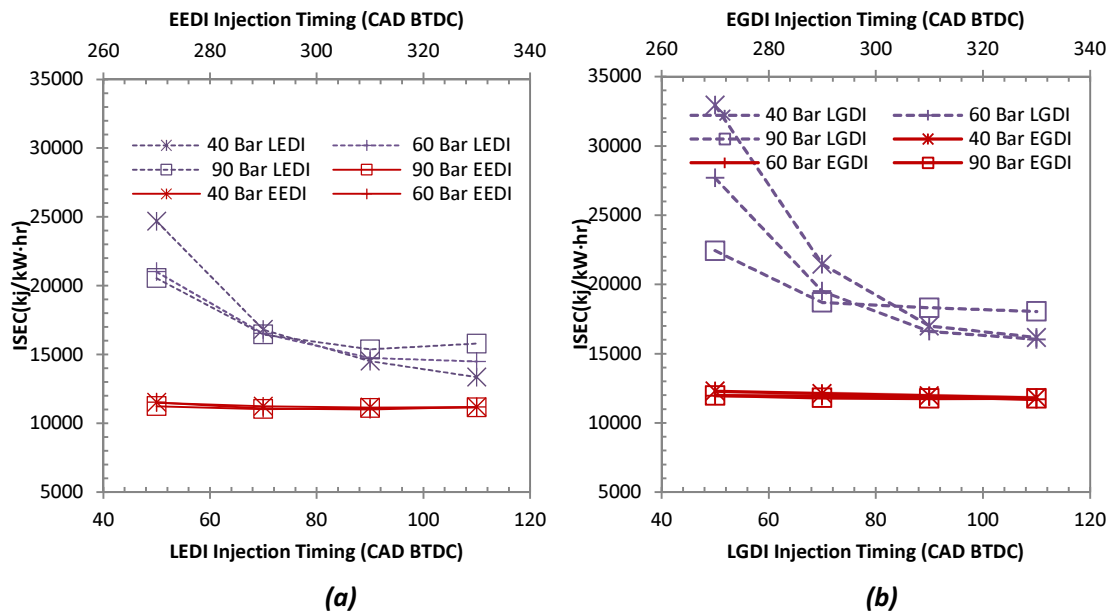


Figure 6.4–Variation of ISEC with SOI timing and pressure in EDI+GPI (a) and EDI+GPI (b) conditions

The ISEC is used in this study to measure the integrated fuel energy consumed rather than the quantity of the fuel consumed. As shown in Figure 6.4 (a), ISEC in EEDI conditions is lower than that in LEDI conditions. It is almost independent of the SOI timing, staying at around 11250 kJ/kW·hr in EEDI conditions and decreasing with the advance of SOI timing in LEDI

conditions. Since the total energy input was kept unchanged in each tested condition, ISEC only varied by the IMEP. Consistent with the timing for the maximum and minimum IMEP in Figure 6.2 (a), the maximum ISEC is 24684 kJ/kW·hr at 40 Bar and SOI timing of 50 CAD BTDC and the minimum is 11039 kJ/kW·hr at 40 Bar and SOI timing of 290 CAD BTDC.

The variation of ISEC with SOI timing and DI pressure in GDI+GPI conditions is illustrated in Figure 6.4 (b). Similar to EDI+GPI conditions, ISEC in EGDI conditions is lower than that in LGDI conditions, and stays stable around 12200 kJ/kW·hr which is greater than the ISEC in LEDI conditions. ISEC in LGDI conditions shows a decline trend with advances in SOI timing. By comparing the Figures 6.4 (a) and 6.4 (b), it can clearly be seen that the ISEC in LGDI conditions is greater than that in LEDI conditions.

6.1.2 Combustion characteristic

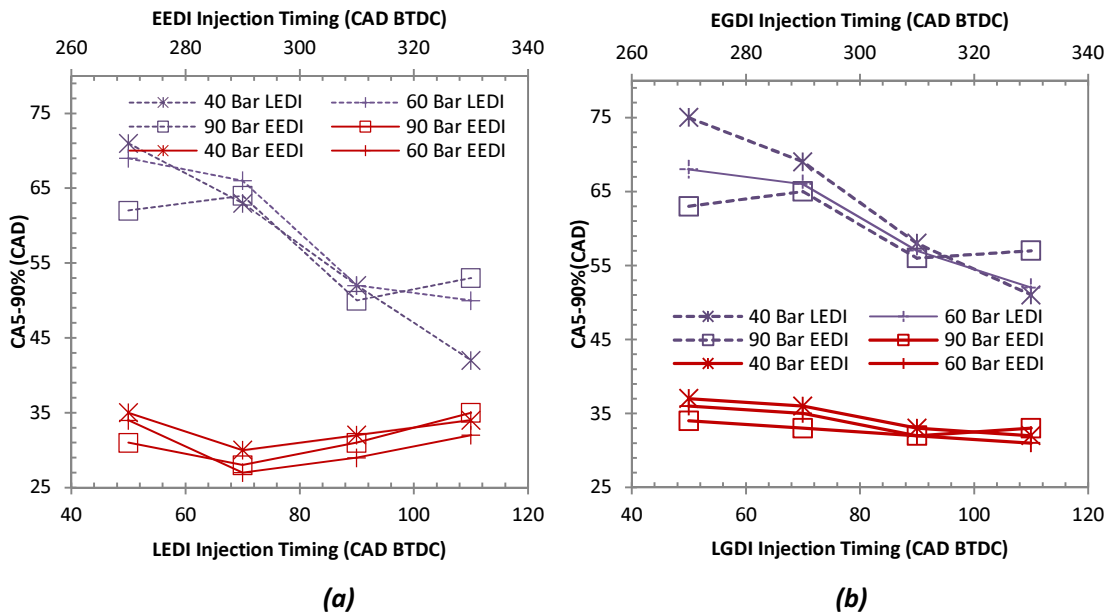


Figure 6.5–Variation of CA5-90% with SOI timing and pressure in EDI+GPI (a) and EDI+GPI (b) conditions

Figure 5.5 (a) shows the variation of the major combustion duration (CA5-90%) with SOI timing. As shown in the figure, the CA5-90% in EEDI conditions is shorter than that in LEDI conditions. CA5-90% in EEDI conditions first reaches its minimum of about 27 CAD when the SOI timing is 290 CAD BTDC, and then slightly increases with further advances in SOI timing. CA5-90% seems independent of the EDI pressure in EEDI conditions as the change of CA5-90%

is insignificant, only about 3 CAD, while the EDI pressure increases from 40 Bar to 90 Bar.

The CA5-90% in LEDI conditions decreases with the increase of SOI timing. As shown in Figure 6.5 (a), at EDI pressures of 40 Bar and 60 Bar, CA5-90% decreases from 69 CAD and 68 CAD to 42 CAD and 50 CAD, respectively. When the EDI pressure is increased to 90 Bar, the effect of advancing SOI timing on CA5-90% becomes weaker. CA5-90% decreases from 62 CAD to 53 CAD. Figure 6.5 (a) also shows that the effect of EDI pressure on CA5-90% varies at different SOI timings. At SOI timing of 50 CAD BTDC, CA5-90% increases with the increase of EDI pressure from 62 CAD to 69 CAD. At SOI timing of 110 CAD BTDC, the CA5-90% decreases gradually from 53 CAD to 42 CAD when the EDI pressure decreases from 90 Bar to 40 Bar. When the SOI timing is in the range from 70 CAD BTDC to 90 CAD BTDC, the effect of EDI pressure on CA5-90% becomes insignificant. The differences in CA5-90% at three EDI pressure levels are minimal in these timings.

The long major combustion duration in LEDI conditions may be caused by the poor mixture quality and low in-cylinder temperature which is caused by the ethanol fuel's vaporisation, therefore deteriorating the combustion and increasing the duration.

The variation CA5-90% in GDI+GPI conditions shows a similar trend with that in EDI+GPI conditions. As shown in Figure 6.5 (b), when the SOI timing is advanced from 50 CAD BTDC to 110 CAD BTDC, the CA5-90% in both conditions decreases. Among the three GDI pressure levels, 40 Bar shows the greatest reduction in the CA5-90% when the SOI timing is advanced from 50 CAD BTDC to 110 CAD BTDC, while the 90 Bar shows the minimum. At SOI timing of 50 CAD BTDC, CA5-90% increases with the increase of GDI pressure, from 63 CAD to 75 CAD. In the SOI timing range from 70 CAD BTDC to 90 CAD BTDC, the CA5-90% is independent of the GDI pressure and the differences in CA5-90% at three GDI pressure levels reduces. At SOI timing of 110 CAD BTDC, the CA10-90% declines from 57 CAD to 52 CAD when the GDI pressure decreases from 90 Bar to 40 Bar.

Figure 6.5 (b) also shows that when the SOI timing is in the range from 270 CAD BTDC to 330

CAD BTDC, the variation of CA5-90% stays stable, and the effect of SOI timing and GDI pressure on CA5-90% becomes less obvious. One difference between GDI+GPI conditions and EDI+GPI conditions is that the CA5-90% in EDI+GPI conditions reaches the minimum at SOI timing of 290 CAD BTDC whereas, the CA5-90% in GDI+GPI conditions reduces with the advance of SOI timing and achieves the minimum at SOI timing of 330 CAD BTDC. This result further supports the previous discussion that the volatility of gasoline is less than that of ethanol which requires more time for vaporisation.

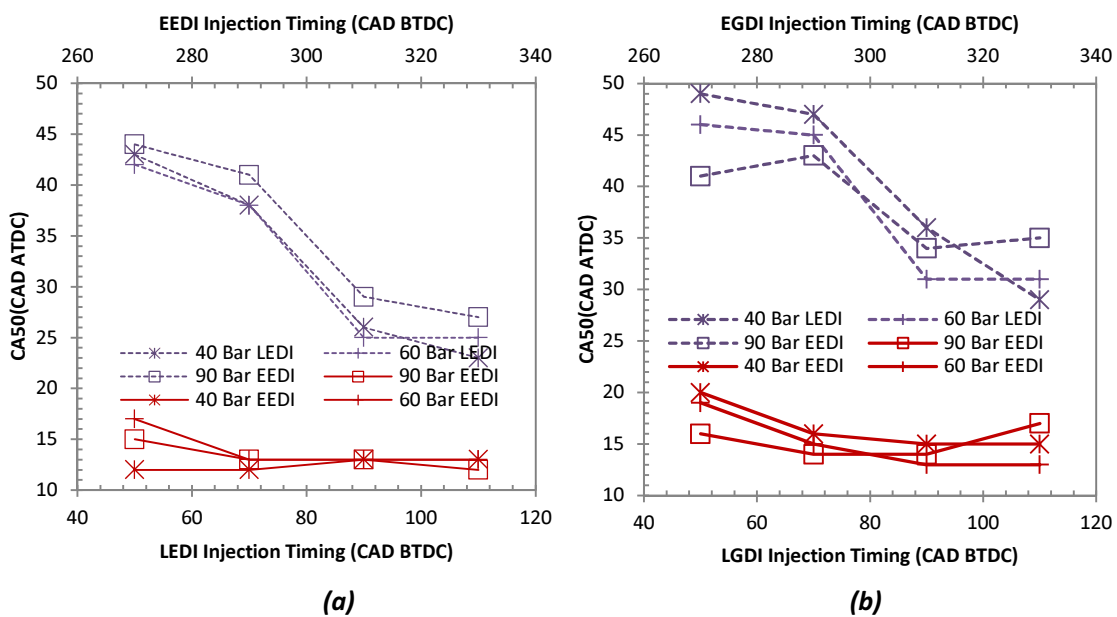


Figure 6.6–Variation of CA50 with SOI timing and pressure in EDI+GPI (a) and EDI+GPI (b) conditions

Figure 6.6 (a) shows the variation of central combustion phasing (CA50) with SOI timing and EDI pressure in the EDI+GPI conditions. As it can be seen, the CA50 in LEDI conditions is more retarded than in EEDI conditions. The CA50 in EEDI conditions almost stays at around 12 CAD ATDC except at SOI timing of 270 CAD BTDC. This means the CA50 in EEDI conditions is closer to the 8 CAD ATDC which is generally regarded as the optimum to achieve the best thermal efficiency. The change of EDI pressure does not show great influence on CA50 in EEDI conditions as shown in Figure 6.6 (a).

The CA50 in LEDI conditions gradually decreases with the advance of SOI timing. At injection pressure of 90 Bar, it decreases from 44 CAD ATDC at SOI timing of 50 CAD BTDC to 27

CAD ATDC at SOI timing of 110 CAD BTDC. Similar trends are also observed at the other two EDI pressures. This may be the result of the improved fuel mixture quality due to the advance of SOI timing which provides more time for the fuel vaporisation and mixing before ignition.

The variation of CA50 with SOI timing and pressure in GDI+GPI conditions is shown in Figure 6.6 (b). When comparing the CA50 in EDI+GPI conditions (Figure 6.6 (a)) with that in GDI+GPI conditions, it can be seen that the trends of CA50 in both conditions are similar. In late direct injection conditions (LEDI and LGDI), the CA50 advances with the increase of SOI timing. In early direct injection conditions (EEDI and EGDI), the variation of CA50 is stable and the effects of SOI timing and injection pressure become insignificant compared to later direct injection conditions. Detailed analysis reveals that the effect of injection pressure on CA50 in LGDI conditions is stronger than that in LEDI conditions. As shown in Figure 6.6 (a), in LEDI conditions, the difference in CA50 at three injection pressure levels is small, whereas the CA50 in LGDI conditions advances with the increase of GDI pressure except at SOI timing of 110 CAD BTDC where the CA50 retards with the raise in GDI pressure. This difference in CA50 can be attributed to the low volatility of gasoline fuel. The gasoline fuel contains more heavy components than that of ethanol fuel. The increase of injection pressure can facilitate the atomisation and vaporisation process of these heavy components. Therefore, the mixture quality is improved with the increase of injection pressure and combustion is improved as well. For ethanol fuel, which contains a single component, the vaporisation requires less pressure than that of gasoline. From Figure 6.6 (a), it can be seen that 40 Bar is enough to result in similar CA50 as that of 60 Bar and 90 Bar. Thus, the fuel pressure for ethanol can be kept at a low level while maintaining similar engine performance.

The difference of CA50 location in EDI+GPI and GDI+GPI conditions may be one of the main contributors to the variation of engine efficiency.

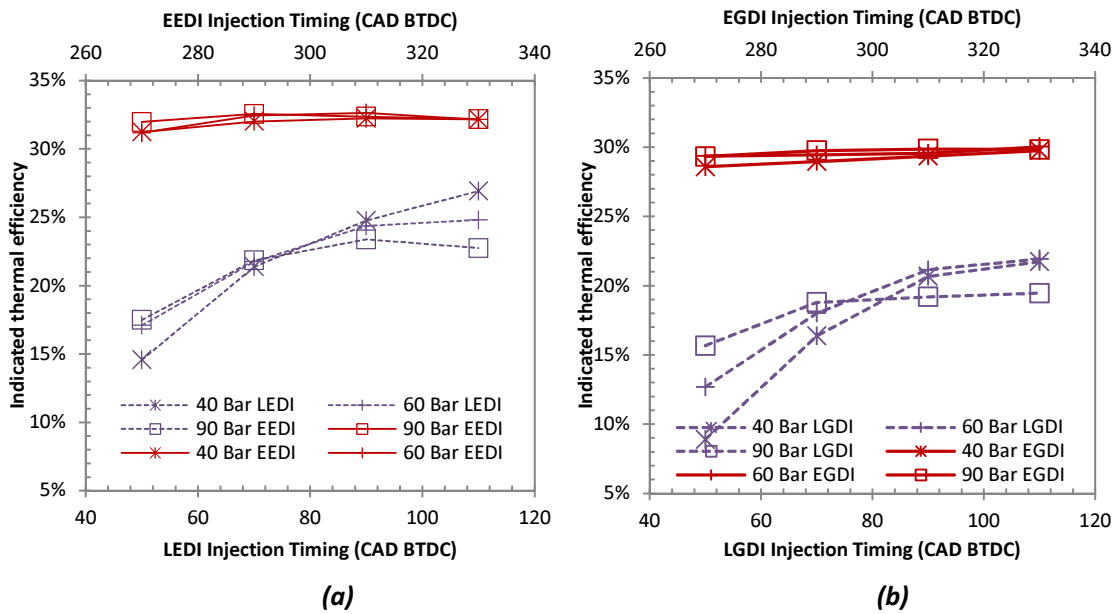


Figure 6.7–Variation of indicated thermal efficiency with SOI timing and pressure in EDI+GPI (a) and EDI+GPI (b) conditions

The effect of SOI timing and EDI pressure on indicated thermal efficiency is illustrated in Figure 6.7 (a). As shown, the highest indicated thermal efficiency is about 32.5% at SOI timing of 290 CAD BTDC. In EEDI conditions, the indicated thermal efficiency is almost independent of the SOI timing and it is greater than in LEDI conditions. Indicated thermal efficiency in LEDI conditions gradually increases with advances in SOI timing. The variation of EDI pressure has a minimal effect on the indicated thermal efficiency when it is in EEDI conditions. However, in LEDI conditions, the indicated thermal efficiency increases with the increase of EDI pressure at SOI timing of 50 CAD BTDC and decreases with the increase of EDI pressure at SOI timing of 110 CAD BTDC.

The volumetric efficiency (Figure 6.3 (a)), CA5-90% (Figure 6.5 (a)) and CA50 (Figure 6.6 (a)) are improved in EEDI conditions. These should be the factors contributing to the higher indicated thermal efficiency in EEDI conditions.

The indicated thermal efficiency result in GDI+GPI conditions is similar to that in EDI+GPI conditions as is shown in Figure 6.7 (b). It can be seen that the indicated thermal in EGGI conditions is stable with a slight increase when the SOI timing advances. In LGDI conditions, the indicated thermal efficiency at three GDI pressures decreases with advances in SOI timing.

The effect of injection pressure on indicated thermal efficiency in LGDI conditions is more significant than in LEDI conditions. For example, at SOI timing of 50 CAD BTDC, the raise of injection pressure from 40 Bar to 90 Bar leads to a 6.7% increase in indicated thermal efficiency in LGDI conditions and this value reduces to 2.9% in LEDI conditions.

6.1.3 Emissions

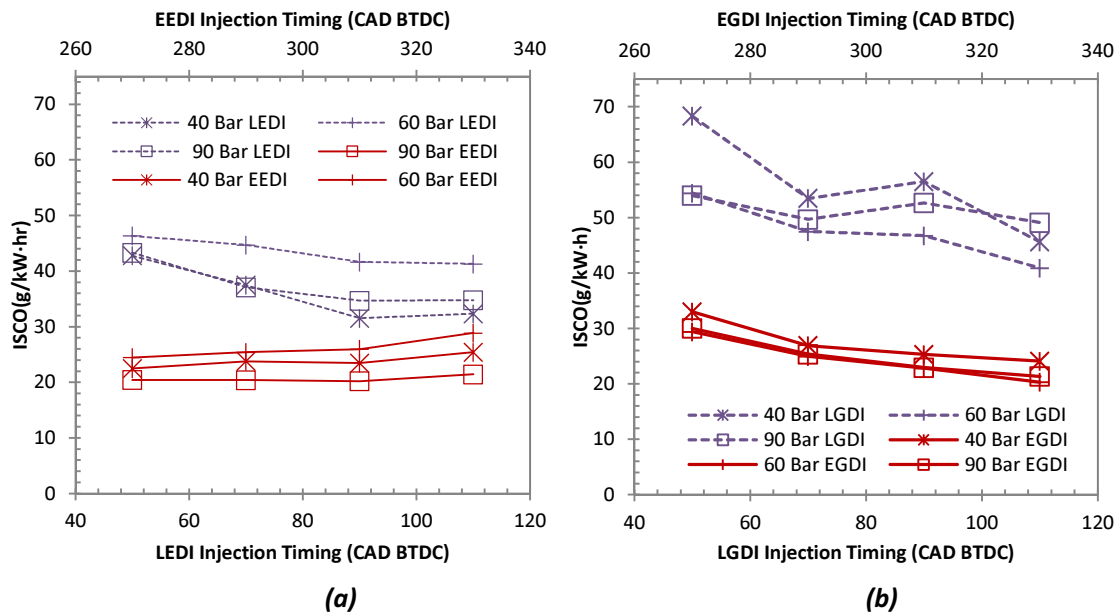


Figure 6.8–Variation of ISCO with SOI timing and pressure in EDI+GPI (a) and EDI+GPI (b) conditions

The variation of ISCO emission with SOI timing and pressure in EDI+GPI conditions is shown in Figure 6.8 (a). As it can be seen, the ISCO in EEDI conditions is lower than that experienced in LEDI conditions. It slightly increases when SOI timing advances. At EDI pressure of 40 Bar, it increases from 24.6 g/kW·hr to 28.8 g/kW·hr when the SOI timing is advanced from 270 CAD BTDC to 310 CAD BTDC. When the injection pressure is 60 Bar, the ISCO is increased from 20.4 g/kW·hr to 25.4 g/kW·hr. The ISCO at 90 Bar almost stays stable at around 20.0 g/kW·hr.

ISCO in LEDI conditions decreases with the advance of SOI timing. The maximum ISCO is 46.3 g/kW·hr at SOI timing of 50 CAD BTDC and EDI pressure of 60 Bar. The minimal ISCO in LEDI conditions is 34.7 g/kW·hr at SOI timing of 110 CAD BTDC and EDI pressure of 40

Bar. CO emission is a product of incomplete combustion. The fuel vaporisation, combustion temperature and in-cylinder flow all have great influence on it. Possibly due to the poor quality of the mixture which has insufficient time to become homogenous, the ISCO in LEDI conditions is higher than that in EEDI conditions.

The exhaust emission of ISCO in GDI+GPI conditions is shown in Figures 6.8 (b). As shown in Figures 6.8 (b), the ISCO in both LGDI and EGDI conditions generally decreases with the advance of SOI timing. The minimum ISCO in LGDI conditions is 40.9 g/kW·hr at SOI timing of 110 CAD BTDC and GDI pressure of 60 Bar. The lowest ISCO in EGDI conditions is 21.4 g/kW·hr at SOI timing of 330 CAD BTDC and GDI pressure of 40 Bar. In the LGDI condition the GDI pressure of 60 Bar produces the lowest CO emissions. However, in the LEDI condition, 40 Bar results in less ISCO than other pressure levels. The ISCO in EGDI conditions shows a decrease trend which is different from that experienced in EEDI conditions where the ISCO slightly increases with the advance of SOI timing. The decrease of ISCO with the advance of SOI timing indicates that advancing the SOI timing may result in a better mixture quality, as the formation of CO emissions is mainly related to the mixture quality.

Figure 6.9 (a) shows the variation of ISHC with SOI timing at three different EDI pressures. As shown in Figure 6.9 (a), the ISHC in both EEDI and LEDI conditions decreases with the advance in SOI timing. There are no distinguishable differences in ISHC in EEDI and LEDI conditions. The ISHC at 60 Bar in LEDI conditions is higher than that in any other conditions. The highest value of ISHC at EDI pressure of 60 Bar is 13.6 g/kW·hr at SOI timing of 290 CAD BTDC. ISHC at 90 Bar reaches the minimum of about 2.32 g/kW·hr. The decrease of ISHC with the increase of SOI timing may be related to the improved mixture quality.

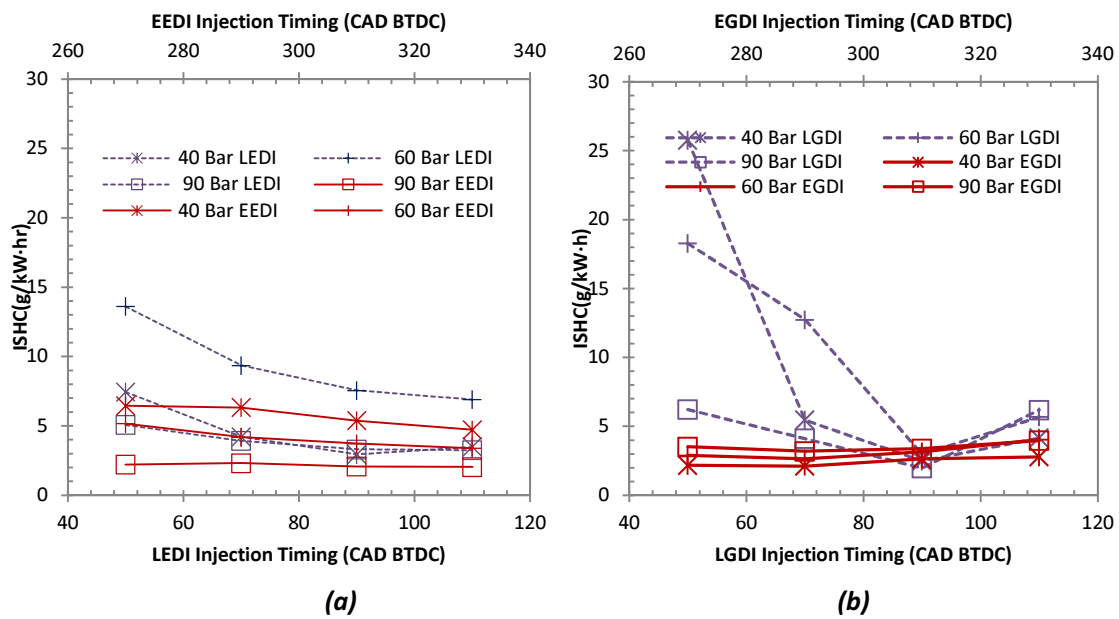


Figure 6.9–Variation of ISHC with SOI timing and pressure in EDI+GPI (a) and EDI+GPI (b) conditions

ISHC in LGDI conditions, as shown in Figure 6.9 (b), generally decreases with the advance of SOI timing. The maximum ISHC in these conditions is 25.8 g/kW·hr at SOI timing of 50 CAD BTDC and GDI pressure of 40 Bar. In EGDI conditions, ISHC stays stable and is almost independent of SOI timing and injection pressure. The maximum ISHC in these conditions is 3.9 g/kW·hr at SOI timing of 110 BTDC and GDI pressure of 40 Bar. Apart from several points (SOI timing of 50 CAD BTDC when GDI pressure is 40 Bar and 60 Bar, and SOI timing of 70 CAD BTDC when GDI pressure is 60 Bar), ISHC in both EGDI and LGDI conditions does not show a distinguishable difference, which is similar to that in EDI+GPI conditions. The high ISHC at SOI timing of 50 CAD BTDC and GDI pressure of 40 Bar and 60 Bar can be attributed to the poor mixture quality, because in GDI+GPI conditions low injection pressure and late SOI timing may result in poor mixture quality.

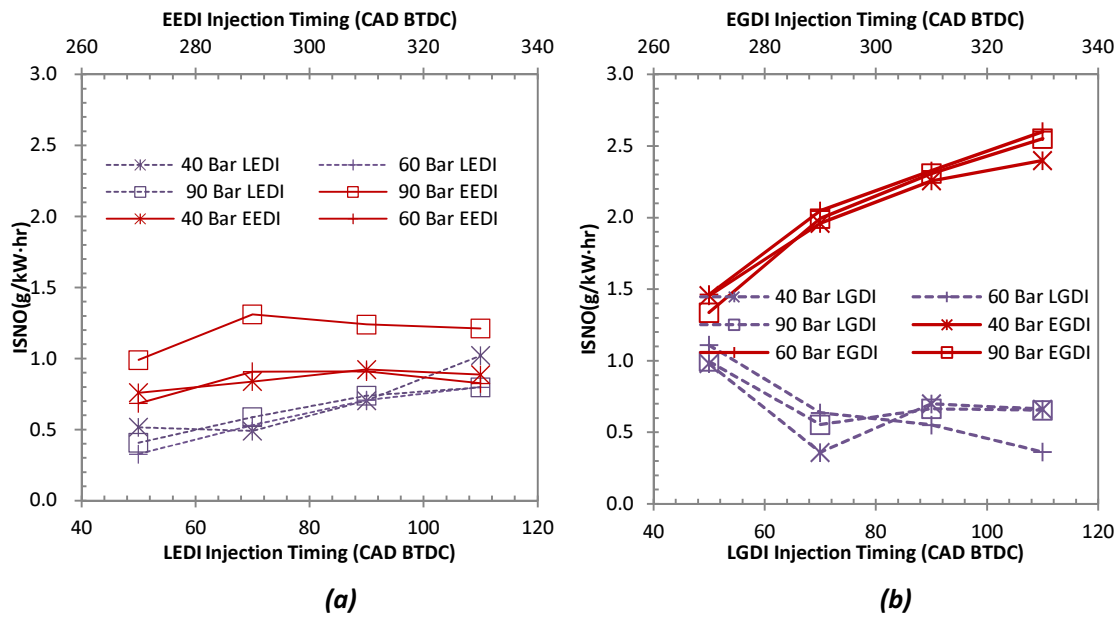


Figure 6.10–Variation of ISNO with SOI timing and pressure in EDI+GPI (a) and EDI+GPI (b) conditions

The effect of varying SOI timing and EDI pressure on ISNO emission is shown in Figure 6.10 (a). As shown in the figure, the ISNO in EEDI conditions is greater than that in LEDI conditions. ISNO in EEDI conditions first increases with the advance of SOI timing and then stays stable when the SOI timing is greater than 290 CAD BTDC. The maximum ISNO is 1.31g/kW·hr at 90 Bar and SOI timing of 270 CAD BTDC.

NO emissions are related to the in-cylinder temperature and its lasting time. Three factors may contribute to this result. Firstly, early injection cools the gas at an early time, increasing the heat transfer from the wall to the gases. Thus the cooling effect of fuel evaporation on the final charge temperature is reduced and therefore NO emissions increase. Secondly, high EDI pressure may lead to more wall-wetting. So most of the fuel is vaporised by absorbing thermal energy from the piston head and cylinder wall and the cooling effect on fresh charge reduced. Thirdly, the combustion process is improved by a more homogenous mixture. The combustion temperature is therefore increased, resulting in an increase of NO emissions.

ISNO in LEDI conditions increases with the advance of SOI timing from about 0.42 g/kW·hr to about 0.80 g/kW·hr when the EDI pressure is 60 Bar and 90 Bar, and from 0.52 g/kW·hr to 1.02 g/kW·hr at EDI pressure of 40 Bar. There is no significant change of ISNO when the EDI

pressure is increased from 40 Bar to 90 Bar. The increase of ISNO with the increase of SOI timing may be due to the reduced cooling effect and increased heat transfer from the wall to the mixture when the SOI timing is advanced.

The variation of ISNO with SOI timing and GDI pressure is shown in Figure 6.10 (b). It can be seen that ISNO in the EGDI condition generally increases with the advance of SOI timing and the variation of GDI pressure has little effect on NO emissions. In LGDI conditions, the ISNO first decreases with the advance of SOI timing. When the SOI timing is earlier than 70 CAD BTDC, it becomes stable with further advances in SOI timing.

By analysing Figures 6.10 (a) and 6.10 (b), it can be seen that the ISNO in GDI+GPI conditions is generally higher than that in EDI+GPI conditions. In EGDI conditions, ISNO shows a monotonous increase trend with the advance of SOI timing, while in EEDI conditions ISNO becomes stable when the SOI timing is earlier than 290 CAD BTDC. These differences in ISNO can be attributed to the difference in ethanol and gasoline's latent heat of vaporisation, the former is about 3 times greater than the latter.

6.2 Effect of SOI timing on knock mitigation

As reviewed in Section 2.2.3, the variation of SOI timing leads to the difference in charge cooling, which, in turn, affects the engine anti-knock ability. Therefore, the effect of SOI timing on EDI+GPI engine knock mitigation is worth investigating.

The tests were performed at 3500rpm with an EER of 24.2% and ethanol injection pressure of 40 Bar. Two engine loads, light (IMEP 4.5~6.5 Bar) and medium (IMEP 6.5~8.5 Bar) were compared. The ethanol direct injection SOI timing was swept from 50 CAD BTDC to 110 CAD BTDC (LEDI) and 270 CAD BTDC to 330 CAD BTDC (EEDI) with 20 CAD intervals. In this way, the effect of EDI on knock mitigation before and after the inlet valve closing was investigated. The ethanol fuel SOI timing from 120 CAD BTDC to 250 CAD BTDC was avoided due to the fluctuation. In each tested condition, the engine spark timing was advanced until the knock was detected from the cylinder pressure. Then the spark timing was retarded 2

CAD and marked as KLSA. Gasoline only conditions were also tested to provide the benchmarks for the results. The engine experimental conditions for this part of tests are listed in Table 6.2.

Table 6.2 Experimental conditions for Section 6.2

Engine speed	4000rpm
Engine load	Medium; Light
Throttle Position	44%@Medium Load, 24%@Light Load
EER	24.2%
Injection timing (CAD BTDC)	50, 70, 90, 110; 270, 290, 310, 330
Injection pressure	60 Bar
Spark timing	KLSA

6.2.1 Engine performance

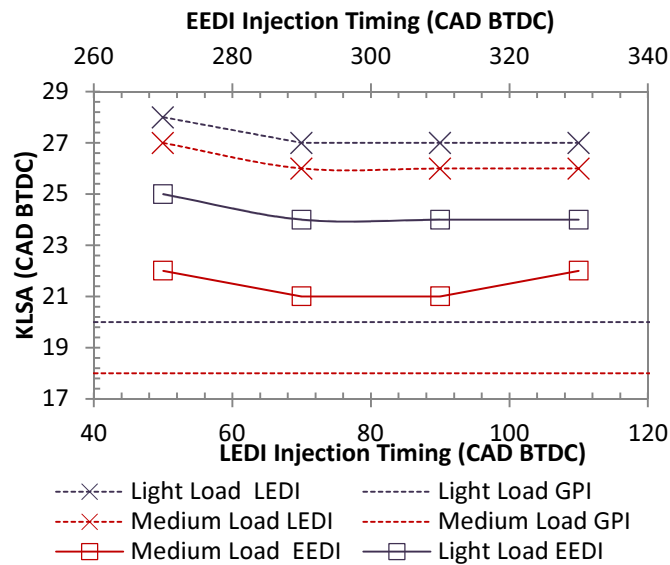


Figure 6.11–Variation of KLSA with SOI timing

The effect of ethanol fuel SOI timing on KLSA is illustrated in Figure 6.11. As shown in the figure, the LEDI demonstrates greater potential for mitigating engine knock than EEDI. KLSA in LEDI conditions is advanced from 20 CAD BTDC (in GPI condition) to 28 BTDC at light load and 18 CAD BTDC (in GPI condition) to 25 CAD BTDC at medium load, whilst in EEDI conditions it can only be advanced to 25 CAD BTDC at light load and 22 CAD BTDC at medium load. As reviewed in Section 2.2.3, early ethanol fuel injection (EEDI) cools the gas at an earlier time, increasing the heat transfer from the wall to the gases. Thus, the cooling effect

of fuel evaporation on the final charge temperature is compromised and the engine anti-knock ability is reduced. For later ethanol fuel injection (LEDI), the heat transfer rate before fuel injection is lower, because the air temperature is higher. When fuel is injected late and it cools the charge, the cooling effect due to fuel evaporation can be well conserved which leads to a lower in-cylinder temperature as well as a knocking tendency. Therefore, LEDI is more effective in suppressing engine knock than EEDI. GPI is the least effective in suppressing the knock, as shown in Figure 6.11. This may be related to two mechanisms. Firstly, in GPI conditions, gasoline fuel is injected into the intake port. Most of the fuel impinges the metal surfaces of the port and valves [172]. The evaporation of this fuel relies mainly on heat transfer from the hot surface of the port and valve to the fuel film, which is unlike the directly injected ethanol fuel that vaporises mainly by absorbing the heat from the charge in cylinder. Therefore, the evaporation of the gasoline fuel in GPI condition cools the charge less effectively than that in EDI conditions. Secondly, gasoline’s latent heat of vaporisation and octane number are lower than ethanol.

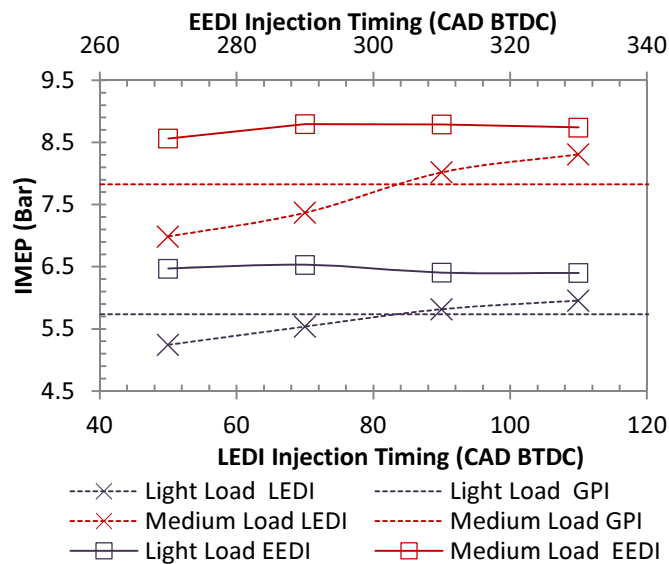


Figure 6.12–Variation of IMEP with SOI timing at KLSA

Although the KLSA is more advanced in LEDI conditions than in LEDI conditions as shown in Figure 6.11, the IMEP does not increase with the advance of KLSA. As shown in Figure 6.12, the IMEP in EEDI conditions is greater than in LEDI and GPI conditions, and it is almost independent of the SOI timing. IMEP in LEDI conditions decreases with the retard of SOI

timing. When the SOI timing is retarded to be later than 90 CAD BTDC, the IMEP at both engine loads is lower than in GPI conditions. This indicates that the effect of EEDI on IMEP improvement is stronger than that of LEDI, although its effect on knock mitigation is weaker than LEDI's. Advanced spark timing, increased volumetric efficiency (Figure 6.13) and more homogeneous mixture which improve the combustion (Figures 6.14 and 6.15) may contribute to the increase of IMEP in EEDI conditions. Among these factors, the mixture quality may play an important role in affecting the final IMEP results.

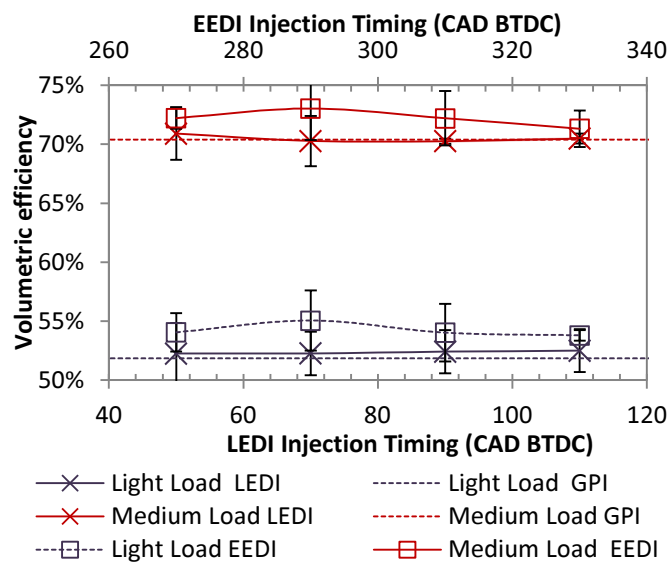


Figure 6.13–Variation of volumetric efficiency with SOI timing at KLSA

Figure 6.13 shows the variation of volumetric efficiency with SOI timing at KLSA. The charge cooling effect of EDI on suppressing engine knock is realised mainly through reducing fresh charge temperature [89]. The charge density is affected by the reduced temperature during this process which may ultimately influence volumetric efficiency. It can be seen in Figure 6.13 that in both engine loads, the volumetric efficiency in EEDI conditions is higher than that in LEDI and GPI conditions. In EEDI conditions, the ethanol fuel is injected during the intake stroke. Volumetric efficiency can be increased by the reduced temperature and volume of the fresh charge due to fuel's evaporation. Moreover, the evaporation of ethanol requires more heat than gasoline to be transferred from the fresh charge and the cylinder wall. Thus the charge temperature can be further reduced when there is DI ethanol which results in higher volumetric efficiency in the EEDI condition. More details for the result presented in Figure 6.13 can be

found in the discussion for Figure 6.3.

6.2.2 Combustion characteristics

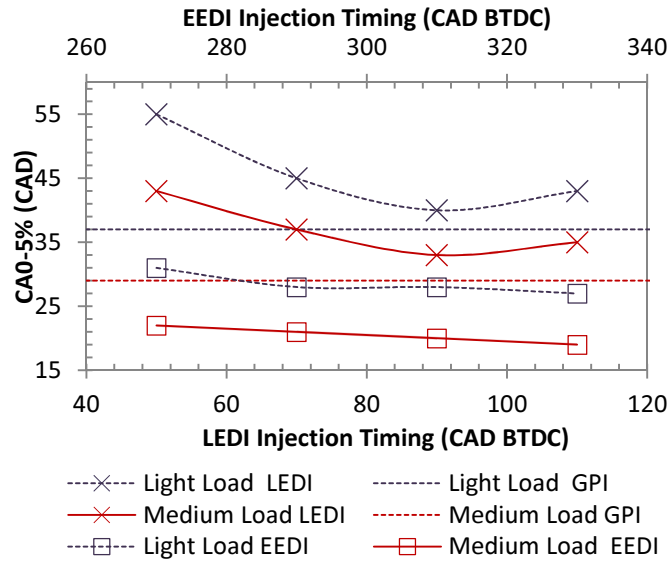


Figure 6.14–Variation of CA0-5% with SOI timing at KLSA

Figure 6.14 shows the variation of combustion initiation duration (CA0-5%) with SOI timing at KLSA. The combustion initiation duration directly relates to the combustion stability and is sensitive to the mixture homogeneous quality and in-cylinder temperature before the ignition [155]. Normally, long combustion initiation duration indicates that the mixture is hard to be ignited. Engine efficiency can be negatively affected because of poor ignition. Therefore, the result presented here is to find an SOI timing range at which the engine knock can be effectively mitigated and the combustion initiation duration is not largely elongated. As shown in Figure 6.14, CA0-5% in EEDI conditions is shorter than in LEDI and GPI conditions. It gradually decreases with the advance of SOI timing in both EEDI and LEDI conditions except at SOI timing of 110 CAD BTDC at which the CA0-5% increases slightly. The minimal values of CA0-5% in LEDI conditions are 40 CAD at light load and 33 CAD at medium load when SOI timing is 90 CAD BTDC. The minimal values of CA0-5% in EEDI conditions are 27 CAD at light load and 19 CAD at medium load when SOI timing is 330 CAD BTDC. This result indicates that EEDI is more effective than LEDI on knock mitigation in the present study, because it results in better combustion. The decrease of CA0-5% with the advance of SOI

timing may be because of the increased time for ethanol fuel vaporisation which results in a more homogeneous mixture and a high in-cylinder temperature. The slight increase in CA0-5% at SOI timing of 110 CAD BTDC can be attributed to the weak in-cylinder flow during ethanol injection at this timing (the inlet valve is just open), which decreases the mixture quality and prolongs the combustion initiation duration.

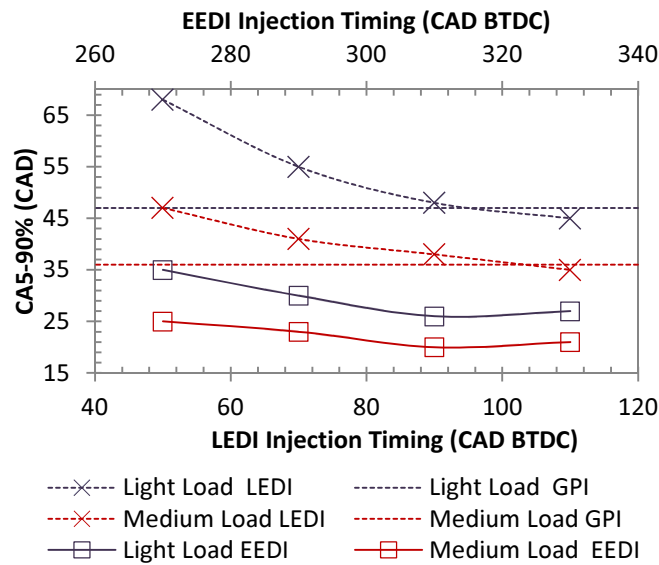


Figure 6.15–Variation of CA5-90% with SOI timing at KLSA

Figure 6.15 shows the variation of major combustion duration, CA5-90%, with SOI timing at KLSA. As shown in Figure 6.15, CA5-90% in EEDI conditions is shorter than in LEDI and GPI conditions. There is an average 20 CAD deduction of CA5-90% in EEDI conditions when compared to that in LEDI conditions. This result indicates that although LEDI is effective in knock mitigation, the major combustion duration is substantially increased in the LEDI condition. The longest CA5-90% is 68 CAD at SOI timing of 50 CAD BTDC and the minimum CA5-90% is 20 CAD at 290 CAD BTDC. CA5-90% generally decreases with the advance of SOI timing in all the tested conditions. This decrease in CA5-90% can be attributed to the improved fuels/air mixture quality when SOI timing is increased. The CA5-90% result, here again, proves that the EEDI can result in better combustion and this should be regarded as one of the main factors that leads to high IMEP in EEDI conditions.

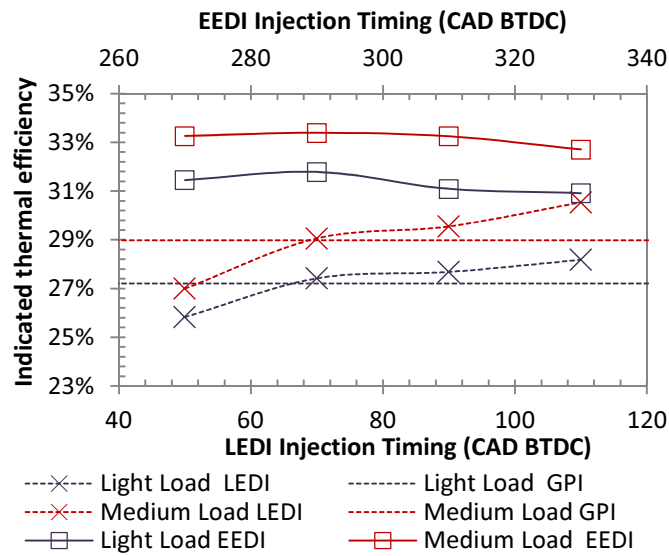


Figure 6.16–Variation of indicated thermal efficiency with SOI timing at KLSA

The effect of SOI timing on indicated thermal efficiency at KLSA is shown in Figure 6.16. Here, the effect of SOI timing on knocking which ultimately affects engine efficiency can be clearly seen. As shown in the figure, the peak indicated thermal efficiency in EEDI conditions is about 33.5% at SOI timing of 290 CAD BTDC and medium load. Whereas, the corresponding indicated thermal efficiency for the GPI condition is only 29% which is because the advent of knock constrains further advances in spark timing. The indicated thermal efficiency in EEDI conditions is almost independent with the variation of SOI timing and it is greater than in LEDI and GPI conditions. Indicated thermal efficiency in LEDI conditions, gradually increases with the advance of SOI timing. It exceeds the value in the GPI condition when the SOI timing is earlier than 70 CAD BTDC. This result indicates that EEDI can result in higher indicated thermal efficiency than LEDI and GPI. The advanced spark timing (Figure 6.11) and reduced combustion duration (Figure 6.15) may be the main reasons that contribute to the higher efficiency in the EEDI condition. In addition, the increased volumetric efficiency which reduces the pumping loss during the intake process [171] and ethanol’s high energy content of stoichiometric mixture per unit mass of air may also contribute to the high indicated thermal efficiency.

6.2.3 Emissions

When the engine is running at KLSA, minimal change of spark timing can lead to moderate variation in engine power output but substantial change in NO_x and HC emissions [155]. The variations of ISNO and ISHC with SOI timing at KLSA are shown in Figures 6.17 and 6.18, respectively. As shown in Figure 6.17, ISNO in LEDI conditions is less than that in GPI and EEDI conditions. At both loads, ISNO gradually increases with the advance of SOI timing in EEDI and LEDI conditions. The lowest ISNO is 0.22 g/kW·hr at SOI timing of 50 CAD BTDC at light load in LEDI condition and the highest ISNO is 3.7 g/kW·hr at SOI timing of 330 CAD BTDC at medium load.

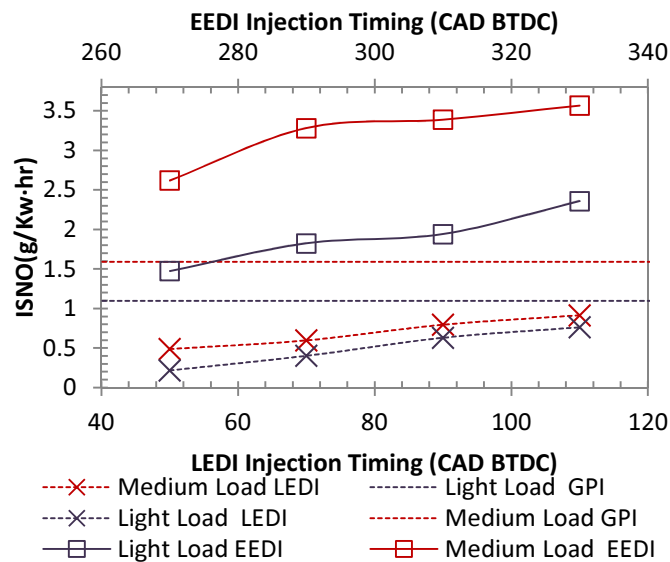


Figure 6.17–Variation of ISNO with SOI timing at KLSA

The increase of ISNO with the advance of SOI timing may be because the heat transfer from the wall to the gases increases with the advance of SOI timing. Further, homogeneous mixture improves the combustion, leading to more intensive heat release and a higher temperature. By analysing Figure 6.11 and Figure 6.17, it can be seen that although the spark timing is more advanced in LEDI conditions, the ISNO is not affected by the more advanced spark timing and it remains at a low level at both light and medium loads. EEDI, though the spark timing is less advanced than that in LEDI conditions, leads to more NO emissions. This result indicates that the mixture homogeneous quality has a more dominant effect on influencing NO formation in this part of study, as it is directly relates to the combustion quality and subsequent combustion temperature.

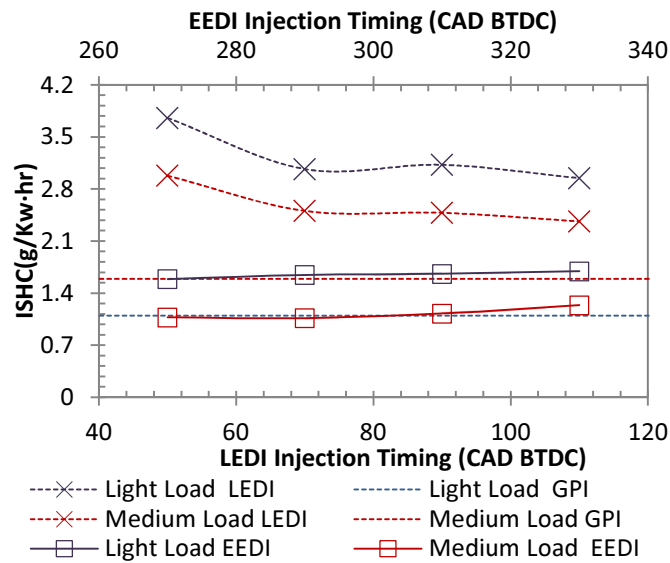


Figure 6.18–Variation of ISHC with SOI timing at KLSA

Figure 6.18 shows the variation of ISHC with SOI timing at KLSA. As shown in the figure, more HC emissions were generated in LEDI conditions than in EEDI and GPI conditions. The ISHC in the LEDI condition generally decreases with the advance of SOI timing and the ISHC in EEDI conditions is almost independent with the advance of SOI timing. At medium load, the ISHC in EEDI conditions is lower than in the GPI condition. At light load, the ISHC in EEDI conditions is slightly higher than the corresponding GPI condition. The maximal value of ISHC is 3.75 g/kW·hr at SOI timing of 50 CAD BTDC at light load and the minimum is 1.07 g/kW·hr at SOI timing of 270 CAD BTDC at medium load. The high ISHC in LEDI conditions can be attributed to the mixture inhomogeneous which leads to incomplete combustion. The decrease of ISHC with the advance of SOI timing in LEDI conditions may be because advancing SOI timing provides more time for fuel vaporisation. Thus, the combustion is more complete and the ISHC decreases.

6.3 Effect of SOI timing on lean burn

6.3.1 Engine performance

In order to further explore the potential in using EDI to improve GPI engine efficiency and reduce emissions, lean burn has been investigated in this study. According to the review in

Section 2.2.5, stratified combustion with fuel directly injected later in the compression stroke (LEDI) has more potential to extend the lean burn limit than homogeneous lean combustion (EEDI and GPI). However, stable combustion in the stratified condition is hard to achieve. The SOI timing needs to be carefully optimised to ensure stable combustion. Therefore, the effect of SOI timing on EDI+GPI engine lean burn is worth investigating.

In the experiments aimed at investigating the effect of SOI timing on lean burn, two test conditions with EERs of 24% and 48% were selected. The direct injection pressure for EER of 24% was 40 Bar and 90 Bar for EER of 48%. This was to keep the same EDI duration and to minimise the influence of the end of injection timing on engine performance. Spark timing was set at 21 CAD BTDC and 25 CAD BTDC for EERs of 24% and 48% respectively, to provide more time for fuel evaporation and to ensure stable combustion according to previous pretests.

During the test of lean burn, the engine conditions of load and SOI timing were first set at the designated values with stoichiometric AFR. Then, the energy flow rates of ethanol and gasoline were fixed, and the throttle opening was increased to make the mixture increasingly lean. When the AFR was increased, the IMEP was first raised and it reached the maximum with an increase of AFR, then it decreased with a further increase of AFR. If the COV_{IMEP} was less than 10% during this process, the AFR for the IMEP which was 2% dropped from the maximum was regarded as the lean burn limit. This method of defining the lean burn limit was suggested by Albert et al. [173]. If the COV_{IMEP} was above 10%, the AFR would be decreased until the COV_{IMEP} was within 10% again. Then the corresponding AFR was recorded as the lean burn limit. Using a 2% drop in IMEP as a marker to lean burn limit is because exploiting the potential of EDI+GPI in improving engine efficiency is one of the major purposes in this study. The total energy input of both ethanol and gasoline fuels was kept unchanged in each of the tested conditions, as previously described, thus the condition at which the IMEP reached the maximum was the condition with the maximum thermal efficiency. In order to ensure the combustion stability in the acceptable range, the upper combustion stability limit of 10% COV_{IMEP} was used as another marker to the lean burn limit. It should be noted that using 10% of COV_{IMEP} as the

upper limit is because the engine used for this test is a single cylinder air cooled engine with a relatively short stroke of 58mm. Previous studies on similar small engines also used the 10% of COV_{IMEP} as the acceptance [174]. The experimental conditions for the tests are listed in Table 6.3.

Table 6.3 Experimental conditions for Section 6.3

Engine speed	4000rpm
EER	0% (GPI), 24%, 48%
Injection timing (CAD BTDC)	50, 70, 90, 110; 270, 290, 310, 330
Injection pressure	40 Bar (EER 24%) 90 Bar (EER 48%)
Spark timing	21 CAD BTDC (EER 24%) 25 CAD BTDC (EER 48%)

Figure 6.19 shows the variation of lean burn limit with SOI timing at two EERs of 24% and 48%. As shown in Figure 6.19, EEDI can keep the engine operating at leaner conditions than LEDI and GPI. The lean burn limit, defined by the maximum λ achievable, in EEDI conditions is greater than in LEDI and GPI conditions. At both EER levels of 24% and 48%, the lean burn limit first reaches its peak at SOI timing of 290 CAD BTDC in EEDI condition and 90 CAD BTDC in LEDI condition. Then, it begins to slightly decrease with further advances in SOI timing. EER of 24% seems to be more suitable for extending the lean burn limit than EER of 48% does. The lean burn limit reaches its maximum of 1.29 when EER is 24% at SOI timing of 290 CAD BTDC. The minimum lean burn limit exists at EER of 48% in LEDI conditions, which is only slightly greater than the stoichiometric AFR ($\lambda=1$) while the other lean burn limits are all above $\lambda=1.1$.

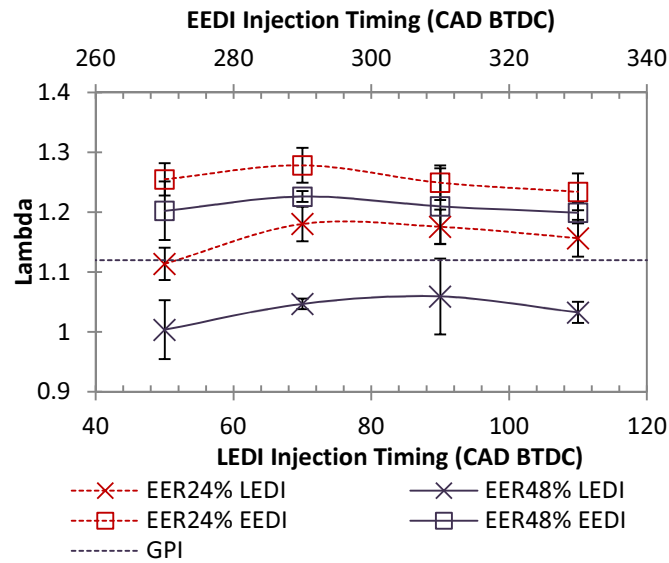


Figure 6.19 –Variation of lean burn limit with SOI timing

As reviewed in Section 2.2.5, LEDI produced stratified charge adjacent to the spark plug, which theoretically has more potential to extend the lean burn limit than the homogeneous lean burn (EEDI and GPI). However in the present study, the effect of LEDI on extending the lean burn limit is weaker than that of EEDI. One possible explanation to this result is that LEDI might lead to severe fuel impingement on the piston crown and cylinder wall as reported in [117]. This wall-wetting negatively affects the mixture formation, combustion, decreasing combustion stability (Figure 6.22) and elongating combustion duration (Figure 6.24). Therefore, the lean burn limit in LEDI conditions is low. The top lean burn limit at SOI timing of 290 CAD BTDC may be due to the improved mixture quality. Similar engine performance improvement at this particular SOI timing is shown in Figures 6.5(a) and 6.6(a).

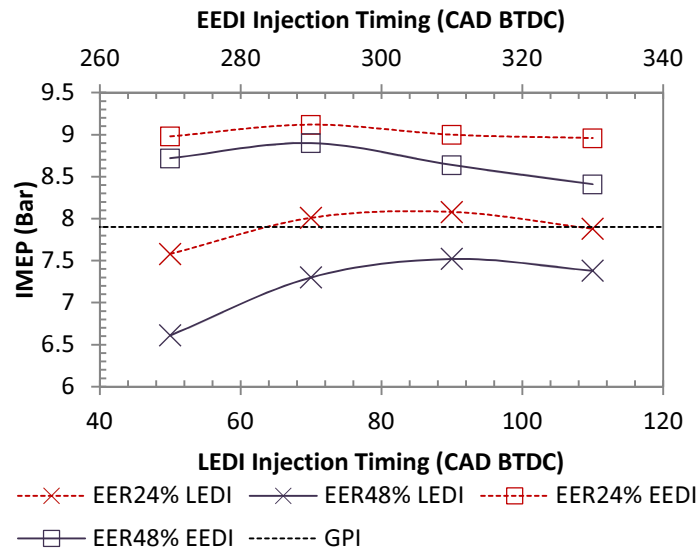


Figure 6.20– Variation of IMEP at lean burn limit

The variation of IMEP with SOI timing at the lean burn limit is shown in Figure 6.20. It can be seen that IMEP is greater in EEDI conditions than in LEDI and GPI conditions. IMEP at EER of 24% is higher than that at EER of 48% in both LEDI and EEDI conditions. As shown in Figure 6.20, IMEP varies with lean burn limit. The IMEP increases when the lean burn limit increases, and decreases when the lean burn limit reduces. This result is mainly due to the 2% drop in IMEP from the maximum to define the lean burn limit.

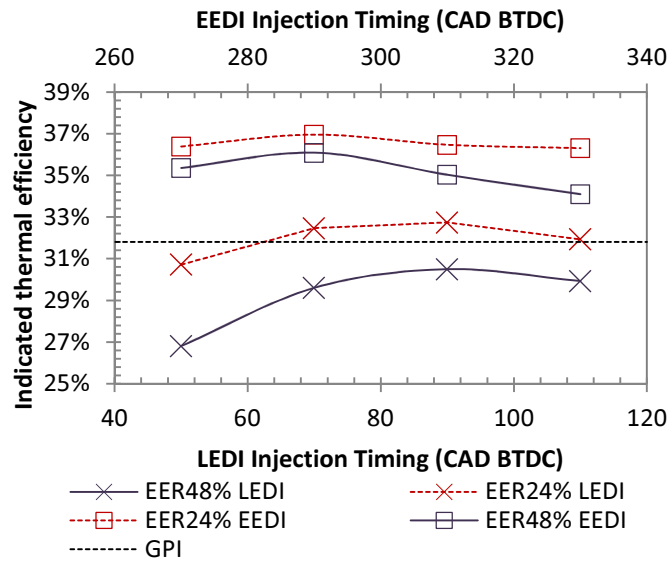


Figure 6.21– Variation of indicated thermal efficiency at lean burn limit

The effect of SOI timing on indicated thermal efficiency at the lean burn limit is shown in Figure 6.21. As shown in Figure 6.21, the indicated thermal efficiency is greater in the EEDI condition than in LEDI and GPI conditions. The peak indicated thermal efficiency is 36.8% at SOI timing of 290 CAD BTDC and EER of 24%. In EEDI conditions, the indicated thermal efficiency at both EER levels (24% and 48%) first slightly increases until it reaches the maximum at SOI timing of 290 CAD BTDC, and then decreases with further advances in SOI timing. In LEDI conditions, the indicated thermal efficiency first increases with the advance of SOI timing and then begins to decrease when the SOI timing is earlier than 90 CAD BTDC.

Results shown in Figure 6.21 may be related to the quality of the ethanol/air mixture. When the SOI timing is at 330 CAD BTDC and 270 CAD BTDC, the mixture quality may be negatively affected by wall-wetting and the reduced time for fuel evaporation respectively, as stated in the discussion for Figure 6.13. Therefore the combustion deteriorates and the indicated thermal efficiency reduces. In LEDI conditions, advancing SOI timing provides more time for ethanol evaporation and heat recovery. As a consequence, the mixture quality is improved and the in-cylinder temperature is increased. Thus the combustion is improved and the indicated thermal efficiency is increased.

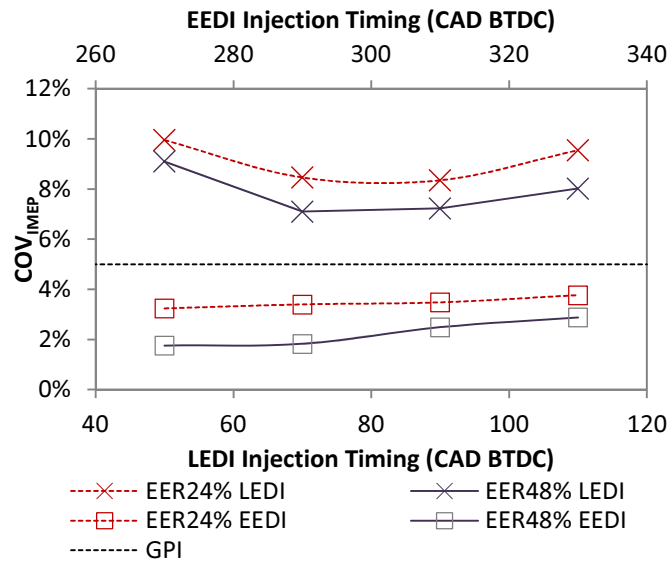


Figure 6.22–Variation of COV_{IMEP} with SOI timing at lean burn limit

The variation of COV_{IMEP} at lean burn limit is shown in Figure 6.22. When the mixture is leaned, the combustion becomes unstable. It is therefore necessary to monitor the COV_{IMEP} to keep the combustion stability in the acceptable range (10% in this study). As shown in Figure 6.22, the COV_{IMEP} in EEDI conditions is almost independent with the SOI timing and stays around 3.8% at EER of 24% and 2.1% at EER of 48% when the SOI timing varies. In LEDI conditions, the COV_{IMEP} reaches its minimum in the SOI timing range between 70 CAD BTDC and 90 CAD BTDC. At SOI timing of 50 CAD BTDC, the COV_{IMEP} at EER of 24% is close to 10% and at EER of 48%, it approaches 9.0%. The minimum COV_{IMEP} , 1.7%, occurs at SOI timing of 270 CAD BTDC and EER of 48%. COV_{IMEP} in GPI condition is 4.8%, which is greater than that in EEDI conditions and lower than that in LEDI conditions.

Previous investigation has shown that the COV_{IMEP} gradually decreased with the increase of EER at original spark advance (15 CAD BTDC) and stoichiometric AFR (Figure 4.17), possibly due to ethanol’s high laminar flame propagation speed and better low temperature combustion stability. In the present work, high EER level also shows an improvement to combustion stability in lean burn. As shown in Figure 6.22, in both EEDI and LEDI conditions, COV_{IMEP} at EER of 48% is lower than at EER of 24%.

6.3.2 Combustion

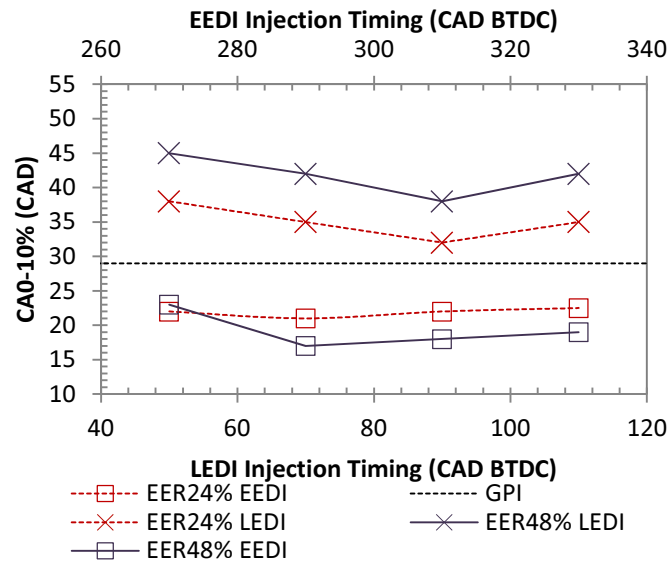


Figure 6.23– Variation of CA0-10% at lean burn limit

The variations of CA0-10% with SOI timing at lean burn limit are shown in Figure 6.23. This result directly reflects the mixture ignition characteristics in lean conditions. It can be seen that CA0-10% in EEDI conditions is shorter than in LEDI and GPI conditions at both EERs of 24% and 48%. In EEDI conditions, CA0-10% is almost independent from SOI timing except at 50 CAD BTDC where the CA0-10% at EER of 48% increases sharply. In LEDI conditions, CA0-10% first decreases with the advance of SOI timing and reaches the minimum at SOI timing of 90 CAD BTDC, then it increases with a further advance of SOI timing. At both EERs of 24% and 48%, the CA0-10% in EEDI conditions is less than 24 CAD, and in LEDI conditions, it is greater than 30 CAD. CA0-10% in GPI condition is 29 CAD which lies between that within EEDI and LEDI conditions.

The variation of CA0-10% is related to the combustion stability (COV) [175]. Previous studies have found a correlation between COV_{IMEP} and CA0-10%. It was reported that when the CA0-10% was over a certain range (30 CAD in their study), the COV_{IMEP} began to increase substantially [176]. In the present work, the CA0-10% of 30 CAD plays a similar role as a threshold. As it can be seen in Figures 6.22 and 6.23, when CA0-10% is longer than 30 CAD, the COV_{IMEP} stays at high level which is greater than 6.5%. When the CA0-10% is shorter than 30 CAD, the combustion stays stable and COV_{IMEP} is less than 4% (in EEDI conditions).

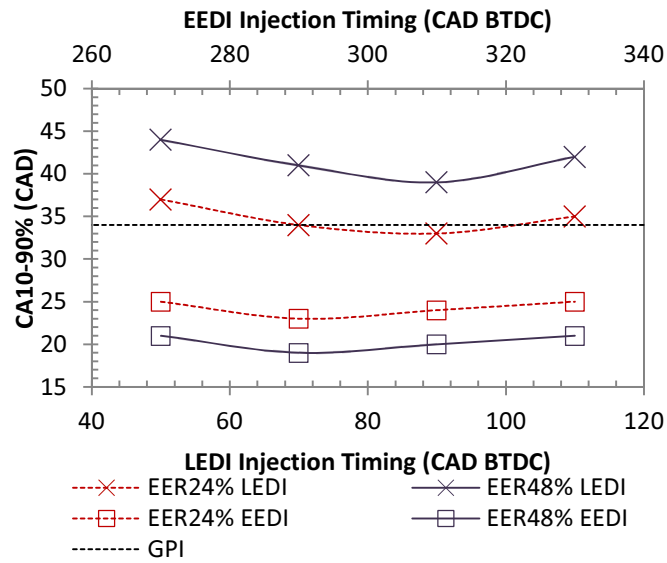


Figure 6.24– Variation of CA10-90% at lean burn limit

The variation of CA10-90% with SOI timing at the lean burn limit is shown in Figure 6.24. As is shown in the figure, CA10-90% generally follows the same trend as that of CA0-10%. In EEDI conditions, CA10-90% first decreases and reaches the minimum at SOI timing of 270 CAD BTDC, then it increases with a further advance in SOI timing. In LEDI conditions, CA10-90% first slightly decreases, then rises with the advance of SOI timing. CA10-90% in GPI condition is 34 CAD which is longer than in EEDI conditions but shorter than in LEDI conditions. It can be also seen from Figure 6.24 that in LEDI conditions, CA10-90% at EER of 48% is higher than at EER of 24%. This may be because the high EER (48%) level leads to more fuel impingement on the cylinder surface due to the increased DI fuel amount, which ultimately prolongs the combustion duration.

6.3.3 Emissions

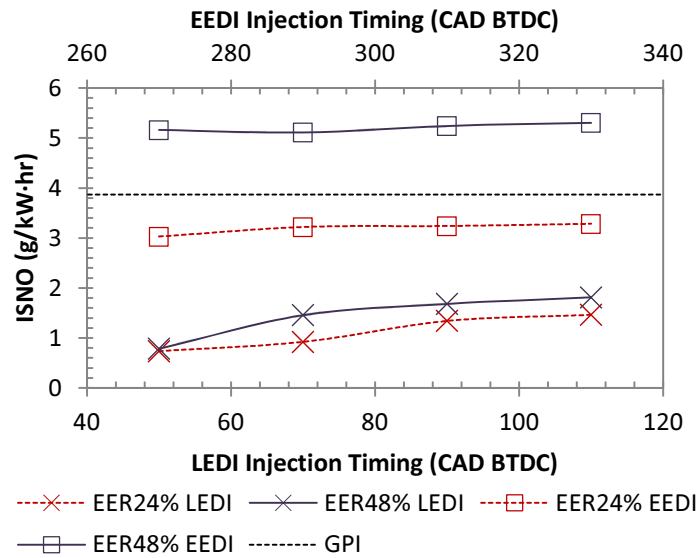


Figure 6.25– Variation of ISNO at lean burn limit

The effects of SOI timing on ISNO emission at lean burn limit are shown in Figure 6.25. It can be seen that in EEDI conditions, ISNO at both EERs is almost independent from SOI timing. ISNO at EER of 48% is about 50% greater than that at EER of 24%. The high ISNO at EER of 48% in EEDI condition may be because at EER of 48% the engine lean burn limit is lower than that at an EER of 24% (Figure 6.19). Richer mixture may result in a higher in-cylinder temperature which increases the formation of NO_x emissions. It can also be seen in Figure 6.25 that in LEDI conditions, the ISNO is lower than in GPI and EEDI conditions, and this slightly increases with the advance of SOI timing. The increase of ISNO with SOI timing may be because the advance of SOI timing provides more time for heat transfer from the cylinder wall to fresh charge, which finally contributes to the increase of the combustion temperature.

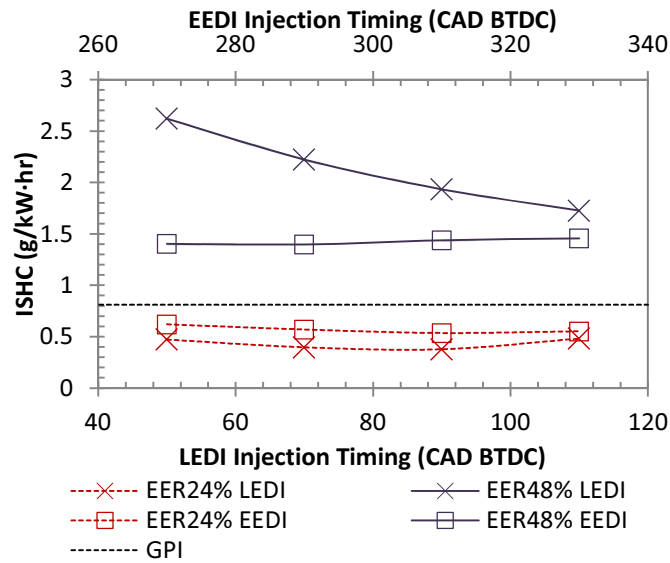


Figure 6.26– Variation of ISHC at lean burn limit

In a certain AFR range (14.7~17.6) [177], lean mixture has great potential for reducing HC emissions. The effect of SOI timing on ISHC at the lean burn limit is shown in Figure 6.26. It can be seen that at both EERs, ISHC in EEDI conditions is less than that experienced in LEDI and GPI conditions. In EEDI conditions, ISHC is almost independent from SOI timing and it is less than 0.62 g/kW·hr. The low ISHC in EEDI conditions can be attributed to a high lean burn limit (Figure 6.19) and better mixture quality. Leaner mixture can provide more oxygen for HC oxidation, thus resulting in less HC emissions. Early fuel direct injection (EEDI) enables more time for fuel evaporation which improves mixture quality and leads to more complete combustion. Therefore, HC emissions are decreased in EEDI conditions due to the above two reasons. In LEDI conditions, ISHC at EER of 24% is almost independent from SOI timing, and ISHC at EER of 48% gradually decreases with the advance of SOI timing. The decrease of ISHC with the advance of SOI timing at an EER of 48% may be because advancing the SOI timing provides more time for improving mixture homogeneity.

6.4 Summary

1. At original spark timing of 15 CAD BTDC, the IMEP was greater and ISEC was less in EEDI and EGDI conditions than in LEDI and LGDI conditions. The charge cooling effect and improved mixture quality may contribute to the increase of IMEP and the decrease of ISEC in

EEDI and EGDI conditions. In EEDI and EGDI conditions, the effect of SOI timing on IMEP was insignificant. In LEDI and LGDI conditions, the IMEP increased with the advance of SOI timing. The IMEP in EEDI and EGDI conditions was quite independent of the injection pressure. However, in LEDI and LGDI conditions, high injection pressure led to an increase of IMEP at a SOI timing of 50 CAD BTDC but a decrease at a SOI timing of 110 CAD BTDC.

2. The major combustion duration (CA5-90%) at spark timing of 15 CAD BTDC in EEDI and EGDI conditions was shorter than in LEDI and LGDI conditions with the central combustion crank angle (CA50) advanced. This indicates that the heat loss during the combustion was low and the engine work increased as the CA50 was advanced. As a result, the indicated thermal efficiency in EEDI and EGDI conditions was higher than in the LEDI and LGDI conditions. The peak of indicated thermal efficiency in EEDI conditions was at the range of SOI timing from 270 CAD BTDC to 290 CAD BTDC and the peak in EGDI conditions was at SOI timing of 330 CAD BTDC.

3. ISCO in EEDI and EGDI conditions was lower than that in LEDI and LGDI conditions. ISNO in EEDI and EGDI conditions was greater than that in LEDI and LGDI conditions. The effect of SOI timing on HC emissions was not significant in EDI+GPI conditions. However, in GDI+GPI mode, the ISHC at SOI timing later than 90 CAD BTDC was greater than that at other timings. ISHC and ISCO in early fuel injection conditions (EEDI and EGDI) and the injection pressure of 90 Bar were generally lower than those at other injection pressure levels. ISNO at that condition reached the maximum.

4. Later fuel injection (LEDI and LGDI) led to the deterioration of combustion and high pollutant emissions of HC and CO. Poor mixture quality which resulted from less time for fuel evaporation should be the main reason to the result. The high volatility of ethanol fuel showed benefits to combustion process and emissions formation in both later fuel injection (LEDI and LGDI) and early fuel injection (EEDI and EGDI) conditions. In EEDI conditions, the indicated efficiency reached the maximum and stayed stable when the SOI timing was advanced to 290 CAD BTDC. However, in LGDI conditions, the indicated efficiency slightly increased with the

advance of SOI timing and reached its maximum at SOI timing of 330 CAD BTDC. The indicated efficiency and emissions of ISHC and ISCO in LGDI conditions were generally higher than those in LEDI conditions.

5. The engine knock was effectively suppressed in LEDI conditions, so that more advanced spark timing could be adopted. However, due to the small improvement of volumetric efficiency and the deterioration of combustion, the IMEP and indicated thermal only slightly increased. The advance of spark timing was less effective in suppressing knock in EEDI than in LEDI. The combined effect of conceded spark advance and volumetric improvement led to higher IMEP and engine efficiency in EEDI conditions than that in LEDI conditions. With further consideration of the ISNO results, SOI timing at 270 CAD BTDC was the optimal injection timing for this particular engine, in terms of both NO emissions reduction and engine efficiency improvements.

6. EEDI was more effective in extending the lean burn limit than LEDI. The maximum lean burn limit (λ) achieved by EEDI was 1.29. COV_{IMEP} and emissions in EEDI conditions were less than that in LEDI conditions. LEDI only slightly increased the lean burn limit which was just over stoichiometric AFR. Poor mixture quality may be the main reason for the low lean burn limit. IMEP in EEDI conditions was greater than in LEDI conditions. EER of 48% resulted in lower IMEP and higher HC and NO emissions than at an EER of 24% in both EEDI and LEDI conditions.

Chapter Seven

7. Conclusions and future work

Introduction

The main aim of this thesis was to investigate the application of ethanol direct injection in a port injection gasoline engine. The effect of ethanol direct injection on potential engine thermal efficiency increment and emissions reduction was explored via leveraging effect, knock suppression and lean burn. Influence of ethanol direct injection on engine control parameters such as SOI timing and spark timing was also studied in order to adapt the conventional port injection gasoline engine to this new fuelling system. The investigation was based on experimental studies which were carried out on a self-developed testing rig system. The research engine was a 250cc, 4-stroke, air cooled single cylinder engine which was modified by adding an ethanol fuel direct injection system and a new ECU. Based on the experimental results, the main conclusion from this work will be presented in this chapter, and these will be followed by some suggestions for future work.

7.1 Conclusion

Leveraging effect on engine performance

In the engine conditions of fixed spark timing (15 CAD BTDC) and throttle position, ISEC decreased with the increase of EER. This indicates that to achieve comparable engine IMEP, less energy input will be required in a SI engine equipped with EDI+GPI. Hence, the total fuel consumption could be reduced by the leveraging use of ethanol fuel. Factors that contribute to the decreased ISEC may include the charge cooling effect, increase of LHV per unit mass of air, changes in the ratio of constant pressure to constant volume heat capacity, increases in products moles and reduced heat losses.

At 3500rpm, when the EER is less than 42.4% at light load and 36.3% at medium load, EDI+GPI has shown positive impact to combustion. The initial combustion period (CA0-5%),

early combustion period (CA5-50%) and major combustion period (CA5-90%) decreased with the increase of EER. A further increase of EER over 42.4% at light load and 36.3% at medium load led to an increase of CA0-5%, CA5-50% and CA5-90%. The deterioration of combustion should be caused by the over charge cooling effect, which may significantly reduce the combustion temperature.

The pollutant emissions of HC, CO and NO were reduced by using EDI+GPI technology. When EER was less than 24.2% at light load and 18.0% at medium load, the ISHC and ISCO decreased with the increase of EER. However, a further increase of EER resulted in an increase of HC and CO emissions, which may be due to the deterioration mixture quality and over charge cooling effect. ISNO displayed an opposite trend with ISHC and ISCO. It first increased with the increase of EER until it reached 24.2% at both light and medium load, then decreased with the further increase of EER.

Compared to the GDI+GPI mode, the EDI+GPI mode was more effective in terms of improving engine efficiency and reducing emissions. At fixed spark timing and throttle position, EDI+GPI generated a higher IMEP and indicated thermal efficiency than that of GDI+GPI. The great charge cooling effect caused by EDI, which increased volumetric efficiency, and improved combustion process due to use of ethanol fuel should be the factors that lead to higher IMEP and indicated thermal efficiency. The emissions of HC and CO increased monotonously with the increase DI/PFI energy ratio in GDI+GPI mode. Conversely, the HC and CO emissions in the EDI+GPI mode first decreased with an increase of the DI/PFI energy ratio until they reached the minimum, then they increased with further increases of the DI/PFI energy ratio .

Leveraging effect enhanced by spark timing and inlet air pressure increment

Experimental results have shown that when the spark timing was in the range from 25 CAD BTDC to 35 CAD BTDC, the effect of spark timing on the gasoline only condition (EER of 0%) was more obvious than that produced in EDI+GPI conditions. For the same spark advance in this range, the gasoline only condition resulted in more IMEP increments than those achieved in EDI+GPI conditions. However, when the spark timing was earlier than 35 CAD BTDC, the

variation of IMEP with spark timing is almost the same at different EERs. When the EER was less 34%, the CA5-50%, CA5-90% and COV_{IMEP} decreased with the increase of EER in the spark timing range from 25 CAD BTDC to 50 CAD BTDC. When the EER was greater than 34%, the CA5-50%, CA5-90% and COV_{IMEP} increased with the increase of EER when the spark timing was in the range between 25 CAD BTDC and 30 CAD BTDC. In the spark timing range from 35 CAD BTDC to 40 CAD BTDC, the CA5-50%, CA5-90% and COV_{IMEP} stayed stable and these were almost independent of the EER. Finally, these combustion parameters decreased with further increases of EER when the spark timing was earlier than 45 CAD BTDC.

EDI+GPI effectively mitigated engine knock and permitted more advanced spark timing when compared with GPI and GDI. The ethanol's great latent heat of vaporisation and high octane rating should be the factors that lead to the great anti-knock ability. At three engine loads of IMEP 7.2 Bar, 7.8 Bar and 8.5 Bar, when the EER was in the range from 15% to 35%, every 2% or 3% increment of EER permitted about 2 CAD advance of KLSA. The advanced spark timing allowed the combustion to take place at a more optimum timing, which increased the indicated thermal efficiency. The maximum indicated thermal efficiency in IMEP 7.2 Bar, 7.8 Bar and 8.5 Bar was 35.7%, 35.4% and 35.1%, respectively, which was 1.7%, 1.6% and 3.1% greater than their GPI counterparts.

In conditions of simulating turbocharging, the inlet air pressure was increased from 1.0 to 1.4 Bar by using compressed air. The EER level was increased with the increase of inlet air pressure in order to handle the raised knock tendency. The engine load and efficiency increased with the increase of inlet air pressure. The highest load achieved in the tests was 10.5 Bar IMEP at inlet air pressure of 1.4 Bar. At this condition, the EER level of 36.9% was required to overcome the knocking caused by both spark advance and high inlet air pressure. The indicated thermal efficiency at 10.5 Bar IMEP was 37.2%.

Influence of SOI timing and injection pressure

The effect of the injection strategy on EDI+GPI engine performance was evaluated at two SOI timing ranges. SOI timing from 50 CAD BTDC to 110 CAD BTDC was the range after the inlet

valve closed, which was defined as LEDI. SOI timing from 270 CAD BTDC to 330 BTDC was the range before the inlet valve closed, which was defined as EEDI. The results showed that the IMEP in EEDI conditions was greater than the IMEP in LEDI conditions due to improved volumetric efficiency and combustion. EDI pressure had an insignificant effect on IMEP in EEDI conditions. In LEDI conditions, IMEP was lower and the major combustion duration was longer than in the EEDI condition, possibly due to the poor mixture quality. In LEDI conditions, high injection pressure led to increased IMEP at an EDI timing of 50 CAD BTDC but the IMEP decreased at 110 CAD BTDC. EEDI resulted in lower CO and higher NO emissions than LEDI conditions. The effect of EDI timing on HC emissions was not significant. HC and CO emissions in EEDI conditions and EDI pressure 90 Bar were lower than those at other pressures. NO emissions in that condition reached the maximum. HC emissions at EDI timing of 50 CAD BTDC in LEDI conditions reached the maximum, however, NO emissions at that timing achieved the minimum. Generally, engine performance in terms of efficiency, combustion and emissions in EEDI conditions was better than engine performance in the LEDI condition.

Experimental results about the effect of the injection strategy on knock mitigation in the EDI+GPI engine indicated that LEDI was effective in suppressing engine knock and permitting more advanced spark timing. The effect of EEDI on knock suppression was less significant than that of LEDI because of the increased heat transfer from the cylinder wall to the fresh charge. Volumetric efficiency and combustion was effectively improved in EEDI conditions. The combined effect of the spark advance and improved volumetric efficiency in EEDI conditions led to higher IMEP and engine indicated thermal efficiency than in LEDI conditions.

EEDI was more effective in extending the lean burn limit than LEDI. The maximum lean burn limit (λ) achieved by EEDI was 1.29. COV_{IMEP} and emissions in EEDI conditions were less than that in LEDI conditions. LEDI only slightly increased the lean burn limit which was just over stoichiometric AFR. Poor mixture quality may be the main reason for the low lean burn limit. IMEP in EEDI conditions was greater than that in LEDI conditions. EER of 48% resulted in lower IMEP and higher HC and NO emissions than that at EER of 24% in both EEDI and LEDI conditions.

7.2 Future work

This work has investigated a wide variety of combustion and emission aspects related to applying ethanol direct injection on the port injection gasoline engine. Several problems have been exposed during the test owing to the constraints of the current engine configuration. The better understanding of these problems needs further modification of the rig system. There are also some problems or phenomena that are unable to be well explained based on current experimental results. Detailed realisation of these problems/phenomena requires the assistance of simulation work. Several outstanding issues are outlined below to serve as recommendations for future work.

Engine test

The engine test results showed that the engine performance significantly deteriorated in later fuel direct injection conditions, most possibly due to the poor mixture quality. This poor mixture quality should be attributed to the arrangement of the direct injector because the current location was chosen based on the packaging constraint of the cylinder head. Future experimental investigation should be performed on a production DISI engine where the arrangement of the DI injector is optimised to facilitate the formation of a homogeneous mixture. In this way, the engine performance may show improvement in later fuel direct injection conditions. LEDI may require less ethanol than EEDI to achieve a similar knock mitigation performance while maintaining the same engine thermal efficiency. Stratified combustion (LEDI) may make the engine achieve leaner conditions.

The experimental results have demonstrated the great potential of EDI+GPI in knock mitigation. However, this part of the test was performed at high engine temperature conditions (oil temperature 398 K) in order to realise knocking at medium load conditions and limit the peak cylinder pressure to protect the prototype engine. Future investigations should be conducted at normal engine temperature conditions (oil temperature 368 K), so that the experimental results of ethanol consumption for mitigating knock will be more meaningful.

In the investigations with boost inlet air pressure, the maximum inlet pressure was limited at 1.4 Bar. This boost level (0.4 Bar) is relatively low when compared with a modern turbo/supercharge engine which is normally around 1.0 Bar. A future downsized engine may adopt a higher boost level (1.0~2.0 Bar) in order to maintain the similar power output of the current large natural aspiration engine. The reason for limiting the boost level at 0.4 Bar in this study was due to the large (66 CAD) overlap of the inlet and exhaust valve in the test engine, which led to over scavenge problems when the inlet air pressure was greater than 1.4 Bar. In future studies, the overlap of the inlet and exhaust valve should be reduced. Thus high boost pressure can be tested and the investigation to EDI+GPI on knock mitigation can be evaluated in a more useful way.

In the present work, the effects of EDI+GPI on knock mitigation, emissions reduction and lean burn have been investigated. However, its impact on mixture physicochemical properties, which can be utilised to control some advanced combustion processes such as HCCI and dual-fuel sequential combustion (DFSC) has not been well explored. Due to the use of two different fuels and injection systems, the EDI+GPI engine has provided more flexibility than the current means available to control these advanced combustion processes. Future study on the EDI+GPI engine can focus on these areas, so that higher efficiency and lower emissions can be reached.

Simulation

The EDI has shown great potential in suppressing engine knock. Ethanol's great latent heat of vaporisation, high octane rating, low adiabatic flame temperature and high laminar flame speed have been regarded that their capacity contributing towards knock suppressing. However, which property has played the more dominant role and what is the order of the effectiveness for these factors? These questions should be answered via simulation works. The results of the simulation work can provide useful feedback for the future design work on the EDI+GPI engine. In such a way, the effectiveness of utilising the EDI to suppress knock can therefore be optimised.

The end gas area is the area in the cylinder where auto-ignition is most likely to occur. Reducing temperature in the end gas area can significantly decrease the knock propensity. EDI can

substantially decrease the charge temperature. However, this potential has not been well utilised to decrease the temperature in the end gas area, because in the current DISI engine the fuel spray is usually optimised to form a homogeneous mixture around the spark plug. Simulation work could help to identify the end gas area for a specific cylinder geometry. Thus in engine design, some of the fuel plumes could be directed to this area in order to decrease its temperature and further enhance the EDI+GPI engine anti-knock properties.

Reference

- [1] Grant, P., Michael, D., "Australia Annual Biofuels 2010", GAIN Report Number: AS1024, 2010.
- [2] Arnaldo, Walter., Biomass and Bioenergy. 32 (2008) 730.
- [3] Brown, Tristan R., and Robert C. Brown. "A review of cellulosic biofuel commercial - scale projects in the United States." *Biofuels, Bioproducts and Biorefining* 7.3 (2013): 235-245.
- [4] Wallington, T.J., Anderson J.E., and Winkler, S.L., "Comment on "Natural and Anthropogenic Ethanol Sources in North America and Potential Atmospheric Impacts of Ethanol Fuel Use"." *Environmental science & technology* 47.4 (2013): 2139-2140.
- [5] Government Report, State of Western Australia, "Western Australia Biofuels Taskforce Interim Report February 2007" 2007.
- [6] Yucesu, H.S., Sozen, A., Topgul, T. and Arcaklioglu, E., "Comparative study of mathematical and experimental analysis of spark ignition engine performance used ethanol-gasoline blend fuel." *Applied Thermal Engineering*, 27.3, (2007): 358-368.
- [7] Orbital Engine Company, "A literature review based assessment on the impacts of a 10% and 20% ethanol gasoline fuel blended on the Australian vehicle fleet, Report to Environment Australia", November 2002.
- [8] Orbital Engine Company, "Market Barriers to the uptake of biofuel study testing gasoline containing 20% ethanol (E20), Phase 2B final report to the Department of the Environment and Heritage", May 2004.
- [9] Miyamoto, N., Kenji Y., and Tadashi M., "Glow plug or spark plug makes the efficient use of neat alcohol fuels possible in a diesel engine." 5th International Symposium on Alcohol Fuel Technology, New Zealand. 1982.
- [10] Adomeit, P., Markus J., Andreas K., and Stefan P., "Glow-plug Ignition of Ethanol Fuels under Diesel Engine Relevant Thermodynamic Conditions". No. 2011-01-1391. SAE Technical Paper, 2011.
- [11] Somandepalli, V., Sean K., and Scott D., "Hot surface ignition of ethanol-blended fuels and biodiesel." No. 2008-01-0402. SAE Technical Paper, 2008.
- [12] LoRusso, J.A.; Cibanek, H.A., "Direct injection ignition assisted alcohol engine" Society of Automotive Engineers international congress and exposition, Detroit, MI, USA, 29 Feb 1988; Other Information: Technical Paper 880495.
- [13] Can, Ö., Çelikten, İ., Usta N., "Effects of ethanol addition on performance and emissions of a turbocharged indirect injection Diesel engine running at different injection pressures," *Energy Conversion and Management*, 45, 15-16, (2004): 2429-2440.
- [14] Karthikeyan, B., Srithar, K., "Performance characteristics of a glowplug assisted low heat rejection diesel engine using ethanol." *Applied Energy*, 88.1, (2011): 323-329.
- [15] Bilgin, A., Durgun, O., Sahin, Z., "The effects of diesel-ethanol blends on diesel engine performance". *Energy sources*, 24.5, (2002): 431-440.
- [16] Surawski N.C., Miljevic B., Roberts B.A., "Particle emissions, volatility, and toxicity from an ethanol fumigated compression ignition engine." *Environmental science &*

- technology, 44.1, (2009): 229-235.
- [17] Prommes K., Apanee L., Samai J., "Solubility of a diesel–biodiesel–ethanol blend, its fuel properties, and its emission characteristics from diesel engine," *Fuel*, 86, 7–8, (2007): 1053–1061.
- [18] Cheenkachorn, K., Fungtammasan, B., "An Investigation to Diesel-Ethanol-Biodiesel Blends for Diesel Engine: Part 1. Emulsion Stability and Fuel Properties." *Energy Sources, Part A: Recovery, Utilization, and Environmental Effects*, 32. 7, (2010).
- [19] Ma, W., Yang, J., Feng, W., "A Discussion about Compound Diesohol by Mechanical Emulsification Blend Ethanol with Diesel." *Energy Technology*, 4, (2004): 25-29.
- [20] Cheenkachorn, K., Narasingha, M., Funghammasan, B., "Biodiesel as Additive for Diesohol: Investigation to Emulsion Stability and Fuel Properties." *Chemeca 2006: Knowledge and Innovation. [Auckland, N.Z.]: Engineers Australia, (2006): 84-89.*
- [21] Demirbas, A., "Emission Characteristics of Gasohol and Diesohol." *Energy Sources, Part A: Recovery, Utilization, and Environmental Effects*, 31.13, (2009):1099-1104.
- [22] Demirbas, A. "Biofuels sources, biofuel policy, biofuel economy and global biofuel projections." *Energy Conversion and Management*, 49.8 (2008): 2106-2116.
- [23] Pan, J., Yang, W., Chou, S., Li, D., Xue, H., Zhao, J., and Tang, A., "Spray And Combustion Visualization Of Biodiesel In A Direct Injection Diesel Engine." *Thermal Science* 17.1 (2013): 279-289.
- [24] Arul Mozhi Selvan, V., Anand, R. B., & Udayakumar, M., "Combustion characteristics of Diesohol using biodiesel as an additive in a direct injection compression ignition engine under various compression ratios." *Energy & Fuels* 23, 11 (2009): 5413-5422.
- [25] Du, B., Long, W., Wei, S., Dong, Q., Xu, F., "A Study on the Combustion and Emission Characteristics of a Diesel Engine Fueled With Ethanol-Diesel-Gasoline Blends." *Automotive Engineering*, 30. 3.
- [26] Yan, Y., Yu-sheng, Z., Si-ping, R., Rui, Z., "Study on Combustion and Emission Characteristics of Diesel Engines Fueled with Ethanol/Diesel Blended Fuel." *SAE Technical Paper 2009-01-2675*, 2009, doi:10.4271/2009-01-2675.
- [27] Masuda, Y. and Chen, Z., "Combustion and Emission Characteristics of a PCI Engine Fueled with Ethanol-Diesel Blends." *SAE Technical Paper 2009-01-1854*, 2009, doi:10.4271/2009-01-1854.
- [28] Anisits, F., Hiemesch, O., "Investigations and results with MWM pilot-ignition ethanol combustion system." *Proceedings of the IV International Symposium on Alcohol Fuels Technology, Guaruja-SP-Brasil, 5-8 Oct. 1980.*
- [29] Pischinger F., Hilger, U., "Operation and Exhaust Emissions Behavior of the Direct-Injection Alcohol Diesel Engines. A-49 VI IAFTS, 1984.
- [30] Satge de Caro, P., Mouloungui, Z., Vaitilingom, G., & Berge, J. C., "Interest of combining an additive with diesel–ethanol blends for use in diesel engines." *Fuel*, 80.4, (2001):565-574.
- [31] Pischinger, Franz F., Peter Burghardt, Cornelis Havenith, and Kurt Weidmann., "Investigations on a passenger car swirl-chamber diesel engine using different alcohol fuels." No. 830552. *SAE Technical Paper*, 1983.
- [32] .Pischinger F., Reuter U.,Scheid E., "Self ignition of diesel sprays and its dependence on fuel properties and injection parameters." *Annual energy-sources technology*

- conference and exhibition, New Orleans, LA, USA, 10 Jan 1988; Other Information: Technical Paper 88-ICE-14.
- [33] Shi, S.X., Zhao, H.K., Fu, M.L., "Investigation of using ethanol-diesel blended in a diesel engine." *Combustion Science*, 1982, No. 2.
- [34] Cui, C.X., Wu, D.Y., Wang, J.Y., "The use of ethanol fuel in a diesel engine equipped with swirl combustion chamber." *Journal of HUST*, 1986, No.4
- [35] Lu, X.C., Ma, J., Ji, L., Huang, Z., "Simultaneous reduction of NO_x emission and smoke opacity of biodiesel-fueled engines by port injection of ethanol." *Fuel*, 87.7, (2008): 1289-1296.
- [36] Abu-Qudais, M., Haddad, O., Qudaisat, M., "The effect of alcohol fumigation on diesel engine." *Energy Conversion & Management*, 41, (2000): 389-399
- [37] Pidol, L., Lecointe, B., Pesant, L., and Jeuland, N., "Ethanol as a Diesel Base Fuel - Potential in HCCI Mode," SAE Technical Paper 2008-01-2506, 2008, doi:10.4271/2008-01-2506
- [38] Yao, C., Liu J., Yang, X., Chen, X., "Emissions and Fuel Economy of a Common Rail Engine Using Diesel/Ethanol Blended with Water Compound Combustion Mode." *Transactions of CSICE*, 02, (2011).
- [39] Kim, Y., Kim, K., and Lee, K., "A Study on the Combustion and Emission Characteristics of Diesel Fuel Blended with Ethanol in an HCCI Engine," SAE Technical Paper 2008-32-0026, 2008, doi:10.4271/2008-32-0026.
- [40] Maurya, Rakesh Kumar, and Avinash Kumar Agarwal. "Experimental study of combustion and emission characteristics of ethanol fuelled port injected homogeneous charge compression ignition (HCCI) combustion engine." *Applied Energy* 88.4 (2011): 1169-1180.
- [41] Lü, X., Hou, H., Zu, L., Huang, Z., "Experimental study on the auto-ignition and combustion characteristics in the homogeneous charge compression ignition (HCCI) combustion operation with ethanol/n-heptane blend fuels by port injection." *Fuel* 85.17 (2006): 2622-2631.
- [42] Di Pardo J., "Outlook for biomass ethanol production and demand." US Energy Information Administration. www.eia.doe.gov/oiaf/analysis/paper/pdf/biomass.pdf, 2000.
- [43] Wikipedia, "Ethanol fuel" 2014 http://en.wikipedia.org/wiki/Ethanol_fuel
- [44] Balat, M., Balat, H., "Recent trends in global production and utilization of bio-ethanol fuel." *Applied Energy*, 86.11, (2011): 2273-2282.
- [45] China Economic Net, "Recently development of flexible fuel Vehicles" Dong, N., 2008 http://paper.ce.cn/jjrb/html/2008-10/29/content_35369.htm
- [46] Stein, R., Polovina, D., Roth, K., Foster, M., "Effect of Heat of Vaporization, Chemical Octane, and Sensitivity on Knock Limit for Ethanol - Gasoline Blends." *SAE Int. J. Fuels Lubr.* 5.2, (2012):823-843, doi:10.4271/2012-01-1277.
- [47] Szybist, J., Foster, M., Moore, W., Confer, K., "Investigation of Knock Limited Compression Ratio of Ethanol Gasoline Blends." SAE Technical Paper 2010-01-0619, 2010, doi:10.4271/2010-01-0619.
- [48] Halle, A. and Pagot, A., "Development of a Flex Fuel Vehicle: Impact on Powertrain's Design and Calibration," SAE Technical Paper 2010-01-2087, 2010,

- doi:10.4271/2010-01-2087.
- [49] Cao, Y., "Thermodynamic Cycles of Internal Combustion Engines for Increased Thermal Efficiency, Constant-Volume Combustion, Variable Compression Ratio, and Cold Start." SAE Technical Paper 2007-01-4115, 2007, doi:10.4271/2007-01-4115.
- [50] Varde, K. and Clark, C., "A Comparison of Burn Characteristics and Exhaust Emissions from Off-Highway Engines Fueled by E0 and E85." SAE Technical Paper 2004-28-0045, 2004, doi:10.4271/2004-28-0045.
- [51] Lupescu, J., Chanko, T., Richert, J., and DeVries, J., "Treatment of Vehicle Emissions from the Combustion of E85 and Gasoline with Catalyzed Hydrocarbon Traps." SAE Int. J. Fuels Lubr. 2(1):485-496, 2009, doi:10.4271/2009-01-1080.
- [52] Varde, K. and Manoharan, N., "Characterization of Exhaust Emissions in a SI Engine using E85 and Cooled EGR." SAE Technical Paper 2009-01-1952, 2009, doi:10.4271/2009-01-1952.
- [53] Thummadetsak, T., Tipdecho, C., Wongjareonpanit, U., and Monnum, P., "Thailand Fuel Performance and Emissions in Flex Fuel Vehicles." SAE Technical Paper 2010-01-2132, 2010, doi:10.4271/2010-01-2132.
- [54] Jiang, Y.L., Xu, J.D., Zhang, K.N., "The Application of Ethanol Fuel on JieFangTruck", Automobile Science, 4, (1985).
- [55] Wang, K.M., "The Combustion Characteristic of Ethanol and Gasoline Dual-fuel Engine", Journal of TaiYan technology institute, 6, (1983).
- [56] Sugarcane, "Brazilian experience in using sugarcane on transportation fleet" <http://sugarcane.org/the-brazilian-experience/brazilian-transportation-fleet>
- [57] Furey, R.L., Jackson, M.W., "Exhaust and evaporative emissions from a Brazilian Chevrolet fueled with ethanol-gasoline blends." Proceedings of 12th Intersoc Energy Convers Engineering Conference, August 28-September 2, 1977. 1977, 1(Paper 779008 Proceeding).
- [58] Kumar, A., Khatri, D., and Babu, M., "Experimental Investigations on the Performance, Combustion and Emission Characteristics of alcohol blended gasoline in a Fuel Injected Spark Ignition Engine." SAE Technical Paper 2008-28-0068, 2008, doi:10.4271/2008-28-0068.
- [59] Wallner, T. and Miers, S., "Combustion Behavior of Gasoline and Gasoline/Ethanol Blends in a Modern Direct-Injection 4-Cylinder Engine." SAE Technical Paper 2008-01-0077, 2008, doi:10.4271/2008-01-0077.
- [60] Anderson, J., Leone, T., Shelby, M., Wallington, T., "Octane Numbers of Ethanol-Gasoline Blends: Measurements and Novel Estimation Method from Molar Composition." SAE Technical Paper 2012-01-1274, 2012, doi:10.4271/2012-01-1274.
- [61] Martínez, F.A., Ganji, A.R., "Performance and exhaust emissions of a single-cylinder utility engine using ethanol fuel." Training, 2006, (2013): 12-05.
- [62] Cooney, C., Wallner, T., McConnell, S., "Effects of blending gasoline with ethanol and butanol on engine efficiency and emissions using a direct-injection, spark-ignition engine." ASME, 2009.
- [63] Sandquist, H., Karlsson, M., and Denbratt, I., "Influence of Ethanol Content in Gasoline on Speciated Emissions from a Direct Injection Stratified Charge SI Engine." SAE Technical Paper 2001-01-1206, 2001, doi:10.4271/2001-01-1206.

- [64] He, B.Q., Wang, J.X., Hao, J.M., Yan, X.G., Xiao, J.H., "A study on emission characteristics of an EFI engine with ethanol blended gasoline fuels." *Atmospheric Environment* 37, (2003): 949–957.
- [65] Delgado, R., and Paz, S., "Effect of Different Ethanol-Gasoline Blends on Exhaust Emissions and Fuel Consumption." SAE Technical Paper 2012-01-1273, 2012, doi:10.4271/2012-01-1273.
- [66] Delgado, R., Paz, S., and Riba, D., "Evaluation of the Effect of Adding Ethanol to Gasoline at Different Percentages on Evaporative Emissions (Regulated and Non-regulated Pollutants)." SAE Technical Paper 2011-36-0202, 2011, doi:10.4271/2011-36-0202.
- [67] Jewitt, C.H., Lewis M., Gibbs, and Beth E., "Gasoline driveability index, ethanol content and cold-start/warm-up vehicle performance." No. 2005-01-3864. SAE Technical Paper, 2005.
- [68] Maheshwari, M., Pal, N.K., Acharya, G.K., Malhotra, R.K., "Indian Experience with the Use of Ethanol-Gasoline Blends on Two Wheelers and Passenger Cars." SAE paper 2004-28-0086, 2004.
- [69] Owen, K. and Coley, T., "Automotive fuels handbook" , Society of Automotive Engineers, 1990.
- [70] British Petroleum Company, "Air BP, Handbook of Products" 2000.
- [71] Black, F., "An overview of the technical implications of methanol and ethanol as highway motor vehicle fuels." No. 912413. SAE Technical Paper, 1991.
- [72] "Lynd, L.R., "Overview and evaluation of fuel ethanol from cellulosic biomass: technology, economics, the environment, and policy." *Annual review of energy and the environment* 21.1 (1996): 403-465.
- [73] Guibet, J.C., "Fuels and Engines", Éditions Technip, 1999.
- [74] Clifford, M., Shiblom and Gary, A.S., "Effect of Intake Valve Deposits of Ethanol and Additives Common to the Available Ethanol Supply." No. 902109. SAE Technical Paper, 1990.
- [75] Owen, K., Coley, T., "Automotive Fuels Reference Book", SAE International, 1995.
- [76] Downstream Alternatives Inc., "Fuel Recommendations Database Non-automotive Gasoline Powered Equipment", Downstream Alternatives Inc. 1999.
- [77] Tenenbaum, D.J., "Food vs. fuel: diversion of crops could cause more hunger[J]. *Environmental Health Perspectives*." 116.6, (2008): A254.
- [78] Pimentel, D., "Ethanol fuels: energy balance, economics, and environmental impacts are negative." *Natural resources research*, 12.2, (2003): 127-134.
- [79] Yang, B., Wyman, C.E., "Pretreatment: the key to unlocking low - cost cellulosic ethanol." *Biofuels, Bioproducts and Biorefining*, 2.1, (2008): 26-40.
- [80] Cohn, D.R., Bromberg, L., and Heywood, J.B., "Direct Injection Ethanol Boosted Gasoline Engines: Biofuel Leveraging For Cost Effective Reduction of Oil Dependence and CO₂ Emissions". 2005, Massachusetts Institute of Technology: Cambridge, MA.
- [81] Bromberg, L. and Cohn, D., "Alcohol Fueled Heavy Duty Vehicles Using Clean, High Efficiency Engines," SAE Technical Paper 2010-01-2199, 2010, doi:10.4271/2010-01-2199.
- [82] Cohn, D.R., Bromberg, L., and Heywood, J.B., Fuel Management System for Variable

- Ethanol Octane Enhancement of Gasoline Engines, U.S. Patent, 2010: US 2010175659, United States Patent and Trademark Office.
- [83] Ikoma, T., Abe, S., Sonoda, Y., Suzuki, H., "Development of V-6 3.5-liter Engine Adopting New Direct Injection System," SAE Technical Paper 2006-01-1259, 2006, doi:10.4271/2006-01-1259.
- [84] Mittal, V., Revier, B., and Heywood, J., "Phenomena that Determine Knock Onset in Spark-Ignition Engines." SAE Technical Paper 2007-01-0007, 2007, doi:10.4271/2007-01-0007.
- [85] Jahn, T., Schuerg, F., and Kempf, S., "Knock Control on Small Four-Two-Wheeler Engines." SAE Technical Paper 2012-32-0052, 2012, doi:10.4271/2012-32-0052.
- [86] Kasseris, E. and Heywood, J., "Charge Cooling Effects on Knock Limits in SI DI Engines Using Gasoline/Ethanol Blends: Part 1-Quantifying Charge Cooling," SAE Technical Paper 2012-01-1275, 2012, doi:10.4271/2012-01-1275.
- [87] Kasseris, E. and Heywood, J., "Charge Cooling Effects on Knock Limits in SI DI Engines Using Gasoline/Ethanol Blends: Part 2-Effective Octane Numbers." SAE Int. J. Fuels Lubr. 5(2):844-854, 2012, doi:10.4271/2012-01-1284.
- [88] Szybist, James P., and Brian H. West. The Impact of Low Octane Hydrocarbon Blending Streams on Ethanol Engine Optimization. Oak Ridge National Laboratory (ORNL); Fuels, Engines and Emissions Research Center; National Transportation Research Center, 2013.
- [89] Achleitner, E., Bäcker, H., and Funaioli, A., "Direct Injection Systems for Otto Engines," SAE Technical Paper 2007-01-1416, 2007, doi:10.4271/2007-01-1416.
- [90] Hemdal, S., Denbratt, I., Dahlander, P., and Warnberg, J., "Stratified Cold Start Sprays of Gasoline-Ethanol Blends," SAE Int. J. Fuels Lubr. 2(1):683-696, 2009, doi:10.4271/2009-01-1496.
- [91] Vuk, C. and Vander Griend, S., "Fuel Property Effects on Particulates In Spark Ignition Engines," SAE Technical Paper 2013-01-1124, 2013, doi:10.4271/2013-01-1124.
- [92] Oh, H., Bae, C., and Min, K., "Spray and Combustion Characteristics of Ethanol Blended Gasoline in a Spray Guided DISI Engine under Lean Stratified Operation," SAE Int. J. Engines 3(2):213-222, 2010, doi:10.4271/2010-01-2152.
- [93] Shayler, P., Jones, S., Horn, G., and Eade, D., "Characterisation of DISI Emissions and Fuel Economy in Homogeneous and Stratified Charge Modes of Operation," SAE Technical Paper 2001-01-3671, 2001, doi:10.4271/2001-01-3671.
- [94] Serras-Pereira, J., Aleiferis, P., Richardson, D., and Wallace, S., "Characteristics of Ethanol, Butanol, Iso-Octane and Gasoline Sprays and Combustion from a Multi-Hole Injector in a DISI Engine," SAE Int. J. Fuels Lubr. 1.1, (2009): 893-909, doi:10.4271/2008-01-1591.
- [95] Zeng, W., Xu, M., Zhang, M., Zhang, Y., "Characterization of Methanol and Ethanol Sprays from Different DI Injectors by Using Mie-scattering and Laser Induced Fluorescence at Potential Engine Cold-start Conditions," SAE Technical Paper 2010-01-0602, 2010, doi:10.4271/2010-01-0602.
- [96] Schifter, I., Vera, M., Díaz, L., Guzmán, E., Ramos, F., Lopez-Salinas, E., "Environmental implications on the oxygenation of gasoline with ethanol in the

- metropolitan area of Mexico City." *Environmental science & technology* 35.10 (2001): 1893-1901.
- [97] Eyidogan, M., Ozsezen, A. N., Canakci, M., & Turkcan, A., "Impact of alcohol-gasoline fuel blends on the performance and combustion characteristics of an SI engine." *Fuel* 89.10 (2010): 2713-2720.
- [98] Liao, S. Y., Jiang, D. M., Huang, Z. H., Zeng, K., Cheng, Q., "Determination of the laminar burning velocities for mixtures of ethanol and air at elevated temperatures." *Applied Thermal Engineering* 27.2 (2007): 374-380.
- [99] Saxena, P., and Forman A.W., "Numerical and experimental studies of ethanol flames." *Proceedings of the Combustion Institute* 31.1 (2007): 1149-1156.
- [100] Geng, P., Furey, R., and Melkvik, L., "Elemental Composition Determination and Stoichiometric Air-Fuel Ratios of Gasoline Containing Ethanol," SAE Technical Paper 2010-01-2112, 2010, doi:10.4271/2010-01-2112.
- [101] Bradley D., "Fundamentals of lean combustion." *Lean Combustion: Technology and Control*, (2008): 19-53.
- [102] *Lean combustion: technology and control*[M]. Access Online via Elsevier, 2011.
- [103] Pannone, G., Johnson, R., "Methanol as a Fuel for a Lean Turbocharged Spark ignition Engine." SAE Technical Paper 890435, 1989, doi: 10.4271/890435.
- [104] Germane, G., Wood, C., and Hess, C., "Lean Combustion in Spark-Ignited Internal Combustion Engines - A Review." SAE Technical Paper 831694, 1983, doi: 10.4271/831694.
- [105] Rousseau, S., Lemoult, B., Tazerout, M., "Combustion characterization of natural gas in a lean burn spark-ignition engine." *Proceedings of the Institution of Mechanical Engineers, Part D: Journal of Automobile Engineering*, 213.5, (1999): 481-489.
- [106] Piock, W., Weyand, P., Wolf, E., and Heise, V., "Ignition Systems for Spray-Guided Stratified Combustion." *SAE Int. J. Engines* 3.1, (2010):389-401, doi:10.4271/2010-01-0598.
- [107] Toulson, E., Schock, H., and Attard, W., "A Review of Pre-Chamber Initiated Jet Ignition Combustion Systems." SAE Technical Paper 2010-01-2263, 2010, doi:10.4271/2010-01-2263.
- [108] Hassaneen, A., Varde, K., Bawady, A., and Morgan, A., "A Study of The Flame Development and Rapid Burn Durations In A Lean-Burn Fuel Injected Natural Gas S.I. Engine." SAE Technical Paper 981384, 1998, doi:10.4271/981384.
- [109] Li, L., Wang, Z., Wang, H., Deng, B., "A Study of LPG Lean Burn for a Small SI Engine," SAE Technical Paper 2002-01-2844, 2002, doi:10.4271/2002-01-2844.
- [110] Saanum, I., Bysveen, M., Tunestål, P., and Johansson, B., "Lean Burn Versus Stoichiometric Operation with EGR and 3-Way Catalyst of an Engine Fueled with Natural Gas and Hydrogen Enriched Natural Gas." SAE Technical Paper 2007-01-0015, 2007, doi:10.4271/2007-01-0015..
- [111] Beeckmann, J., Kruse, S., and Peters, N., "Effect of Ethanol and n-Butanol on Standard Gasoline Regarding Laminar Burning Velocities," SAE Technical Paper 2010-01-1452, 2010, doi:10.4271/2010-01-1452.
- [112] Beeckmann, J., Röhl, O., and Peters, N., "Experimental and Numerical Investigation of Iso-Octane, Methanol and Ethanol Regarding Laminar Burning Velocity at Elevated

- Pressure and Temperature." SAE Technical Paper 2009-01-1774, 2009, doi:10.4271/2009-01-1774..
- [113] Wu, C.W., Chen, R.H., Pu, J.Y., "The influence of air–fuel ratio on engine performance and pollutant emission of an SI engine using ethanol–gasoline-blended fuels." *Atmospheric Environment*, 38.40, (2004): 7093-7100..
- [114] Alexandrian, M., Schwalm, M., 1992. Comparison of ethanol and gasoline as automotive fuels. ASME papers 92-WA/DE-15
- [115] Warnberg, J., Boehmer, M., and Denbratt, I., "Optimised Neat Ethanol Engine with Stratified Combustion at Part-load; Particle Emissions, Efficiency and Performance," SAE Technical Paper 2013-01-0254, 2013, doi:10.4271/2013-01-0254..
- [116] Liang, C., Ji, C., Gao, B., Liu, X., Zhu, Y., "Investigation on the performance of a spark-ignited ethanol engine with DME enrichment." *Energy Conversion and Management* 58 (2012): 19-25.
- [117] Brehob, D., Fleming, J., Haghgooie, M., and Stein, R., "Stratified-Charge Engine Fuel Economy and Emission Characteristics," SAE Technical Paper 982704, 1998, doi:10.4271/982704..
- [118] Adomeit, P., Lang, O., Pischinger, S., Aymanns, R., "Analysis of Cyclic Fluctuations of Charge Motion and Mixture Formation in a DISI Engine in Stratified Operation," SAE Technical Paper 2007-01-1412, 2007, doi:10.4271/2007-01-1412.
- [119] Hanabusa, H., Kondo, T., Hashimoto, K., Sono, H., "Study on Homogeneous Lean Charge Spark Ignition Combustion," SAE Technical Paper 2013-01-2562, 2013, doi:10.4271/2013-01-2562.
- [120] Weber, H.J., Mack, A., Roth, P., "Combustion and pressure wave interaction in enclosed mixtures initiated by temperature nonuniformities." *Combustion and flame* 97.3 (1994): 281-295..
- [121] Martz, J. B., Kwak, H., Im, H.G., Lavoie, G.A., Assanis, D.N., *Proc. Combust. Inst.*, 33, (2011): 3001-3006.
- [122] Shayler, P.J., Jones, S.T., Horn, G., & Eade, D., "Characterisation of DISI Emissions and Fuel Economy in Homogeneous and Stratified Charge Modes of Operation." SAE Technical Paper 2001-01-3671, 2001, doi: 10.4271/2001-01-3671.
- [123] Subramanian, K. A., Singal, S. K., Saxena, M., Singhal, S., "Utilization of liquid biofuels in automotive diesel engines: an Indian perspective." *Biomass and Bioenergy* 29.1 (2005): 65-72.
- [124] Sementa, Paolo, Bianca Maria Vaglieco, and Francesco Catapano. Non-intrusive investigation in a small GDI optical engine fuelled with gasoline and ethanol. No. 2011-01-0140. SAE Technical Paper, 2011.
- [125] Delgado, R., Paz, S., and Riba, D., "Evaluation of the Effect of Adding Ethanol to Gasoline at Different Percentages on Evaporative Emissions (Regulated and Non-regulated Pollutants)." SAE Technical Paper 2011-36-0202, 2011, doi:10.4271/2011-36-0202.
- [126] Wallner, T., Miers, S.A., McConnell, S., "A comparison of ethanol and butanol as oxygenates using a direct-injection, spark-ignition engine." *Journal of Engineering for Gas Turbines and Power* 131.3, (2009): 032802-032809.
- [127] Tanaka, H., Matsumoto, T., Funaki, R., Kato, T., Mitsutake, K., Sekimoto, M.,

- Watanabe, H., "Effects of Ethanol or ETBE Blending in Gasoline on Evaporative Emissions for Japanese In-Use Passenger Vehicles." No. 2007-01-4005. SAE Technical Paper, 2007.
- [128] Martínez, F., Ganji, A., "Performance and Exhaust Emissions of a Single-Cylinder Utility Engine Using Ethanol Fuel," SAE Technical Paper 2006-32-0078, 2006, doi:10.4271/2006-32-0078.
- [129] Li, L., Liu, Z., Wang, H., Deng, B., "Combustion and Emissions of Ethanol Fuel (E100) in a Small SI Engine," SAE Technical Paper 2003-01-3262, 2003, doi:10.4271/2003-01-3262.
- [130] Celik, M. Bahattin. "Experimental determination of suitable ethanol–gasoline blend rate at high compression ratio for gasoline engine." *Applied Thermal Engineering* 28.5 (2008): 396-404.
- [131] Bresenham D, Reisel J, Neusen K. Spindt air–fuel ratio method generalization for oxygenated fuels. SAE Tec Pap Ser 1998; No. 982054; 1998.
- [132] Obital Engine Company, "A literature Review Based Assessment on the Impacts of a 10% and 20% Ethanol Gasoline Fuel Blend on Non-Automotive Engines", Report to Environment Australia, December, 2002, Obital Engine Company.
- [133] Blumberg, P., Bromberg, L., Kang, H., and Tai, C., "Simulation of High Efficiency Heavy Duty SI Engines Using Direct Injection of Alcohol for Knock Avoidance," *SAE Int. J. Engines* 1(1):1186-1195, 2009, doi:10.4271/2008-01-2447.
- [134] Cohn, D.R., Bromberg, L., Heywood, J.B., Optimized fuel management system for direct injection ethanol enhancement of gasoline engines, U.S. Patent 7,225,787, June 5 2007.
- [135] Stein, R., House, C., and Leone, T., "Optimal Use of E85 in a Turbocharged Direct Injection Engine," *SAE Int. J. Fuels Lubr.* 2.1, (2009): 670-682, doi:10.4271/2009-01-1490.
- [136] Daniel, R., Wang, C., Xu, H., Tian, G., "Dual-Injection as a Knock Mitigation Strategy Using Pure Ethanol and Methanol," *SAE Int. J. Fuels Lubr.* 5.2, (2012):772-784, doi:10.4271/2012-01-1152.
- [137] Ikoma, T., Abe, S., Sonoda, Y., Suzuki, H., Suzuki, Y., Basaki, M., "Development of V-6 3.5-liter engine adopting new direct injection system." *SAE Technical Papers* 2006-01 (2006): 1259.
- [138] Wurms, R., Jung, M., Adam, S., Dengler, S., Heiduk, T. and Eiser, A., "Innovative Technologies in Current and Future TFSI Engines from Audi", 20th Aachen Colloquium Automobile and Engine Technology 2011. 2011.
- [139]. Ritchie, D., Wang, C.M., Xu, H., Tian, G., "Split-Injection Strategies at Wide Open Throttle using Gasoline, Ethanol and 2,5-Dimethylfuran in a Direct-Injection SI Engine", SAE Paper 2012-01-0403.
- [140] Zhu, G., Stuecken, T., Schock, H., Yang, X., Hung, D.L., & Fedewa, A., "Combustion characteristics of a single-cylinder engine equipped with gasoline and ethanol dual-fuel systems." No. 2008-01-1767. SAE Technical Paper, 2008.
- [141] Daniel, R., Tian, G., Xu, H., Wyszynski, M.L., Wu, X., Huang, Z., "Effect of spark timing and load on a DISI engine fuelled with 2, 5-dimethylfuran." *Fuel* 90.2 (2011): 449-458.

- [142] Wurms, R., Jung, M., Adam, S., Dengler, S., Heiduk, T. and Eiser, A., "Innovative Technologies in Current and Future TFSI Engines from Audi", 20th Aachen Colloquium Automobile and Engine Technology 2011. 2011.
- [143] Kistler, "Image of Kistler 6115B Pressure transducer" 2010 www.kistler.com/au/en/product/pressure/6115BFD16A41
- [144] Horiba, "Image of Horiba Mexa 5841 five gas analyzer" 2008 www.horiba.com/uk/automotive-test-systems/products/emission-measurement-systems/portable-emission-analyzers/details/mexa-5841-826/
- [145] Heywood, J.B., "Two-Stroke Cycle Engine: It's Development, Operation and Design (Combustion)." Taylor & Francis; 1 edition, 1999.
- [146] Heywood, J.B., Internal Combustion Engine Fundamentals, McGraw-Hill. 1988.
- [147] Anderson, J., Leone, T., Shelby, M., Wallington, T., "Octane Numbers of Ethanol-Gasoline Blends: Measurements and Novel Estimation Method from Molar Composition." SAE Tech. Pap. Ser. 2012, Paper No. 2012-01-1274.
- [148] Christensen, M., Johansson, B., "Supercharged Homogeneous Charge Compression Ignition (HCCI) with Exhaust Gas Recirculation and Pilot Fuel." SAE Tech. Pap. Ser. 2000, Paper No. 2000-01-1835.
- [149] Mittal, V., Revier, B., and Heywood, J., "Phenomena that Determine Knock Onset in Spark-Ignition Engines," SAE Technical Paper 2007-01-0007, 2007, doi:10.4271/2007-01-0007.
- [150] YBR 250 Service Manual, First edition, February 2007.
- [151] Rassweiler, Gerald M., and Lloyd Withrow., "Motion pictures of engine flames correlated with pressure cards." No. 380139. SAE Technical Paper, 1938.
- [152] Ball, J. K., Raine, R. R., & Stone, C. R., "Combustion analysis and cycle-by-cycle variations in spark ignition engine combustion Part 1: An evaluation of combustion analysis routines by reference to model data." Proceedings of the Institution of Mechanical Engineers, Part D: Journal of Automobile Engineering 212.5 (1998): 381-399.
- [153] Christensen, M., Johansson, B., "Supercharged Homogeneous Charge Compression Ignition (HCCI) with Exhaust Gas Recirculation and Pilot Fuel," SAE Technical Paper 2000-01-1835, 2000, doi:10.4271/2000-01-1835.
- [154] Nakata, K., Utsumi, S., Ota, A., Kawatake, K., "The Effect of Ethanol Fuel on a Spark Ignition Engine", SAE Technical Paper 2006-01-3380, 2006. doi: 10.4271/2006-01-3380.
- [155] Daniel, R., Wang, C., Xu, H., and Tian, G., "Effects of Combustion Phasing, Injection Timing, Relative Air-Fuel Ratio and Variable Valve Timing on SI Engine Performance and Emissions using 2,5-Dimethylfuran," SAE Int. J. Fuels Lubr. 5.2, (2012): 855-866, doi:10.4271/2012-01-1285.
- [156] Smith, J.M., Van Ness H.C., Abbot M.M.. Introduction to Chemical Engineering Thermodynamics, Fifth Edition. McGraw-Hill. New York, NY. 1996. p 283.
- [157] Smith, J.M., Van Ness H.C., Abbot M.M.. Introduction to Chemical Engineering Thermodynamics, Seventh Edition. McGraw-Hill. New York, NY. 2006. p 648.
- [158] Piyaboot Ornman, Chinda Charoenphonphanich, "Combustion Characteristics of Direct Injection Stratified Charge of Gasohol Fuels", The First TSME International

- Conference on Mechanical Engineering, 20-22 October, 2010, Ubon Ratchathani.
- [159] Chareonphonphanich, C., and Srichai, P., "Flame Propagation of Bio-Ethanol in a Constant Volume Combustion Chamber." JSAE paper No. 2009-32- 0113 / 20097113.
- [160] Sezer, İ., Altın İ., Bilgin A.. "Exergetic Analysis of Using Oxygenated Fuels in Spark-Ignition (SI) Engines." *Energy & Fuels*, 23, (2009): 1801-1807.
- [161] Marriott, C.D, Wiles, M.A., Gwidt, J.M., Parrish. S.E., "Development of a Naturally Aspirated Spark Ignition Direct-Injection Flex-Fuel Engine," *SAE Int. J. Engines* 1.1, (2008): 267-295.
- [162] Turner D, Xu H., Cracknell R.F., "Combustion performance of bio-ethanol at various blend ratios in a gasoline direct injection engine." *Fuel*, 90.5, (2011): 1999-2006.
- [163] Topgül, T., Yücesu, H. S., Cinar, C., & Koca, A., "The effects of ethanol–unleaded gasoline blends and ignition timing on engine performance and exhaust emissions." *Renewable energy* 31.15 (2006): 2534-2542.
- [164] Zhuang Y, Hong G., "The Effect of Direct Injection Timing and Pressure on Engine Performance in an Ethanol Direct Injection Plus Gasoline Port Injection (EDI+GPI) SI Engine." *SAE Technical Paper* 2013-01-0892, 2013, doi:10.4271/2013-01-0892.
- [165] Sayin, C., "The impact of varying spark timing at different octane numbers on the performance and emission characteristics in a gasoline engine." *Fuel* 97 (2012): 856-861
- [166] Wang, C., Xu, H., Daniel, R., Ghafourian, A., Herreros, J. M., Shuai, S., Ma, X., "Combustion characteristics and emissions of 2-methylfuran compared to 2, 5-dimethylfuran, gasoline and ethanol in a DISI engine." *Fuel* 103 (2013): 200-211.
- [167] Da Silva, R., Cataluña, R., Menezes, E.W.D., Samios, D., & Piatnicki, C.M.S., "Effect of additives on the antiknock properties and Reid vapor pressure of gasoline." *Fuel* 84.7 (2005): 951-959.
- [168] Zhao, F., Harrington, D., and Lai, M.C., "Automotive Gasoline Direct-Injection Engines," *Society of Automotive Engineers, Inc., Warrendale, PA, ISBN* 978-0-7680-0882-1, 2002.
- [169] Wu, X., Daniel, R., Tian, G., Xu H., Huang, Z.H., Dave R., "Dual-Injection: the Flexible, Bi-fuel Concept for Spark-Ignition Engines fuelled with various Gasoline and Biofuel blends," *Applied Energy* 88 (2011) 2305–2314, 2011.
- [170] Zhu, G.G., Haskara, I. and Winkelman, J., "Closed-Loop Ignition Timing Control for SI Engines Using Ionization Current Feedback." *IEEE Transactions on Control Systems Technology*, 15.3, (2007): 12.
- [171] Yang J, and Anderson R. Fuel Injection Strategies to Increase Full-Load Torque Output of a Direct-Injection SI Engine. *SAE Technical Paper* 980495, 1998, doi:10.4271/980495.
- [172] Achleitner E, Bäcker H, Funaioli A., "Direct Injection Systems for Otto Engines." *SAE Technical Paper* 2007-01-1416, 2007, doi:10.4271/2007-01-1416.
- [173] Lee, A. T., Wilcutts, M., Tunestål, P., & Hedrick, J. K., "A method of lean air-fuel ratio control using combustion pressure measurement." *JSAE review* 22.4 (2001): 389-393.
- [174] Ayala, F., Gerty, M., and Heywood, J., "Effects of Combustion Phasing, Relative Air-fuel Ratio, Compression Ratio, and Load on SI Engine Efficiency," *SAE Technical*

- Paper 2006-01-0229, 2006, doi:10.4271/2006-01-0229.
- [175] Kiyota, Y., Akishino, K., and Ando, H., "Concept of Lean Combustion by Barrel-Stratification," SAE Technical Paper 920678, 1992, doi:10.4271/920678.
- [176] Topinka, J. A., Gerty, M.D., Heywood, J.B., & Keck, J.C., "Knock behavior of a lean-burn, H₂ and CO enhanced, SI gasoline engine concept." No. 2004-01-0975. SAE Technical Paper, 2004.
- [177] Brehob, D., Fleming, J., Haghgoobie, M., and Stein, R., "Stratified-Charge Engine Fuel Economy and Emission Characteristics," SAE Technical Paper 982704, 1998, doi:10.4271/982704.